

THE THREE-NUCLEON CONTINUUM: ACHIEVEMENTS, CHALLENGES AND APPLICATIONS

W. GLÖCKLE^a, H. WITALA^b, D. HÜBER^a, H. KAMADA^a, J. GOLAK^b

^a*Institut für theoretische Physik II, Ruhr-Universität Bochum, D-44780 Bochum, Germany*

^b*Institute of Physics, Jagellonian University, PL-30059 Cracow, Poland*



AMSTERDAM – LAUSANNE – NEW YORK – OXFORD – SHANNON – TOKYO

The three-nucleon continuum: achievements, challenges and applications

W. Glöckle^a, H. Witała^b, D. Hüber^a, H. Kamada^{a,1}, J. Golak^b

^a Institut für theoretische Physik II, Ruhr-Universität Bochum, D-44780 Bochum, Germany

^b Institute of Physics, Jagellonian University, PL-30059 Cracow, Poland

Received November 1995; editor: G.E. Brown

Contents:

1. Introduction	110	7.8. 3NF effects at higher energies	249
2. Theoretical formulation	114	8. Other rigorous techniques and open questions	250
2.1. Heuristic approach	114	8.1. Configuration space treatment	250
2.2. Algebraic approach	119	8.2. The method of continued fractions	254
2.3. Inclusion of three-nucleon forces	122	8.3. The pair correlated hyperspherical	
2.4. 3N scattering observables	124	harmonic basis method	256
3. Technical performance	134	8.4. Finite rank expansions	257
4. Numerical algorithms and techniques	139	8.5. The Coulomb problem in pd scattering	258
5. Accuracy tests	145	8.6. Relativistic 3N equations	260
6. Comparison of theory and experiment	151	9. Applications	262
6.1. NN force picture only	155	9.1. Inclusive and exclusive electron scattering	
6.2. 3N scattering including 3NF's	201	on ${}^3\text{He}$ and ${}^3\text{H}$	262
7. Special topics	218	9.2. Photodisintegration and pd capture in the	
7.1. Survey of breakup cross sections	218	3N system	263
7.2. Extraction of the nn scattering length a_{nn}	224	9.3. Pion absorption on ${}^3\text{He}$ and ${}^3\text{H}$	263
from the 3N breakup process		9.4. Nonmesonic decay of the hypertriton	264
7.3. The A_y puzzle	229	10. Conclusions and outlook	264
7.4. Eigen phase shifts and mixing parameters	230	Appendix A. Cross sections	267
for elastic nd scattering above the breakup		Appendix B. Breakup kinematics	270
threshold		Appendix C. Geometrical quantities related to	
7.5. High energy limit	233	permutation operators	271
7.6. The nucleon-deuteron optical potential and	243	Appendix D. List of international few-body	
its high energy limit		conferences	271
7.7. Connection between total nd and nn and		References	273
np cross sections in the high energy limit	246		

¹ Present address: Paul Scherrer Institut, CH-5232, Villigen PSI, Switzerland.

Abstract

After a brief historic overview the basic equations for three-nucleon (3N) scattering based on general two-nucleon and 3N forces are reviewed and the main steps for their derivation are given. Also the expressions for the various observables, elastic and breakup cross sections, as well as the great variety of spin observables are displayed and derived. The treatment of the 3N Faddeev equations in momentum space and in a partial wave decomposition is outlined in some detail, the handling of the singularities in the integral kernel described and the algorithms and techniques used to solve the large set of equations in the discretized form are presented. Accuracy tests in form of benchmark calculations, where our results are compared to the ones of other techniques, are given. The bulk part of this review, however, is devoted to the comparison of very many observables in elastic nucleon-deuteron (Nd) scattering and the breakup process to the predictions based on the most modern nucleon-nucleon (NN) forces AV18, Nijmegen93, Nijmegen I and II and a recently updated OBE-potential CD Bonn. Overall the agreement with the data is excellent and there is little room left for the action of a three-nucleon force (3NF). The effects of the $\pi-\pi$, $\pi-\rho$ and $\rho-\rho$ exchange 3NF's of the Tucson-Melbourne model are studied. They are in general small and in the few cases where discrepancies to data occur using NN forces only, they go into the wrong direction. We propose quite a few measurements, which should help to get more information on the potential energy of three nucleons. Several special topics are discussed: Do certain 3N scattering observables scale with the triton binding energy? Which of the 3N breakup cross sections are totally insensitive to the choice of the NN force and which are very sensitive? How well can one extract the nn scattering length from the 3N breakup? We discuss the outsticking discrepancy of the 3N analyzing power A_y in low energy elastic Nd scattering; the eigen phase shifts and mixing parameters in elastic nd scattering; the simplifications of 3N scattering at high energies and the formulation of the optical potential for elastic nd scattering and its limiting form at high energies. Alternative approaches to solve 3N scattering: in configuration space, using finite rank expansions of NN forces, variational techniques and the hybrid Sendai method are briefly described as well as the proton-proton Coulomb force problem in the pd system and the question how to incorporate relativity. Finally some applications are sketched where a 3N final state occurs and where the interaction among the nucleons requires a correct treatment. We mention inelastic electron scattering as well as π -absorption on ${}^3\text{He}$ (${}^3\text{H}$) and nonmesonic decay of the hypertriton.

PACS: 21.45.+v; 24.10.-i; 25.10.+s

1. Introduction

Since the early days of nuclear physics the few-nucleon systems received special attention. We cite a few of the very early articles: [503,476,132,133,393]. It was natural that one wanted to see whether the NN force models of those days had a chance to provide the binding energies of ^2H , ^3H and ^3He and also of ^4He by estimating solutions to the nonrelativistic Schrödinger equation. These estimates led to important insights, among them [476], that the NN forces have to have a finite range in order to avoid a collapse. There was a long period where variational and other approximate techniques have been used, whose spirit can be found in [54], for instance. Nuclear reaction theory written out in the form of multiple rescattering was formulated [497,148,267], especially for nucleon scattering on a nucleus. Thereby already interactions within a pair of nucleons were summed up to infinite order into a t-matrix, where however at intermediate states Hamiltonians of subclusters were carried along. The KMT formulation [267] of nucleon–nucleus scattering led recently to a successful application in working out optical potentials [87]. Interestingly enough one of the nontrivial ingredients in that approach is the three-body problem formed by the projectile, one active nucleon in the target and the remaining nucleons considered as a whole through a mean field. In the formal approaches of the fifties like the ones mentioned above, the 3N scattering problem in the form of multiple scattering was apparently not in the center of the interest. We are aware only of the work by Everett [126], who concentrated on the 3N system. He wrote down the multiple rescattering series for nucleon–deuteron scattering in terms of the two-nucleon off-shell t-matrices (including the kinetic energy of the third particle in the intermediate free propagator between two pair interactions), but he did not take the next step to split that infinite series into three parts, which would obey a set of three coupled integral equations. These would have been already the Faddeev equations. The work on general nucleon–nucleus scattering mentioned above did in fact that step with respect to the different nucleon target–nucleon interactions, however in the context of a many body system. It was Faddeev, who wrote down these coupled equations for three particles and for general interactions the first time [128]. Mitra [343], studying the bound state problem of three particles with separable pair forces, found, that the Schrödinger equation could be reduced exactly to an equation (or coupled equations) for amplitude(s) in one vector variable. They are known nowadays to be Faddeev equations specialized to those forces. Amado [23] found a linear equation for an off-shell nucleon–deuteron scattering amplitude, assuming the deuteron to be an elementary particle with a decay vertex into two nucleons. The resulting equation was a special case of the Faddeev equations based on separable forces but the general case as formulated by Faddeev was not obvious from that very first step.

The well-founded mathematical structure of the Faddeev equations was worked out by Faddeev himself [129]. Important for us here is, that the once iterated kernel of the Faddeev integral equations is connected and that for short range pair forces, typical for nuclear physics, it is compact, which guarantees the convergence of the numerically discretized form of it. Also the uniqueness of the solution of the Faddeev equations is of equal importance.

The actual application of the Faddeev equations posed severe problems at that time due to the very restricted computer facilities, and simplifications were eagerly searched for. The separable structure of the two-nucleon t-matrix in the spin-angular momentum state of the deuteron close to the deuteron pole invited to search for finite rank approximations for two-nucleon t-matrices. The virtual state in the NN state 1S_0 was also such a natural source of separability. This was pushed quite strongly and beautifully by Lovelace [318] and led to the Lovelace formulation of the Faddeev equations, a

coupled set of one-dimensional equations, which were then feasible for numerical treatments. This was generalized in [13] starting from suitable transition operators and separating the general two-nucleon t-matrices into a part of finite rank and a remainder. The resulting set of multi-channel two-particle Lippmann–Schwinger equations was then the starting point for numerous numerical studies using finite rank NN forces. This set runs under the name Alt–Grassberger–Sandhas (AGS)-equations. We cite from this work [13], that the direct solution of the Faddeev equations without using finite rank devices "reveals nearly unsurmountable calculational difficulties". It is exactly that what we are doing and what will be the technical message contained in this article. The physical aim will be the test of nuclear Hamiltonians.

One of the reasons Faddeev formulated his equations was that the Lippmann–Schwinger equations (LSE) [316] for three particles have serious drawbacks. Their kernel is not compact or connected even after any number of iterations and such a LSE does not have a unique solution. This was pointed out before in [138, 124, 161]. What was considered to be a drawback was turned into something useful [168] by demanding, that a specific 3N scattering state should not obey just one LSE equation but three at the same time. In this manner it could be shown that the solution is uniquely defined, in other words all the boundary conditions are fixed. Such a set of three LSE's equations is called nowadays the triad of LSE's [315]. They are well suited for formal manipulations. Thus the Faddeev equations or the AGS equations for the arrangement operators follow from that triad directly [172]. That triad can be generalized to four [479, 420, 489, 78, 172] and even to a general number N of particles, like the Faddeev equations, the generalization of which have been worked out by Yakubovsky [528] and carry his name. An equivalent coupling scheme was given in [198, 14]. One way to solve the triad directly has been already indicated in [168] and appeared later again as "Faddeev choice" [420].

For some time in the seventies interest turned into deriving connected kernel equations [447, 43, 212, 295, 399, 478, 420, 81, 299, 490], different from the Faddeev–Yakubovsky ones. Thereby often states with auxiliary indices, dummy indices, were introduced [420, 421], which obey a set of coupled equations and whose solutions are such that the states collapse just to one, the desired solution. Unfortunately nearly all of these formulations turned out to possess not only one solution, the physical one, but also on top spurious ones [131, 81, 299, 491, 5, 172].

The first numerical calculations [1, 2] using separable spin-dependent s-wave Yamaguchi forces gave qualitative agreement to the simple low energy data: angular distributions in elastic nd scattering, the total nd breakup cross section, the total cross section and some kinematically incomplete nd breakup cross sections. This was considered to be a success, since it showed, that the correct treatment of the quantum mechanics of three particles was an important key for understanding at least qualitatively the data, independent whether the forces are chosen to be fully realistic. Including a separable three-body force chosen ad hoc on top of separable Yamaguchi forces led to an even better agreement [373] with the same type of data. This very first period was followed by a rapidly increasing number of studies, where ad hoc chosen separable forces, also of second and higher ranks, including also p- and d-wave forces, more or less adjusted to NN phases known at that time, were applied. Representative work can be found in [72, 381, 3, 59, 113, 119, 382, 383, 114, 384, 69, 115, 278, 372, 439, 535, 211, 70, 205, 472, 207, 455, 116, 280, 456, 442, 426, 532, 223, 457, 533]. Certainly some qualitative insights could be achieved like sensitivities of certain 3N observables to the 1S_0 force, to the ${}^3S_1 - {}^3D_1$ tensor force, to 3P wave forces, etc., but conclusions drawn from a quantitative agreement or disagreement have to be considered with great caution. For instance the 3N analyzing power A_y turned out to be well

described in [207], while nowadays we know that modern NN forces adjusted to the most recent NN phase shift analysis (PSA) are not able to achieve it and a serious problem exists. Some pd breakup data [68] are well described by [119], while the same forces are not able to reproduce more modern data [397], which however are well described by modern NN interactions.

The beginning of investigations using realistic forces, which were well adjusted to NN data, like the Paris [310], Nijmegen [349], AV14 [505] and OBE-potentials [320], came with high rank approximations to those potentials (see Section 8.4). Thus the first time one saw the beautiful agreement of that Faddeev theory with the low energy data of the differential cross sections and the angular distribution of certain spin transfer coefficients in elastic nd scattering [282,386,283,284], but also the first time a clear statement was made that the 3N analyzing power A_y in elastic nd scattering shows a significant discrepancy [283]. In that work of the Graz–Osaka collaboration the breakup process was not dealt with, since their codes relying on contour deformation have some technical difficulty to evaluate the breakup amplitude.

The Utrecht group started already quite early [275,276] using nonseparable local forces, though still restricted to s-wave interactions, the so called Malfliet–Tjon (MT) potentials [324]. They lead to two-dimensional integral equations in contrast to the one-dimensional ones for finite rank forces. This was a decisive technical step forward. In that work the determination of the breakup cross section was now included and a very interesting study [275] covering the whole phase space was performed. Using different s-wave forces regions in phase space were identified which were very sensitive to the choice of the forces and others which were not. We shall repeat that study but based on the most modern forces and including all the relevant higher partial wave NN force components in Section 7.1.

This first pioneering study was later followed by more advanced work [463–465] using now the more realistic Reid potential [400]. However, tensor force couplings and higher NN force components were still treated only approximately, in a perturbative manner. As we know now [513] this was not justified and therefore those results do not represent the correct predictions of that force. Nevertheless it was a significant step forward and the rich variety of cross sections and spin observables in elastic neutron–deuteron (nd) scattering and the breakup process were investigated. Another remarkable step forward was done in [44], where the Faddeev equations in configuration space were solved for the local de Tourreil and Sprung NN interaction [488] including some higher partial wave NN force components exactly, some d-wave force components however still perturbatively. In view of very recent investigations [179,370] on the asymptotic behavior of Faddeev amplitudes in the breakup channel and the special care required for its correct treatment the accuracy of the results in [44] cannot be judged by us since not sufficient information in that respect was provided in that article. Altogether the situation remained open in an unfortunate sense, that the existing discrepancies to data could possibly be considered to be caused by the hopelessly complicated nature of the 3N potential energy and not by the simple fact that the reason might be that just the 3N Schrödinger equation with fully realistic NN forces was not solved sufficiently accurate enough. This only changed when it finally turned out to be possible [510,511] to solve the Faddeev equations exactly for any type of realistic NN force, for elastic scattering and the breakup process, and the true predictions of all the different NN forces could be gained and compared to data. (See also [475,64].) The outcome of that new development is the subject of this review.

In Section 2 the basic 3N equations are reviewed and briefly derived in a heuristic, physically transparent (Subsection 2.1) and a more formal algebraic approach (Subsection 2.2). The extension necessary to include 3N forces (3NF) are given in Subsection 2.3. We display in Subsection 2.4 the

expressions for the very many 3N scattering observables discussed in this review. The partial wave decomposition in momentum space including two representations of particle permutation operators, which are central to any three-body problem, and the complexity of the partial wave decomposition of a 3NF are presented in Section 3. The way we handle the singularities of the momentum space Faddeev kernel, the skew arguments introduced into the unknown amplitudes by the permutation operators and the big matrices are described in Section 4. The technical sections are finished by the description of accuracy tests and presentations of benchmark calculations in Section 5. The bulk part of the review lies in Sections 6 and 7, where theory is compared to experimental data. In Section 6 we cover very many of the measured cross sections and spin observables for elastic Nd scattering and the breakup process. First we use only NN forces (Subsection 6.1) and then we also show effects of the Tuscon–Melbourne 3NF [96] in a great variety of 3N scattering observables (Subsection 6.2). Section 7 is devoted to the following special topics: a survey of 3N breakup cross sections over all phase-space with the aim to separate it into domains which are very insensitive to the choice of NN forces and domains with the opposite property (Subsection 7.1); a presentation of the difficulties and the chances for extracting the nn scattering length from the 3N breakup process (Subsection 7.2); the discussion of the A_y puzzle in low energy elastic nucleon–deuteron scattering (Subsection 7.3); a display of the complex eigen phase shift and mixing parameters for elastic nd scattering above the breakup threshold (Subsection 7.4); simplifications for 3N scattering at high energies (Subsection 7.5); the formulation and the properties of the optical nucleon–deuteron potential (Subsection 7.6); the connection between the total nd and np and nn cross sections in the high energy limit (Subsection 7.7) and finally possible 3NF effects at higher energies between 100 and 150 MeV (Subsection 7.8).

Up to that point all the theoretical analysis of the data is based on the momentum space treatment of the Faddeev equations. In Section 8 we present then competing rigorous techniques carried through: in configuration space (Subsection 8.1), in form of the Sendai approach, which uses the method of continued fractions and works partially in configuration and partially in momentum space (Subsection 8.2), the pair correlated hyperspherical harmonic basis method (Subsection 8.3) and last not least the progress achieved using high-rank expansions of realistic NN forces (Subsection 8.4). The pending difficult pp Coulomb force problem in pd scattering is touched in Subsection 8.5 and the equally challenging question to incorporate relativity into 3N equations in Subsection 8.6.

Finally some selected applications of 3N scattering theory to cases, where one has to expect a strong final state interaction among three final nucleons are described briefly in Section 9. These are inclusive and exclusive electron scattering on ${}^3\text{He}$ (${}^3\text{H}$) (Subsection 9.1), photodisintegration and pd capture in the 3N system (Subsection 9.2), pion- and muon absorption on ${}^3\text{He}$ (${}^3\text{H}$) (Subsection 9.3) and the nonmesonic decay of the hypertriton (Subsection 9.4).

We finish with conclusions and an outlook in Section 10. Appendices contain additional and more detailed information. We also list the specialized workshops and conferences we are aware of and which are a very useful additional source of information on the subject of this article.

2. Theoretical formulation

2.1. Heuristic approach

Let us assume three particles, numbered 1, 2, and 3, where 2 and 3 are bound to each other and are hit by the free particle 1 in the initial state. Let the three particles interact by pairwise-forces. Then the amplitude for the breakup process, where in the final state all three particles are free, is described by the following obvious Born- or Neumann series:

$$\begin{aligned}
 & \text{Diagram 1: } 1 \text{ (projectile)} \rightarrow U_0^{(1)} \text{ (circle)} \text{ (target 2,3)} \\
 & = \text{Diagram 2: } 1 \text{ (projectile)} \rightarrow 2 \text{ (particle 2)} \rightarrow 3 \text{ (particle 3)} \\
 & + \text{Diagram 3: } 1 \text{ (projectile)} \rightarrow 2 \text{ (particle 2)} \rightarrow 3 \text{ (particle 3)} \\
 & + \dots
 \end{aligned}$$

$$\equiv V_3\phi_1 + V_2\phi_1 + V_1G_0V_3\phi_1 + V_3G_0V_3\phi_1 + V_3G_0V_2\phi_1 + \dots \quad (1)$$

We denoted the pair interactions like $V_{12} \equiv V_3$, etc., the initial state by ϕ_1 and the free three-particle propagator between consecutive pair interactions by G_0 . This is the whole physics, a sum over terms which are composed of interactions within all pairs and free propagations in between. The first interactions to the right have to be of course between the projectile numbered 1 and the constituents of the target, the particles numbered 2 and 3. The superscript 1 for the breakup operator $U_0^{(1)}$ stands for the projectile to be particle 1.

We would like to work with the Faddeev scheme. Then one splits that infinite sequence of processes into three parts, which will be shown to be coupled by three integral equations. The natural way to define the three parts is to combine all processes which end up with one specific pair interaction to the left. Thus

$$\begin{aligned}
 & 1 \text{ (projectile)} \rightarrow U_0^{(1)} \text{ (circle)} \text{ (target 2,3)} \\
 & =
 \end{aligned}$$

$$\begin{aligned}
 & \left\{ \begin{array}{c} \text{Diagram 1} \\ \text{Diagram 2} \\ \text{Diagram 3} \end{array} \right. + \left\{ \begin{array}{c} \text{Diagram 4} \\ \text{Diagram 5} \\ \text{Diagram 6} \end{array} \right. + \dots \\
 + & \left\{ \begin{array}{c} \text{Diagram 7} \\ \text{Diagram 8} \\ \text{Diagram 9} \end{array} \right. + \left\{ \begin{array}{c} \text{Diagram 10} \\ \text{Diagram 11} \\ \text{Diagram 12} \end{array} \right. + \dots \\
 + & \left\{ \begin{array}{c} \text{Diagram 13} \\ \text{Diagram 14} \\ \text{Diagram 15} \end{array} \right. + \left\{ \begin{array}{c} \text{Diagram 16} \\ \text{Diagram 17} \\ \text{Diagram 18} \end{array} \right. + \dots
 \end{aligned}$$

$$\equiv (U_0^{(1,3)} + U_0^{(1,2)} + U_0^{(1,1)}) \phi_1 \quad (2)$$

where the second superscript denotes the free particle to the left. A little inspection reveals that

$$\begin{aligned}
 U_0^{(1,3)} \phi_1 = & \left. \begin{array}{c} \text{Diagram 1} \\ \text{Diagram 2} \\ \text{Diagram 3} \end{array} \right. + \left. \begin{array}{c} \text{Diagram 4} \\ \text{Diagram 5} \\ \text{Diagram 6} \end{array} \right. \\
 & + \left. \begin{array}{c} \text{Diagram 7} \\ \text{Diagram 8} \\ \text{Diagram 9} \end{array} \right. + \left. \begin{array}{c} \text{Diagram 10} \\ \text{Diagram 11} \\ \text{Diagram 12} \end{array} \right. \\
 & + \left. \begin{array}{c} \text{Diagram 13} \\ \text{Diagram 14} \\ \text{Diagram 15} \end{array} \right. + \left. \begin{array}{c} \text{Diagram 16} \\ \text{Diagram 17} \\ \text{Diagram 18} \end{array} \right.
 \end{aligned}$$

$$\quad (3)$$

$$\begin{aligned}
 U_0^{(1,2)} \phi_1 &= \text{Diagram 1} + \text{Diagram 2} \\
 &+ \text{Diagram 3} + \text{Diagram 4} \quad (4) \\
 U_0^{(1,1)} \phi_1 &= \text{Diagram 5} \\
 &+ \text{Diagram 6} + \text{Diagram 7} \quad (5)
 \end{aligned}$$

The diagrams consist of two horizontal lines representing nucleons. A vertical dashed line connects them. A circle labeled $U_0^{(1,3)}$ is placed between the two lines. In diagram 1, the circle is at the top. In diagram 2, it is at the bottom. In diagram 3, it is on the left. In diagram 4, it is on the right. In diagram 5, it is at the top. In diagram 6, it is at the bottom. In diagram 7, it is on the right.

In other words, after the last pair interaction to the left and a free propagation one encounters again the infinite three subseries.

Now comes the decisive step to sum up the pair interaction within one and the same pair to infinite order. This is accomplished by putting the amplitude on the right hand side, which has the same second index as the amplitude on the left hand side, to the left and inverting the operator acting on it,

$$(1 - V_3 G_0) U_0^{(1,3)} \phi_1 = V_3 \phi_1 + V_3 G_0 (U_0^{(1,2)} + U_0^{(1,1)}) \phi_1 \quad (6)$$

$$U_0^{(1,3)} \phi_1 = t_3 \phi_1 + t_3 G_0 (U_0^{(1,2)} + U_0^{(1,1)}) \phi_1 \quad (7)$$

The quantity t_3 has been defined by

$$t_3 \equiv (1 - V_3 G_0)^{-1} V_3 \quad (8)$$

and is obviously the two-nucleon t -matrix for particles 1 and 2 living in the space of three nucleons. It obeys the LSE

$$t_3 = V_3 + V_3 G_0 t_3 \quad (9)$$

Similarly we get

$$U_0^{(1,2)} \phi_1 = t_2 \phi_1 + t_2 G_0 (U_0^{(1,3)} + U_0^{(1,1)}) \phi_1 \quad (10)$$

$$U_0^{(1,1)} \phi_1 = t_1 G_0 (U_0^{(1,3)} + U_0^{(1,2)}) \phi_1 \quad (11)$$

Eqs. (7), (10), and (11) form a set of three coupled Faddeev equations.

The last step is to antisymmetrize. It is sufficient to do that for the initial state. Thus we replace ϕ_1 by

$$\phi_a \equiv \phi_1 + \phi_2 + \phi_3 \quad (12)$$

In ϕ_i particle i is the free one and the remaining ones form the two-body bound state, which is assumed to be antisymmetric. This guarantees that the linear combination, Eq. (12), is antisymmetric in all three particles. Clearly one can repeat now the above steps for ϕ_2 and ϕ_3 separately. The properly antisymmetrized breakup amplitude is then

$$U_0 \phi_1 \equiv U_0^{(1)} \phi_1 + U_0^{(2)} \phi_2 + U_0^{(3)} \phi_3 = \sum_i \sum_k U_0^{(k,i)} \phi_k \equiv \sum_i U_{0,i} \phi_i \quad (13)$$

Adding the three sets for $U_0^{(k)}$ one easily derives

$$U_{0,1} \phi_1 = t_1(\phi_2 + \phi_3) + t_1 G_0(U_{0,2} + U_{0,3}) \phi_1 \quad (14)$$

$$U_{0,2} \phi_1 = t_2(\phi_3 + \phi_1) + t_2 G_0(U_{0,3} + U_{0,1}) \phi_1 \quad (15)$$

$$U_{0,3} \phi_1 = t_3(\phi_1 + \phi_2) + t_3 G_0(U_{0,1} + U_{0,2}) \phi_1 \quad (16)$$

The three equations (14)–(16) look remarkably similar and one expects that the second and third one are just a cyclic and an anticyclic permutation of the first one. Inspection of $U_{0,i}$ as defined in Eq. (13) reveals that indeed

$$U_{0,2} = P_{12} P_{23} U_{0,1} \quad (17)$$

$$U_{0,3} = P_{13} P_{23} U_{0,1} \quad (18)$$

Thus defining

$$P \equiv P_{12} P_{23} + P_{13} P_{23} \quad (19)$$

and

$$T \equiv U_{0,1} \quad (20)$$

we end up with

$$T\phi = tP\phi + tP G_0 T\phi \quad (21)$$

(we dropped the index 1 at t and ϕ). This is our basic Faddeev-like equation. Its iteration generates a multiple scattering series in two-nucleon t -matrices among all pairs. The full breakup operator is then given as

$$U_0 = (1 + P)T \quad (22)$$

Once T is known the operator for elastic scattering follows by quadrature. Again we would like to sketch that feature first heuristically, using the Neumann series, which nicely describes all of the ongoing physics. Let us start from the analog of Eq. (1), now for elastic scattering

(23)

Note all processes are initiated from the right by the projectile-target interactions except that to the very left a pair interaction between particles 2 and 3 forming the final bound state is not allowed to occur. Thus processes like

(24)

do not occur in the above infinite sum. Namely to the very left one encounters in the graph (24) the state $\langle \phi_1 | V_1 G_0$, which is just $\langle \phi_1 |$, due to the two-body Schrödinger equation and the on-the-energy-shell condition of the final free particle numbered 1. Thus all these processes (24) are already taken into account in the set (23).

Let us now antisymmetrize the initial state as above,

(25)

Inserting the corresponding sums it is very easy to recognize the relation

$$U\phi = PG_0^{-1}\phi + PT\phi \quad (26)$$

Thus the operator for elastic scattering follows from T . This ends the heuristic approach.

2.2. Algebraic approach

There are various ways to derive the Faddeev equations for scattering states or transition operators, as quoted in the introduction. Here we would like to start from the basic set of LSE's [168], often called "triad of Lippmann–Schwinger equations" [315]. A (stationary) scattering state initiated by an asymptotic arrangement of particles, described by a state ϕ (like ϕ_1 in Section 2.1) is given by

$$\Psi^{(+)} = \lim_{\epsilon \rightarrow 0} i\epsilon \frac{1}{E + i\epsilon - H} \phi \quad (27)$$

where H is the total Hamiltonian and E the energy connected to ϕ . In the three-body system the Hamiltonian can be decomposed as

$$H = H_0 + V_i + V^i \equiv H_i + V^i \quad (28)$$

where H_0 is the kinetic energy, H_i the so-called channel Hamiltonian with one pair interaction $V_i \equiv V_{jk}$ ($j \neq i, k \neq i$) and V^i the sum of the remaining two interactions with the particle i . (We shall use this convenient notation to denote a pair by the number of the third particle.) Obviously ϕ_i is an eigenstate of H_i to the energy E . Now using the resolvent identities

$$\frac{1}{E + i\epsilon - H} = \frac{1}{E + i\epsilon - H_i} + \frac{1}{E + i\epsilon - H_i} V^i \frac{1}{E + i\epsilon - H} \quad (29)$$

for $i = 1, 2, 3$ one is led to

$$\Psi^{(+)} = \lim_{\epsilon \rightarrow 0} \frac{i\epsilon}{E + i\epsilon - H_i} \phi + \lim_{\epsilon \rightarrow 0} \frac{1}{E + i\epsilon - H_i} V^i \frac{i\epsilon}{E + i\epsilon - H} \phi \quad (30)$$

As an example let us choose $\phi \equiv \phi_1$, then it is not difficult to show that

$$\lim_{\epsilon \rightarrow 0} \frac{i\epsilon}{E + i\epsilon - H_i} \phi_1 = \delta_{ii} \phi_1 \quad (31)$$

This is called the Lippmann identity [317,45]. Disregarding the subtleties connected with the limits in the second term and denoting the special scattering state initiated by ϕ_1 as $\Psi_1^{(+)}$ one gets ($G_i \equiv \lim_{\epsilon \rightarrow 0} (E + i\epsilon - H_i)^{-1}$)

$$\Psi_1^{(+)} = \delta_{ii} \phi_1 + G_i V^i \Psi_1^{(+)} \quad (32)$$

These are three equations which form the triad, one inhomogeneous and two homogeneous ones. It is shown in [168] that this set fixes all the boundary conditions and defines therefore $\Psi_1^{(+)}$ uniquely. The argument is very simple. The states $\Psi_2^{(+)}$ and $\Psi_3^{(+)}$ initiated by ϕ_2 and ϕ_3 , respectively, obey corresponding sets, where the driving terms occur for $i = 2$ and $i = 3$, respectively. Clearly requiring the three equations of the set (32) to be fulfilled simultaneously, rules out a possible admixture of

$\Psi_2^{(+)}$ and $\Psi_3^{(+)}$ in the general solution of the set (32). Furthermore it is also obvious that any solution of the set (32) has to be a solution of the Schrödinger equation at the energy E . The only other scattering states are the ones with three free particles in the initial state, described by three-particle plane wave states ϕ_0 . Now the application of $i\epsilon G_i$ onto ϕ_0 is not zero, but generates two-body scattering states in the subsystem $(jk) \neq i$. Therefore the specific driving terms (ϕ_1 or zero) in the set (32) rule out any admixture of that last group of scattering states and the set (32) generates $\Psi_1^{(+)}$ uniquely.

As a sideremark we mention that in the case of four particles one needs a set of seven homogeneous and inhomogeneous LSE's in order to fix all boundary conditions and to define a specific scattering state uniquely [420,78]. This has been generalized also to N particles [479,420,489].

In scattering processes one is usually interested in transition operators from a specific asymptotic configuration to the same or other ones. Regarding the asymptotic behavior of $G_i V^i \Psi_1^{(+)}$ in configuration space in the channel, where the pair jk , ($j \neq i \neq k$) is bound and particle i is free one reads off the amplitude accompanying the outgoing radial wave as

$$A_{i1} \equiv \langle \phi_i | V^i | \Psi_1^{(+)} \rangle \quad (33)$$

Clearly the transition operator connected to that amplitude is

$$U_{i1} |\phi_1\rangle \equiv V^i |\Psi_1^{(+)}\rangle \quad (34)$$

The set (32) provides now in a very natural manner three coupled equations for the three operators U_{i1} , $i = 1, 2, 3$. Namely regarding

$$U_{11} |\phi_1\rangle = (V_2 + V_3) |\Psi_1^{(+)}\rangle \quad (35)$$

we operate by V_2 and V_3 onto the equations with $i = 2$ and 3 , respectively, and correspondingly for U_{21} and U_{31} by V_1 on the equation with $i = 1$ and get

$$U_{11} \phi_1 = V_2 G_2 U_{21} \phi_1 + V_3 G_3 U_{31} \phi_1 \quad (36)$$

$$U_{21} \phi_1 = V_1 \phi_1 + V_1 G_1 U_{11} \phi_1 + V_3 G_3 U_{31} \phi_1 \quad (37)$$

$$U_{31} \phi_1 = V_1 \phi_1 + V_1 G_1 U_{11} \phi_1 + V_2 G_2 U_{21} \phi_1 \quad (38)$$

Since

$$V_1 \phi_1 = G_0^{-1} \phi_1 \quad (39)$$

and

$$V_i G_i \equiv t_i G_0 \quad (40)$$

the set (36)–(38) can be rewritten as ($\bar{\delta}_{i1} \equiv 1 - \delta_{i1}$)

$$U_{i1} \phi_1 = \bar{\delta}_{i1} G_0^{-1} \phi_1 + \sum_{j \neq i} t_j G_0 U_{j1} \phi_1 \quad (41)$$

which are the Alt–Grassberger–Sandhas (AGS) equations [13] for the arrangement amplitudes.

Let us now antisymmetrize. Again we assume that the channel state ϕ is already antisymmetrized in the two-body subsystem, which is in a bound state. Then

$$\Psi_a^{(+)} \equiv \lim_{\epsilon \rightarrow 0} i\epsilon \frac{1}{E + i\epsilon - H} (\phi_1 + \phi_2 + \phi_3) \equiv \Psi_1^{(+)} + \Psi_2^{(+)} + \Psi_3^{(+)} \quad (42)$$

is antisymmetric. Therefore the transition operator into the state ϕ_i resulting from a fully antisymmetrized scattering state is

$$U_i \phi_1 \equiv \sum_k U_{ik} \phi_k \quad (43)$$

From the three equations (41) follows again a set of three coupled equations

$$U_i \phi_1 = \sum_{k \neq i} G_0^{-1} \phi_k + \sum_{j \neq i} t_j G_0 U_j \phi_1 \quad (44)$$

Now we can see directly the relations between U_1 , U_2 and U_3 . According to Eqs. (43), (34) and (42) one has

$$U_1 \phi_1 = \sum_k U_{1k} \phi_k = \sum_k V^1 |\Psi_k^{(+)}\rangle = V^1 \Psi_a^{(+)} \quad (45)$$

$$U_2 \phi_1 = V^2 \Psi_a^{(+)} \quad (46)$$

$$U_3 \phi_1 = V^3 \Psi_a^{(+)} \quad (47)$$

Consequently

$$U_2 \phi_1 = P_{12} P_{23} U_1 \phi_1 \quad \text{and} \quad U_3 \phi_1 = P_{13} P_{23} U_1 \phi_1 \quad (48)$$

and as expected only one operator, say U_1 , is independent. Therefore we can choose one equation from the set (44) and get ($U \equiv U_1$)

$$U \phi = G_0^{-1} P \phi + P t G_0 U \phi \quad (49)$$

to generate the operator for elastic scattering. Again we dropped the indices on ϕ and t . Eq. (49), however, provides also information on the full breakup process. General scattering theory tells (it follows directly from the homogeneous LSE using the free resolvent operator G_0 instead of the G_i 's in Eq. (30)) that the transition amplitude into the state, where all particles are free, is given by

$$A_0 \equiv \langle \phi_0 | \sum_i V_i |\Psi_a^{(+)}\rangle \quad (50)$$

Therefore the transition operator is

$$U_0 \phi \equiv \sum_i V_i \sum_k \Psi_k^{(+)} \quad (51)$$

Let us now use again the basic set (32) for $k = 1$ and the corresponding sets for $k = 2$ and 3 , respectively. One easily reads off

$$U_0 \phi = \sum_i V_i \phi_i + \sum_l t_l G_0 U \phi \quad (52)$$

Since $V_i\phi_i = G_0^{-1}\phi_i$ the first terms in Eq. (52) will not contribute to the on-the-energy shell amplitude in Eq. (50) and we can make a choice for U_0 dropping them. Then

$$U_0\phi \equiv (1 + P)tG_0U\phi \quad (53)$$

This equation provides the breakup operator, once the operator for elastic scattering, U , is known. Getting U_0 is just a quadrature.

We shall show in Section 4 that this formulation has serious drawbacks [57] for general forces. However it is ideal and has been essentially always used in case of finite rank forces [318,13], [430,385]. Since we shall work with general forces throughout we now identically rewrite Eq. (49). Define

$$T \equiv tG_0U \quad (54)$$

Then it follows from (49)

$$T\phi = tP\phi + tG_0PT\phi \quad (55)$$

which is the equation found before in Section 2.1 for the breakup process. Again we see

$$U_0\phi = (1 + P)T\phi \quad (56)$$

and the connection to the operator for elastic scattering

$$U\phi = PG_0^{-1}\phi + PT\phi \quad (57)$$

The central equation for all our numerical performance is Eq. (55). This concludes the formal derivation of our basic equations (55)–(57) valid for arbitrary two-body forces.

2.3. Inclusion of three-nucleon forces

Quark physics, meson theory and relativistic extensions, all tell that 3NF's should be present. Their strength is still under debate, but they will be there. Therefore we would like to extend the formalism for the inclusion of 3NF's. We shall be more brief now and refer the reader to [297,298,172,173,175] and [236] where both algebraic and heuristic (in the sense of the Neumann series) approaches are displayed. We denote the 3NF by V_4 . Then the set (32) is just modified by the occurrence of the additional interaction V_4 in all three integral kernels. It appears natural to add a fourth equation

$$\Psi_1^{(+)} = G_4(V_1 + V_2 + V_3)\Psi_1^{(+)} \quad (58)$$

This directly results from Eq. (27) using the resolvent identity with the Green operator

$$G_4 \equiv \lim_{\epsilon \rightarrow 0} \frac{1}{E + i\epsilon - H_0 - V_4} \quad (59)$$

and

$$\lim_{\epsilon \rightarrow 0} i\epsilon G_4\phi_1 = 0 \quad (60)$$

Then we introduce an auxiliary transition operator

$$U_{41}\phi_1 \equiv (V_1 + V_2 + V_3)\Psi_1^{(+)} \quad (61)$$

and derive the slight generalization of Eq. (41)

$$U_{11}\phi_1 = \bar{\delta}_{11}G_0^{-1}\phi_1 + \sum_{j \neq i} t_j G_0 U_{j1}\phi_1 + V_4 G_4 U_{41}\phi_1 \quad (62)$$

$$U_{41}\phi_1 = G_0^{-1}\phi_1 + \sum_{j=1}^3 V_j G_j U_{j1}\phi_1 \quad (63)$$

which can be combined into the compact notation

$$U_{\alpha 1}\phi_1 = \bar{\delta}_{\alpha 1}G_0^{-1}\phi_1 + \sum_{\beta \neq \alpha} t_\beta G_0 U_{\beta 1}\phi_1 \quad (64)$$

with $\alpha, \beta = 1, \dots, 4$. We introduced the three-body t -matrix t_4 driven alone by V_4 :

$$t_4 = V_4 + V_4 G_0 t_4 \quad (65)$$

The antisymmetrization follows from the same steps as above and we end up with the generalization of Eq. (49)

$$U\phi = PG_0^{-1}\phi + PtG_0U\phi + t_4G_0U_4\phi \quad (66)$$

$$U_4\phi = (1 + P)G_0^{-1}\phi + (1 + P)tG_0U\phi \quad (67)$$

Here U is again the operator for elastic scattering and U_4 is defined by

$$U_4\phi = \sum_{k=1}^3 U_{4k}\phi_k \quad (68)$$

This set (66)–(67) is suitable for finite rank forces and has been used in [334]. For general forces we rewrite it by defining

$$T \equiv tG_0U \quad (69)$$

$$T_4 \equiv t_4G_0U \quad (70)$$

into

$$T\phi = tP\phi + tG_0T_4\phi + tPG_0T\phi \quad (71)$$

$$T_4\phi = (1 + P)t_4\phi + (1 + P)t_4G_0T\phi \quad (72)$$

(Note that the operator P commutes with t_4). From Eq. (66) we directly read off the operator for elastic scattering

$$U\phi = PG_0^{-1}\phi + PT\phi + T_4\phi \quad (73)$$

and the operator for the breakup process turns out to be a nearly obvious generalization of Eq. (56), namely

$$U_0\phi = (1 + P)T\phi + T_4\phi \quad (74)$$

It is the set (71)–(74), which we shall use later in the numerical applications, when 3NF's are present.

2.4. 3N scattering observables

The main dynamical ingredients for calculating observables are the transition amplitudes $\langle \phi' | U | \phi \rangle$ for elastic scattering and $\langle \phi_0 | U_0 | \phi \rangle$ for the breakup process. Now we have to be more specific and concentrate from now on on nucleon–deuteron scattering. The initial channel state $|\phi\rangle$ carries the information about the spin quantum numbers m_d and m_N of the incoming deuteron and nucleon, respectively, as well as the relative momentum \mathbf{q}_0 of the nucleon with respect to the deuteron. Also later on we shall add the charge states of the particles in an isospin formalism. Thus for now

$$|\phi\rangle = |\varphi_d m_d\rangle |\mathbf{q}_0 m_N\rangle \quad (75)$$

and $|\phi'\rangle$ carries corresponding primed quantum numbers. The free state ϕ_0 describes the relative motions of three free particles and their spin magnetic quantum numbers. Again later on one has to add for each particle the information, whether it is a proton or a neutron.

We describe the relative motions for three particles by standard Jacobi momenta

$$\mathbf{p}_i = \frac{1}{2}(\mathbf{k}_j - \mathbf{k}_k) \quad (76)$$

$$\mathbf{q}_i = \frac{2}{3}(\mathbf{k}_i - \frac{1}{2}(\mathbf{k}_j + \mathbf{k}_k)) \quad (77)$$

for $ijk = 123$ and cyclically, expressed in terms of the individual momenta \mathbf{k}_i of the three particles. The free motion can be described in terms of any of the three pairs of Jacobi momenta. For brevity we now just write

$$|\phi_0\rangle = |\mathbf{p} \mathbf{q} m_1 m_2 m_3\rangle \quad (78)$$

We normalize the momentum states as

$$\langle \mathbf{p} | \mathbf{p}' \rangle = \delta(\mathbf{p} - \mathbf{p}') \quad (79)$$

$$\langle \mathbf{q} | \mathbf{q}' \rangle = \delta(\mathbf{q} - \mathbf{q}') \quad (80)$$

2.4.1. Cross sections

One can derive the cross sections in two ways. Either one regards the asymptotically outgoing fluxes in the elastic and breakup channels as it follows from the LSE's for the fully antisymmetric scattering state $\Psi_a^{(+)}$ or one uses the standard time dependent scattering theory which leads to the transition rate in the distant future.

Let us begin with the first approach. The antisymmetrized scattering state $\Psi_a^{(+)}$ obeys three inhomogeneous LSE's [168]. Each one of them can be used to extract the asymptotic behavior in the elastic channel. Take for example

$$\Psi_a^{(+)} = \phi_1 + G_1 V^1 \Psi_a^{(+)} \quad (81)$$

Let us denote by

$$\mathbf{r} = \mathbf{x}_2 - \mathbf{x}_3 \quad (82)$$

$$\mathbf{R} = \mathbf{x}_1 - \frac{1}{2}(\mathbf{x}_2 + \mathbf{x}_3) \quad (83)$$

the standard Jacobi vectors conjugate to the Jacobi momenta \mathbf{p}_1 and \mathbf{q}_1 . Then the Green function G_1 in configuration space and restricted to the deuteron channel is

$$\begin{aligned} \langle \mathbf{r} \mathbf{R} | G_1 | \mathbf{r}' \mathbf{R}' \rangle |_d &= \varphi_d(\mathbf{r}) \int \frac{d\mathbf{q}}{(2\pi)^3} \frac{e^{i\mathbf{q} \cdot (\mathbf{R} - \mathbf{R}')}}{E + i\epsilon - \epsilon_d - (3/4m)q^2} \varphi_d(\mathbf{r}') \\ &= -\varphi_d(\mathbf{r}) \frac{2m}{3} \frac{1}{2\pi} \frac{e^{i\sqrt{(4m/3)(E-\epsilon_d)}|\mathbf{R}-\mathbf{R}'|}}{|\mathbf{R}-\mathbf{R}'|} \varphi_d(\mathbf{r}') \end{aligned} \quad (84)$$

The (negative) binding energy of the deuteron is denoted by ϵ_d and the nucleon mass by m . Thus the asymptotic behavior of $\Psi_a^{(+)}$ in the deuteron channel is

$$\begin{aligned} \Psi_a^{(+)}(\mathbf{r}, \mathbf{R}) |_d &\rightarrow \varphi_d(\mathbf{r}) \left\{ \frac{e^{i\mathbf{q} \cdot \mathbf{R}}}{(2\pi)^{3/2}} - \frac{2m}{3} \frac{1}{2\pi} \frac{e^{i\sqrt{(4m/3)(E-\epsilon_d)}R}}{R} \right. \\ &\quad \times \left. \int d\mathbf{r}' d\mathbf{R}' \varphi_d(\mathbf{r}') e^{-i\mathbf{q}' \cdot \mathbf{R}'} \langle \mathbf{r}' \mathbf{R}' | V^1 | \Psi_a^{(+)} \rangle \right\} \end{aligned} \quad (85)$$

where $\mathbf{q}' \equiv \sqrt{\frac{4}{3}m(E-\epsilon_d)}\hat{\mathbf{R}} \equiv q_0\hat{\mathbf{R}}$ points into the direction of observation $\hat{\mathbf{R}}$. It follows immediately that the differential cross section for elastic Nd scattering in the center of mass system is given by

$$\frac{d\sigma}{d\Omega} = |M_{m'_d m'_N m_d m_N}(\mathbf{q}', \mathbf{q}_0)|^2 \quad (86)$$

where

$$M_{m'_d m'_N m_d m_N}(\mathbf{q}', \mathbf{q}_0) \equiv -\frac{2}{3}m(2\pi)^2 \langle \phi' | U | \phi \rangle \quad (87)$$

is the elastic scattering amplitude expressed with the help of the operator U from Section 2.2. We added the more detailed information on magnetic spin quantum numbers present in the states ϕ' and ϕ on top of \mathbf{q}' and \mathbf{q}_0 .

In case of the breakup process it is most convenient to use a homogeneous LSE with the free Green operator G_0

$$\Psi_a^{(+)} = G_0 \Psi_a^{(+)} \quad (88)$$

(Note that V denotes here the full potential energy.) The configuration space representation of G_0 is known [410] and given as

$$\langle \mathbf{r} \mathbf{R} | G_0 | \mathbf{r}' \mathbf{R}' \rangle = \frac{i}{(4\pi)^2} \left(\frac{4}{3}\right)^{3/2} \frac{m^2 E}{X^2} H_2^{(1)}(X\sqrt{mE}) \quad (89)$$

with $X^2 \equiv (\mathbf{r} - \mathbf{r}')^2 + \frac{4}{3}(\mathbf{R} - \mathbf{R}')^2$.

Let us now regard the limit $|\mathbf{r}|$ and $|\mathbf{R}| \rightarrow \infty$ for fixed \mathbf{r}' and \mathbf{R}' :

$$X \rightarrow \rho - \hat{r}\mathbf{r}' \cos\xi + \sqrt{\frac{4}{3}}\hat{\mathbf{R}}\mathbf{R}' \sin\xi \quad (90)$$

where we introduced the polar coordinates ρ and ξ

$$r = \rho \cos \xi \quad (91)$$

$$R = \sqrt{\frac{3}{4}} \rho \sin \xi \quad (92)$$

Consequently using the asymptotic form of the Hankel function one has

$$\langle \mathbf{r} \mathbf{R} | G_0 | \mathbf{r}' \mathbf{R}' \rangle \rightarrow \frac{i}{(4\pi)^2} \left(\frac{4}{3}\right)^{3/2} \sqrt{\frac{2}{\pi}} \frac{m^2 E}{(mE)^{1/4}} e^{-i\frac{3}{4}\pi} \frac{e^{i\sqrt{mE}\rho}}{\rho^{5/2}} e^{-ipr'} e^{-iqR'} \quad (93)$$

with

$$\mathbf{p} \equiv \sqrt{mE} \hat{\mathbf{r}} \cos \xi \quad (94)$$

$$\mathbf{q} \equiv \sqrt{mE} \sqrt{\frac{4}{3}} \hat{\mathbf{R}} \sin \xi \quad (95)$$

Note that the way r and R tend towards infinity fixes the asymptotic relative momenta \mathbf{p} and \mathbf{q} . Then using Eq. (93) it follows immediately from Eq. (88)

$$\Psi_a^{(+)}(\mathbf{r}, \mathbf{R}) \rightarrow \frac{i}{(4\pi)^2} \left(\frac{4}{3}\right)^{3/2} \sqrt{\frac{2}{\pi}} \frac{m^2 E}{(mE)^{1/4}} e^{-i\frac{3}{4}\pi} \frac{e^{i\sqrt{mE}\rho}}{\rho^{5/2}} (2\pi)^3 \langle \mathbf{pq} | V | \Psi_a^{(+)} \rangle \quad (96)$$

One encounters an outgoing wave in the hyperradius ρ modulated by the breakup amplitude

$$\langle \phi_0 | U_0 | \phi \rangle \equiv \langle \mathbf{pq} | V | \Psi_a^{(+)} \rangle \quad (97)$$

which tells how the energy is distributed over the two relative motions and which depends on the directions of observations $\hat{\mathbf{r}}$ and $\hat{\mathbf{R}}$. Regarding the continuity equation it follows that the flux passing the surface element at asymptotically large ρ as fixed by $\hat{\mathbf{p}} \equiv \hat{\mathbf{r}}, \hat{\mathbf{q}} \equiv \hat{\mathbf{R}}$ is given by

$$\begin{aligned} dN &= \frac{1}{m} \left(\frac{3}{4}\right)^{3/2} d\hat{\mathbf{r}} d\hat{\mathbf{R}} \cos^2 \xi \sin^2 \xi d\xi 2 \left(\frac{(2\pi)^3}{(4\pi)^2} \left(\frac{4}{3}\right)^{3/2} \sqrt{\frac{2}{\pi}} \frac{m^2 E}{(mE)^{1/4}} \right)^2 \sqrt{mE} |\langle \phi_0 | U_0 | \phi \rangle|^2 \\ &= \pi m p q^2 d\hat{\mathbf{q}} d\hat{\mathbf{r}} d\hat{\mathbf{R}} |\langle \phi_0 | U_0 | \phi \rangle|^2 \end{aligned} \quad (98)$$

Therefore dividing by the incoming flux one is lead to the five-fold differential cross section in the center of mass system:

$$\frac{d^5 \sigma}{d\hat{\mathbf{p}} d\hat{\mathbf{q}} dq} = \frac{(2\pi)^4 m^2}{3 q_0} p q^2 |\langle \phi_0 | U_0 | \phi \rangle|^2 \quad (99)$$

The second more standard way to arrive at the breakup cross section is to use the result of time-dependent scattering theory [121, 254, 241]. We sketch the derivation in Appendix A. Thereby we follow very closely the steps used in potential scattering as outlined for instance in [172]. The results, Eqs. (A.17) and (A.24), agree with the expressions found in the time independent approach.

The transition rate, Eq. (A.23) from Appendix A, for the breakup process

$$dN = 2\pi |\langle \phi_0 | U_0 | \phi \rangle|^2 \int dp dq \delta \left(\frac{3q_0^2}{4m} + \epsilon_d - \frac{p^2}{m} - \frac{3q^2}{4m} \right) \quad (100)$$

can be rewritten as

$$dN = 2\pi |\langle \phi_0 | U_0 | \phi \rangle|^2 \int dk_1 dk_2 dk_3 \delta(\mathbf{k}_{\text{lab}} - \mathbf{k}_1 - \mathbf{k}_2 - \mathbf{k}_3) \delta \left(E_{\text{lab}} + \epsilon_d - \frac{\mathbf{k}_1^2}{2m} - \frac{\mathbf{k}_2^2}{2m} - \frac{\mathbf{k}_3^2}{2m} \right) \quad (101)$$

Thereby we introduced the projectile momentum in the laboratory system \mathbf{k}_{lab} , its energy $E_{\text{lab}} \equiv (1/6m)\mathbf{k}_{\text{lab}}^2 + (3/4m)\mathbf{q}_0^2$ and the final laboratory momenta \mathbf{k}_i of the three nucleons.

It is natural to define and separate the phase space factor. For certain directions $d\hat{k}_1$, $d\hat{k}_2$ and an energy interval dE_1 around $E_1 \equiv \mathbf{k}_1^2/2m$ the phase space factor k_E is

$$\begin{aligned} k_E d\hat{k}_1 d\hat{k}_2 dE_1 &\equiv \int dk_1 dk_2 dk_3 \delta(\mathbf{k}_{\text{lab}} - \mathbf{k}_1 - \mathbf{k}_2 - \mathbf{k}_3) \delta(E_{\text{lab}} + \epsilon_d - \sum \mathbf{k}_i^2/2m) \\ &= d\hat{k}_1 d\hat{k}_2 dE_1 \frac{m^2 \sqrt{2mE_1 k_2^2}}{|-(\mathbf{k}_{\text{lab}} - \mathbf{k}_1) \cdot \hat{\mathbf{k}}_2 + 2k_2|}. \end{aligned} \quad (102)$$

Here k_2 is given by the zero's of the argument of the energy conserving δ -function:

$$k_2^2 - \mathbf{k}_2 \cdot (\mathbf{k}_{\text{lab}} - \mathbf{k}_1) + \mathbf{k}_1^2 - \mathbf{k}_1 \cdot \mathbf{k}_{\text{lab}} - m\epsilon_d = 0 \quad (103)$$

This equation (103) apparently defines an ellipse in the k_1 - k_2 plane. The physically accessible k_1 , k_2 -values have to be nonnegative. Depending on the external parameter \mathbf{k}_{lab} , the momentum \mathbf{k}_1 and the directions $\hat{\mathbf{k}}_1$ and $\hat{\mathbf{k}}_2$, either the whole ellipse lies in the first quadrant, or only parts of it or there are no physical solutions at all. The points lying on that ellipse or on the corresponding curve in the E_1 - E_2 plane comprise the so-called kinematically allowed S-curve on which the physically accessible events have to lie. We provide an overview over all cases in Fig. 1. Let θ_1 and θ_2 be the angles between the beam axis and $\hat{\mathbf{k}}_1$ and $\hat{\mathbf{k}}_2$, respectively. Then, as shown in Appendix B, certain regions of θ_i -values are kinematically forbidden. These are the values $\theta^{(-)} \leq \theta_1$, $\theta_2 \leq \theta^{(+)}$, except for the triangular like area at $\theta_i \gtrsim \theta^{(-)}$. In the area surrounded by the circle like dashed curve in the center of Fig. 1 there are no real solutions to Eq. (103). All the curves shown in Fig. 1 are ellipses in the k_1 - k_2 plane. The dot defines our convention for the starting value of the arclength $S = 0$, which is measured counterclockwise.

The form of the phase space factor in Eq. (102) has the disadvantage that it diverges at the k_1 -values at which the ellipse has an infinite derivative. Therefore one replaces usually the E_1 -variable by an arclength S along that curve. It is a matter of convention to choose the location $S = 0$ on that curve and we use the one defined in Fig. 1. Now one has

$$dS = dE_1 \sqrt{1 + \left(\frac{dE_2}{dE_1} \right)^2} = dE_1 \sqrt{1 + \left(\frac{k_2}{k_1} \frac{2k_1 - \hat{\mathbf{k}}_1 \cdot (\mathbf{k}_{\text{lab}} - \mathbf{k}_2)}{2k_2 - \hat{\mathbf{k}}_2 \cdot (\mathbf{k}_{\text{lab}} - \mathbf{k}_1)} \right)^2} \quad (104)$$

Consequently

$$k_S \equiv k_E \frac{dE_1}{dS} = \frac{m^2 k_1^2 k_2^2}{\sqrt{k_1^2 (2k_2 - \hat{\mathbf{k}}_2 \cdot (\mathbf{k}_{\text{lab}} - \mathbf{k}_1))^2 + k_2^2 (2k_1 - \hat{\mathbf{k}}_1 \cdot (\mathbf{k}_{\text{lab}} - \mathbf{k}_2))^2}} \quad (105)$$

Finally dividing by the incoming flux in the lab. system the breakup cross section is

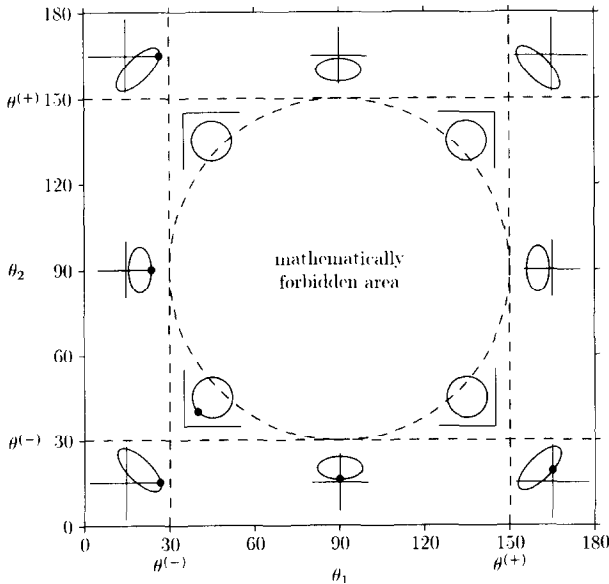


Fig. 1. The different types of kinematically allowed loci in the k_1 - k_2 plane as a function of θ_1 , θ_2 and $\phi_{12} = 90^\circ$. Only the positive k_1 and k_2 values are physically allowed. The border of the mathematically forbidden area is given by the dashed circle like curve. The dashed straight lines separate physically allowed from physically forbidden regions (see text). The definition of the arclength $S = 0$ is given by the thick dots and S is measured counterclockwise. For further explanation see text.

$$\begin{aligned} \frac{d^5\sigma}{d\hat{k}_1 d\hat{k}_2 dS} &= (2\pi)^4 |\langle \phi_0 | U_0 | \phi \rangle|^2 \frac{2m}{3q_0} k_S \\ &= \frac{(2\pi)^4 |\langle \phi_0 | U_0 | \phi \rangle|^2 m^2 k_1^2 k_2^2}{\sqrt{k_1^2 (2k_2 - \hat{k}_2 \cdot (\mathbf{k}_{lab} - \mathbf{k}_1))^2 + k_2^2 (2k_1 - \hat{k}_1 \cdot (\mathbf{k}_{lab} - \mathbf{k}_2))^2}} \frac{2m}{3q_0} \end{aligned} \quad (106)$$

All the cross section formulas presented up to now refer to specified magnetic quantum numbers of all particles in the initial and final states. Not observing polarizations one has to sum over the final magnetic quantum numbers and average over the initial ones.

The total cross section σ_{tot} for neutron-deuteron scattering is most easily determined via the optical theorem (see Appendix A and Section 5):

$$-\frac{1}{(2\pi)^3} \frac{3q_0}{4} \frac{1}{m} \sigma_{tot} = \text{Im} \langle \phi | U | \phi \rangle \quad (107)$$

Again strictly spoken this refers to definite spin magnetic quantum numbers.

2.4.2. Spin observables in elastic scattering

In 3N scattering there is a rich variety of spin-observables. Besides the vector polarizations of the nucleons there are also vector and tensor polarizations of the deuteron - and this for elastic scattering and the breakup process.

Let us first regard elastic scattering. A basis in spin space is

$$\{|\lambda_i\rangle\} \equiv \{|m_N\rangle|m_d\rangle\} \quad (108)$$

where m_N and m_d assume all allowed values. In terms of that basis one can express an arbitrary initial pure spin state as

$$|n\rangle = \sum_i a_i^{(n)} |\lambda_i\rangle \quad (109)$$

The density operator for a mixed state formed with probabilities p_n is then

$$\hat{\rho} = \sum_n |n\rangle p_n \langle n| = \sum_{ij} |\lambda_i\rangle \rho_{ij} \langle \lambda_j| \quad (110)$$

with

$$\rho_{ij} = \sum_n a_i^{(n)} p_n a_j^{(n)*} \quad (111)$$

This 6×6 matrix ρ can be expanded in the complete set of 6×6 matrices

$$\{S^\mu\} \equiv \{\sigma^{(i)} \otimes S^{(j)}\} \quad (112)$$

with the 2×2 matrices $\sigma^{(0)} = 1$, $\sigma^{(k)} = \sigma_k$, $k = 1, 2, 3$ (the usual Pauli matrices) and the 3×3 matrices $S^{(j)}$, $j = 0, \dots, 8$ for spin 1 [357]. The latter ones are constructed from the spin 1 angular momentum operators

$$S_x = \frac{1}{\sqrt{2}} \begin{pmatrix} 0 & 1 & 0 \\ 1 & 0 & 1 \\ 0 & 1 & 0 \end{pmatrix}, \quad S_y = \frac{1}{\sqrt{2}} \begin{pmatrix} 0 & -i & 0 \\ i & 0 & -i \\ 0 & i & 0 \end{pmatrix}, \quad S_z = \begin{pmatrix} 1 & 0 & 0 \\ 0 & 0 & 0 \\ 0 & 0 & -1 \end{pmatrix} \quad (113)$$

and the unit 3×3 matrix. A convenient set [357] is

$$\begin{aligned} S^{(0)} &= I, \quad S^{(1)} = \sqrt{\frac{3}{2}} \mathcal{P}_x = \sqrt{\frac{3}{2}} S_x, \quad S^{(2)} = \sqrt{\frac{3}{2}} \mathcal{P}_y = \sqrt{\frac{3}{2}} S_y, \quad S^{(3)} = \sqrt{\frac{3}{2}} \mathcal{P}_z = \sqrt{\frac{3}{2}} S_z, \\ S^{(4)} &= \sqrt{\frac{2}{3}} \mathcal{P}_{xy} = \sqrt{\frac{2}{3}} 3 S_x S_y, \quad S^{(5)} = \sqrt{\frac{2}{3}} \mathcal{P}_{yz} = \sqrt{\frac{2}{3}} 3 S_y S_z, \quad S^{(6)} = \sqrt{\frac{2}{3}} \mathcal{P}_{xz} = \sqrt{\frac{2}{3}} 3 S_x S_z \\ S^{(7)} &= \sqrt{\frac{1}{6}} (\mathcal{P}_{xx} - \mathcal{P}_{yy}) = \sqrt{\frac{1}{6}} (3 S_x S_x - 3 S_y S_y), \quad S^{(8)} = \sqrt{\frac{1}{2}} \mathcal{P}_{zz} = \sqrt{\frac{1}{2}} (3 S_z S_z - 2I) \end{aligned} \quad (114)$$

The set of 36 matrices S^μ is orthonormal with respect to the trace

$$\text{Tr}(S^\mu S^\nu) = (2 \cdot \frac{1}{2} + 1)(2 \cdot 1 + 1) \delta_{\mu\nu} = 6 \delta_{\mu\nu} \quad (115)$$

Now one can expand ρ and using Eq. (115) one gets

$$\rho = \frac{1}{6} \sum_\mu S^\mu \text{Tr}(\rho S^\mu) \quad (116)$$

For a given density matrix the expectation value of any operator \hat{O} is

$$\langle \hat{O} \rangle = \frac{\text{Tr}(\rho \hat{O})}{\text{Tr}(\rho)} \quad (117)$$

with

$$O_{ij} \equiv \langle \lambda_i | \hat{O} | \lambda_j \rangle \quad (118)$$

Thus we have

$$\rho_i = \frac{1}{6} \text{Tr} (\rho_i) \sum_{\mu} S^{\mu} \langle S^{\mu} \rangle_i \quad (119)$$

In Eq. (119) we added an index i in order to denote the case of the initial state density matrix ρ_i expressed in terms of the initial state expectation values $\langle S^{\mu} \rangle_i$.

What is the spin state in the final state of elastic scattering? Supplementing the notation in Eq. (85) for spin states (see [172] for instance), the state accompanying the outgoing wave is

$$|f^{(n)}\rangle \equiv \sum_i |\lambda_i\rangle \sum_j M_{ij} a_j^{(n)} \quad (120)$$

with

$$M_{ij} \equiv -\frac{2}{3}m(2\pi)^2 \langle \phi' | U | \phi \rangle = -\frac{2}{3}m(2\pi)^2 \langle \lambda_i | \langle q' | U | q \rangle | \lambda_j \rangle. \quad (121)$$

Eq. (120) defines the coefficients

$$(a_f)_i^{(n)} \equiv \sum_j M_{ij} a_j^{(n)} \quad (122)$$

for the superposition of spin states and thus the density matrix for the final state is

$$(\rho_f)_{ij} = \sum_n (a_f)_i^{(n)} p_n (a_f)_j^{(n)*} = \sum_{kl} M_{ik} (\rho_i)_{kl} M_{lj}^{\dagger} \quad (123)$$

Now one can calculate the expectation value of any quantity S^{μ} :

$$\langle S^{\mu} \rangle_f = \frac{\text{Tr} (\rho_f S^{\mu})}{\text{Tr} (\rho_f)} = \frac{1}{6} \text{Tr} (\rho_i) \frac{\sum_{\nu} \langle S^{\nu} \rangle_i \text{Tr} (MS^{\nu} M^{\dagger} S^{\mu})}{\text{Tr} (M \rho_i M^{\dagger})} \quad (124)$$

Defining

$$I = \frac{\text{Tr} (M \rho_i M^{\dagger})}{\text{Tr} (\rho_i)} \quad (125)$$

which is easily seen to be the elastic cross section of Eq. (86) summed over the spin orientations in the final state, one ends up with the most general expression for spin observables

$$\langle S^{\mu} \rangle_f I = \frac{1}{6} \sum_{\nu} \langle S^{\nu} \rangle_i \text{Tr} (MS^{\nu} M^{\dagger} S^{\mu}) \quad (126)$$

For later use we also need the unpolarized cross section. Assume the initial state to be unpolarized:

$$\langle S^{\mu} \rangle_i = 0 \text{ for all } S^{\mu} \text{ except for } S^0 \equiv 1_{2 \times 2} \otimes 1_{3 \times 3} \quad (127)$$

Then the initial density matrix is simply given by

$$\rho_i = \frac{1}{6} \text{Tr} (\rho_i) 1_{2 \times 2} \otimes 1_{3 \times 3} \quad (128)$$

and from Eq. (125) the resulting spin averaged (unpolarized) differential cross section I_0 is found to be

$$I_0 = \frac{1}{6} \text{Tr} (MM^\dagger) \quad (129)$$

Let us now regard the spin observables, in turn, which have been measured up to now.

The nucleon analyzing power A_y

Assume the nucleon spin to be polarized in the initial state described by the polarization vector

$$\mathbf{P} = \langle \boldsymbol{\sigma} \rangle_i \quad (130)$$

All other initial state expectation values are assumed to be zero (unpolarized deuteron), except for the one of the unit matrix, of course.

We regard now the cross section ($\mu = 0$) and get from Eq. (126)

$$I = I_0 \left(1 + \sum_k P_k \frac{\text{Tr} (M\sigma_k M^\dagger)}{\text{Tr} (MM^\dagger)} \right) \quad (131)$$

Because of the initial state polarization there is an additional contribution on top of I_0 , which defines the nucleon analyzing powers

$$A_k \equiv \frac{\text{Tr} (M\sigma_k M^\dagger)}{\text{Tr} (MM^\dagger)} \quad (132)$$

In all what follows we choose the scattering plane according to the Madison convention [39] to coincide with the x - z plane and the y axis to point into the direction $\mathbf{k}_{in} \times \mathbf{k}_{out}$, where \mathbf{k}_{in} and \mathbf{k}_{out} are the momenta of the incoming and outgoing particles, respectively. The parity conservation leads then to the statement [357] that $A_x = A_z = 0$.

The deuteron analyzing powers

As a spin 1 object the deuteron can be both vector and tensor polarized. The two cases are described by the polarization vector $P_i \equiv \langle \mathcal{P}_i \rangle$ and the polarization tensor $P_{jk} = \langle \mathcal{P}_{jk} \rangle$, respectively. Note that $P_{xx} + P_{yy} + P_{zz} = 0$ [357], thus only two of the three are independent.

For an unpolarized nucleon but vector and tensor polarized deuterons the cross section picks up again contributions on top of I_0 (see Eq. (126) for $\mu = 0$)

$$I = I_0 \left(1 + \frac{3}{2} \sum_i P_i A_i + \frac{1}{3} \sum_{jk} P_{jk} A_{jk} \right) \quad (133)$$

This defines the so-called vector and tensor analyzing powers of the deuteron, A_i and A_{jk} , respectively,

$$A_i = \frac{\text{Tr} (M\mathcal{P}_i M^\dagger)}{\text{Tr} (MM^\dagger)}, \quad A_{jk} = \frac{\text{Tr} (M\mathcal{P}_{jk} M^\dagger)}{\text{Tr} (MM^\dagger)} \quad (134)$$

Again [357] parity conservation puts A_x , A_z , A_{xy} and A_{yz} to zero. In spherical tensor notation the nonvanishing and independent analyzing powers are defined by

$$iT_{11} = \frac{\sqrt{3}}{2} A_y, \quad T_{20} = \frac{1}{\sqrt{2}} A_{zz}, \quad T_{21} = -\frac{1}{\sqrt{3}} A_{xz}, \quad T_{22} = \frac{1}{2\sqrt{3}} (A_{xx} - A_{yy}) \quad (135)$$

The spin transfer coefficients

In this case some of the spin directions are fixed in the initial state as well as in the final state. Assuming that only the incoming nucleon is polarized, the polarization of the outgoing nucleon in the final state (denoted with primes) can, according to Eq. (126), be written as

$$P'_l \cdot I \equiv \langle \sigma_l \rangle_f \cdot I = I_0 \left(P_l'^{(0)} + \sum_{k=1}^3 P_k K_k^{l'} \right) \quad (136)$$

Here P_k describes the polarization of the incoming nucleon beam and $P_l'^{(0)}$ is the polarization of the outgoing nucleon as generated by the unpolarized nucleon beam ($P_k = 0$)

$$P_l'^{(0)} = \frac{\text{Tr} (MM^\dagger \sigma_l)}{\text{Tr} (MM^\dagger)} \quad (137)$$

The polarization transfer coefficients $K_k^{l'}$ provide information about the transfer of the incoming polarization to the outgoing nucleon and are given by

$$K_k^{l'} \equiv \frac{\text{Tr} (M\sigma_k M^\dagger \sigma_l)}{\text{Tr} (MM^\dagger)} \quad (138)$$

The vector and tensor polarizations of the outgoing deuteron can be expressed in an analogous way

$$P'_l \cdot I = I_0 \left(P_l'^{(0)} + \sum_k P_k K_k^{l'} \right), \quad P'_{li} \cdot I = I_0 \left(P_{li}'^{(0)} + \sum_k P_k K_k^{li'} \right) \quad (139)$$

Here the vector and tensor polarizations of the outgoing deuteron created in unpolarized nucleon-deuteron scattering are

$$P_l'^{(0)} = \frac{\text{Tr} (MM^\dagger \mathcal{P}_l)}{\text{Tr} (MM^\dagger)}, \quad P_{li}'^{(0)} = \frac{\text{Tr} (MM^\dagger \mathcal{P}_{li})}{\text{Tr} (MM^\dagger)} \quad (140)$$

and the nucleon to deuteron polarization transfer coefficients are

$$K_k^{l'} = \frac{\text{Tr} (M\mathcal{P}_l M^\dagger \sigma_k)}{\text{Tr} (MM^\dagger)}, \quad K_k^{li'} = \frac{\text{Tr} (M\mathcal{P}_{li} M^\dagger \sigma_k)}{\text{Tr} (MM^\dagger)} \quad (141)$$

Again parity conservation allows only the following coefficients to be different from zero: $P_y'^{(0)}$, $K_x^{x'}, K_x^{z'}, K_y^{y'}, K_z^{x'},$ and $K_z^{z'}$ for nucleon to nucleon transfers, and $P_{y'}^{(0)}, P_{x'x'}^{(0)}, P_{x'z'}^{(0)}, P_{y'y'}^{(0)}, P_{z'z'}^{(0)}, K_x^{x'}, K_x^{z'}, K_y^{y'}, K_z^{z'}, K_x^{x'y'}, K_y^{y'z'}, K_y^{x'z'}, K_y^{y'z'}, K_z^{x'y'},$ and $K_z^{y'z'}$ for nucleon to deuteron polarization transfers.

The spin correlation coefficients

In the past even more complicated spin observables for elastic proton-deuteron scattering were measured with both protons and deuterons polarized in the initial state. In such a case on top of already known quantities new terms defining the spin correlation coefficients C_{ji} and $C_{jk,i}$ (see Eq. (126)) arise:

$$I = I_0 \left(1 + \sum_k P_k^N A_k^N + \frac{3}{2} \sum_k P_k^d A_k^d + \frac{1}{3} \sum_{jk} P_{jk}^d A_{jk} + \frac{1}{3} \sum_{kl} P_k^N P_l^d C_{k,l} + \frac{2}{3} \sum_{kli} P_k^N P_{li}^d C_{li,k} \right) \quad (142)$$

with indices N and d referring to nucleon and deuteron, respectively. The spin correlation coefficients are given by

$$C_{k,l} = \frac{\text{Tr} (M \sigma_k \mathcal{P}_l M^\dagger)}{\text{Tr} (MM^\dagger)}, \quad C_{li,k} = \frac{\text{Tr} (M \sigma_k \mathcal{P}_{li} M^\dagger)}{\text{Tr} (MM^\dagger)} \quad (143)$$

Again, parity conservation reduces significantly the number of nonzero coefficients to $C_{x,x}$, $C_{z,x}$, $C_{xy,x}$, $C_{yz,x}$, $C_{y,y}$, $C_{xz,y}$, $C_{xx,y}$, $C_{yy,y}$, $C_{zz,y}$, $C_{x,z}$, $C_{z,z}$, $C_{xy,z}$, and $C_{yz,z}$.

One also uses the notation, for instance $S \equiv -\frac{1}{2} C_{yy,y}$ and $T \equiv -\frac{1}{2} C_{xx,y} - C_{xy,x}$.

2.4.3. Spin observables in the breakup process

Let us now regard the breakup process. Here the spin state accompanying the outgoing wave in Eq. (96) is (up to a constant which drops out)

$$|g^{(n)}\rangle \equiv \sum_i |\Lambda_i\rangle \sum_j N_{ij} a_j^{(n)}, \quad (144)$$

where the spin basis for the three final nucleons is now

$$\{|\Lambda_i\rangle\} = \{|m_1\rangle|m_2\rangle|m_3\rangle\} \quad (145)$$

and where we introduced the notation

$$N_{ij} \equiv \langle \phi^0 | U_0 | \phi \rangle = \langle \Lambda_i | \langle \mathbf{p} \cdot \mathbf{q} | U_0 | q_0 \rangle | \lambda_j \rangle \quad (146)$$

for the breakup amplitude.

From Eq. (144) we read off the coefficients

$$(a_f)_i^{(n)} \equiv \sum_j N_{ij} a_j^{(n)} \quad (147)$$

which define the density matrix for the final state

$$(\rho_f)_{ij} = \sum_{kl} N_{ik} (\rho_i)_{kl} N_{lj}^\dagger \quad (148)$$

In comparison to Eq. (123) only the elastic amplitudes M_{ik} are replaced by the breakup amplitudes N_{ik} . Therefore all the expressions for the various spin observables given above remain formally the same for the breakup process. Up to now only some vector and tensor analyzing powers, as well as some spin transfer coefficients have been measured.

It should also be noted, that for the breakup process, in which two of the three final nucleons are detected, one can consider either coplanar (all momenta including the beam momentum lie in one plane) or non-coplanar configurations. In case of the coplanar geometries parity conservation causes the observables to vanish which correspond to the ones vanishing in elastic nucleon-deuteron scattering. However, for non-coplanar configurations parity conservation does not rule out any of the spin observables. For the discussion of this interesting aspect we refer to [357,359].

This concludes the description of the basic formalism.

3. Technical performance

We work in momentum space and in a partial wave representation. Partial wave projected states $|plm\rangle$ are defined in relation to the full momentum states of Eqs. (79)–(80) as

$$\langle p'|p\ lm\rangle \equiv \frac{\delta(p' - p)}{pp'} Y_{lm}(\hat{p}') \quad (149)$$

Then we can introduce states of total angular momentum in the two-nucleon subsystem as

$$|p\ (ls)jm\rangle \equiv \sum_{\mu} C(ls, \mu\ m - \mu) |p\ l\mu\rangle |s\ m - \mu\rangle \quad (150)$$

where $|s\ m_s\rangle$ are states of total two-nucleon spin $s = 0, 1$. The motion of the third nucleon in relation to that two-nucleon subsystem is described correspondingly by

$$|q\ (\lambda\frac{1}{2})Im_I\rangle \equiv \sum_{\mu} C(\lambda\frac{1}{2}I, \mu\ m_I - \mu) |q\ \lambda\mu\rangle |\frac{1}{2}\ m_I - \mu\rangle \quad (151)$$

States of total three-nucleon angular momentum are then given as

$$\begin{aligned} |pq\ \alpha\rangle &\equiv |pq\ (ls)j\ (\lambda\frac{1}{2})I\ (JI)JM\ (t\frac{1}{2})T\ M_T\rangle \\ &\equiv \sum_{\mu} C(jIJ, \mu\ M - \mu) |p\ (ls)j\mu\rangle |q\ (\lambda\frac{1}{2})I\ M - \mu\rangle \sum_{\nu} C(t\frac{1}{2}T, \nu\ M_T - \nu) |t\ \nu\rangle |\frac{1}{2}\ M_T - \nu\rangle \end{aligned} \quad (152)$$

We added the isospin state to total isospin T and magnetic quantum number M_T coupled out of two-nucleon isospin $t = 0, 1$ and the isospin $\frac{1}{2}$ of the third particle. Summing over all discrete quantum numbers and integrating over p and q one has a complete set of states in the three-nucleon space. Of course the states $|pq\ \alpha\rangle$ are orthonormalized:

$$\langle p'q'\ \alpha'|pq\ \alpha\rangle = \frac{\delta(q - q')}{qq'} \frac{\delta(p - p')}{pp'} \delta_{\alpha\alpha'} \quad (153)$$

The basic equation to be solved is (see Eq. (55))

$$T|\phi\rangle = tP|\phi\rangle + tPG_0T|\phi\rangle \quad (154)$$

The state $|\phi\rangle$ composed of a deuteron and a momentum state of the third particle is antisymmetric in the two-nucleon subsystem. Thus its representation in the basis $|pq\ \alpha\rangle$ requires not all states but only the antisymmetric ones in that subsystem. This is simply achieved by restricting the two-nucleon quantum numbers to

$$l + s + t = \text{odd} \quad (155)$$

Since the operator tP is symmetric under exchanges of the particles in that two-nucleon subsystem also the representation of $tP|\phi\rangle$ needs only that subset of basis states. From Eq. (154) it then follows trivially that this is true also for $T|\phi\rangle$. Thus $T|\phi\rangle$ is antisymmetric under exchange of the two nucleons in that subsystem. This is of course required to guarantee the overall antisymmetrization of the breakup amplitude in Eq. (56).

To be specific let us number the two nucleons in that subsystem by 2 and 3 in the following. Henceforth the decomposition of unity will always be

$$\sum_{\alpha} \int_0^{\infty} dp p^2 \int_0^{\infty} dq q^2 |pq\alpha\rangle \langle pq\alpha| = I \quad (156)$$

where the condition (155) applies.

Let us now embark into the representation of Eq. (154) in the basis of Eq. (152). One gets in a first step

$$\langle pq\alpha|T|\phi\rangle = \langle pq\alpha|tP|\phi\rangle + \sum' \sum'' \langle pq\alpha|t|p'q'\alpha'\rangle \langle p'q'\alpha'|P|p''q''\alpha''\rangle \langle p''q''\alpha''|G_0T|\phi\rangle \quad (157)$$

The t-matrix element is relatively simple. The quantum numbers of the third particle are not affected and the free propagator in the LSE for t picks up just the eigenvalue of the kinetic energy of the third particle. Thus

$$\begin{aligned} \langle pq\alpha|t(E)|p'q'\alpha'\rangle &= \frac{\delta(q - q')}{qq'} \delta_{\lambda\lambda'} \delta_{H''} \\ &\times \langle p (ls)j (t\frac{1}{2})T M_T | \tilde{t} \left(E - \frac{3}{4m}q^2 \right) | p' (l's')j' (t'\frac{1}{2})T' M'_T \rangle \end{aligned} \quad (158)$$

as follows from an easy algebra. The NN t-matrix \tilde{t} is to a very high degree of approximation diagonal in spin s and isospin t , but at least in the state 1S_0 (we use standard spectroscopic notation ${}^{2s+1}l_j$) it depends on the charge state of the two nucleons. Thus

$$\begin{aligned} \langle pq\alpha|t(E)|p'q'\alpha'\rangle &= \frac{\delta(q - q')}{qq'} \delta_{\lambda\lambda'} \delta_{H''} \delta_{ss'} \delta_{tt'} \delta_{jj'} \delta_{M_T M'_T} \sum_{\nu} C(t\frac{1}{2}T, \nu M_T - \nu) C(t'\frac{1}{2}T', \nu M_T - \nu) \\ &\times \langle p (ls)j t\nu | \tilde{t} \left(E - \frac{3}{4m}q^2 \right) | p' (l's')j t\nu \rangle \end{aligned} \quad (159)$$

Obviously $\nu = 1, 0, -1$ refer to the pp, np and nn systems, respectively. Since we neglect the Coulomb force throughout, there is no difference between pd and nd scattering and we can restrict ourselves to nd scattering for instance, which has $M_T = -\frac{1}{2}$. On the right hand side we encounter the two-nucleon t-matrix depending on the energy $E - \frac{3}{4m}q^2$, which is the total energy minus the relative energy of the third particle, on the relative momenta p and p' and the discrete quantum numbers l , l' , s , j and t . Clearly l can be different from l' due to the action of the tensor force.

Let us now just concentrate on the isospin features [516] and drop all other dependencies. Evaluating the Clebsch–Gordan coefficients one gets

$$\begin{aligned} \langle (0\frac{1}{2})\frac{1}{2} - \frac{1}{2}|t|(0\frac{1}{2})\frac{1}{2} - \frac{1}{2} \rangle &= \tilde{t}_{np}^{t=0} \\ \langle (1\frac{1}{2})\frac{1}{2} - \frac{1}{2}|t|(1\frac{1}{2})\frac{1}{2} - \frac{1}{2} \rangle &= \frac{2}{3}\tilde{t}_{nn}^{t=1} + \frac{1}{3}\tilde{t}_{np}^{t=1} \\ \langle (1\frac{1}{2})\frac{1}{2} - \frac{1}{2}|t|(1\frac{1}{2})\frac{3}{2} - \frac{1}{2} \rangle &= \langle (1\frac{1}{2})\frac{3}{2} - \frac{1}{2}|t|(1\frac{1}{2})\frac{1}{2} - \frac{1}{2} \rangle = \frac{1}{3}\sqrt{2} (\tilde{t}_{nn}^{t=1} - \tilde{t}_{np}^{t=1}) \\ \langle (1\frac{1}{2})\frac{3}{2} - \frac{1}{2}|t|(1\frac{1}{2})\frac{3}{2} - \frac{1}{2} \rangle &= \frac{1}{3}\tilde{t}_{nn}^{t=1} + \frac{2}{3}\tilde{t}_{np}^{t=1} \end{aligned} \quad (160)$$

We explicitly see the need of the $T = 3/2$ state in order to be able to distinguish between the $\tilde{t}_{np}^{l=1}$ and $\tilde{t}_{nn}^{l=1}$ interactions.

In reality only in the two-nucleon state 1S_0 charge independence breaking has been clearly established experimentally, that is $\tilde{t}_{nn}^{l=1} \neq \tilde{t}_{np}^{l=1}$. As seen from Eq. (160) this will couple $T = 3/2$ states to the initial $T = 1/2$ states. For certain observables the inclusion of $T = 3/2$ states is crucial, for others not. This will be discussed in Section 6. Even neglecting $T = 3/2$ admixtures, the linear combination $\frac{2}{3}\tilde{t}_{nn}^{l=1} + \frac{1}{3}\tilde{t}_{np}^{l=1}$ from Eq. (160) can easily be taken into account without enlarging the set of coupled equations. From now on we shall write Eq. (159) as

$$\langle pq\alpha | t(E) | p'q'\alpha' \rangle = \frac{\delta(q-q')}{qq'} \delta_{\lambda\lambda'} \delta_{ll'} \delta_{ss'} \delta_{tt'} \delta_{jj'} \tilde{t}_{\bar{\alpha}\bar{\alpha}'} \left(p, p', E - \frac{3}{4m}q^2 \right) \quad (161)$$

where $\bar{\alpha}$ includes the information $lsjtT$.

The matrix representation of the permutation operator requires more work. This is a purely geometrical problem, though, and its solution is presented in [172]. There are various ways to evaluate P , see for instance [237]. For Eq. (157) the most convenient form is

$$\langle p'q'\alpha' | P | pq\alpha \rangle = \int_{-1}^{+1} dx \frac{\delta(p' - \pi_1)}{p''^{l'+2}} \frac{\delta(p - \pi_2)}{p^{l+2}} G_{\alpha'\alpha}(q'qx) \quad (162)$$

with

$$\pi_1 = \sqrt{q^2 + \frac{1}{4}q'^2 + qq'x}, \quad \pi_2 = \sqrt{q'^2 + \frac{1}{4}q^2 + qq'x} \quad (163)$$

and

$$G_{\alpha'\alpha}(q'qx) = \sum_k P_k(x) \sum_{l'_1+l'_2=l'} \sum_{l_1+l_2=l} q'^{l'_2+l_2} q^{l'_1+l_1} g_{\alpha'\alpha}^{k l'_1 l'_2 l_1 l_2} \quad (164)$$

The purely geometrical quantity $g_{\alpha'\alpha}^{k l'_1 l'_2 l_1 l_2}$ is given in Appendix C.

Finally G_0 is of course diagonal with the eigenvalue $(E + i\epsilon - (1/m)p^2 - (3/4m)q^2)^{-1}$. Equipped with all that we arrive at the following set of coupled equations:

$$\begin{aligned} \langle pq\alpha | T | \phi \rangle &= \langle pq\alpha | tP | \phi \rangle + \sum_{\alpha'} \sum_{\alpha''} \int_0^\infty dq' q'^2 \int_{-1}^{+1} dx \frac{\tilde{t}_{\bar{\alpha}\bar{\alpha}'}(p, \pi_1, E - (3/4m)q^2)}{\pi_1''} \\ &\times G_{\alpha'\alpha''}(qq'x) \frac{1}{E + i\epsilon - q^2/m - q'^2/m - qq'x/m} \frac{\langle \pi_2 q'\alpha'' | T | \phi \rangle}{\pi_2''} \end{aligned} \quad (165)$$

It remains to display the driving term. We need ϕ in the basis of Eq. (152). It is an easy exercise to arrive at

$$\langle pq\alpha | tP | \phi \rangle = \sum_{\alpha'} \int_{-1}^{+1} dx \tilde{t}_{\bar{\alpha}\bar{\alpha}'}(p, \pi_1, E - \frac{3}{4m}q^2) \sum_{\alpha''} \delta_{\alpha''\alpha_d} G_{\alpha'\alpha''}(q, q_0, x) \frac{\varphi_{l''}(\pi_2)}{\pi_2''} C_{\alpha''}^{m_d m_N} \quad (166)$$

where

$$C_{\alpha}^{m_d m_N} = \sqrt{\frac{2\lambda+1}{4\pi}} C(\lambda \frac{1}{2} I, 0 m_N) C(1IJ, m_d m_N) \quad (167)$$

and α_d is the set of discrete quantum numbers which in the two-nucleon subsystem contains $l = 0, 2$, $s = 1, j = 1$, and $t = 0$, the deuteron quantum numbers. We assumed that the initial relative momentum q_0 points into the z -direction. Of course π_1 and π_2 are now defined through q and q_0 .

For each fixed total angular momentum J and parity Eq. (165) represents an infinite set of coupled integral equations in the two continuous variables p and q . There are three sorts of singularities in this set. The two-nucleon t-matrix $\tilde{t}(p, p', z)$ has a pole singularity for $z = \epsilon_d$, the deuteron binding energy, if the channel indices coincide with ${}^3S_1 - {}^3D_1$. Since the momentum q varies between 0 and ∞ one hits that pole for a specific q -value for E above the deuteron threshold, which lies at $E = \epsilon_d$. Clearly that singularity generates the elastic cut. Next there is the singularity of the free propagator. The x -integration generates logarithmic singularities in the variable q' whose positions move with q . Finally the t-matrix \tilde{t} generates a square root singularity in q at $q = \sqrt{(4m/3)E}$ in the amplitude $\langle pq\alpha | T | \phi \rangle$. All that will be displayed in some detail in Section 4.

Let us now regard the set (71), (72) which includes the 3NF.

For larger computers than available right now (at least to us) the three-body operator t_4 driven by the 3NF V_4 can be evaluated directly solving Eq. (65). This requires a tremendous amount of storage resources and computer time. Then the solution of the set (71), (72) could be obtained directly as for the simpler case without 3NF. Instead we have to use a perturbative expansion, where several orders, however, have to be taken into account. This reduces the amount of necessary computer resources substantially and then gets feasible. In zeroth order in V_4 the set (71), (72) is

$$T^{(0)} = tP + tPG_0T^{(0)}, \quad T_4^{(0)} = 0 \quad (168)$$

The contribution $T^{(1)}$ and $T_4^{(1)}$ of first order in V_4 is

$$T^{(1)} = tG_0T_4^{(1)} + tPG_0T^{(1)}, \quad T_4^{(1)} = V_4(1 + P) + V_4(1 + P)G_0T^{(0)} \quad (169)$$

The integral kernel in the first of the Eqs. (169) is the same as in Eq. (168), only the driving term has changed. This is very important from a numerical point of view.

Expanding t_4 of Eq. (65) in powers of V_4 one easily finds the contribution of n th order in V_4 to be ($n \geq 1$):

$$\begin{aligned} T^{(n)} &= tG_0T_4^{(n)} + tPG_0T^{(n)} \\ T_4^{(n)} &= V_4(G_0V_4)^{n-1}(1 + P) + \sum_{k=1}^n V_4(G_0V_4)^{k-1}G_0(1 + P)T^{(n-k)} \end{aligned} \quad (170)$$

This can be identically rewritten into a more convenient form, which requires only the amplitudes of one order below the actual one ($n \geq 2$):

$$T_4^{(n)} = V_4G_0(1 + P)T^{(n-1)} + V_4G_0T_4^{(n-1)} \quad (171)$$

Then the full amplitudes are

$$T = \sum_{i=0}^{\infty} T^{(i)}, \quad T_4 = \sum_{i=0}^{\infty} T_4^{(i)} \quad (172)$$

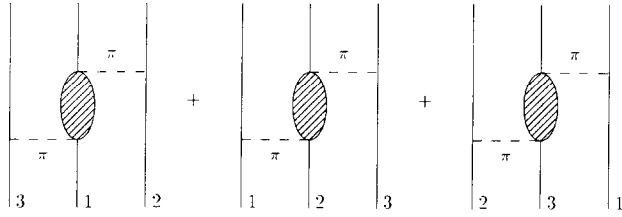


Fig. 2. The $\pi - \pi$ exchange three-nucleon force. The shaded areas do not include the forward propagating nucleon.

The 3NF's [97,406,100], based on the $\pi - \pi$, $\pi - \rho$ and $\rho - \rho$ exchanges split naturally into three parts according to the nucleon that undergoes (virtual) meson–nucleon scattering. Then V_4 has the structure

$$V_4(1 + P) = (1 + P)V_4^{(1)}(1 + P) \quad (173)$$

where $V_4^{(1)}$ is one of the three parts. Consequently we can write

$$T_4^{(1)} \equiv (1 + P)\hat{T}_4^{(1)}, \quad \hat{T}_4^{(1)} = V_4^{(1)}(1 + P)(1 + G_0 T^{(0)}) \quad (174)$$

and for $n \geq 2$

$$T_4^{(n)} \equiv (1 + P)\hat{T}_4^{(n)}, \quad \hat{T}_4^{(n)} = V_4^{(1)}(1 + P)G_0(T^{(n-1)} + \hat{T}_4^{(n-1)}) \quad (175)$$

The set of Eqs. (172)–(175) is the one we employ.

The partial wave representation is analogous to the one displayed above for the zeroth order (Eq. (168)) and we refer the reader to the detailed exposition in [235].

A new feature, however, is the partial wave representation of the 3NF itself, which requires some explanation. The $\pi - \pi$ exchange 3NF [97] is a prominent process and is depicted in Fig. 2. The shaded area represents the full πN off-the-mass-shell scattering amplitude except for the forward propagating nucleon, which generates just an iteration of the one-pion-exchange among the three nucleons and which is of course included in the NN force itself. The $\pi - \pi$ Tucson–Melbourne 3NF model [96,97] has the following form:

$$\begin{aligned} \langle \mathbf{k}'_1 \mathbf{k}'_2 \mathbf{k}'_3 | V_4^{(1)} | \mathbf{k}_1 \mathbf{k}_2 \mathbf{k}_3 \rangle &= \frac{1}{(2\pi)^6} \delta(\mathbf{k}_1 + \mathbf{k}_2 + \mathbf{k}_3 - \mathbf{k}'_1 - \mathbf{k}'_2 - \mathbf{k}'_3) \frac{g^2}{4m_N^2} \\ &\times \frac{H(Q^2)}{(Q^2 + \mu^2)} \frac{H(Q'^2)}{(Q'^2 + \mu^2)} \left\{ \boldsymbol{\tau}_2 \cdot \boldsymbol{\tau}_3 \boldsymbol{\sigma}_2 \cdot \mathbf{Q} \boldsymbol{\sigma}_3 \cdot \mathbf{Q}' \left[a + b \mathbf{Q} \cdot \mathbf{Q}' + c (Q^2 + Q'^2) \right] \right. \\ &\left. + d \boldsymbol{\tau}_3 \times \boldsymbol{\tau}_2 \boldsymbol{\sigma}_2 \cdot \mathbf{Q} \boldsymbol{\sigma}_3 \cdot \mathbf{Q}' \boldsymbol{\sigma}_1 \cdot (\mathbf{Q} \times \mathbf{Q}') \right\} \end{aligned} \quad (176)$$

where

$$H(Q^2) = \left(\frac{\Lambda^2 - \mu^2}{\Lambda^2 + Q^2} \right)^2 \quad (177)$$

stands for the strong form factors at both ends of the pion lines. Λ is a suitable cut-off parameter and a , b , c , and d are constants of the theory. The task is to present that form in the basis given in Eq. (152). This leads to quite formidable expressions, which are outlined in detail in [97] and

[460]. Here we would like to point out only the most elementary structure, which illustrates already the complexity [175].

Let us neglect spin- and isospin dependencies and keep only the meson-propagators

$$\langle \mathbf{p}'\mathbf{q}'|V_4^{(1)}|\mathbf{pq}\rangle = \frac{1}{Q^2 + \mu^2} \frac{1}{Q'^2 + \mu^2} \quad (178)$$

This corresponds in configuration space to a product of two (regularized) Yukawa potentials between particles 1 and 2 and 1 and 3, which obviously is a 3NF. Now the pion momenta expressed in term of the Jacobi variables are

$$Q = \mathbf{p} - \mathbf{p}' - \frac{1}{2}(\mathbf{q} - \mathbf{q}'), \quad Q' = \mathbf{p} - \mathbf{p}' + \frac{1}{2}(\mathbf{q} - \mathbf{q}') \quad (179)$$

and one can see that the individual angular dependencies with respect to \hat{p} , \hat{p}' , \hat{q} , and \hat{q}' are buried in the expression (178). Thus

$$\begin{aligned} \langle p'q'(l'\lambda')L'M'|V_4^{(1)}|pq(l\lambda)LM\rangle &= \int d\hat{p}' d\hat{q}' d\hat{p} d\hat{q} \mathcal{Y}_{l'\lambda'}^{L'M'*}(\hat{p}'\hat{q}') \\ &\times \frac{1}{(p - p' - \frac{1}{2}(\mathbf{q} - \mathbf{q}'))^2 + \mu^2} \times \frac{1}{(p - p' + \frac{1}{2}(\mathbf{q} - \mathbf{q}'))^2 + \mu^2} \mathcal{Y}_{l\lambda}^{LM}(\hat{p}\hat{q}) \\ &= \delta_{LL'}\delta_{MM'} \frac{(4\pi)^2}{8} (-)^{l+\lambda'+L} \sum_{l_1l_2l_3} \hat{l}_1\hat{l}_2\hat{l}_3 H_{l_1l_2l_3} \\ &\times \sum_{\lambda_1+\lambda_2=l_1} p^{\lambda_1} p'^{\lambda_2} \sqrt{\frac{(2l_1+1)!}{(2\lambda_1)!(2\lambda_2)!}} \sum_{\lambda_3+\lambda_4=l_2} q^{\lambda_3} q'^{\lambda_4} \sqrt{\frac{(2l_2+1)!}{(2\lambda_3)!(2\lambda_4)!}} \\ &\times C(\lambda_1l_2l, 00) C(\lambda_2l_2l', 00) C(\lambda_3l_3\lambda, 00) C(\lambda_4l_3\lambda', 00) \\ &\times \left\{ \begin{array}{ccc} \lambda_2 & \lambda_1 & l_1 \\ l & l' & l_2 \end{array} \right\} \left\{ \begin{array}{ccc} \lambda_4 & \lambda_3 & l_1 \\ \lambda & \lambda' & l_3 \end{array} \right\} \left\{ \begin{array}{ccc} l & l' & l_1 \\ \lambda' & \lambda & L \end{array} \right\} \end{aligned} \quad (180)$$

with

$$H_{l_1l_2l_3} = \int_{-1}^{+1} dx_1 \int_{-1}^{+1} dx_2 \int_{-1}^{+1} dx_3 P_{l_1}(x_1) P_{l_2}(x_2) P_{l_3}(x_3) \frac{1}{A_1^{l_2} A_2^{l_3} ((A_1^2 + \frac{1}{4}A_2^2 + \mu^2)^2 - A_1^2 A_2^2 x_1^2)} \quad (181)$$

and

$$A_1 = \sqrt{p^2 + p'^2 - 2pp'x_2}, \quad A_2 = \sqrt{q^2 + q'^2 - 2qq'x_3} \quad (182)$$

One encounters unavoidably a threefold x -integral. Including the spin dependencies the expressions get even more complicated and experienced programming is required in order to make the expressions tractable in a reasonable time. This has been achieved [235,460].

4. Numerical algorithms and techniques

Though the number of equations in the set (165) is infinite the short range nature of the NN force allows a very systematic truncation. For a given energy the two-nucleon t-matrix can be neglected

beyond a certain total two-body angular momentum j_{max} . Therefore under this assumption for a given total three-body angular momentum, the number of discrete sets of α 's, called channels in the following, is strictly finite. The concrete realization will be described in Section 6. As an example we display in Table 1 a small subset of discrete quantum numbers hidden in the index α . In praxis the number of coupled equations is of the order 60. This together with the two continuous variables p and q , which require typically 30 and 40 grid points, respectively, leads to a matrix representation of the integral kernel of a typical dimension 72000×72000 . A direct inversion appears right now not to be possible. Consequently we used an iterative procedure, which requires only matrix-multiplications and where the integral kernel is built up for each iteration from pieces, which are evaluated beforehand. See [511,103,236] for detailed information. Putting Eq. (165) into the form

$$T = T^{(0)} + KT \quad (183)$$

one gets the multiple scattering series by iteration

$$T = T^{(0)} + KT^{(0)} + K^2T^{(0)} + K^3T^{(0)} + \dots \quad (184)$$

Obviously the different terms are generated recursively as

$$T^{(n)} = KT^{(n-1)} \quad (n \geq 1) \quad (185)$$

The Born series

$$T = \sum_{n=0}^{\infty} T^{(n)} \quad (186)$$

diverges for the state of total angular momentum and parity $J^\pi = 1/2^+$, the quantum numbers of the 3N bound state. This is even true at ≈ 100 MeV and beyond. For all other J^π states the Born series converges but rather slowly for $J^\pi = 3/2^+$. Therefore it is mandatory to use an algorithm which makes sense out of that divergent series and which provides a fast result in case of convergence. The method of Padé approximants [33,493] turned out to be very convenient and very accurate. For 3N scattering it has been used the first time in [276]. As an example we display in Table 2 the individual terms of the Born series, the partial sums up to a certain n and the Padé approximants to that order. The example refers to $J^\pi = 1/2^+$, the first channel from Table 1 and to $p = 0.50 \text{ fm}^{-1}$ and $q = 0.43 \text{ fm}^{-1}$. Clearly the Born series is strongly diverging, whereas the series of Padé approximants is beautifully converging. The second example in Table 2 is for $J^\pi = 3/2^+$, where the Born series is slowly converging and the Padé approximants reach the final sum significantly faster. The examples in Table 2 are based on the realistic NN force AV18 [507] and incoming nucleon lab. energy $E = 22.7$ MeV.

Let us now regard the singularities in the set (165). The deuteron pole $1/(z - \epsilon_d)$ of $\tilde{T}(z)$ carries over to the amplitude T as is obvious from (165). Therefore it is advisable to define new quantities

$$\langle pq\alpha|T|\phi\rangle \equiv \begin{cases} \frac{\langle pq\alpha|\hat{T}|\phi\rangle}{E + i\epsilon - (3/4m)q^2 - \epsilon_d} & \text{for } \alpha = \alpha_d \\ T = \hat{T} & \text{for } \alpha \neq \alpha_d \end{cases} \quad (187)$$

and

Table I

A subset of discrete quantum numbers α defined in Eq. (152) corresponding to $J^{\Pi} = 1/2^+$.

No	l	s	j	λ	I	t	T	J
1	0	0	0	0	1/2	1	1/2	1/2
2	0	0	0	0	1/2	1	3/2	1/2
3	1	1	0	1	1/2	1	1/2	1/2
4	1	0	1	1	1/2	0	1/2	1/2
5	1	0	1	1	3/2	0	1/2	1/2
6	0	1	1	0	1/2	0	1/2	1/2
7	0	1	1	2	3/2	0	1/2	1/2
8	2	1	1	0	1/2	0	1/2	1/2
9	2	1	1	2	3/2	0	1/2	1/2
10	1	1	1	1	1/2	1	1/2	1/2
11	1	1	1	1	3/2	1	1/2	1/2

$$\tilde{t}_{\bar{\alpha}\bar{\alpha}'} \left(p, p', E - \frac{3}{4m} q^2 \right) \equiv \begin{cases} \frac{\hat{t}_{\bar{\alpha}\bar{\alpha}'}(p, p', E - (3/4m)q^2)}{E + i\epsilon - (3/4m)q^2 - \epsilon_d} & \text{for } \alpha = \alpha_d \\ \tilde{t} = \hat{t} & \text{for } \alpha \neq \alpha_d \end{cases} \quad (188)$$

It results

$$\begin{aligned} \langle pq\alpha|\hat{T}|\phi\rangle &= \langle pq\alpha|\hat{t}P|\phi\rangle + \sum_{\alpha'} \sum_{\alpha''} \int_0^\infty dq' q'^2 \int_{-1}^{+1} dx \frac{\hat{t}_{\bar{\alpha}\bar{\alpha}'}(p, \pi_1, E - (3/4m)q^2)}{\pi_1^{l'}} \\ &\times G_{\alpha'\alpha''}(qq'x) \frac{1}{E + i\epsilon - q^2/m - q'^2/m - qq'x/m} \\ &\times \left(\delta_{\alpha''\alpha_d} \frac{\langle \pi_2 q' \alpha'' | \hat{T} | \phi \rangle}{\pi_2^{l''}} \frac{1}{E + i\epsilon - (3/4m)q^2 - \epsilon_d} + \bar{\delta}_{\alpha''\alpha_d} \frac{\langle \pi_2 q' \alpha'' | \hat{T} | \phi \rangle}{\pi_2^{l''}} \right) \end{aligned} \quad (189)$$

The integral over q' can be discretized in the usual manner using Gaussian quadrature points for instance after an appropriate substitution. We cut off the integral at a value $q = \bar{q}$, which is sufficiently large to guarantee convergence and independence of that specific choice. The deuteron pole is then treated by a standard subtraction technique. Much more delicate is the free propagator singularity. One can rewrite the free propagator as

$$\frac{1}{E + i\epsilon - (1/m)(q^2 + q'^2 + qq'x)} = -\frac{m}{qq'} \frac{1}{x - x_0 - i\epsilon} \quad (190)$$

with

$$x_0 = \frac{mE - q^2 - q'^2}{qq'} \quad (191)$$

For suitable q and q' values $|x_0| \leq 1$ and we encounter a singularity in the x -integration. Collecting the x -dependence of the other terms into $f(x)$ one has the following structure treated again by subtraction:

Table 2

The Born terms of Eq. (186), its partial and Padé sums. An element $\langle pq\alpha|T|\phi\rangle$ for $\alpha = 1$, $p = 0.50 \text{ fm}^{-1}$, $q = 0.43 \text{ fm}^{-1}$ at $E = 22.7 \text{ MeV}$ has been chosen. The upper part refers to $J^{\Pi} = 1/2^+$, the lower part to $J^{\Pi} = 3/2^+$. The realistic NN force AV18 was used.

n	$T_{\alpha}^{(n)}(p, q)$	$\sum_{i=1}^n T_{\alpha}^{(n)}(p, q)$	$\sum_{i=1}^n T_{\alpha}^{(n)}(p, q)$ Padé
1	16.026 – 29.292 i	16.026 – 29.292 i	16.026 – 29.292 i
2	10.134 + 54.000 i	26.160 + 24.708 i	– 11.835 – 8.850 i
3	– 54.328 + 24.747 i	– 28.168 + 49.455 i	– 13.774 + 1.211 i
4	– 55.570 – 54.848 i	– 83.738 – 5.393 i	– 11.793 – 3.429 i
5	44.977 – 84.504 i	– 38.761 – 89.897 i	– 11.149 – 4.964 i
6	120.522 + 18.136 i	81.761 – 71.761 i	– 11.047 – 4.378 i
7	23.629 + 150.770 i	105.390 + 79.009 i	– 10.894 – 4.343 i
8	– 170.670 + 88.851 i	– 65.280 + 167.860 i	– 10.871 – 4.476 i
9	– 172.330 – 169.791 i	– 237.610 – 1.931 i	– 10.820 – 4.432 i
10	134.710 – 272.919 i	– 102.900 – 274.850 i	– 10.813 – 4.415 i
11	379.050 + 54.490 i	276.150 – 220.360 i	– 10.818 – 4.420 i
12	83.880 + 474.290 i	360.030 + 253.930 i	– 10.817 – 4.420 i
13	– 534.210 + 286.130 i	– 174.180 + 540.060 i	– 10.818 – 4.420 i
14	– 551.600 – 526.114 i	– 725.780 + 13.946 i	– 10.818 – 4.420 i
15	412.620 – 865.716 i	– 313.160 – 851.770 i	– 10.818 – 4.420 i
16	1196.580 + 153.550 i	883.420 – 698.220 i	– 10.818 – 4.420 i
17	285.780 + 1490.540 i	1169.200 + 792.320 i	– 10.818 – 4.420 i
18	– 1669.470 + 926.280 i	– 500.270 + 1718.600 i	– 10.818 – 4.420 i
19	– 1762.030 – 1632.221 i	– 2262.300 + 86.379 i	– 10.818 – 4.420 i
1	– 6.291 – 7.546 i	– 6.291 – 7.546 i	– 6.291 – 7.546 i
2	0.504 – 0.732 i	– 5.787 – 8.278 i	– 6.074 – 7.999 i
3	– 0.821 – 0.527 i	– 6.608 – 8.805 i	– 6.414 – 8.122 i
4	– 0.301 + 0.739 i	– 6.909 – 8.066 i	– 6.491 – 8.296 i
5	0.669 + 0.090 i	– 6.240 – 7.976 i	– 6.501 – 8.276 i
6	– 0.078 – 0.593 i	– 6.318 – 8.569 i	– 6.524 – 8.283 i
7	– 0.492 + 0.202 i	– 6.809 – 8.367 i	– 6.510 – 8.269 i
8	0.285 + 0.378 i	– 6.524 – 7.989 i	– 6.509 – 8.270 i
9	0.261 – 0.331 i	– 6.263 – 8.320 i	– 6.509 – 8.270 i
10	– 0.344 – 0.150 i	– 6.607 – 8.470 i	– 6.509 – 8.270 i
11	– 0.051 + 0.330 i	– 6.659 – 8.140 i	– 6.509 – 8.270 i
12	0.296 – 0.030 i	– 6.363 – 8.171 i	– 6.509 – 8.270 i

$$\int_{-1}^{+1} dx \frac{f(x)}{x - x_0 - i\epsilon} = f(x_0) \int_{-1}^{+1} dx \frac{1}{x - x_0 - i\epsilon} + \int_{-1}^{+1} dx \frac{f(x) - f(x_0)}{x - x_0 - i\epsilon} \quad (192)$$

The first integral in Eq. (192) dropping $f(x_0)$ leads to

$$\ln \left| \frac{1 - x_0}{1 + x_0} \right| + i\pi\Theta(1 - |x_0|) = \ln \left| \frac{qq' + q^2 + q'^2 - mE}{qq' - q^2 - q'^2 + mE} \right| + i\pi\Theta \left(1 - \left| \frac{mE - q^2 - q'^2}{qq'} \right| \right) \quad (193)$$

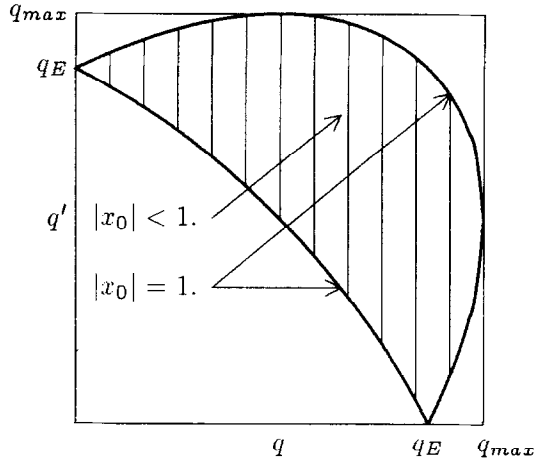


Fig. 3. The location of the logarithmic singularities in Eq. (193). Along the solid lines the logarithm is singular, in the shaded area the θ -function contributes.

and the second one, with the singularity removed, can be discretized conventionally. We always use Gaussian quadrature. The logarithm in Eq. (193) gets singular along two lines in the q - q' -plane, which form a moon shape region and which are displayed in Fig. 3. In the interior of that moon shape the imaginary part in Eq. (193) is present. Except for $q = 0$, $q_E = \sqrt{mE}$ and $q = \sqrt{\frac{4}{3}mE} \equiv q_{max}$ in the interval $q \leq q_{max}$ the integral in q' hits two logarithmic singularities. Their positions depend on q and are known as the notorious moving singularities in every three-body problem [430]. We treat them again by subtraction. One can also use special integration rules based on logarithmic weight functions [103]. This obviously requires quadrature points which change with q . It appears therefore unavoidable to interpolate the amplitude $\langle \pi_2 q' \alpha'' | \hat{T} | \phi \rangle$ in the variable q' . We use a Spline interpolation of the form

$$f(q') = \sum_{k=1}^n S_k(q') f(q_k) \quad (194)$$

which is based on cubic Splines and has been worked out in [171]. The detailed and rather lengthy layout of that whole subject of singularities can be found in [511,103,236].

The complicated x -dependence buried in π_1 and π_2 requires also an interpolation of the two-nucleon t-matrix and the amplitude \hat{T} . Again we use the same Spline method.

The integration for $q' \geq q_{max}$ does not require interpolation and is standard except for the deuteron pole subtraction mentioned before.

Finally we mention that $\langle pq\alpha | \hat{T} | \phi \rangle$ behaves as

$$\langle pq\alpha | \hat{T} | \phi \rangle = A + B\sqrt{q_{max}^2 - q^2} \quad (195)$$

for $q \rightarrow q_{max}$ from below. This follows trivially from the fact that the two-nucleon t-matrix has exactly that behavior as a function of the subsystem energy ($E - (3/4m)q^2$). In the interpolation in the variable q one has to take that into account by changing to the variable $\sqrt{q_{max}^2 - q^2}$ in a proper interval below q_{max} . For more details we refer the reader to [103,236].

If one would have worked with Eq. (49) for the operator U the deuteron pole would have been affected by the x -integration, too, which is introduced through the permutation operator P . Thus that simple pole would have also been "smeared out" into logarithmic singularities. This is the reason, why we work with the breakup operator T and its integral equation given in Eq. (55).

Since the moving logarithmic singularities are the main challenge to be overcome in solving the three-body equations above the breakup threshold, we would like to finally mention a recent investigation [237] which avoids that difficulty, but unfortunately aggravates the treatment of the virtual pole position of the NN t-matrix in the state 1S_0 . For other three-body systems, which do not have nearby t-matrix pole singularities, that new approach might be very profitable. Looking back to Eq. (154), inserting intermediate states and exhibiting the deuteron pole as in Eqs. (187), (188) one has

$$\begin{aligned} \langle pq\alpha|\hat{T}|\phi\rangle &= \langle pq\alpha|\hat{t}P|\phi\rangle \\ &+ \sum' \sum'' \langle pq\alpha|\hat{t}|p'q'\alpha'\rangle \langle p'q'\alpha'|P|p''q''\alpha''\rangle \frac{1}{E + i\epsilon - p''^2/m - (3/4m)q''^2} \\ &\times \left\{ \frac{\delta_{\alpha''\alpha_d}}{E + i\epsilon - (3/4m)q''^2 - \epsilon_d} \langle p''q''\alpha''|\hat{T}|\phi\rangle + \bar{\delta}_{\alpha''\alpha_d} \langle p''q''\alpha''|\hat{T}|\phi\rangle \right\} \end{aligned} \quad (196)$$

The second part of the kernel on the right hand side contains only one pole. Instead of using the form (162) of the permutation operator one can use another one. Altogether there are six different forms corresponding to different momenta as arguments in the δ -functions and their possible usage is discussed in [237]. Thus let us consider

$$\langle p'q'\alpha'|P|p''q''\alpha''\rangle = \int_{-1}^{+1} dx \frac{\delta(p'' - \tilde{\pi}_1)}{p''^{l''+2}} \frac{\delta(q'' - \tilde{\pi}_2)}{q''^{l''+2}} \tilde{G}_{\alpha'\alpha''}(p'q'x) \quad (197)$$

with

$$\begin{aligned} \tilde{\pi}_1 &= \sqrt{\frac{1}{4}p'^2 + \frac{9}{16}q'^2 + \frac{3}{4}p'q'x} \\ \tilde{\pi}_2 &= \sqrt{p'^2 + \frac{1}{4}q'^2 - p'q'x} \end{aligned} \quad (198)$$

and \tilde{G} given in Appendix C. Then the second part of the kernel will become

$$\sum' \sum'' \langle pq\alpha|\hat{t}|p'q'\alpha'\rangle \frac{1}{E + i\epsilon - p'^2/m - (3/4m)q'^2} \bar{\delta}_{\alpha''\alpha_d} \int_{-1}^{+1} dx \tilde{G}_{\alpha'\alpha''}(p'q'x) \frac{\langle \tilde{\pi}_1 \tilde{\pi}_2 \alpha''|\hat{T}|\phi\rangle}{\tilde{\pi}_1^{l''} \tilde{\pi}_2^{l''}} \quad (199)$$

Since the \hat{t} -matrix is diagonal in q the free propagator has just a simple pole in p' whose position is determined by q , which can simply be treated by subtraction like in a two-body LSE. However one faces a two-fold interpolation for \hat{T} .

Now the first part in Eq. (196) is the more interesting one. Using there also the same permutation operator would introduce into the deuteron pole a x -dependence and consequently logarithmic singularities. Therefore nothing would have been gained. The simple trick is now to write the product of two poles as a difference of two terms

$$\frac{1}{E + i\epsilon - p''^2/m - (3/4m)q''^2} \frac{1}{E + i\epsilon - (3/4m)q''^2 - \epsilon_d} \\ = \left\{ \frac{1}{E + i\epsilon - p''^2/m - (3/4m)q''^2} - \frac{1}{E + i\epsilon - (3/4m)q''^2 - \epsilon_d} \right\} \frac{1}{p''^2/m - \epsilon_d} \quad (200)$$

Since $\epsilon_d < 0$ the last factor is nonsingular and well behaved. The first part on the right hand side can be treated as above using Eq. (197), which just leads to a simple pole. In the second part one can use the first type of permutation operator given in Eq. (162), which does not affect q'' and again one just encounters a simple pole. This form has been applied in [237] to realistic calculations. Though the programming is much simpler the code is more time consuming because of the two-fold interpolation. However, the most serious drawback of that approach is the reliable control of the virtual state pole in the 1S_0 NN t-matrix. It lies on the second energy sheet and leads to a q -dependence

$$\langle pq\alpha|\hat{T}|\phi\rangle = \mathcal{O}\left(\frac{1}{\sqrt{E - (3/4m)q^2 + i\sqrt{|E_V|}}}\right) \quad (201)$$

where $E_V \approx -100$ keV is the location of the virtual state in the second sheet. In the approach described before, which we are actually using, that pole can be safely handled by cumulating a sufficient number of quadrature points near $q_{max} = \sqrt{\frac{4}{3}mE}$. In the approach avoiding logarithmic singularities one has to put much more effort in treating that pole safely. The difficulties are caused by the numerically small value of $|E_V|$. For more details we refer to [237].

5. Accuracy tests

Our internal tests lead us to the result that the observables, cross sections and spin observables in elastic Nd scattering and the breakup process, have at most numerical errors of 1–2%. More convincing for the readers, however, might be comparisons to the other work performed by other groups using independent and quite different algorithms. Before we come to that we would like to mention one simple test. A necessary requirement for having solved the 3N equations correctly is to fulfill unitarity. The Faddeev equations as an exact framework have unitarity built in. The unitarity relation for the elastic transition operator coupled to the breakup process can easily be derived from Eq. (49):

$$\langle\phi'|\mathbf{U}|\phi\rangle^* - \langle\phi|\mathbf{U}|\phi'\rangle = \int d\mathbf{q} \langle\phi_q|\mathbf{U}|\phi\rangle^* 2\pi i\delta\left(E - \frac{3}{4m}q^2 - \epsilon_d\right) \langle\phi_q|\mathbf{U}|\phi'\rangle \\ + \int dp d\mathbf{q} \langle\phi_0|\mathbf{U}_0|\phi\rangle^* 2\pi i\delta\left(E - \frac{p^2}{m} - \frac{3q^2}{4m}\right) \langle\phi_0|\mathbf{U}_0|\phi'\rangle \quad (202)$$

Choosing specifically $\phi' = \phi$ one gets the optical theorem (see also Appendix A)

$$-\text{Im} \langle\phi|\mathbf{U}|\phi\rangle = \pi^2 q_0 m \int d\hat{q} |\langle\phi_q|\mathbf{U}|\phi\rangle|^2 + \frac{1}{2}\pi m \int_0^{\sqrt{4mE/3}} d\hat{p} d\hat{q} q^2 pdq |\langle\phi_0|\mathbf{U}_0|\phi\rangle|^2$$

Table 3

Verification of the optical theorem (203). I_1 and I_2 denote the two integrals on the right hand side of Eq. (203), I_3 the left hand side.

E_{lab} [MeV]	I_1 [mbarn]	I_2 [mbarn]	$I_1 + I_2$ [mbarn]	I_3 [mbarn]
10.0	0.2629	0.0433	0.3052	0.3053
22.7	0.1608	0.0707	0.2315	0.2319
65.0	0.0519	0.0688	0.1210	0.1215
180.0	0.0148	0.0615	0.0763	0.0760

$$= \frac{3}{4m} q_0 \frac{1}{(2\pi)^3} \sigma_{tot} \quad (203)$$

We evaluated the forward scattering amplitude and the two integrals and verified Eq. (203) to be fulfilled within less than 0.5%. Examples are given in Table 3 for various energies and using the Bonn B NN force [321]. The numbers in Table 3 are fully converged with respect to the number of partial waves.

A more detailed and independent test was to compare individual observables evaluated also by other groups. In one study [102] we used approximations of finite rank to the Paris potential [310], including all relevant partial wave NN force components. In other words the NN forces in all its complexity has been involved (see Section 8.4). Since our algorithm is general we can use also these finite rank forces without making use of their special feature. On the other hand that feature allows to reduce the Faddeev equations to a coupled set of one-dimensional integral equations, which are easier to solve than the two-dimensional ones we are using. Moreover the complex structure of the moving logarithmic singularities can be avoided in these one-dimensional equations by rotating the contour of integration to complex momenta. In that special form the Faddeev equations look quite differently from ours and the comparison of 3N observables achieved by the two methods represents a highly nontrivial test. We compared in [102] observables for elastic nd scattering obtained by our method to the ones of the Graz–Osaka group using the one-dimensional equations. One example (the tensor analyzing power T_{21}) is shown in Fig. 4. The agreement is essentially perfect.

In a second study [238] we compared elastic Nd phase-shift and mixing parameters below the breakup threshold to results achieved in a totally different approach in configuration space. There wave function components are written as a product of a short range correlation function and a part which can be expanded in hyperspherical harmonics. That treatment is called the pair correlated hyperspherical harmonic basis method and will be described in Section 8.3.

The partial wave projected S-matrix for elastic Nd scattering is defined through the asymptotic behavior of the Faddeev component

$$\begin{aligned} \psi(\mathbf{r}, \mathbf{R}) &\rightarrow \sum_{l=0,2} \varphi_l(r) \sum_{\lambda' I'} \left\{ \{Y_l(\hat{r})\chi_1\}_{j=1} \left\{ Y_\lambda(\hat{R})\chi_{1/2}\right\}_I \right\}^{JM} \\ &\times \left(-\frac{1}{2iq_0 R} \right) [\delta_{\lambda\lambda'} \delta_{II'} e^{-i(q_0 R - \frac{1}{2}\lambda\pi)} - e^{i(q_0 R - \frac{1}{2}\lambda'\pi)} S_{\lambda' I', \lambda I}^J] \end{aligned} \quad (204)$$

As shown in [238] that S-matrix is connected to the U-matrix of Section 2.2 via

$$S_{\lambda' I', \lambda I}^J = \delta_{\lambda' \lambda} \delta_{II'} - \frac{4}{3} \pi i q_0 m i^{\lambda' - \lambda} U_{\lambda' I', \lambda I}^J \quad (205)$$

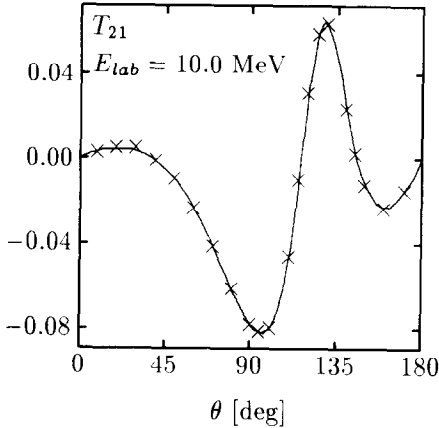


Fig. 4. A comparative study based on finite rank approximations of the Paris potential, see text. The solid line is our momentum space result at $E = 10$ MeV, the crosses are the Graz-Osaka results.

where

$$U_{\lambda' I', \lambda I}^J \equiv \sum_{l' l} \int dp' p'^2 \varphi_{l'}(p') \int dp p^2 \varphi_l(p) \langle p' q_0(l' 1) 1(\lambda' \frac{1}{2}) I' JM | U | p q_0(l 1) 1(\lambda \frac{1}{2}) IJM \rangle \quad (206)$$

In Eqs. (204) and (206) φ_l are the deuteron wave function components in configuration and momentum space, respectively. Following Seyler [438] we used the channel spin representation, which is based on the channel spin Σ

$$\Sigma \equiv j_d + s_N \quad (207)$$

and which requires the following recoupling:

$$U_{\lambda' \Sigma', \lambda \Sigma}^J = \sum_{l'} \sum_I \sqrt{\hat{I}' \hat{\Sigma}'} (-)^{J-I'} \begin{Bmatrix} \lambda' & \frac{1}{2} & I' \\ j_d & J & \Sigma' \end{Bmatrix} \sqrt{\hat{I} \hat{\Sigma}} (-)^{J-I} \begin{Bmatrix} \lambda & \frac{1}{2} & I \\ j_d & J & \Sigma \end{Bmatrix} U_{\lambda' I', \lambda I}^J \quad (208)$$

The S-matrix given in Eq. (205) in the λI - or in the above introduced channel spin representation is unitary below the breakup threshold. For the two parities $\pi = (-)^{J \pm \frac{1}{2}}$ it is, except for $J = \frac{1}{2}$, a 3×3 matrix describing the following couplings:

$$S = (S_{\lambda' \Sigma', \lambda \Sigma}^J) = \begin{pmatrix} S_{J \mp \frac{3}{2}, J \mp \frac{3}{2}}^J & S_{J \mp \frac{3}{2}, J \pm \frac{1}{2}}^J & S_{J \mp \frac{3}{2}, J \pm \frac{1}{2}}^J \\ S_{J \pm \frac{1}{2}, J \mp \frac{3}{2}}^J & S_{J \pm \frac{1}{2}, J \pm \frac{1}{2}}^J & S_{J \pm \frac{1}{2}, J \pm \frac{1}{2}}^J \\ S_{J \pm \frac{1}{2}, J \mp \frac{3}{2}}^J & S_{J \pm \frac{1}{2}, J \pm \frac{1}{2}}^J & S_{J \pm \frac{1}{2}, J \pm \frac{1}{2}}^J \end{pmatrix} \quad (209)$$

In case of $J = \frac{1}{2}$ it is only two-dimensional. The S-matrix can be diagonalized

$$S = U^T e^{2i\Delta} U \quad (210)$$

where Δ is the diagonal matrix of eigen phases $\delta_{\lambda \Sigma}^J$ and the unitary matrix U can be chosen as

$$U = v \ w \ x \quad (211)$$

with

$$v = \begin{pmatrix} 1 & 0 & 0 \\ 0 & \cos \epsilon & \sin \epsilon \\ 0 & -\sin \epsilon & \cos \epsilon \end{pmatrix} \quad (212)$$

$$w = \begin{pmatrix} \cos \xi & 0 & \sin \xi \\ 0 & 1 & 0 \\ -\sin \xi & 0 & \cos \xi \end{pmatrix} \quad (213)$$

$$x = \begin{pmatrix} \cos \eta & \sin \eta & 0 \\ -\sin \eta & \cos \eta & 0 \\ 0 & 0 & 1 \end{pmatrix} \quad (214)$$

It is important to use a convention to built up U out of the three eigenvectors of S . In that respect we refer to [238]. As examples we depict in Table 4 some eigen phases and mixing parameters obtained with the realistic AV14 NN potential [505]. The agreement between our results and the one achieved by the pair correlated hyperspherical harmonic basis method is essentially perfect. For the complete survey see [238].

At the energy of the Nd threshold (incoming nucleon lab. energy $E = 0$) only the s-wave scattering lengths survive, the doublet ($\Sigma = \frac{1}{2}$) and the quartet ($\Sigma = \frac{3}{2}$) ones. They are defined as the limits $q_0 \rightarrow 0$ of the corresponding eigen phases

$$\begin{aligned} \delta_{\frac{1}{2}0}^{\frac{1}{2}} &\rightarrow -^2 a \cdot q_0 \\ \delta_{\frac{3}{2}0}^{\frac{3}{2}} &\rightarrow -^4 a \cdot q_0 \end{aligned} \quad (215)$$

We show various results in Table 5. The agreement among different groups is very good. Due to the wrong 3H binding energy given by the potentials used in Table 5 the doublet scattering length, which is correlated to the 3H binding energy, deviates from the experimental value of 0.65 ± 0.04 fm [110]. We come back to that point in Section 6. The quartet case is less sensitive and theory agrees reasonably well with the experimental value of 6.53 ± 0.02 fm [110].

In case of the breakup process we had to be satisfied up to now with two somewhat restricted comparisons. One is within our momentum space approaches. In Section 4 we showed that logarithmic singularities can be totally avoided. This leads to a quite different kernel as defined in Eqs. (196)–(200) of the corresponding Faddeev equation in comparison to the one given in Eq. (189) we normally are using. Since that alternative method runs into difficulties in treating the 1S_0 virtual pole singularity we dropped that force component totally, but kept all others up to $j_{max} = 2$. Again the Bonn B NN force has been used. The agreement for elastic and breakup observables using both methods was very good. For breakup the nn QFS posed the most difficult task and the maximal difference there was up to 3%. That can be reduced if necessary by increasing the number of discretization points. We refer the reader to the detailed presentation in [237].

The other comparison [156] is for the breakup amplitude in a model calculation using the Malfliet–Tjon (MT) spin-dependent s-wave NN forces [324]. The comparative study was a configuration space solution of the Faddeev equations (see Section 8.1 for a brief description of that method). In configuration space the Faddeev component has the following asymptotic form

$$\psi(r, R) \sim \frac{\sin q_0 R}{R} \varphi_d(r) + A(\xi) \frac{e^{i\sqrt{mE}\rho}}{(\sqrt{mE}\rho)^{5/2}} + \dots \quad (216)$$

Table 4

Comparison of nd eigen phase shifts $\delta_{\lambda\Sigma}^J$ and mixing parameters (in degrees) determined in our momentum space Faddeev method (Bochum) and in the pair correlated hyperspherical harmonic basis method (Pisa).

J^{ll}	$\delta_{\Sigma\lambda}$	$E_{lab} = 1$ MeV		$E_{lab} = 2$ MeV		$E_{lab} = 3$ MeV	
		Bochum	Pisa	Bochum	Pisa	Bochum	Pisa
$1/2^+$	$\delta_{\frac{1}{2}2}$	-0.999	-1.00	-2.57	-2.58	-3.91	-3.91
	$\delta_{\frac{1}{2}0}$	-17.8	-17.7	-28.0	-27.9	-34.9	-34.9
	η	1.03	1.04	1.20	1.21	1.25	1.26
$1/2^-$	$\delta_{\frac{1}{2}1}$	-4.20	-4.20	-6.66	-6.67	-7.54	-7.54
	$\delta_{\frac{3}{2}1}$	12.4	12.4	20.5	20.5	25.0	25.0
	ϵ	3.73	3.73	5.37	5.38	7.23	7.24
$3/2^+$	$\delta_{\frac{3}{2}0}$	-47.2	-47.2	-61.3	-61.3	-70.5	-70.5
	$\delta_{\frac{1}{2}2}$	0.579	0.579	1.54	1.55	2.41	2.42
	$\delta_{\frac{3}{2}2}$	-1.07	-1.08	-2.77	-2.77	-4.22	-4.22
	ϵ	0.651	0.651	0.716	0.717	0.779	0.783
	ξ	0.544	0.546	1.01	1.01	1.43	1.44
	η	-0.113	-0.113	-0.246	-0.245	-0.386	-0.385
$3/2^-$	$\delta_{\frac{3}{2}3}$	0.124	0.125	0.502	0.501	0.942	0.943
	$\delta_{\frac{1}{2}1}$	-4.14	-4.15	-6.50	-6.52	-7.21	-7.25
	$\delta_{\frac{3}{2}1}$	14.3	14.3	22.7	22.7	26.3	26.3
	ϵ	-1.31	-1.29	-1.96	-1.94	-2.75	-2.72
	ξ	-0.186	-0.182	-0.273	-0.272	-0.265	-0.268
	η	-1.11	-1.10	-2.30	-2.30	-3.78	-3.77
$5/2^+$	$\delta_{\frac{3}{2}4}$	-0.0153	-0.0151	-0.0923	-0.0926	-0.211	-0.211
	$\delta_{\frac{1}{2}2}$	0.574	0.575	1.53	1.53	2.38	2.38
	$\delta_{\frac{3}{2}2}$	-1.14	-1.14	-2.98	-2.98	-4.57	-4.57
	ϵ	-0.286	-0.285	-0.306	-0.311	-0.323	-0.331
	ξ	-0.286	-0.287	-0.516	-0.520	-0.727	-0.733
	η	-0.873	-0.872	-1.58	-1.58	-2.17	-2.16
$5/2^-$	$\delta_{\frac{3}{2}1}$	13.4	13.3	22.0	21.9	26.3	26.2
	$\delta_{\frac{1}{2}3}$	-0.0644	-0.0645	-0.258	-0.258	-0.478	-0.477
	$\delta_{\frac{3}{2}3}$	0.130	0.131	0.523	0.523	0.969	0.969
	ϵ	0.470	0.467	0.493	0.491	0.518	0.513
	ξ	0.417	0.416	0.734	0.732	0.993	0.993
	η	-0.132	-0.132	-0.258	-0.257	-0.365	-0.364
$7/2^+$	$\delta_{\frac{3}{2}2}$	-1.06	-1.06	-2.73	-2.73	-4.14	-4.15
	$\delta_{\frac{1}{2}4}$	0.00792	0.00783	0.0480	0.0481	0.110	0.110
	$\delta_{\frac{3}{2}4}$	-0.0160	-0.0159	-0.0966	-0.0969	-0.220	-0.219
	ϵ	0.377	0.361	0.383	0.383	0.367	0.370
	ξ	0.452	0.453	0.838	0.846	1.21	1.21
	η	-0.152	-0.152	-0.317	-0.318	-0.484	-0.490

Table 5

nd doublet and quartet scattering lengths for NN forces only. (cd denotes charge dependence of the potential; in all these cases the NN forces were kept up to $j_{max} = 4$.)

Potential	2a [fm]			4a [fm]				
	Bochum	[86]	[270]	[271]	Bochum	[86]	[270]	[271]
MT I-III	0.70		0.70		6.45		6.44	
RSC		1.520				6.302		
AV14	1.19	1.20		1.196	6.39	6.372		6.380
AV18(cd)	1.27			1.27	6.33			6.33
Nijm93(cd)	1.20				6.35			
NijmI(cd)	1.15				6.32			
NijmII(cd)	1.24				6.35			
Reid93(cd)	1.22				6.34			
CD-Bonn(cd)	0.924				6.35			

Table 6

Doublet breakup amplitudes $A(\theta)$ of Eq. (217) for nd scattering in units of $fm^{-5/2}$. The format is $x.xx[n] \hat{x}.xx 10^n$.

θ	Re $A(\theta)$ (1S_0)		Im $A(\theta)$ (1S_0)		Re $A(\theta)$ (3S_1)		Im $A(\theta)$ (3S_1)	
	Bochum	LA/Iowa	Bochum	LA/Iowa	Bochum	LA/Iowa	Bochum	LA/Iowa
0°	4.99[-1]	5.01[-1]	5.56[-1]	5.56[-1]	-1.17[-2]	-1.30[-2]	2.64[-1]	2.63[-1]
10°	4.92[-1]	4.94[-1]	5.91[-1]	5.91[-1]	1.48[-2]	1.33[-2]	2.66[-1]	2.66[-1]
20°	4.58[-1]	4.59[-1]	6.70[-1]	6.70[-1]	1.00[-1]	1.00[-1]	2.85[-1]	2.85[-1]
30°	3.63[-1]	3.62[-1]	6.67[-1]	6.66[-1]	2.37[-1]	2.42[-1]	3.67[-1]	3.70[-1]
40°	2.18[-1]	2.19[-1]	4.63[-1]	4.63[-1]	3.85[-1]	3.85[-1]	5.39[-1]	5.39[-1]
50°	8.73[-2]	8.78[-2]	2.09[-1]	2.09[-1]	5.06[-1]	5.07[-1]	7.23[-1]	7.23[-1]
60°	-3.50[-2]	-3.50[-2]	-2.53[-2]	-2.57[-2]	6.19[-1]	6.20[-1]	9.33[-1]	9.34[-1]
70°	-2.10[-1]	-2.10[-1]	-2.98[-1]	-2.99[-1]	7.00[-1]	7.00[-1]	1.25[0]	1.25[0]
80°	-7.05[-1]	-7.05[-1]	-8.14[-1]	-8.14[-1]	5.67[-1]	5.69[-1]	1.70[0]	1.70[0]
90°	-4.45[0]	-4.46[0]	1.63[0]	1.63[0]	-8.54[-2]	-8.52[-2]	1.83[0]	1.83[0]

where the scattered elastic waves have been ignored. The hyperspherical (polar) coordinates ρ and ξ are defined as in Section 2.4. The breakup amplitude $A(\xi)$ is connected to the (on-shell) breakup amplitude T introduced in Section 2 and Eq. (165):

$$A(\xi) = \left(\frac{4\pi}{3} \right)^{3/2} (mE)^2 e^{i\pi/4} q_0 \langle pq | T | \phi \rangle \quad (217)$$

where $(1/m)p^2 + (3/4m)q^2 = \epsilon_d + (3/4m)q_0^2 = E$

As an example we display in Table 6 the two doublet amplitudes of the Los Alamos–Iowa group in comparison to ours for $E_{lab} = 42.0$ MeV. The agreement is essentially perfect. For more results see [156] where also various breakup cross sections have been displayed, which perfectly overlap.

Our results for phase shifts in nd scattering above the breakup threshold could be compared up to now only for the MT model potential. The perfect agreement between our and the Los Alamos–Iowa results is demonstrated in Table 7. See also [155] for comparison with other methods.

This concludes the comparison of our results to the ones of other groups and techniques.

Table 7
nd elastic scattering phase shifts and inelasticities based on the MT potentials.

14.1 MeV doublet	Bochum	LA/Iowa
$Re(\delta)$	105.50°	105.48°
η	0.4649	0.4648
14.1 MeV quartet		
$Re(\delta)$	68.96°	68.95°
η	0.9782	0.9782
42.0 MeV doublet	Bochum	LA/Iowa
$Re(\delta)$	41.37°	41.34°
η	0.5022	0.5024
42.0 MeV quartet		
$Re(\delta)$	37.71°	37.71°
η	0.9033	0.9035

6. Comparison of theory and experiment

In the first attempt we choose a 3N Hamiltonian with only two-body forces. The two-body forces are taken to be the unmodified NN interactions acting between two isolated nucleons. There are several so-called realistic NN forces in the literature, purely phenomenological ones and forces which are linked to meson theory. Up to very recently the most prominent representatives were the Paris [310], the Nijmegen [349], the AV14 [505] and the Bonn B [320,321] potentials. The Bonn B and the Nijmegen interactions are of the OBE type, the Paris interaction has a background in dispersion relations and the AV14 potential is essentially phenomenological with a one pion exchange tail. These potentials give a fairly good description of the NN data, but in detail one finds that their NN phase-shift parameters differ quite a bit. We shall be more quantitative later and show that these on-shell differences show up clearly in some of the 3N observables. This blurs the aim of the whole study, since ideally one would like to answer the question, whether one can see clearly defects in that most simple choice of the Hamiltonian, choosing just unperturbed NN forces. Therefore on-shell deficiencies should be absent. An important step forward in that respect occurred very recently and was connected to the most recent phase-shift analysis (PSA) of the Nijmegen group [466] performed between 0 and 350 MeV for the pp and np systems. In [277] a PSA based on np data alone using information from energies up to 500 MeV was announced. They claim that the available 2N data constrain the NN phases in a multi energy PSA very well leading to very small error bars (less than 1%) for the "experimental" phases. Adjusted to those phases and to the 2N data appeared now some new potentials: the AV18 [507], Nijmegen93 and three new phenomenological potentials Nijmegen I, II and Reid93 [467]. They all are charge dependent and have a χ^2 per degree of freedom very close to 1 (with the exception of Nijmegen93, which is less perfect), in contrast to the older NN potentials mentioned before with a χ^2 of $\approx 2\text{--}4$. Also Bonn B has been updated to CD Bonn and achieved

$\chi^2 \approx 1$ [322]. Thus five new NN potentials are now available with a perfect χ^2 and predictions from the corresponding 3N Hamiltonians will be now more conclusive than before. Possible deviations to experimental 3N data can no longer be attributed to defects in the description of the NN data. If they will occur they have to be either caused by wrong off-shell behavior or 3NF effects, which includes changes of NN forces due to the presence of the third nucleon. We display in Table 8 examples of NN phase shifts for the various potentials and compare them to the values of the Nijmegen PSA and the Arndt PSA [26–28,417]. Unfortunately the two PSA's do not agree sufficiently well. The necessary theoretical assumptions entering into the multi-energy PSA's differ in the two approaches. In the Nijmegen approach the NN force is parametrized for each partial wave between $0 \leq r \leq 1.4$ fm by energy dependent constants and for $r \geq 1.4$ fm a potential is chosen consisting of an electromagnetic part and a nuclear part. The electromagnetic part comprises the Coulomb potential, the magnetic moment interaction and the vacuum polarization potential in case of pp and for np it is the magnetic moment interaction only. The nuclear part has the OPE tail, allowing for different pion masses, and the intermediate range force given by heavy boson exchanges in form of the Nijmegen 78 potential [349]. Moreover the latter one is modified by an overall multiplication factor in order to allow for a more perfect fit to the NN data. One can say a NN force model is fitted to the data and interrelates the information from all energies. In the Virginia Polytechnic Institute and State University (VPI-SU) approach by Arndt and coworkers [26–28] the NN phase shifts are parametrized in terms of an energy dependent K -matrix, which consists of an OPE part and a sum over contributions resulting from Yukawa forces of different ranges with free adjustable strength constants. The discrete ranges are replaced by continuous mass distributions in the more recent analysis.

In both analysis the high partial wave phase shifts are taken from the OPE; the Nijmegen analysis introduces in addition an intermediate range of j -values, where the phases are not freely adjusted but taken from the Nijmegen NN potential prediction.

The amount of 2N data and their precision is not good enough to unambiguously carry through a single energy PSA. Thus there appears to be still room for some doubts, whether the present day "experimental" NN phase shifts are the final and true ones, since they necessarily depend on the choice of the parametrization of the energy dependence in the multi-energy analysis. We come back to that point later.

Looking again into Table 8 we see that the phases of the Arndt group deviate from the ones of the Nijmegen group rather strongly, for instance in 1P_1 and ϵ_1 up to nearly 30%, in 3P states up to 6% and in 1D_2 up to 10%. Since the newest potentials addressed in Table 8 are also fits to the NN data directly, they can be considered as other PSA's and they can equally well be claimed to be the "true" phases of the NN systems. Thus there are still ambiguities in modern PSA's. The table reveals that there are very significant deviations among these phases and in relation to the Nijmegen and Virginia PSA's. For ϵ_1 , 1P_1 , 3D_1 , 3P_0 , 3P_2 and 1D_2 these deviations are often 3–8% and sometimes even higher. This does not include the energy ranges, where phases cross zero, of course, and where the deviations can be much larger; also around 200 MeV and higher the deviations are quite large. All that tells that the very basic requirement for nuclear physics, the "true" NN phases and correspondingly adjusted NN potentials, leaves still room for improvements. Nevertheless the optimal χ^2 value very close to 1 for the newest five potentials is a significant improvement over the previous situation.

In solving the Faddeev equations the action of the NN force has still to be truncated to the dominant lower partial waves, up to a certain total two-nucleon angular momentum j_{max} . By increasing j_{max} we checked that the changes in observables caused by that truncation stay well below the experimental

Table 8

Selected NN phases for various NN forces in comparison to the results of the Nijmegen and Virginia phase-shift analysis.

E_{lab} [MeV]	Nijm PSA	Arndt PSA	Nijm 93	Nijm I	Nijm II	Reid93	AV18	CD-Bonn
1S_0 np								
1	62.069	62.156	62.065	62.113	62.087	61.892	62.015	62.078
2	64.465	64.573	64.460	64.533	64.491	64.202	64.388	64.478
3	64.656	64.762	64.650	64.740	64.686	64.334	64.560	64.671
5	63.627	63.708	63.619	63.735	63.663	63.884	63.503	63.645
10	59.96	60.00	59.94	60.10	59.99	59.46	59.78	59.97
20	53.57	53.77	53.54	53.72	53.58	53.05	53.31	53.56
30	48.49	49.00	48.42	48.61	48.44	48.02	48.16	48.43
50	40.54	41.66	40.38	40.56	40.35	40.18	40.09	40.37
100	26.78	27.86	26.17	26.44	26.18	26.32	26.02	26.26
200	8.94	7.86	7.07	8.27	7.92	7.83	8.00	8.14
300	-4.46	-5.55	-7.18	-4.43	-4.84	-5.17	-4.54	-4.45
1S_0 pp								
1	32.684	32.591	32.817	32.798	32.804	32.795	32.682	32.788
2	45.637	45.466	45.836	45.769	45.782	45.754	45.605	45.712
3	51.003	50.730	51.252	51.147	51.164	51.124	50.948	51.055
5	54.832	54.366	55.154	54.989	55.012	54.957	54.744	54.857
10	55.22	54.42	55.67	55.39	55.42	55.36	55.09	55.22
20	50.94	50.02	51.58	51.11	51.15	51.12	50.78	50.93
30	46.51	45.87	47.29	46.67	46.71	46.72	46.34	46.48
50	38.93	38.98	39.76	38.88	38.90	39.00	38.78	38.90
100	24.99	25.67	26.15	24.93	24.89	25.07	25.01	24.96
200	6.55	6.44	7.45	6.64	6.55	6.60	6.99	6.67
300	-6.15	-6.40	-6.62	-6.20	-6.13	-6.11	-5.64	-6.15
3P_0 np								
1	.180	.190	.182	.178	.177	.177	.180	.177
2	.480	.506	.488	.476	.473	.474	.483	.474
3	.836	.876	.851	.831	.824	.826	.843	.826
5	1.626	1.690	1.660	1.617	1.604	1.611	1.643	1.608
10	3.65	3.74	3.75	3.64	3.61	3.64	3.71	3.62
20	6.95	7.06	7.14	6.96	6.90	7.00	7.10	6.92
30	9.04	9.23	9.27	9.09	9.02	9.21	9.26	9.04
50	10.70	11.16	10.81	10.81	10.76	11.13	10.99	10.79
100	8.46	9.42	7.87	8.57	8.65	9.22	8.69	8.70
200	-1.44	-1.39	-3.21	-1.60	-1.42	-.74	-1.43	-1.31
300	-11.47	-12.62	-13.38	-11.46	-11.43	-10.57	-11.06	-11.23

Table 8 — continued

E_{lab} [MeV]	Nijm PSA	Arndt PSA	Nijm 93	Nijm I	Nijm II	Reid93	AV18	CD-Bonn
3P_0 pp								
1	.134	.140	.137	.134	.133	.133	.136	.134
2	.416	.431	.425	.415	.412	.412	.421	.415
3	.769	.792	.787	.768	.763	.763	.780	.768
5	1.582	1.612	1.621	1.580	1.568	1.570	1.607	1.580
10	3.73	3.73	3.83	3.73	3.70	3.71	3.80	3.73
20	7.28	7.21	7.50	7.29	7.23	7.28	7.45	7.29
30	9.58	9.52	9.83	9.61	9.53	9.64	9.81	9.60
50	11.48	11.67	11.62	11.55	11.48	11.67	11.75	11.56
100	9.45	10.35	8.88	9.50	9.55	9.79	9.61	9.63
200	−.37	.14	−2.14	−.63	−.47	−.32	−.50	−.38
300	−10.39	−10.78	−12.30	−10.49	−10.49	−10.29	−10.17	−10.33
1P_1 np								
1	−.187	−.175	−.186	−.189	−.190	−.187	−.190	−.189
2	−.482	−.449	−.477	−.486	−.490	−.480	−.489	−.487
3	−.810	−.753	−.802	−.818	−.824	−.808	−.823	−.818
5	−1.487	−1.375	−1.471	−1.502	−1.515	−1.484	−1.514	−1.503
10	−3.04	−3.77	−3.00	−3.08	−3.11	−3.04	−3.11	−3.08
20	−5.40	−4.78	−5.31	−5.48	−5.55	−5.43	−5.54	−5.47
30	−7.11	−6.24	−6.97	−7.23	−7.34	−7.20	−7.31	−7.19
50	−9.67	−8.60	−9.42	−9.80	−9.96	−9.89	−9.85	−9.69
100	−14.52	−13.74	−13.96	−14.42	−14.59	−14.91	−14.20	−14.15
200	−22.18	−21.94	−20.77	−21.51	−21.52	−22.15	−20.79	−21.34
300	−27.58	−27.28	−24.87	−26.52	−26.43	−26.69	−26.28	−27.52
3S_1 np								
1	147.747	147.781	147.768	147.757	147.747	147.731	147.749	147.748
2	136.463	136.488	136.495	136.476	136.461	136.442	136.465	136.463
3	128.784	128.788	128.826	128.798	128.780	128.760	128.786	128.783
5	118.178	118.129	118.240	118.193	118.171	118.152	118.182	118.175
10	102.61	102.41	102.72	102.62	102.59	102.59	102.62	102.60
20	86.12	85.67	86.35	86.11	86.08	86.12	86.16	86.09
30	76.06	75.46	76.40	76.00	75.98	76.06	76.12	75.99
50	62.77	62.12	63.36	62.64	62.62	62.78	62.89	62.63
100	43.23	42.98	44.33	42.98	42.95	43.18	43.51	42.93
200	21.22	20.88	22.82	21.08	20.98	21.31	21.94	20.88
300	6.60	5.08	8.44	7.00	6.90	7.55	8.13	6.70

errors. If not otherwise stated j_{max} is chosen to be three. Only at the highest energies (about 100 MeV and higher) we could see significant effects of the NN forces in the states $j = 4$. Thus the results to be displayed now can be considered to be the "full" predictions of the various NN forces.

Quite a few results of recent years, achieved with the help of the "older" generation of NN forces, are to a large extend reviewed in [177,178,180,519,261,183,184,187].

Table 8—continued

E_{lab} [MeV]	Nijm PSA	Arndt PSA	Nijm 93	Nijm I	Nijm II	Reid93	AV18	CD-Bonn
3D_1 np								
1	-.005	-.004	-.005	-.005	-.005	-.005	-.003	-.005
2	-.026	-.020	-.025	-.026	-.026	-.025	-.018	-.026
3	-.063	-.049	-.062	-.063	-.063	-.062	-.052	-.063
5	-.183	-.144	-.182	-.183	-.183	-.181	-.167	-.184
10	-.68	-.55	-.67	-.68	-.67	-.67	-.65	-.68
20	-2.05	-1.76	-2.02	-2.05	-2.05	-2.01	-1.99	-2.06
30	-3.55	-3.17	-3.50	-3.56	-3.55	-3.49	-3.46	-3.58
50	-6.43	-6.01	-6.32	-6.45	-6.45	-6.31	-6.28	-6.49
100	-12.23	-11.91	-11.99	-12.26	-12.31	-12.07	-12.04	-12.37
200	-19.71	-19.12	-19.52	-19.62	-19.85	-19.46	-19.82	-19.79
300	-24.14	-22.86	-24.36	-24.21	-24.26	-23.64	-24.83	-24.03
ϵ_1 np								
1	.105	.109	.104	.104	.104	.104	.106	.105
2	.253	.262	.250	.251	.249	.249	.252	.254
3	.402	.414	.396	.399	.396	.396	.399	.403
5	.672	.683	.661	.667	.660	.660	.664	.674
10	1.16	1.16	1.14	1.15	1.13	1.14	1.14	1.16
20	1.66	1.78	1.61	1.64	1.61	1.61	1.63	1.66
30	1.89	2.26	1.81	1.87	1.81	1.83	1.87	1.90
50	2.11	2.89	1.97	2.09	2.00	2.03	2.11	2.12
100	2.42	3.26	2.16	2.44	2.25	2.36	2.52	2.45
200	3.13	3.22	2.86	3.27	3.03	3.40	3.43	3.22
300	4.03	4.41	4.00	4.10	4.12	4.74	4.43	4.04
3P_1 np								
1	-.108	-.108	-.105	-.108	-.107	-.107	-.107	-.108
2	-.286	-.286	-.277	-.284	-.283	-.283	-.283	-.284
3	-.491	-.492	-.476	-.489	-.487	-.487	-.486	-.489
5	-.937	-.941	-.907	-.933	-.928	-.929	-.927	-.932
10	-.2.06	-.2.07	-.1.99	-.2.05	-.2.04	-.2.05	-.2.04	-.2.05
20	-.4.03	-.4.01	-.3.88	-.4.02	-.4.00	-.4.01	-.3.99	-.4.01
30	-.5.65	-.5.56	-.5.45	-.5.63	-.5.61	-.5.63	-.5.58	-.5.62
50	-.8.25	-.8.01	-.8.02	-.8.25	-.8.24	-.8.26	-.8.15	-.8.23
100	-.13.24	-.12.83	-.13.17	-.13.30	-.13.33	-.13.38	-.13.07	-.13.23
200	-.21.30	-.21.32	-.21.33	-.21.41	-.21.38	-.21.55	-.21.22	-.21.25
300	-.28.07	-.28.67	-.27.68	-.28.17	-.27.85	-.28.31	-.28.49	-.28.08

6.1. NN force picture only

6.1.1. Total cross section

Experimental results are compared to various NN force predictions in Table 9. We see that there is negligible dependence on the choice of NN forces (differences less than 1–3%) and therefore we

Table 8 — continued

E_{lab} [MeV]	Nijm PSA	Arndt PSA	Nijm 93	Nijm I	Nijm II	Reid93	AV18	CD-Bonn
3P_1 pp								
1	-.081	-.082	-.079	-.081	-.081	-.081	-.081	-.081
2	-.247	-.251	-.241	-.246	-.245	-.246	-.246	-.247
3	-.450	-.458	-.438	-.448	-.446	-.447	-.447	-.450
5	-.902	-.920	-.877	-.898	-.894	-.896	-.896	-.901
10	-2.06	-2.10	-2.00	-2.05	-2.04	-2.05	-2.05	-2.06
20	-4.07	-4.13	-3.94	-4.06	-4.04	-4.05	-4.04	-4.07
30	-5.71	-5.73	-5.52	-5.69	-5.67	-5.68	-5.66	-5.71
50	-8.32	-8.23	-8.10	-8.31	-8.30	-8.30	-8.23	-8.32
100	-13.26	-13.09	-13.19	-13.30	-13.33	-13.30	-13.11	-13.28
200	-21.25	-21.52	-21.27	-21.32	-21.29	-21.26	-21.16	-21.20
300	-27.99	-28.79	-27.57	-28.02	-27.71	-27.86	-28.37	-27.97
1D_2 np								
1	.001	.001	.001	.001	.001	.001	.001	.001
2	.006	.006	.006	.006	.006	.006	.006	.006
3	.014	.014	.014	.014	.014	.014	.014	.014
5	.042	.042	.042	.042	.042	.041	.042	.042
10	.16	.16	.16	.16	.16	.16	.16	.16
20	.49	.48	.49	.50	.49	.48	.49	.49
30	.88	.85	.88	.89	.88	.87	.88	.89
50	1.73	1.62	1.71	1.72	1.72	1.69	1.70	1.72
100	3.90	3.53	3.75	3.83	3.85	3.79	3.81	3.86
200	7.29	7.01	6.88	7.43	7.38	7.26	7.30	7.45
300	9.69	9.95	8.77	9.82	9.73	9.63	9.43	9.75
1D_2 pp								
1	.001	.001	.001	.001	.001	.001	.001	.001
2	.005	.006	.005	.006	.005	.005	.006	.005
3	.014	.014	.014	.014	.014	.014	.014	.014
5	.043	.044	.044	.044	.044	.043	.044	.044
10	.17	.17	.17	.17	.17	.16	.17	.17
20	.51	.50	.51	.51	.51	.50	.51	.51
30	.89	.87	.89	.90	.89	.88	.90	.90
50	1.71	1.62	1.70	1.71	1.70	1.68	1.73	1.72
100	3.79	3.46	3.67	3.73	3.75	3.71	3.84	3.78
200	7.06	6.83	6.69	7.20	7.15	7.08	7.37	7.28
300	9.42	9.68	8.52	9.52	9.42	9.40	9.52	9.54

saved computer time and did not calculate all cases in the table. The agreement with the data is excellent and well within the error bars. A pictorial overview is given in Fig. 5, where for the sake of a better presentation at each energy always only one potential prediction has been included. The stability of that dynamical picture under exchange of the NN force is an important fact to be noted. We shall see that this remains essentially true for all observables, not only integrated ones. It is also

Table 8 — continued

E_{lab} [MeV]	Nijm PSA	Arndt PSA	Nijm 93	Nijm I	Nijm II	Reid93	AV18	CD-Bonn
3P_2 np								
1	.022	.022	.024	.022	.022	.022	.022	.022
2	.062	.064	.069	.063	.063	.064	.064	.064
3	.115	.118	.128	.117	.116	.118	.119	.118
5	.251	.267	.276	.254	.252	.256	.257	.255
10	.71	.73	.77	.71	.71	.72	.72	.72
20	1.90	1.94	2.01	1.91	1.90	1.93	1.91	1.92
30	3.24	3.29	3.36	3.25	3.24	3.30	3.24	3.26
50	5.89	5.98	5.92	5.88	5.87	6.00	5.86	5.91
100	10.94	11.31	10.67	10.89	10.88	11.20	11.00	10.98
200	15.46	16.49	15.51	15.48	15.42	16.01	15.86	15.62
300	16.95	17.76	17.02	17.08	16.99	17.34	16.91	17.04
3P_2 pp								
1	.014	.013	.015	.014	.014	.014	.014	.014
2	.046	.045	.051	.047	.046	.046	.047	.047
3	.092	.091	.102	.093	.092	.092	.094	.093
5	.214	.212	.236	.217	.216	.215	.219	.217
10	.65	.64	.70	.66	.66	.65	.66	.66
20	1.83	1.80	1.93	1.84	1.83	1.83	1.83	1.84
30	3.17	3.11	3.29	3.18	3.17	3.16	3.16	3.18
50	5.85	5.73	5.89	5.85	5.84	5.83	5.79	5.84
100	11.01	10.95	10.75	10.96	10.97	10.97	10.98	10.97
200	15.63	16.03	15.70	15.65	15.63	15.63	15.91	15.68
300	17.17	17.26	17.28	17.26	17.21	17.15	17.01	17.12
3F_2 np								
1	.000	.000	.000	.000	.000	.000	.000	.000
2	.000	.000	.000	.000	.000	.000	.000	.000
3	.000	.000	.000	.000	.000	.000	.000	.000
5	.002	.002	.002	.002	.002	.002	.002	.002
10	.01	.01	.01	.01	.01	.01	.01	.01
20	.06	.06	.06	.06	.06	.06	.05	.06
30	.13	.14	.13	.13	.13	.13	.12	.12
50	.30	.34	.32	.31	.31	.30	.28	.29
100	.76	.83	.84	.76	.77	.75	.67	.68
200	1.33	1.21	1.26	1.28	1.31	1.27	1.15	1.15
300	1.19	.89	.44	1.06	1.14	1.12	.77	1.18

interesting to see how the 3N observables are built up out of the various NN force components. To that aim we performed separate calculations, where the NN force was truncated to act only in the states 1S_0 and $^3S_1 - ^3D_1$ (called "s-waves" in the following), in all states up to $j_{max} = 1$, $j_{max} = 2$, $j_{max} = 3$ and $j_{max} = 4$, respectively. The result of such an investigation for σ_{tot} is displayed in Fig. 6. The relative changes in relation to the value of σ_{tot} calculated with $j_{max} = 3$ are shown. One sees that

Table 8—continued

E_{lab} [MeV]	Nijm PSA	Arndt PSA	Nijm 93	Nijm I	Nijm II	Reid93	AV18	CD-Bonn
3F_2 pp								
1	.000	.000	.000	.000	.000	.000	.000	.000
2	.000	.000	.000	.000	.000	.000	.000	.000
3	.000	.000	.000	.000	.000	.000	.000	.000
5	.002	.002	.002	.002	.002	.002	.002	.002
10	.01	.01	.01	.01	.01	.01	.01	.01
20	.07	.07	.07	.07	.07	.07	.07	.07
30	.15	.16	.15	.15	.15	.15	.14	.14
50	.34	.38	.36	.34	.34	.34	.32	.32
100	.82	.90	.90	.82	.83	.81	.73	.74
200	1.42	1.31	1.36	1.39	1.42	1.36	1.24	1.24
300	1.34	1.00	.59	1.20	1.29	1.25	.90	1.29
ϵ_2 np								
1	−.001	.000	−.001	−.001	−.001	−.001	−.001	−.001
2	−.007	−.015	−.007	−.007	−.007	−.007	−.007	−.007
3	−.016	−.018	−.016	−.016	−.016	−.016	−.017	−.016
5	−.049	−.048	−.049	−.049	−.049	−.048	−.049	−.049
10	−.18	−.18	−.18	−.18	−.18	−.18	−.19	−.18
20	−.56	−.55	−.56	−.55	−.55	−.55	−.56	−.56
30	−.95	−.92	−.96	−.94	−.94	−.94	−.97	−.95
50	−1.63	−1.57	−1.66	−1.61	−1.62	−1.60	−1.68	−1.63
100	−2.58	−2.50	−2.67	−2.54	−2.54	−2.54	−2.69	−2.62
200	−2.70	−2.73	−2.77	−2.73	−2.71	−2.79	−2.82	−2.76
300	−2.30	−2.13	−1.91	−2.36	−2.35	−2.36	−2.21	−2.05
ϵ_2 pp								
1	−.001	.000	−.001	−.001	−.001	−.001	−.001	−.001
2	−.007	−.015	−.007	−.007	−.007	−.007	−.007	−.007
3	−.017	−.017	−.017	−.017	−.017	−.017	−.017	−.017
5	−.052	−.052	−.053	−.052	−.052	−.052	−.053	−.053
10	−.20	−.20	−.20	−.20	−.20	−.20	−.20	−.20
20	−.60	−.59	−.61	−.60	−.60	−.60	−.61	−.60
30	−1.01	−.99	−1.02	−1.01	−1.01	−1.00	−1.03	−1.02
50	−1.71	−1.66	−1.74	−1.70	−1.70	−1.69	−1.77	−1.72
100	−2.66	−2.60	−2.76	−2.63	−2.64	−2.61	−2.78	−2.71
200	−2.76	−2.82	−2.84	−2.80	−2.79	−2.77	−2.88	−2.83
300	−2.34	−2.22	−1.95	−2.41	−2.41	−2.26	−2.23	−2.10

the $j = 2$ NN force contributions start to play a significant role already below 10 MeV. The $j = 4$ contributions evaluated only around 100 MeV show up only at 140 MeV where they give about 2% contribution.

Table 8 — continued

E_{lab} [MeV]	Nijm PSA	Arndt PSA	Nijm 93	Nijm I	Nijm II	Reid93	AV18	CD-Bonn
3D_2 np								
1	.006	.006	.006	.006	.006	.006	.006	.006
2	.030	.031	.030	.030	.030	.030	.030	.030
3	.075	.078	.075	.075	.075	.075	.075	.075
5	.222	.231	.224	.222	.222	.223	.222	.222
10	.85	.88	.86	.85	.85	.85	.85	.85
20	2.67	2.77	2.73	2.68	2.68	2.69	2.67	2.67
30	4.77	4.92	4.92	4.78	4.78	4.80	4.77	4.76
50	8.97	9.12	9.36	8.98	8.97	9.00	8.94	8.93
100	17.28	17.08	18.34	17.26	17.22	17.11	17.10	17.28
200	24.51	23.82	26.30	24.61	24.49	23.96	24.20	24.80
300	25.45	24.32	27.47	25.32	25.52	24.84	25.01	25.45

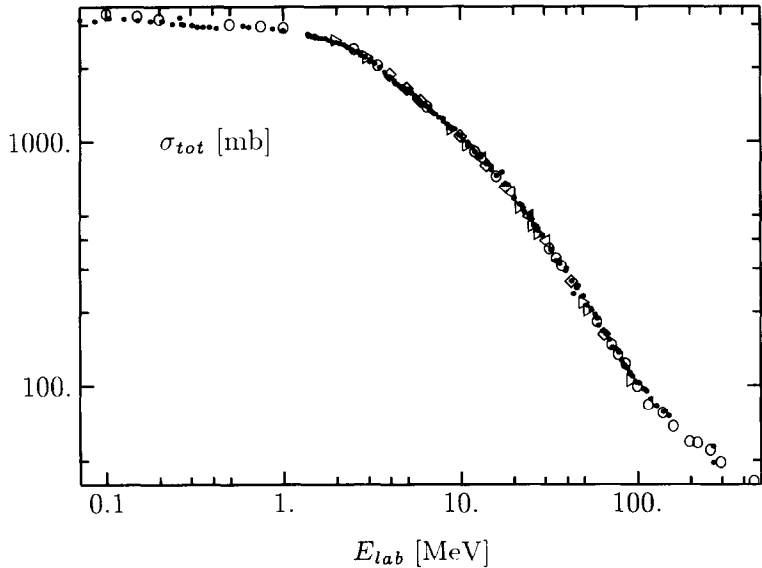


Fig. 5. The total nd cross section. Comparison of experimental data (for references see Table 9) and theory. Predictions of different potentials are shown: Bonn B (\circ), Paris (\diamond), AV18 (\triangleright), Nijmegen93 (\triangleleft).

6.1.2. Elastic nd scattering

Differential cross section

The next simple observable is the differential cross section for elastic Nd scattering. Unfortunately there are not too many nd measurements and we are forced to regard also the pd cross sections, which are much more numerous and have smaller error bars. In our theory we neglect up to now the pp Coulomb force totally, which introduces some uncertainty in the judgement how well theory describes the pd data. Fortunately at a few energies there exist both, nd and pd data. Their comparison allows to constrain Coulomb force effects to be very small except at forward angles, where Rutherford scattering finally has to dominate. Some examples are shown in Fig. 7. We see that except at the

Table 9

Comparison of experimental (taken at $E(\text{exp})$) and theoretical (evaluated at the nucleon lab energy E) total nd cross sections.

E [MeV]	exp [mb]	$E(\text{exp})$ [MeV]	AV18	Bonn B	Nijm 93 [mb]	Nijm I	Nijm II	Paris
1.0	2893.6 ± 18.2 2854 ± 39 3110 ± 200	(1.0031) [92] (0.995) [435] (1.0) [353]		2902				
2.0	2550.6 ± 11.1 2537 ± 10 2600 ± 80	(1.9999) [92] (1.981) [374] (2.0) [353]		2554				
3.0	2158.0 ± 7.2 2240 ± 90 2160 ± 86	(2.9873) [92] (3.00) [353] (3.01) [504]		2163				
8.0	1207 ± 13 1213.3 ± 5.58 1224 ± 10	(8.0) [107] (8.038) [92] (8.0) [431]	1212	1212	1214	1209	1210	
9.0	1118 ± 10 1124.8 ± 5.84 1120 ± 10	(9.015) [107] (9.0251) [92] (8.77) [60]	1119	1119				
10.0	1055 ± 10 1051.1 ± 6.9	(10.0) [107] (10.026) [92]		1039				
11.0	968 ± 13 990.4 ± 7.6	(11.0) [107] (11.016) [92]	968.8	966.6				
12.0	913 ± 13 918.48 ± 8.11 923 ± 10	(12.0) [107] (12.118) [92] (12.0) [431]	906.7	910.4				
13.0	867 ± 12	(12.995) [107]	851.4		854.6	851.0	852.0	
14.1	803 ± 14 790 ± 20 809 ± 6 778 ± 22 806 ± 6 810 ± 30	(14.1) [391] (14.1) [95] (14.1) [289] (14.1) [440] (14.1) [440] (14.2) [340]	797.2	797.0				798.5
19.0	627.96 ± 12.16 632 ± 14	(18.932) [92] (19.01) [435]	614.6		617.6			615.6
22.0	544.68 ± 14.549	(22.079) [92]	534.9	539.4				535.8
24.0	495.49 ± 16.043	(23.955) [92]	490.8	495.5	493.6			491.8
26.0	455 ± 12 451.47 ± 17.72	(26.015) [107] (26.082) [92]	452.5	459.6	455.1			
42.5	267.7 ± 3.9	(42.5) [403]	263.0	266.5				

Table 9—continued

E [MeV]	exp [mb]	E(exp) [MeV]	AV18	Bonn B	Nijm 93 [mb]	Nijm I	Nijm II	Paris
65.0	166.5 ± 2.9 161.7 ± 2.8	(63.5) [403] (66.5) [403]	158.5	162.7				
93.5	110 ± 7 107 ± 1.8 104 ± 4 109.4 ± 2.3	(93.4) [104] (98.1) [332] (95.0) [258] (93.5) [403]	104.8	108.1				
140.0	78.4 ± 1.3	(140.9) [332]		77.2				
270.0	49 ± 5 57 ± 3	(270.0) [147] (270.0) [259]		54.66				

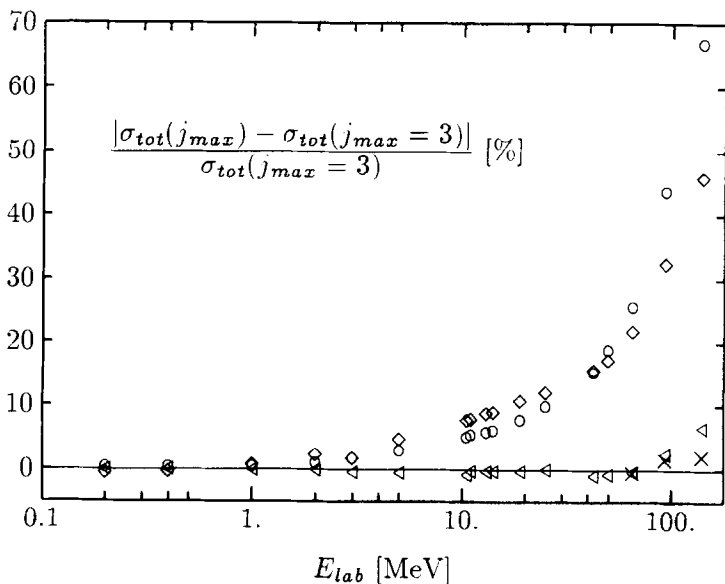


Fig. 6. The relative total nd cross section evaluated for "s-waves" (\circ), $j_{max} = 1$ (\diamond), 2 (\triangleleft), and 4 (\times) in relation to $j_{max} = 3$.

forward angles the experimental nd and pd cross sections practically overlap. Thus if there would be no charge independence breaking (CIB) or charge symmetry breaking (CSB) in the NN forces then the equality of the two cross sections would tell, that Coulomb force effects at the larger angles cannot be greater than the experimental error bars. Well established right now is only CIB in the state 1S_0 . It is manifest in the different scattering lengths for the np and pp (nn) systems. The recommended values [342] are $a_{np} = -23.48 \pm 0.009$ fm and $a_{pp}^{strong} = -17.36 \pm 0.4$ fm. The nn scattering length is less well known. From π^- -absorption on the deuteron [159,433] the value -18.6 ± 0.3 fm has been extracted. The analysis of the nn final state interaction in nd breakup processes remain still very controversial (see Section 7.2) and does not constrain the value of a_{nn} sufficiently well. The $^3\text{He}-^3\text{H}$ mass difference can be "explained" [527] if a small CSB is assumed and the nn force in the state

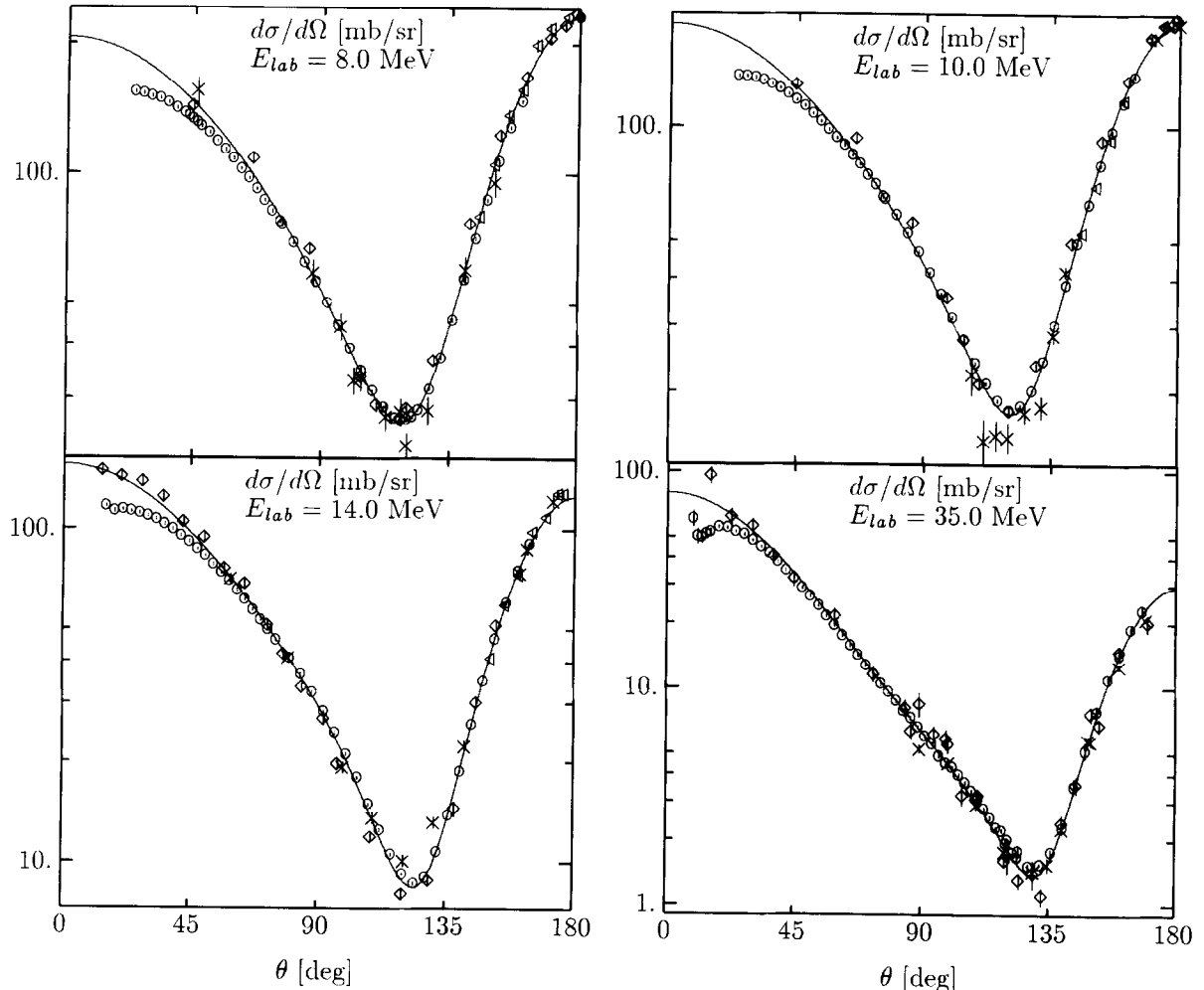


Fig. 7. Angular distributions for elastic Nd scattering. Comparison of pd and nd data. 8 MeV: nd data (\diamond) [431], (\bullet) [252], (\times) [436], (\triangleleft) [234]; pd data (\circ) [416]. 10 MeV: nd data (\diamond) (10.3 MeV) [431], (\times) [24], (\triangleleft) [234]; pd data (\circ) [416]. 14 MeV: nd data (\times) [440], (\triangleleft) [234], (\diamond) [47]; pd data (\circ) [416]. 35 MeV: nd data (\times) [62], (\diamond) (36 MeV) [411]; pd data (\circ) [71]. The solid curve is the AV18 NN force prediction for 8, 10 and 14 MeV and the Nijm I NN force prediction for 35 MeV.

1S_0 is slightly stronger than the corresponding pp force. Let us now regard the influence of CIB and CSB on the differential cross section. In Fig. 8 we display the effect of choosing different 1S_0 NN forces using the Bonn B NN force as an example. Several curves are shown. The first set of curves is based just on "s-wave" forces, using the original 1S_0 np force, a modified 1S_0 pp force and the correct treatment distinguishing between np and pp (= nn) forces. The three curves are essentially indistinguishable. The second set of curves includes on top of the "s-wave" forces the higher partial wave NN force components up to $j_{max} = 2$. Again the effects of CIB are hardly noticeable. We conclude that the effect of that CIB in the state 1S_0 is very small for the differential cross section and the equality of the experimental pd or nd cross sections shown in Fig. 7 indicates strongly that Coulomb force effects should be very small for that observable (except at forward angles).

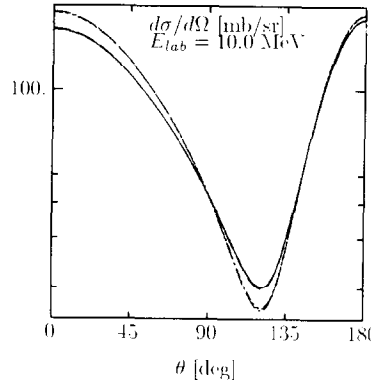


Fig. 8. Insensitivity of the angular distribution in elastic Nd scattering against CIB in the state 1S_0 . Both groups of curves contain three overlapping results (see text). The $j_{max} = 2$ curves are the lowest in the minimum and the largest at forward angles.

Let us now compare theory with experimental data [427,79,392,308,197,411,242,365,305,442,206, 426,431,223,71,396,413,416].

This is shown in Fig. 9 in the energy range starting from a few MeV to about 200 MeV. We do not display all of them, but the ones not shown are very similar. At the very low energies (below about 6 MeV) Coulomb force effects at forward and at backward angles are clearly visible. In the minimum of the cross section the agreement with theory is perfect. There is one nd measurement at 3 MeV, which overlaps with the pd data in the minimum and therefore rules out significant Coulomb force effects for that angular range. (We also checked the effect of CIB at 3 MeV and found it to be negligible for the differential cross section.) This picture of large Coulomb force effects on the angular distributions in the forward and backward angular regions at very small energies is supported by recent results of the Pisa group [271], see Section 8.5. Between 8 MeV (see also Fig. 7) and 35 MeV the agreement with the data is essentially perfect. At 47.5 MeV and 65 MeV the nd data are in good agreement with theory, but pd data with smaller errors appear to be a bit above theory in the minimum. Since the known CIB has no visible effect we have to assume right now that this deviation between nd and pd data is due to Coulomb force effects. While at 93 MeV we still seem to agree with the data at 140 MeV and higher the data are significantly higher than theory, especially for c.m. scattering angles around 120° and beyond. We evaluated the relativistic phase space factor and the relativistic current in the total momentum zero frame. This leads to an increase of the cross section of 1–2% at 100 MeV and higher in relation to the nonrelativistic one. This percentage number refers to the choice of a relativistic momentum space volume element $d\mathbf{p}/\sqrt{m^2 + \mathbf{p}^2}$ against a nonrelativistic one, $d\mathbf{p}/m$. Using just $d\mathbf{p}$ in both cases increases the percentage change to about 10 %. In any case that kinematical correction does not explain the discrepancy to the data around 150 MeV. It remains to be seen, whether one encounters here the onset of dynamical relativistic effects.

It is also very important to note that the theoretical predictions are very stable against interchanges of the NN forces. We show in Fig. 9 at the energies 3, 22.7, 47.5 and 93.5 MeV, representative for the whole energy range under study, that the detailed properties of the forces, like having softer (Nijm I) or harder core (AV18, Nijm93), being strictly local (Nijm II) or having a mild nonlocality (Nijm I, Nijm93) do not show up in the differential cross section. Even the substantially nonlocal Bonn B interaction introduces no change in the differential cross section.

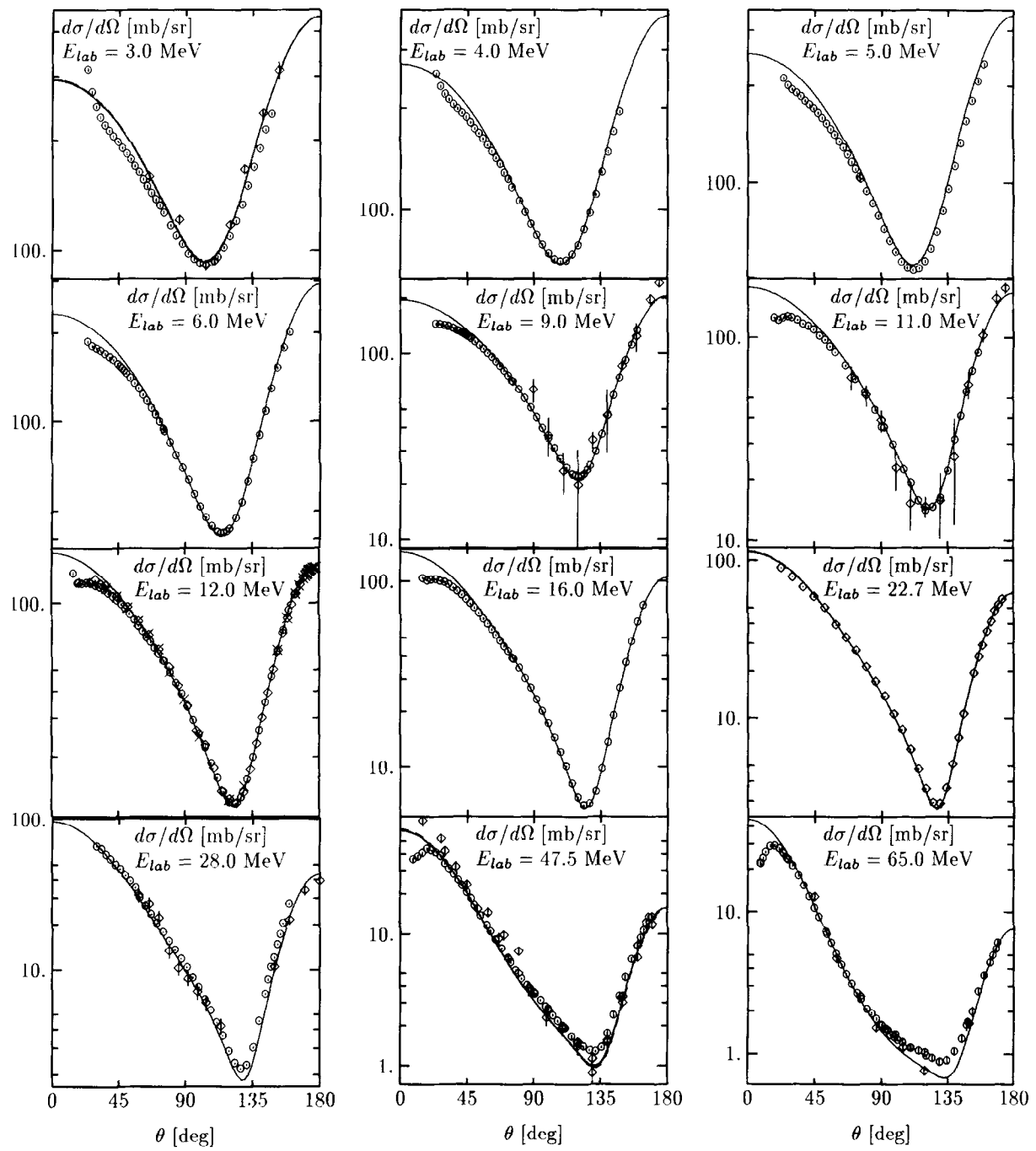


Fig. 9.

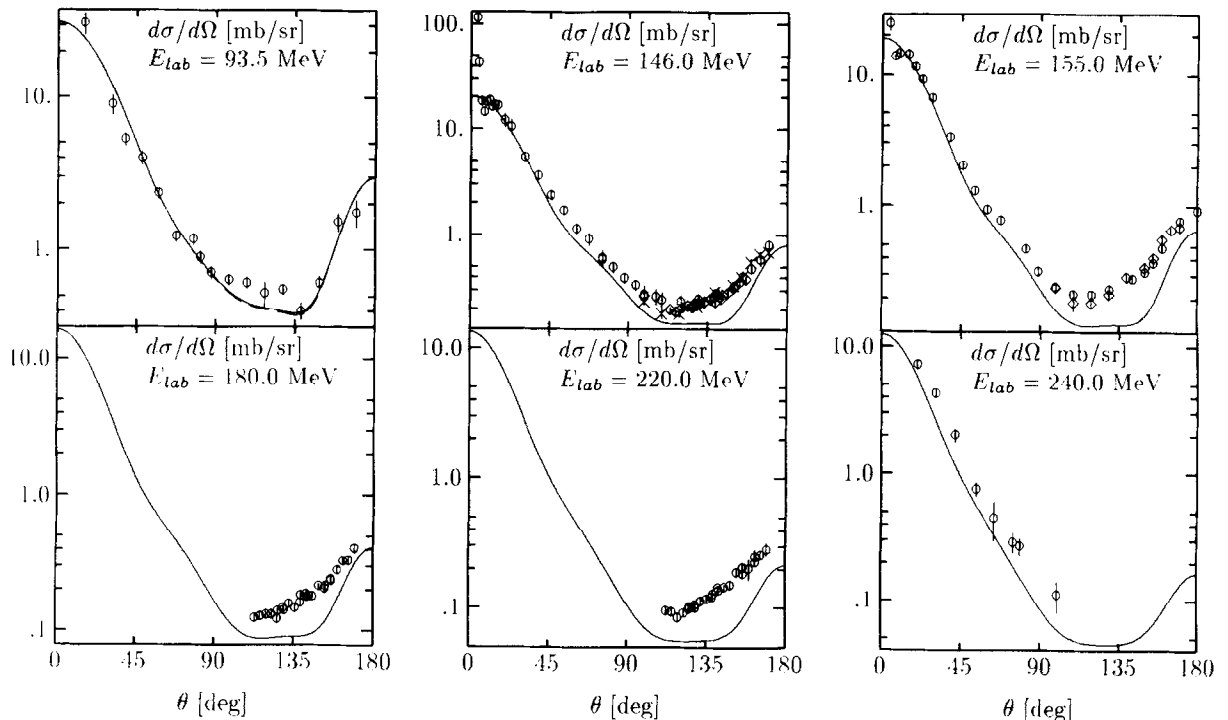


Fig. 9. Angular distributions for elastic Nd scattering. Comparison of data to various potential predictions. 3 MeV: pd data (○) [416]; nd data (◇) [431]; predictions (—) Nijm I, (---) Nijm II, (- - -) Nijm 93, (· · ·) AV18. 4, 5 and 6 MeV: pd data (○) [416]; prediction (—) Nijm I. 9 MeV: pd data (○) [416]; nd data (◇) [305]; prediction (—) Nijm I. 11 MeV: pd data (○) (11.1 MeV) [426]; nd data (◇) [305]; prediction (—) AV18. 12 MeV: pd data (○) [416], (◇) [206], (×) [396]; prediction (—) AV18. 16 MeV: pd data (○) [416]; prediction (—) Nijm I. 22.7 MeV: pd data (○) [416], (◇) [206]; predictions (—) Nijm I, (---) Nijm II, (- - -) Nijm 93, (· · ·) AV18. 28 MeV: pd data (○) [223]; nd data (◇) [197]; prediction (—) Nijm I. 47.5 MeV: pd data (○) (46.3 MeV) [71]; nd data (◇) [411]; predictions (—) Nijm I, (---) Nijm II, (- - -) Nijm 93, (· · ·) AV18. 65 MeV: pd data (○) (64.5 MeV) [442]; nd data (◇) [413]; prediction (—) AV18. 93.5 MeV: pd data (○) (95 MeV) [79]; predictions (—) Nijm I, (---) AV18. 146 MeV: pd data (○) [392], (◇) (145.5 MeV) [242]; nd data (×) (152 MeV) [365]; prediction (—) AV18. 155 MeV: pd data (○) [308]; nd data (◇) (152 MeV) [365]; prediction (—) AV18. 180 MeV: pd data (○) (181 MeV) [242]; prediction (—) AV18. 220 MeV: pd data (○) (216.5 MeV) [242]; prediction (—) AV18. 240 MeV: pd data (○) [427]; prediction (—) AV18.

As a further information we display in Fig. 10 the way the differential cross section is built up out of the different NN force components. At 10 MeV we see that $j_{max} = 2$ is sufficient; this is even true at 93 MeV, except that around 60° c.m. angle the contribution of the $j = 3$ forces removes the little hump of the $j_{max} = 2$ calculation. At 180 MeV the small oscillations present in the $j_{max} = 3$ calculation are reduced significantly by including $j = 4$ NN force components. It is obvious that the $j = 5$ force components would only represent a cosmetic modification for that observable and are not needed.

Some time ago there was indication that at extreme backward angles a discrepancy between theory and experiment [431] might exist [513]. Renewed measurements [234] could not confirm that set of data [431] and now theory and experiment agree perfectly well, see Fig. 7.

It might be of interest to point out that the differential cross section is dominated by quartet

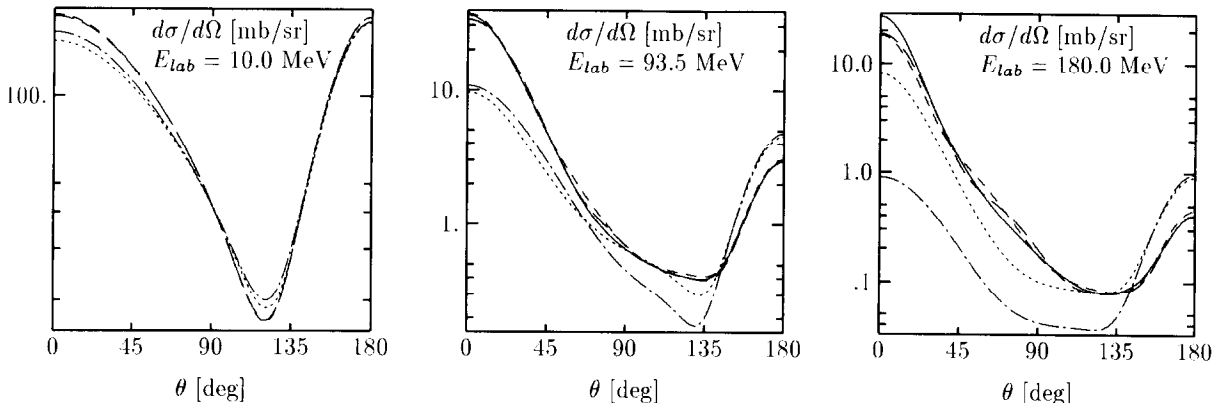


Fig. 10. The dependence of the angular distribution for elastic Nd scattering on the NN force components used: "s-waves" (---), $j_{max} = 1$ (· · · · ·), $j_{max} = 2$ (— · — · —), $j_{max} = 3$ (— · — · — · —) and $j_{max} = 4$ (— — —).

scattering. This has been known for quite some time [2] and emphasized especially in [281].

Let us now turn to spin observables in elastic Nd scattering.

Vector analyzing powers

Nucleon and deuteron vector analyzing powers exhibit a serious problem. We shall devote a special section to that puzzle below. It occurs only at energies below ≈ 30 MeV. For higher energies there is perfect agreement between theory and experiment, as shown in Fig. 11. Note that also pd and nd data agree among themselves, indicating small Coulomb force effects. In Fig. 12 we show how A_y builds up in terms of the different NN force components. Clearly the NN "s-waves" are totally insufficient, as is also the inclusion of all forces up to $j = 1$. Even at 10 MeV and at higher energies the $j = 2$ NN forces crucially contribute. More detailed, the $^3P_2 - ^3F_2$ forces are the most important ones among the $j = 2$ forces. At 180 MeV also the $j = 3$ and 4 NN force components are significant. Now if we regard the small energies, say below 30 MeV, then the contributions of the 3P_j NN force components are really the dominant ones. Moreover the three 3P_j forces determine the analyzing powers in very specific manners. That is displayed in Fig. 13. Switching off the NN force component 3P_0 and keeping all others the maximum of A_y jumps up, while turning off the 3P_1 or $^3P_2 - ^3F_2$ forces separately has an opposite effect. Thus one can expect that even small changes in these specific forces can, via that interplay, lead to substantial shifts in the peak heights of A_y . At the very low energies there is just one maximum around $\theta_{c.m.} = 120^\circ$. Now the comparison to the data shown in Fig. 14 reveals a strong discrepancy: theory underestimates the data by about 30%. This is true also for all neighboring energies [480,482] (see Section 7.3). We also see from Fig. 14 that the pd data lie a bit below the nd data in the maximum of A_y . This is presumably a Coulomb force effect (see Section 8.5). The prediction of the AV14 potential deviates most strongly. The reason is that its 3P_j NN phases differ from the ones of the other potentials. This demonstrates how sensitively A_y reacts to the very details of the NN force input. All the other potentials give essentially the same A_y values in agreement with the fact that their 3P_j phases are very close to each other (see Table 8). We shall come back to that puzzle in Section 7.3.

The deuteron vector analyzing power iT_{11} looks very similar to A_y and exhibits perfect agreement above 30–40 MeV and strong disagreement below. Examples are shown in Fig. 15. Note again the

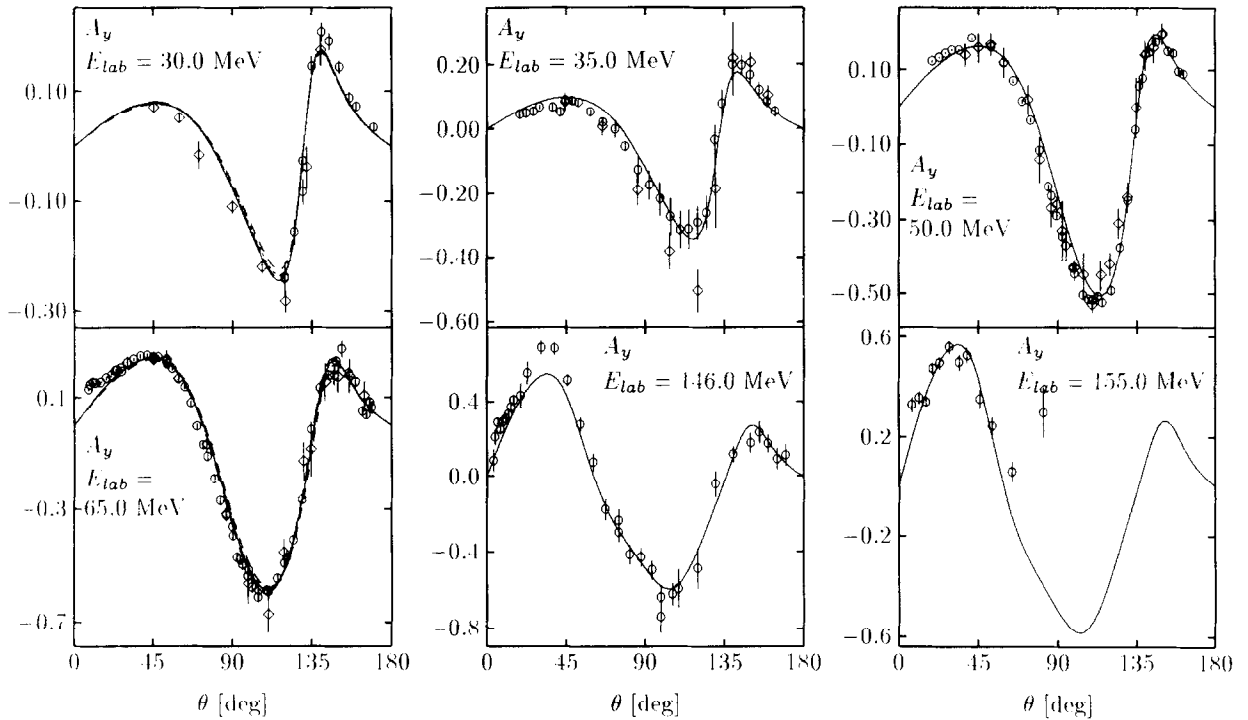


Fig. 11. The nucleon analyzing power A_y for elastic Nd scattering. Comparison of data to various potential predictions. 30 MeV: pd data (\circ) (30.2 MeV) [255]; nd data (\diamond) (29.6 MeV) [112]; predictions (—) Nijm I, (---) Nijm II, (- - -) Nijm 93, (.....) AV18. 35 MeV: pd data (\circ) [71]; nd data (\diamond) [531]; prediction (—) Nijm I. 50 MeV: pd data (\circ) (49.3 MeV) [272]; nd data (\diamond) [412,498]; prediction (—) AV18. 65 MeV: pd data (\circ) (64.5 MeV) [442]; nd data (\diamond) [413]; predictions (—) Nijm I, (---) Nijm II, (- - -) Nijm 93, (.....) AV18. 146 MeV: pd data (\circ) [392]; prediction (—) AV18. 155 MeV: pd data (\circ) [308]; prediction (—) AV18.

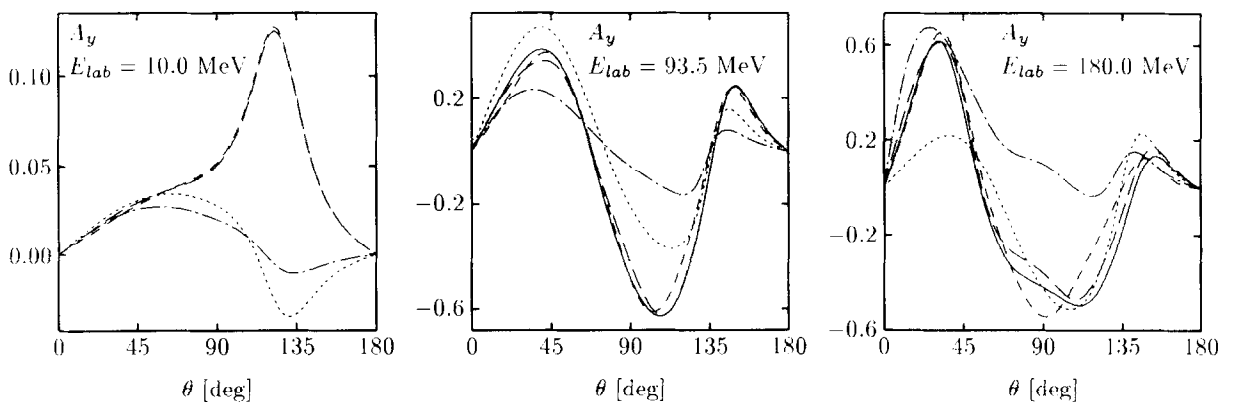


Fig. 12. The dependence of the analyzing power A_y for elastic Nd scattering on the NN force components used: "s-waves" (— · — · —), $j_{max} = 1$ (.....), $j_{max} = 2$ (— · — · —), $j_{max} = 3$ (---) and $j_{max} = 4$ (—).

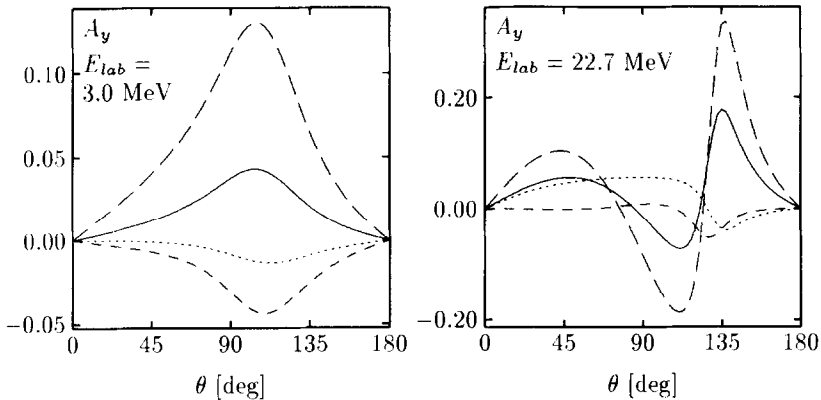


Fig. 13. The sensitivity of the analyzing power A_y in elastic Nd scattering on the 3P_j NN force components, which are switched off separately: (---) without 3P_0 , (- - -) without 3P_1 , and (.....) without $^3P_2 - ^3F_2$. Full calculations are given by the solid lines.

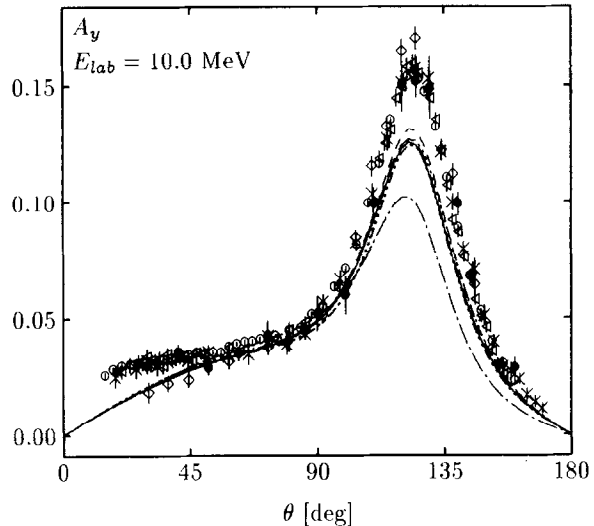


Fig. 14. The analyzing power A_y for elastic Nd scattering at 10 MeV. Comparison of pd data (○) [416], (×) [457], (△) [396], (●) [91] and nd data (◊) [232] to various NN force predictions: (—) Nijm I, (---) Nijm II, (- - - -) Nijm 93, (.....) AV18, (- - - ·) AV14, and (· - - - -) Nijm78.

independence on the choice of NN force.

Tensor analyzing powers

The deuteron tensor analyzing powers T_{20} , T_{21} , and T_{22} have been measured up to now only in the pd system. Thus there remains an uncertainty about Coulomb force effects. As shown in Fig. 16 the deuteron tensor analyzing powers are very well described by theory except at very low energies for T_{20} and T_{21} , where obviously Coulomb force effects are visible at extreme forward angles. Where we show different potential predictions we find essentially no dependence on the choice of the NN force. At the higher energies experimental data with smaller error bars would be very desirable. It is instructive to see how the T_{2k} 's built up, which is displayed in Fig. 17. Clearly the "s-waves" together

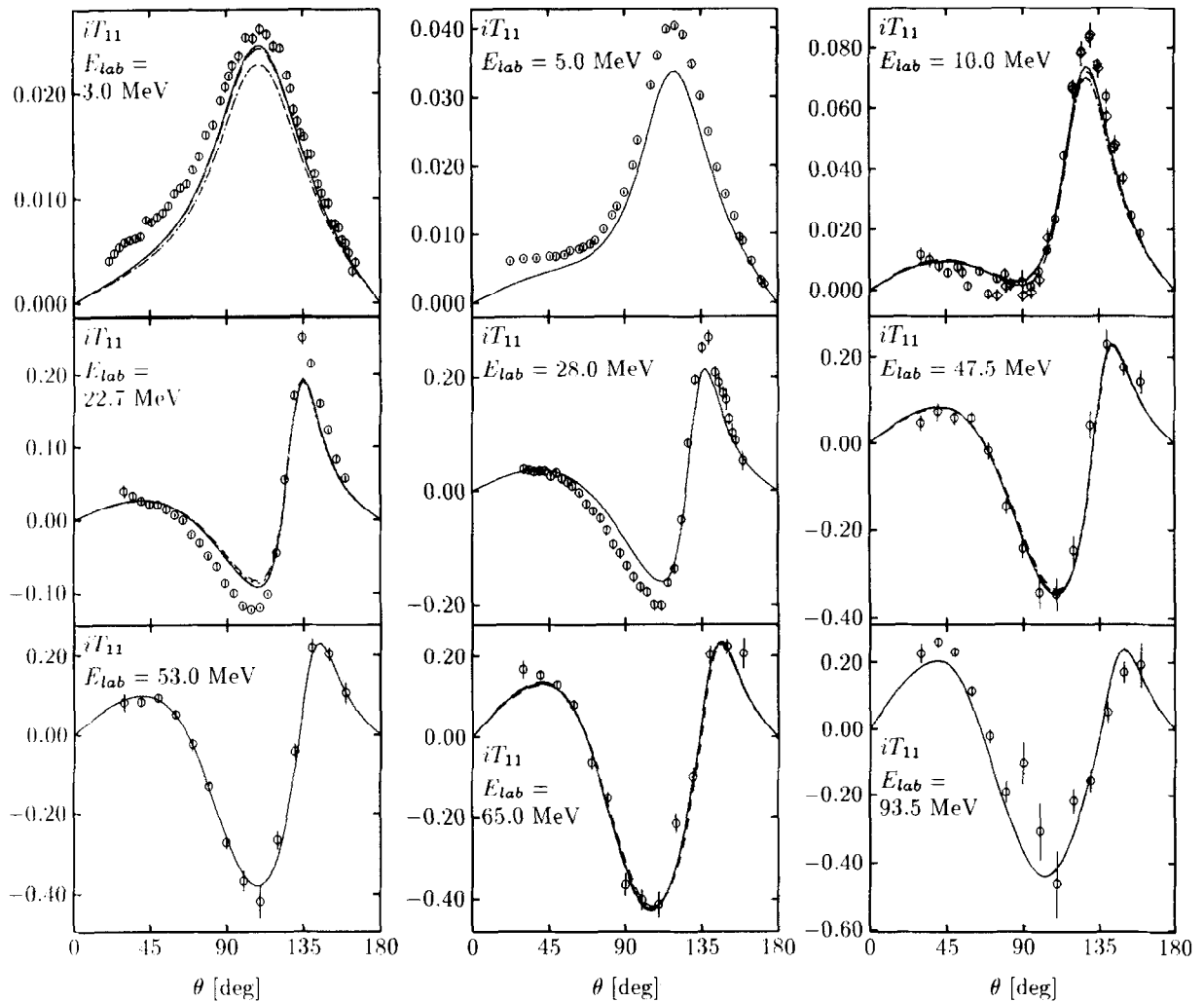


Fig. 15. The deuteron vector analyzing power iT_{11} in elastic Nd scattering. Comparison of data to the NN force predictions. 3 MeV: pd data (○) [416]; predictions (—) Nijm I, (---) Nijm II, (- - -) Nijm 93, (.....) AV18. 5 MeV: pd data (○) (5.05 MeV) [127]; prediction (—) Nijm I. 10 MeV: pd data (○) [457], (○) [426]; predictions (—) Nijm I, (---) Nijm II, (- - -) Nijm 93, (.....) AV18. 22.7 MeV: pd data (○) [206]; predictions (—) Nijm I, (---) Nijm II, (- - -) Nijm 93, (.....) AV18. 28 MeV: pd data (○) [223]; prediction (—) Nijm I. 47.5 MeV: pd data (○) [521]; predictions (—) Nijm I, (---) Nijm II, (- - -) Nijm 93, (.....) AV18. 53 MeV: pd data (○) [521]; prediction (—) Nijm I. 65 MeV: pd data (○) [521]; predictions (—) Nijm I, (---) Nijm II, (- - -) Nijm 93, (.....) AV18. 93.5 MeV: pd data (○) [521]; predictions (—) Nijm I, (---) Nijm II.

with the $j = 1$ NN forces are highly insufficient, even at 10 MeV. While at 10 MeV the addition of $j = 2$ forces essentially provides the final answer, $j = 3$ and even $j = 4$ forces are needed around 100 MeV and at 180 MeV. Especially for T_{21} and T_{22} one has to expect that even $j = 5$ NN forces will be significant around 180 MeV.

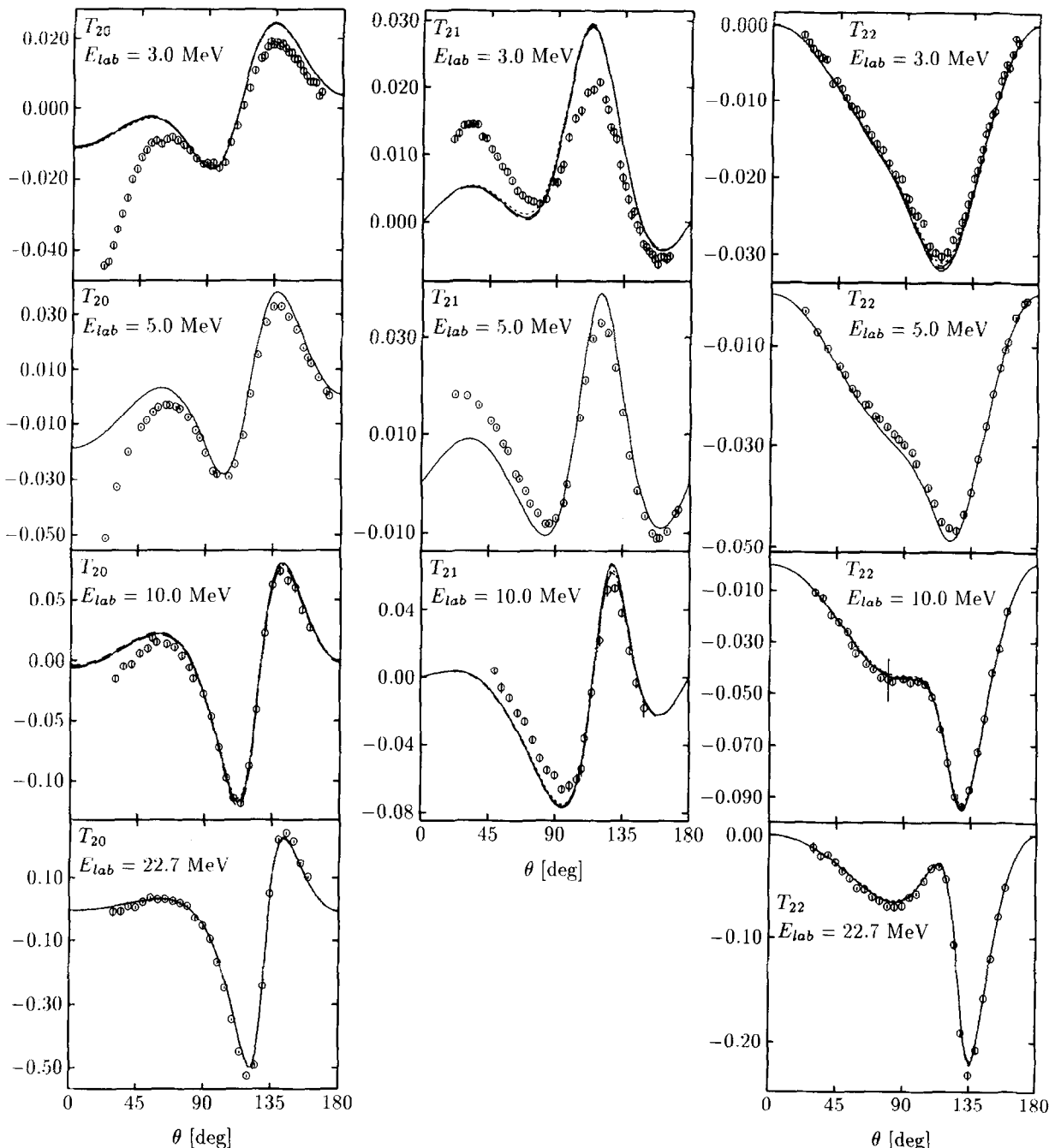


Fig. 16. The deuteron tensor analyzing powers T_{20} , T_{21} , and T_{22} in elastic Nd scattering. Comparison of data to the NN force predictions. References to the data and the choice of NN force predictions are the same as in Fig. 15 except for 5 MeV: pd data (○) [454]; prediction (—) Nijm I.

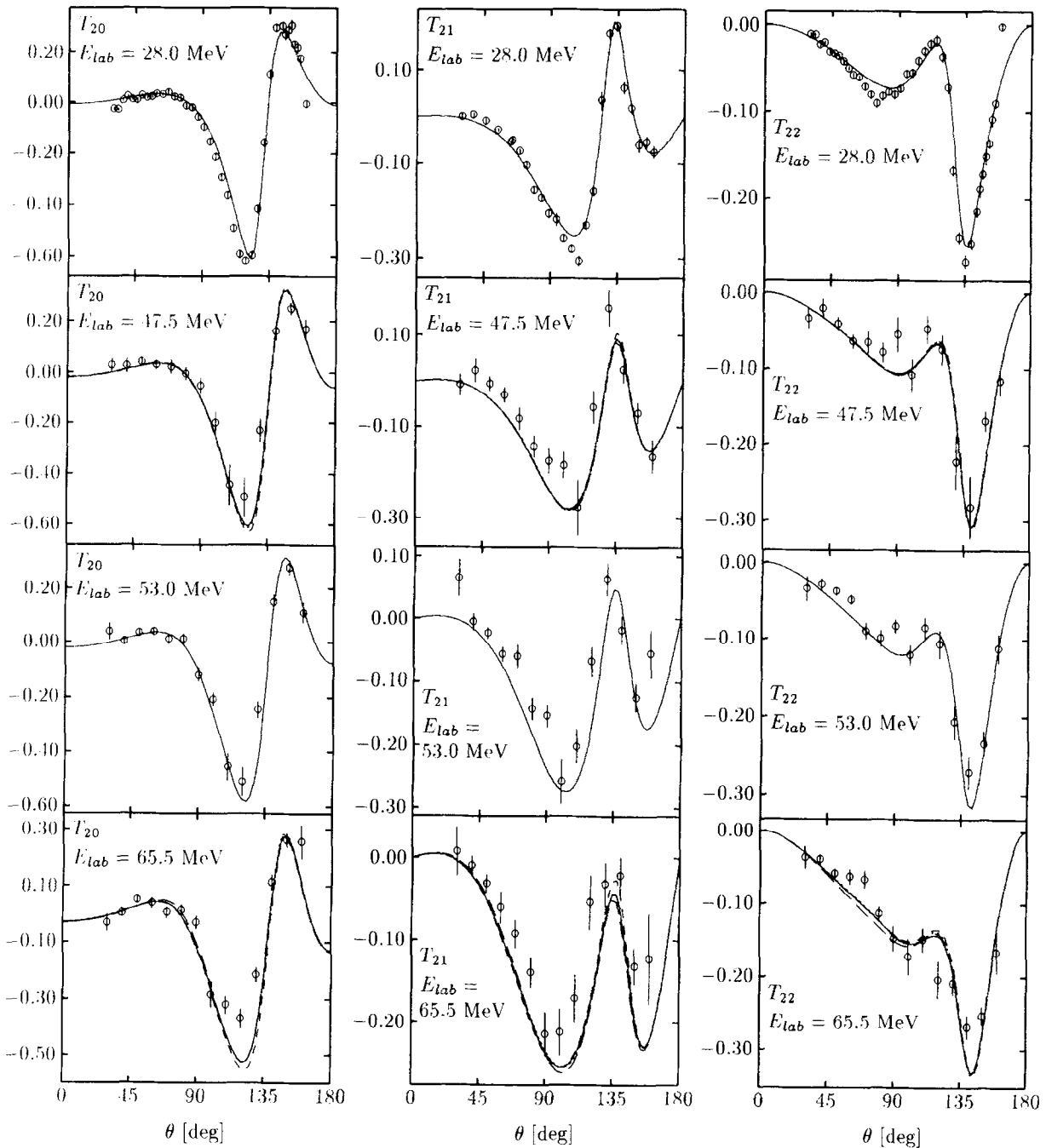


Fig. 16—continued.

Spin transfer coefficients

Let us now turn to the spin transfer coefficients. Three nucleon to nucleon spin-transfer-coefficients $K_x^{'}$, $K_z^{'}$ and $K_y^{'}$ have been measured. We show in Fig. 18 the way they built up out of different NN force components. In addition to the measured ones we add $K_x^{z'}$ and $K_z^{z'}$. Again $j_{max} = 1$

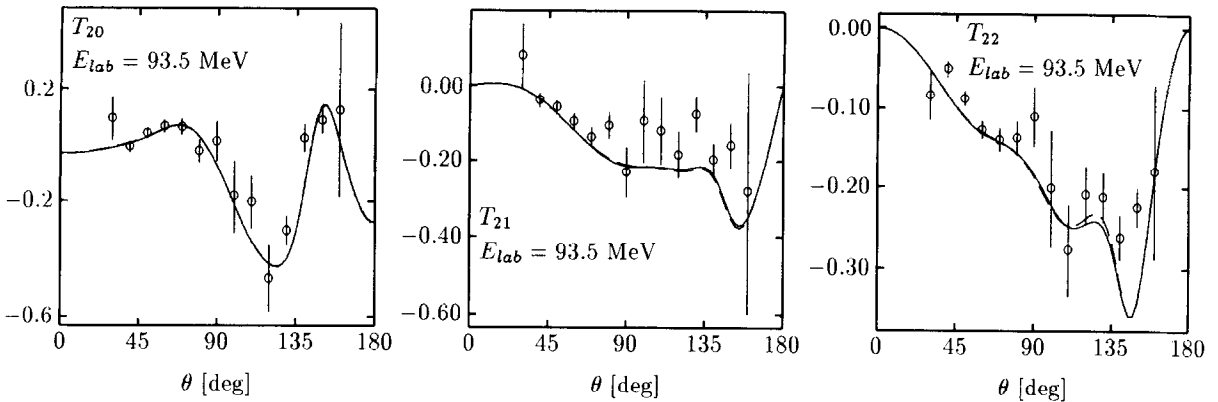


Fig. 16—continued.

would be insufficient even at 10 MeV but $j_{max} = 2$ works well. For 100 and 180 MeV $j_{max} = 3$ is absolutely mandatory to come close to the final structure. Again at 180 MeV presumably $j = 5$ forces should better be included. Fig. 19 shows the comparison of theory and experimental data for $K_y^{y'}$. The agreement is fairly good. Again there is no dependence on the choice of the NN force among the most recent ones. For 19 and 22.7 MeV in the minimum of $K_y^{y'}$ theory appears to be slightly above the data. One reason could be Coulomb force effects, another unsettled details of the $^3S_1 - ^3D_1$ tensor force and of the 1P_1 force component. In the two-nucleon system the ϵ_1 -mixing parameter between the 3S_1 and 3D_1 waves and the δ_{1P_1} phase shift quite often act in a very similar way and are hard to disentangle. For the 3N observable $K_y^{y'}$ we found [474] a similar interplay between the corresponding force components. We would like to add two studies displayed in Fig. 20. The new CD Bonn potential and the Nijmegen force describes the NN data equally well and also their NN phases are very close to each other. Nevertheless CD Bonn has a significantly lower D-state probability of the deuteron (4.83%) than the NijmI (5.68%) potential. That quantity can also be considered as a measure of the strength of the $^3S_1 - ^3D_1$ coupling. Fig. 20 shows their predictions at 19.0 MeV. While CD Bonn passes straight through the data, NijmI stays a bit above. The reason lies in the $^3S_1 - ^3D_1$ force. Namely performing a NijmI calculation with the $^3S_1 - ^3D_1$ force replaced by the one of CD Bonn shifts the NijmI prediction practically to the values of CD Bonn. (Note that also the deuteron wave functions are replaced). The second study highlights the danger of using predictions of outdated NN forces like the Nijm78 potential. The resulting $K_y^{y'}$ describes the data beautifully, but its phase shift parameters δ_{1P_1} and ϵ_1 deviate quite significantly from the ones of the Nijmegen and Virginia PSA. The 1P_1 phase is too weak and the ϵ_1 too strong. If we perform a NijmI calculation and replace its 1P_1 force by the one of Nijm78, we lower the minimum and if in addition we also replace the $^3S_1 - ^3D_1$ force by the one of Nijm78 we get a nearly identical result as for Nijm 78. In view of that latter point it appears very important to settle unambiguously the problem of the true ϵ_1 - and δ_{1P_1} values in NN scattering. The Arndt PSA values [417] still differ significantly from the ones of Nijmegen [466] and another study [224] claims even a third result, see Fig. 21. Based on the recent Nijmegen PSA alone and the related updated potentials Nijm 93, Nijm I, II, and AV18 there is a slight discrepancy in the minimum of $K_y^{y'}$, as we saw in Fig. 19. Note, however, that the new CD Bonn provides a perfect description at 19.0 MeV. CD Bonn has a significantly smaller deuteron D-state probability than all the other forces. It would be very important to fix the Coulomb force effects theoretically, in order to clarify the situation. Another possibility is to measure $K_y^{y'}$ in the nd

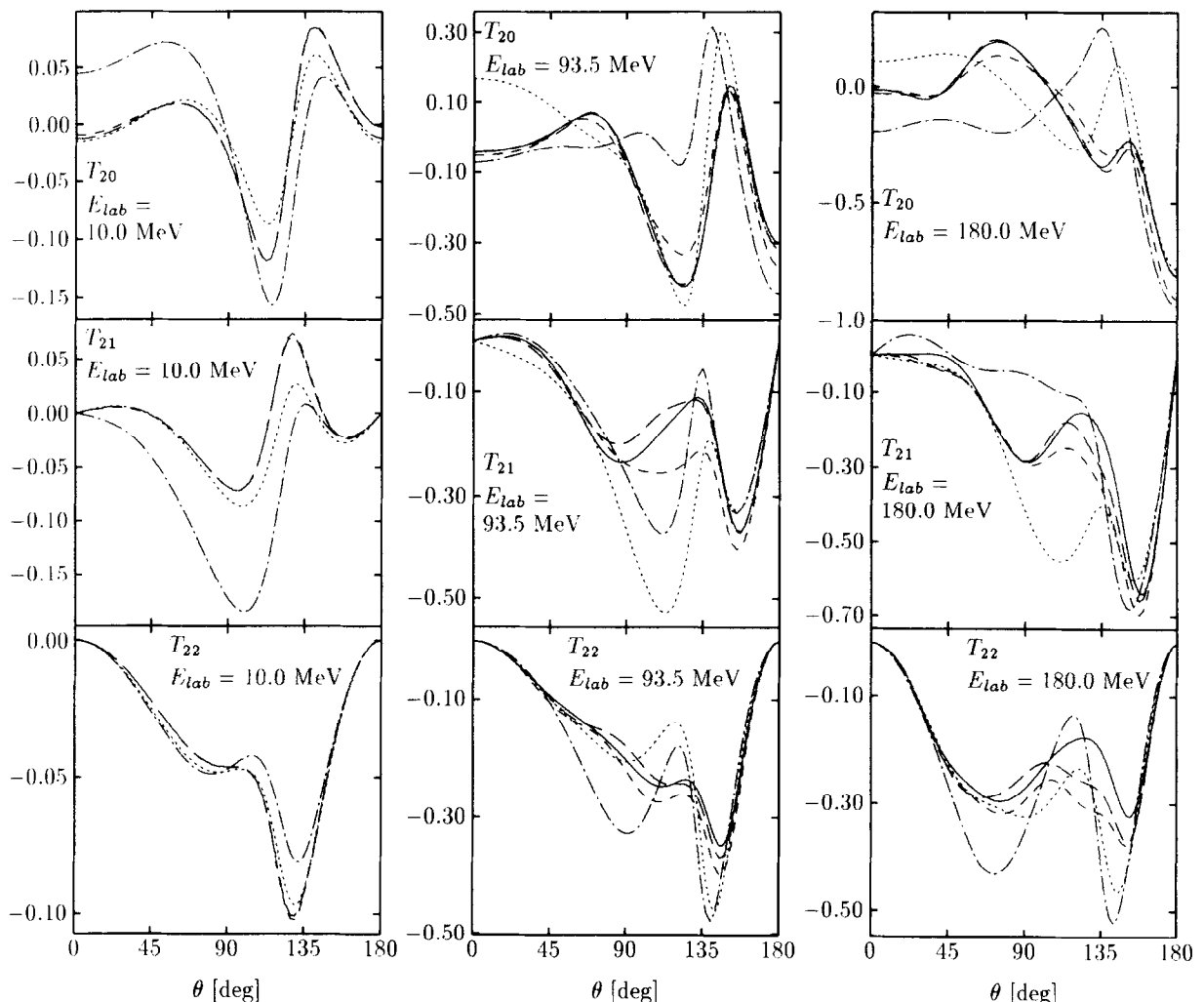


Fig. 17. The dependence of the tensor analyzing powers T_{20} , T_{21} , and T_{22} for elastic Nd scattering on the NN force components used: "s-waves" ($\cdots\cdots$), $j_{max} = 1$ ($\cdot\cdot\cdot$), $j_{max} = 2$ ($\cdots\cdots\cdots$), $j_{max} = 3$ ($- - -$) and $j_{max} = 4$ ($- -$).

system. Such an experimental study in the nd system just in the minimum of K_y' is in preparation [492].

Conclusions from that 3N observable K_y' about specific properties of NN forces, like weaker tensor forces, [89,90], might be misleading as we know now, since 3N forces might do a similar job and lower the minimum. We shall come back to their possible effects in Section 6.2.

The observable K_z' exhibits similar sensitivities [474], however less pronounced and our theoretical results are compared to data in Fig. 22.

Finally K_x' is very insensitive to details of NN forces [150,514] and is very well described by theory, see Fig. 23.

Fig. 24 displays the nucleon to deuteron polarization transfer coefficients K_y' , K_z' , and K_x' . The overall agreement between theory and experiment is good. Data with reduced error bars especially at

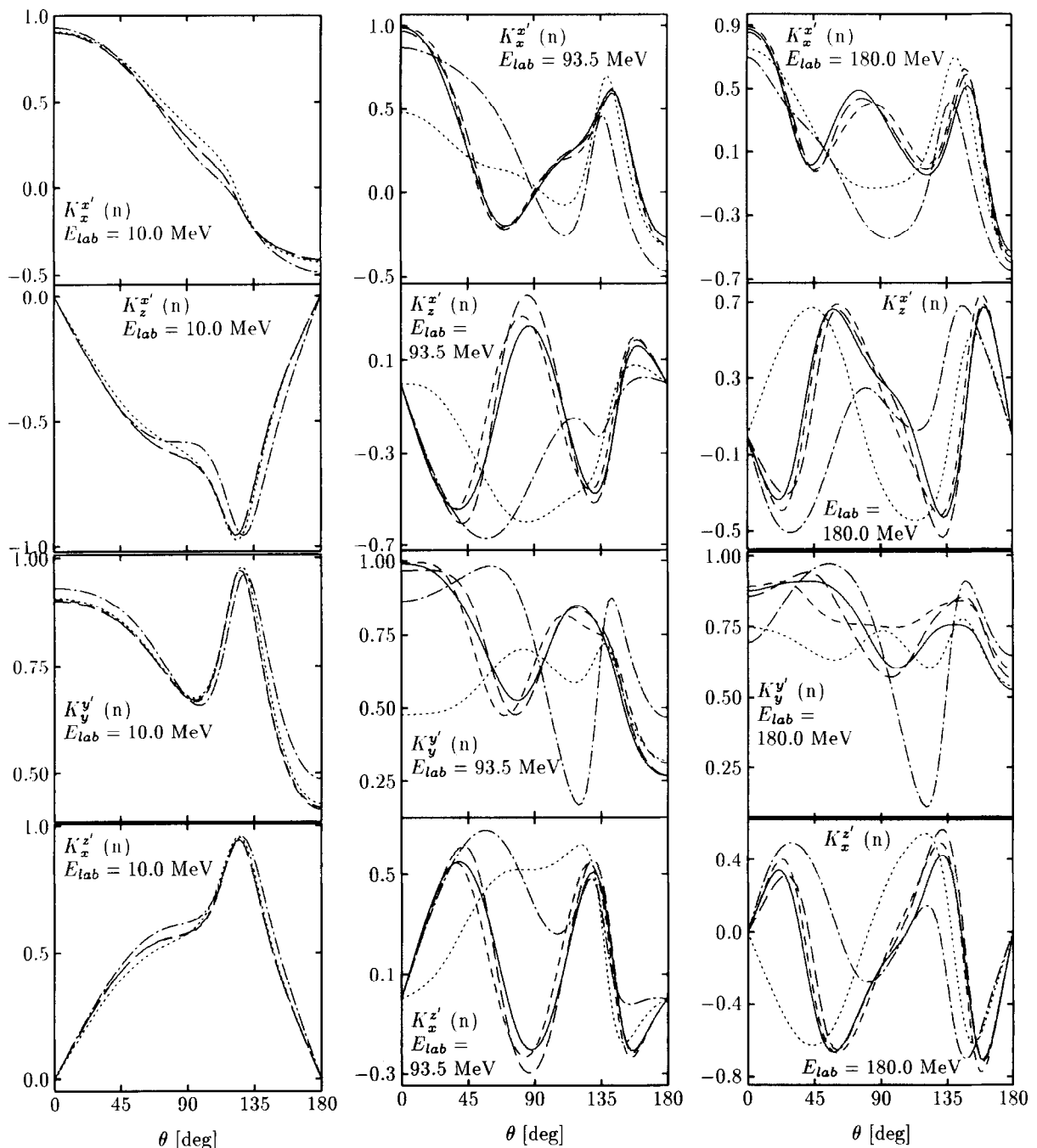


Fig. 18. The dependence of the nucleon to nucleon spin transfer coefficients $K_x^{x'}$, $K_z^{x'}$, $K_y^{y'}$, $K_x^{z'}$, and $K_z^{z'}$ for elastic Nd scattering on the NN force components used: "s-waves" ($- \cdot -$), $j_{max} = 1$ ($\cdots \cdots$), $j_{max} = 2$ ($- \cdot - \cdot$), $j_{max} = 3$ ($- \cdot - \cdot -$) and $j_{max} = 4$ ($- - -$).

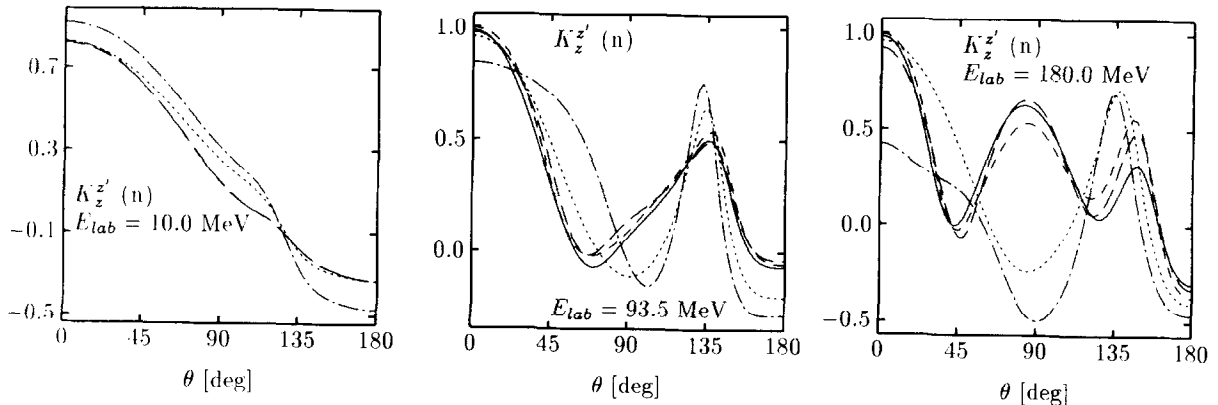


Fig. 18—continued.

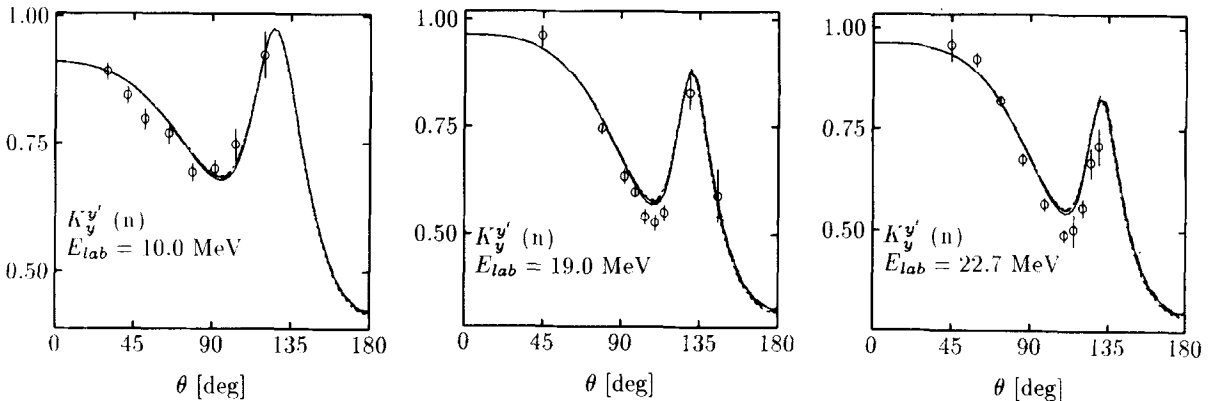


Fig. 19. The nucleon to nucleon spin transfer coefficient K_y' for elastic Nd scattering. Comparison of data with NN force predictions. 10 MeV: pd data (○) [457]. 19 MeV: pd data (○) [474]. 22.7 MeV: pd data (○) [89]. The NN force predictions are (—) Nijm I, (---) Nijm II, (- - -) Nijm 93, and (· · ·) AV18. Note that the zero on the y-axis is suppressed.

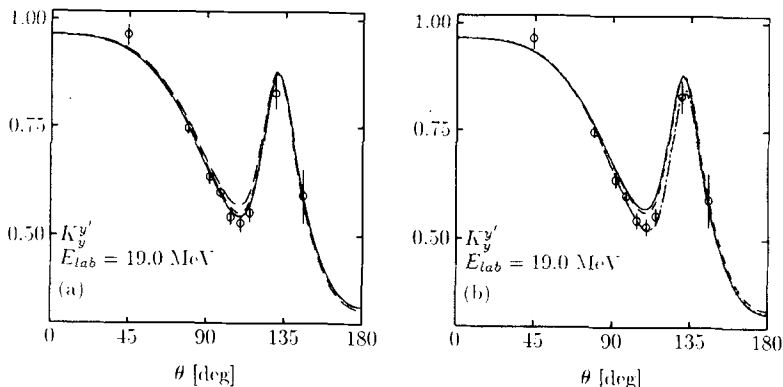


Fig. 20. Studies to the nucleon to nucleon spin transfer coefficient K_y' at 19 MeV: (a): (—) CD-Bonn, (---) Nijm I, and (- - -) Nijm I with the $^3S_1 - ^3D_1$ force of CD-Bonn; (b): (—) Nijm I, (---) Nijm 78, (- - -) Nijm I with the 1P_1 force of Nijm 78, and (· · ·) Nijm I with the 1P_1 and the $^3S_1 - ^3D_1$ force of Nijm 78. Data are taken from [474].

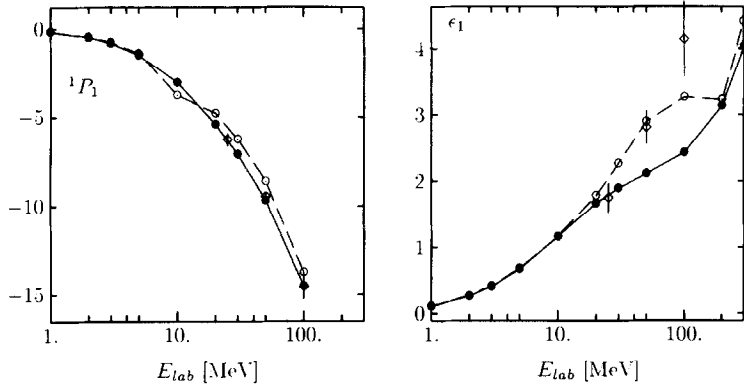


Fig. 21. PSA results for ϵ_1 and 1P_1 from two multi energy investigations: (●) Nijmegen [466] and (○) Virginia [417] and from selected energy intervals (◇) [224].

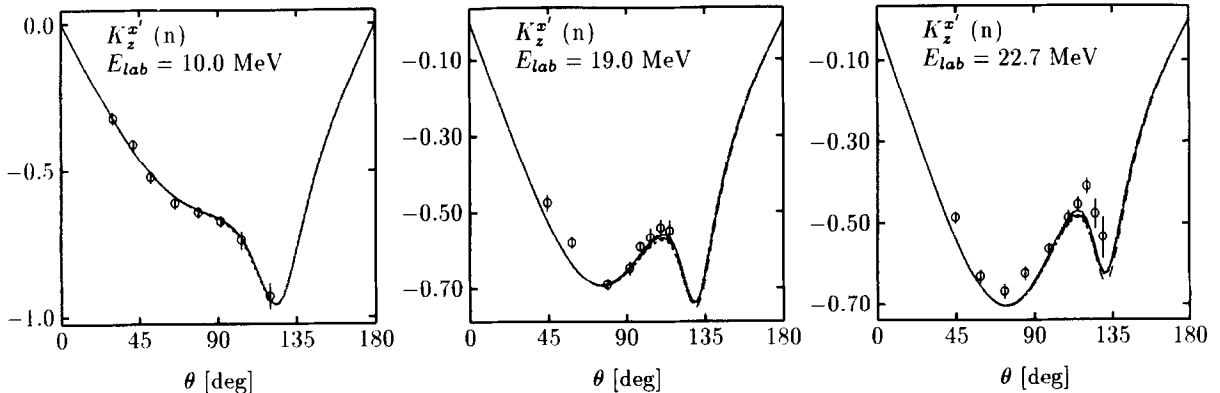


Fig. 22. The nucleon to nucleon spin transfer coefficient K_z' for elastic Nd scattering. Comparison of data with NN force predictions. 10 MeV: pd data (○) [457]. 19 MeV: pd data (○) [474]. 22.7 MeV: pd data (○) [300,301,186]. The NN force predictions are (—) Nijm I, (---) Nijm II, (- - -) Nijm 93, and (.....) AV18.

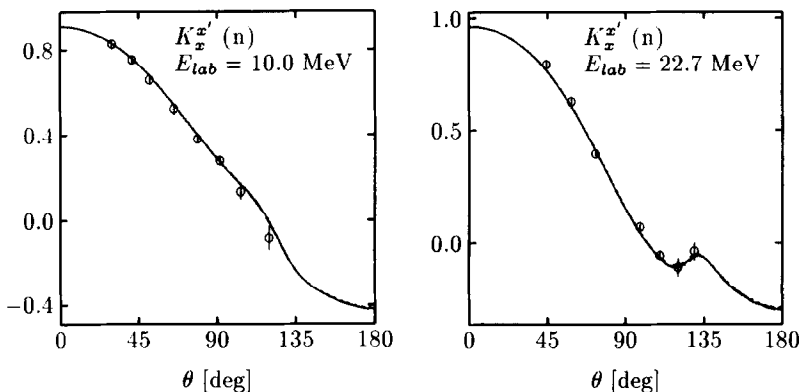


Fig. 23. The nucleon to nucleon spin transfer coefficient K_x' for elastic Nd scattering. Comparison of data with NN force predictions. 10 MeV: pd data (○) [457]. 22.7 MeV: pd data (○) [300,301,186]. The NN force predictions are (—) Nijm I, (---) Nijm II, (- - -) Nijm 93, and (.....) AV18.

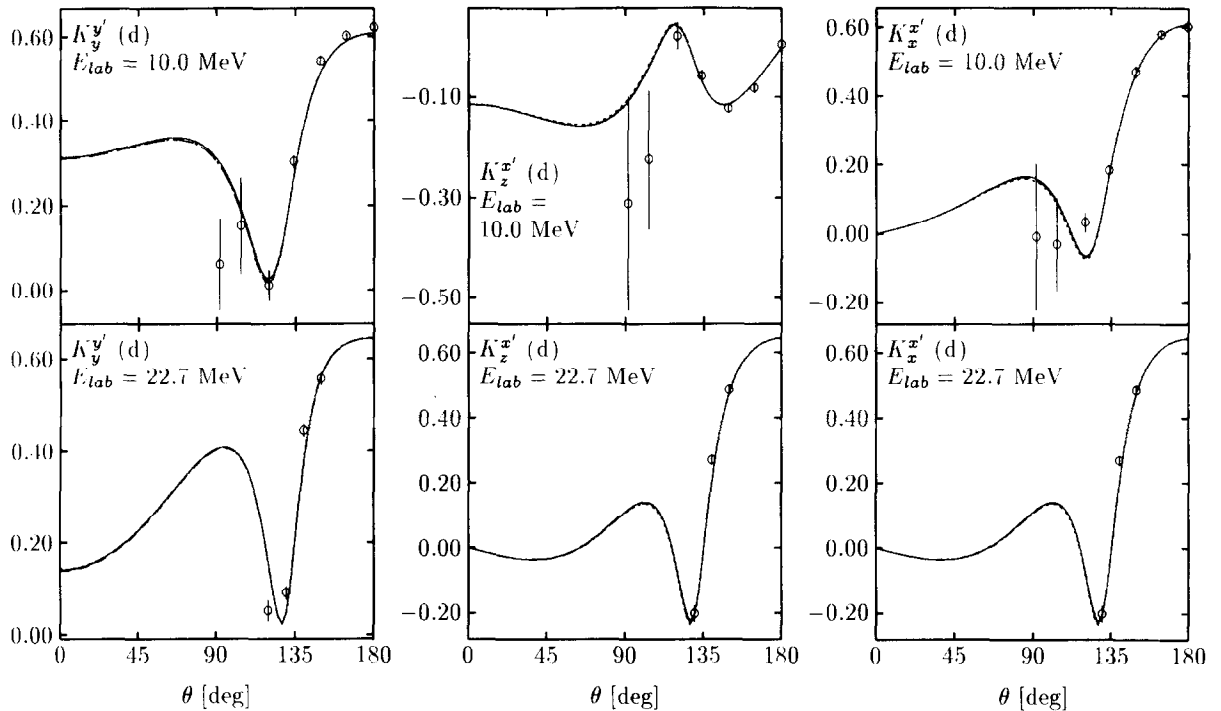


Fig. 24. Neutron to deuteron vector spin transfer coefficients for elastic Nd scattering. Comparison of data with NN force predictions. 10 MeV: pd data (\circ) [457]. 22.7 MeV: pd data (\circ) [300,301,186]. The NN force predictions are (—) Nijm I, (---) Nijm II, (- - -) Nijm 93, and (· · ·) AV18.

the smaller angles would be helpful to clarify even better the situation.

Finally the spin-transfer-coefficients $K_z^{y'z'}$, $K_z^{x'y'}$, $K_z^{x'x'} - K_y^{y'y'}$, $K_x^{x'y'}$, $K_x^{y'z'}$, $K_y^{x'z'}$, $K_y^{z'z'}$ from the nucleon to tensor polarized deuterons, have been measured. Among them $K_z^{y'z'}$, $K_x^{x'y'}$, and $K_y^{x'z'}$, show a remarkable sensitivity to 3P_j NN forces like A_y . Interestingly it is different from the one of A_y [177,178,517]. While the maximum in A_y at low energies decreases by weakening the strength of both the 3P_1 and $^3P_2 - ^3F_2$ force components and increases by weakening the 3P_0 strength, the weakening of the 3P_0 and 3P_1 forces acts similarly in $K_x^{x'y'}$ and $K_y^{x'z'}$ and the effects for $K_z^{y'z'}$ are different in relative strengths in comparison to A_y . This is displayed in Fig. 25. Therefore precise measurements of these observables at low energies could provide useful information on that pending problem of the 3P_j NN force components. Existing pd data at low energies where Coulomb force effects still might play a nonnegligible role are compared in Fig. 26 to various NN force predictions. The agreement is relatively good and all the NN forces lead essentially to the same results. Whether possible small discrepancies are Coulomb force effects or defects in the strong force remains open right now. Recent experimental data at the higher energy 22.7 MeV do not always cover all the angles where the observables show prominent structure as can be seen in Fig. 27. The agreement with theory is good except for $K_z^{y'z'}$ and $K_y^{x'z'}$. All of the existing data for spin-transfers are at low energies, none as far as we know exists around 60 or 140 MeV. It is interesting to note that some of these spin-transfer-coefficients show big 3NF effects at higher energies, see Section 7.8. Measurements would be important to fill that gap and exclude or detect surprises.

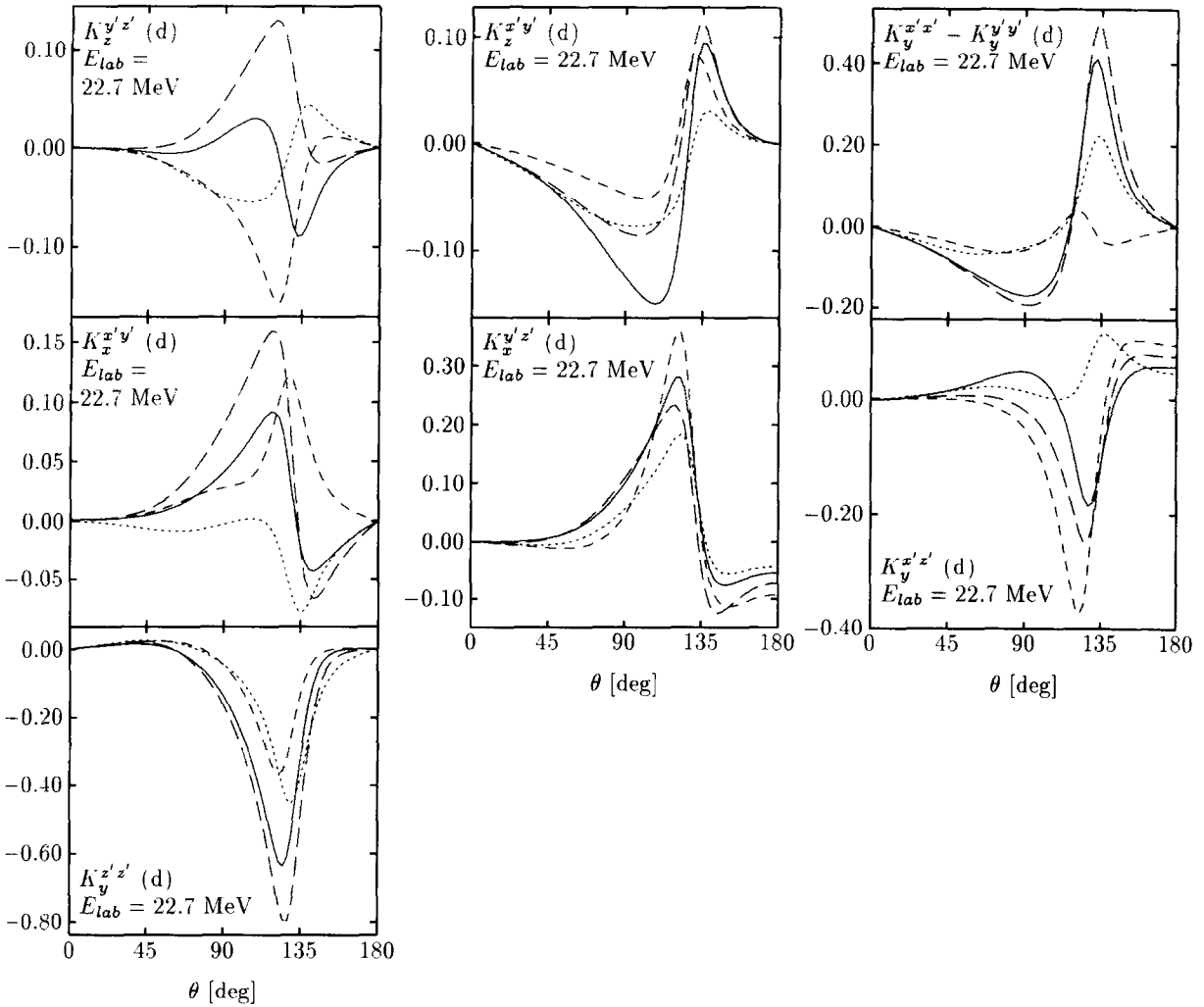


Fig. 25. The sensitivity of the nucleon to deuteron tensor spin transfer coefficients $K_z^{y'z'}$, $K_z^{x'y'}$, $K_y^{x'x'} - K_y^{y'y'}$, $K_x^{x'y'}$, $K_x^{y'z'}$, $K_y^{z'z'}$, and $K_z^{z'z'}$ for elastic Nd scattering on the 3P_j NN force components, which are switched off separately: (---) without 3P_0 , (----) without 3P_1 , and (.....) without $^3P_2 - ^3F_2$. Full calculations are given by the solid lines.

Spin correlation coefficients

There are many more spin observables in elastic Nd scattering, like spin correlation coefficients where in the initial state both, nucleon and deuteron, are polarized. A few spin correlation coefficients have already been measured and are displayed in Fig. 28. The agreement, with the exception of C_{yy} at 12 MeV, is mostly good, but also the quality of the data leave room for improvements. In Fig. 29 we show how C_{xx} , C_{yy} , and S depend on the NN force components. It is interesting to see that even at 10 MeV the $j = 2$ force components for S are absolutely crucial. At the highest energy even $j = 4$ forces are presumably not sufficient. We would like to further point out that some of the spin-correlation coefficients ($C_{xy,x}$, $C_{xx,y} - C_{yy,y}$ and $C_{yy,y}$) reveal at low energies (3 and 10 MeV) sensitivity to 3P_j NN force components (see Fig. 30). However the magnitudes of these observables are of the order

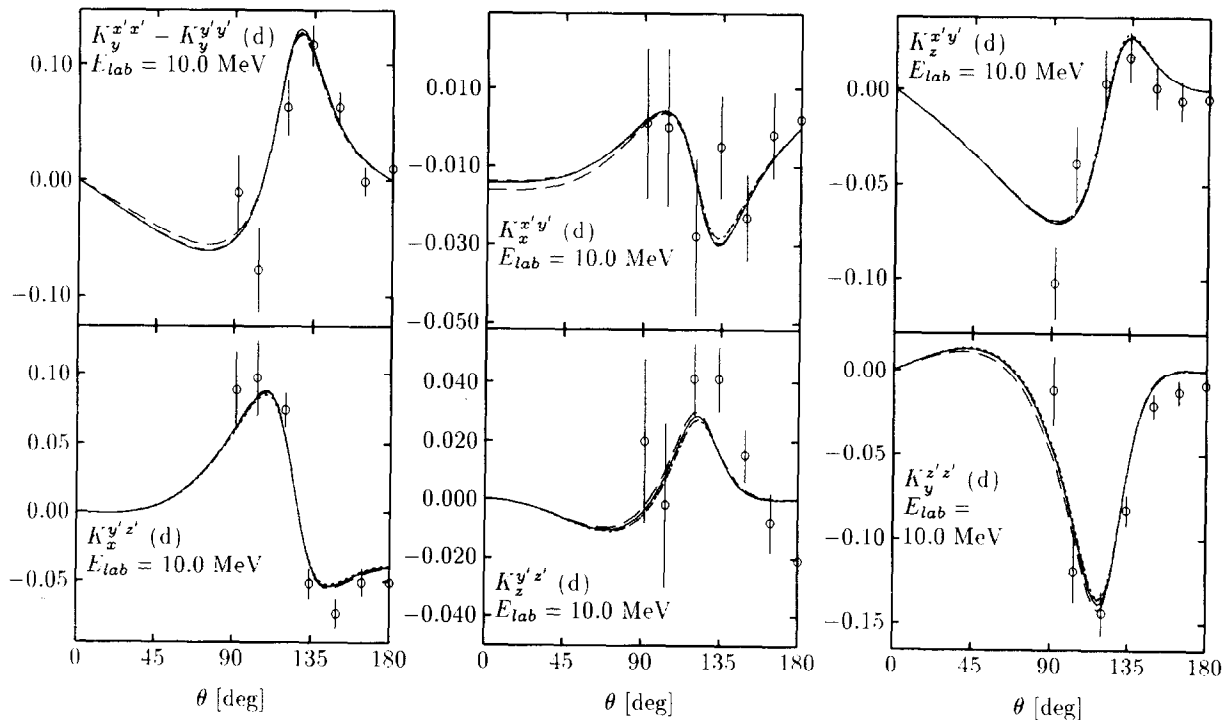


Fig. 26. The nucleon to deuteron spin transfer coefficients $K_y^{x'x'} - K_y^{y'y'}$, $K_x^{x'y'}$, $K_z^{x'y'}$, $K_x^{y'z'}$, $K_z^{y'z'}$, and $K_y^{z'z'}$ at the nucleon lab. energy of 10 MeV. Comparison of data with the NN force predictions: pd data (○) [457]; predictions Nijm I (—), Nijm II (---), Nijm 93 (- · -) and AV18 (·····).

of a few percent only. In addition C_{xx} and C_{yy} depend on 3NF effects showing interesting scaling behavior at low energies (see Section 6.2). At higher energies C_{zz} , $C_{yz,z}$ and $C_{yz,x}$ show also big 3NF effects, see Section 7.8.

Let us now regard the 3N breakup process.

6.1.3. 3N breakup process

Energy and momentum conservation reduces the number of independent momentum components of the final three nucleons to five. Thus using two detectors and measuring two particles in coincidence four angles are fixed and it remains to measure the energy of one of the two detected nucleons in order to fix the kinematics. Since, however, the relation between the energies of the two detected particles is not unique and allows for two solutions, see Section 2.4, one usually has to measure both energies. Let us number the two detected nucleons in such a kinematically complete experiment by 1 and 2. Thus the allowed energies E_1 and E_2 are restricted to lie on a curve, as already explained in Section 2.4. In reality the angular and energy resolutions of the detectors, the finite size of the target and the energy resolution of the beam itself, broaden the curve into a band, especially in case of nd breakup. Now one could also fill that band with theoretical events by performing corresponding simulations and compare contents of certain segments thereof to experimental data. Since the statistical errors would be too large, this has never been done. Instead the experimental data are projected, following special procedures, onto a central curve situated in the middle of the band and corresponding to

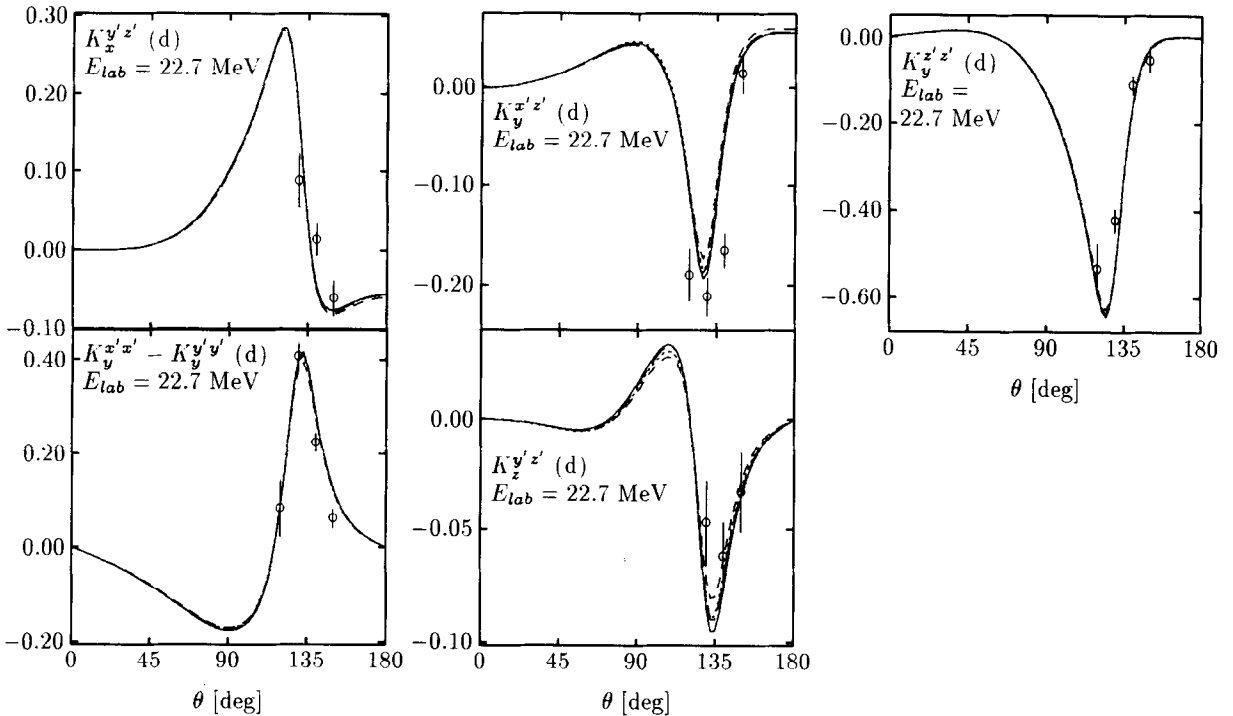


Fig. 27. The nucleon to deuteron spin transfer coefficients $K_x^{y'z'}(d)$, $K_y^{x'z'}(d)$, $K_y^{z'z'} - K_y^{x'x'}(d)$, $K_z^{y'z'}(d)$, $K_z^{y'z'}(d)$ at the nucleon lab. energy of 22.7 MeV. Comparison of data with the NN force predictions: pd data (○) [300], [301], [186]; predictions Nijm I (—), Nijm II (---), Nijm 93 (- - -) and AV18 (· · · · ·).

point geometry and zero energy resolutions. Different groups are using quite different projection procedures. We refer the interested reader to original articles [535,191,263,192,135,354], where various procedures are described. Ideally theory should be handled in much the same manner as the data. This requires however extensive numerical studies, since all the causes for the width of the band have to be simulated. In the case of the pd breakup process usually the two protons are detected and the experimental conditions can be kept rather close to point geometry. Thus averaging of the theoretical data has there little effect, except for observables which show a strong variation in their angular or energy dependence, like e.g. final state interaction peaks [397,9].

Two breakup configurations stick out, since they have a simple two-body reaction mechanism underneath and historically have been analyzed in corresponding rough approximations [83,496,304]. This is the quasifree scattering (QFS) process, where in the final state one nucleon is at rest in the lab. system. The simple minded picture is, that the projectile interacts with one of the two constituents of the deuteron and the other is a spectator. We shall see that this simple mechanism is not at all true below about 100 MeV, but that rescattering among all three particles is strongly present. The other configuration is, when two particles leave the interaction region with equal momenta. Then there is strong final state interaction between the two. Their relative energy is zero and the NN t-matrix at zero energy is strongly enhanced, both in the np as well as in the nn system, due to the nearby pole in the state 1S_0 . This leads to the so-called final state interaction (FSI) peak. In reality the peak height is not only determined by the NN t-matrix describing that interacting pair but also by the production

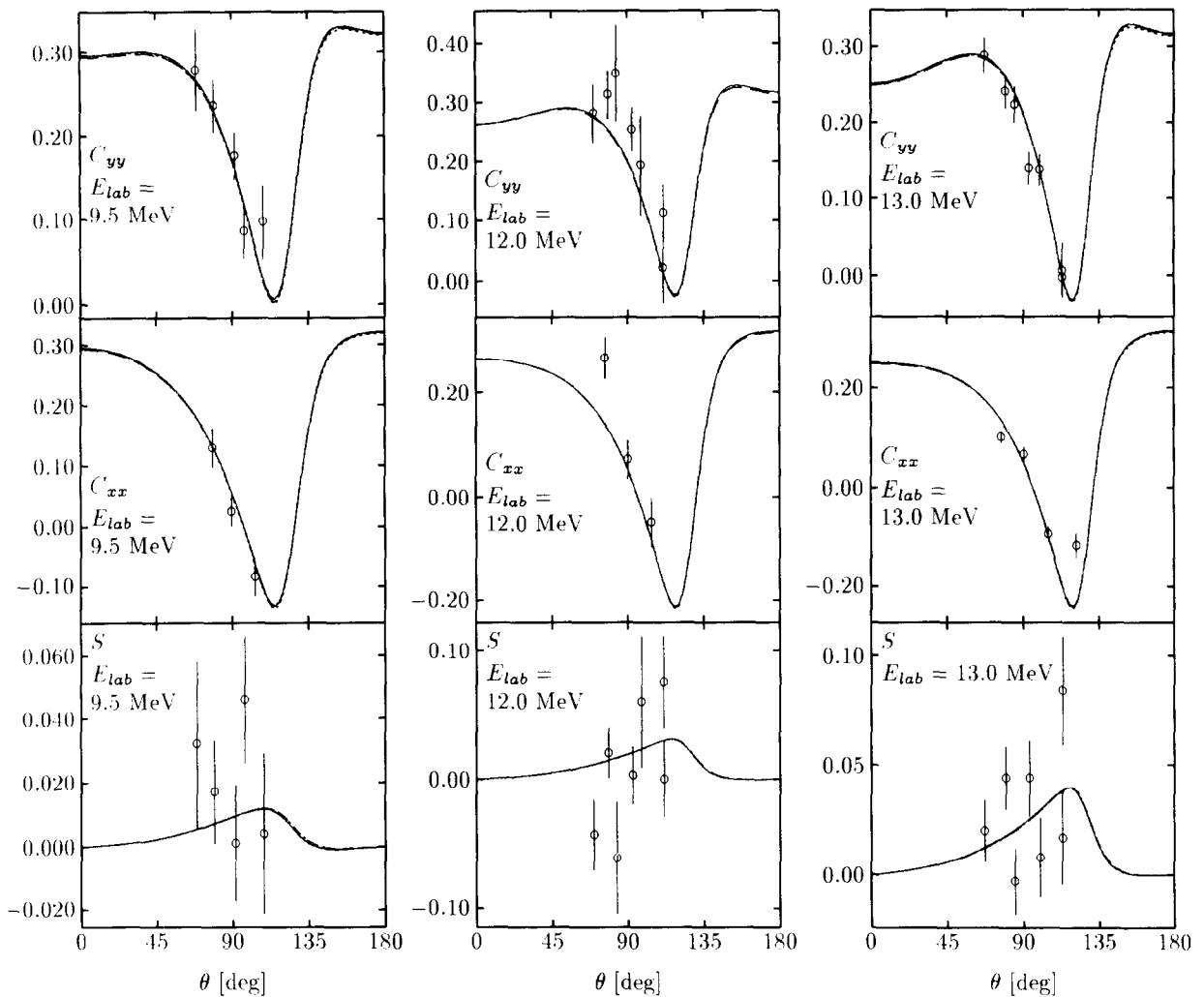


Fig. 28. The spin correlation coefficients C_{yy} , C_{xx} , and S for elastic Nd scattering at various nucleon lab. energies. Comparison of data with the NN force predictions: pd data (\circ) [80]; predictions are Nijm I (—), Nijm II (---), Nijm 93 (- - -) and AV18 (· · · · ·) at 9.5 and 13 MeV and Nijm I (—) and AV18 (---) at 12 MeV.

amplitude for this specific configuration. That amplitude varies with the angle under which that pair leaves with respect to the beam axis.

Two more configurations found special interest, the collinear one [264,311,158,529,358,53,56,473, 263,101] and the star configuration [275,462]. In the collinear case one nucleon is at rest in the center of mass system, consequently the other two leave back to back. The line on which the three final nucleons are moving can have any angle to the beam axis. In the star configuration the three nucleons have equal energies and interparticle angles of 120° in the center of mass system. The plane spanned by the three nucleons can have any orientation with respect to the beam axis. If orthogonal to the beam axis that configuration is often called the space star; if the beam axis lies in that plane one speaks of coplanar stars. These two configurations were expected [334] to be especially good

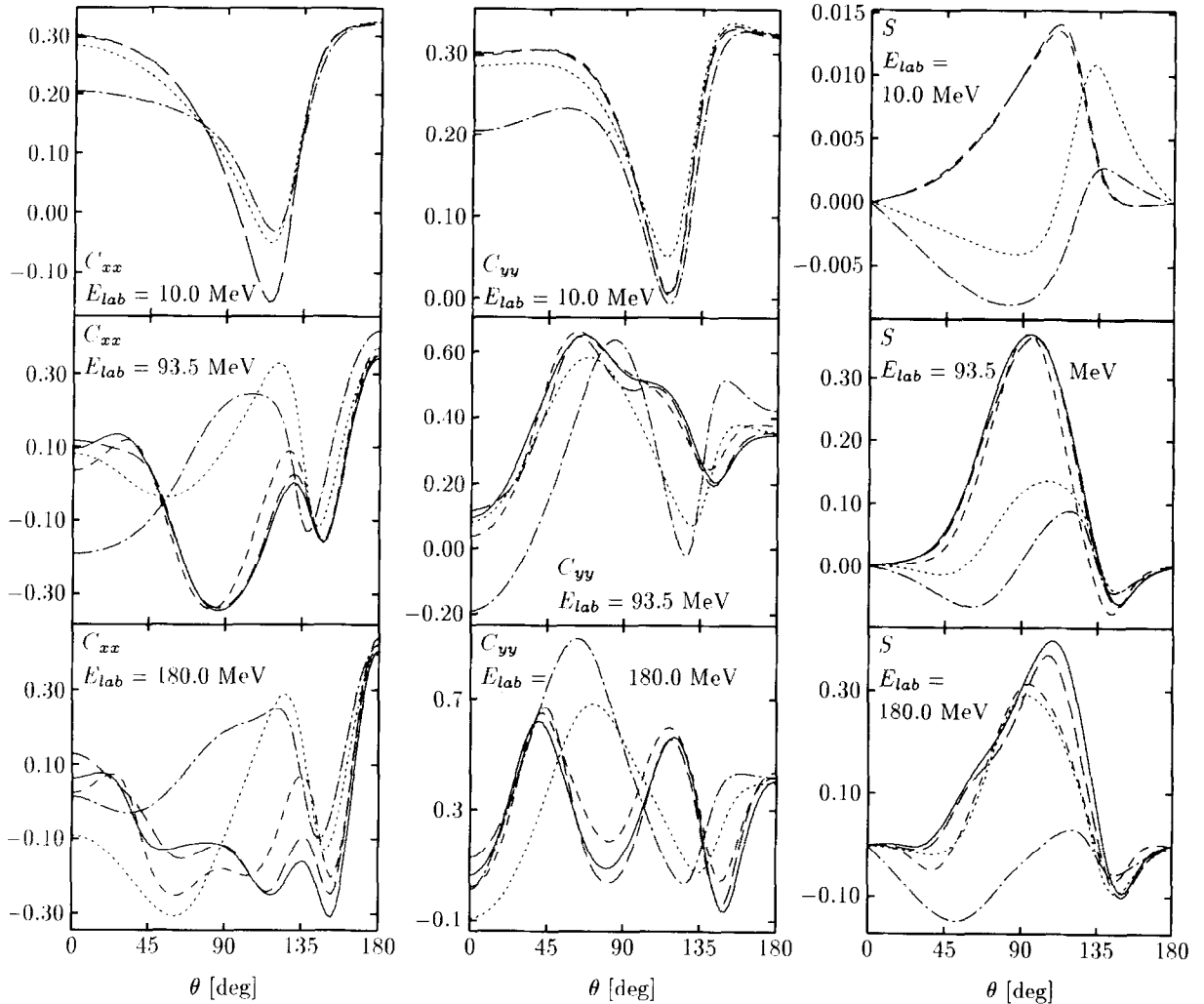


Fig. 29. The dependence of the spin correlation coefficients C_{xx} , C_{yy} , and S for elastic Nd scattering on the NN force components used: "s-waves" ($\cdots\cdots$), $j_{max} = 1$ ($\cdot\cdot\cdot$), $j_{max} = 2$ ($-\cdot-\cdot$), $j_{max} = 3$ ($--$) and $j_{max} = 4$ ($-$ —).

candidates to see effects of 3NF's. One reason was that the most simple 3NF, the $\pi - \pi$ exchange with an intermediate Δ [157], has the property, that it is repulsive when the three nucleons lie on a line and attractive, when they are at the corners of an equilateral triangle [35,63]. This refers to the spin-isospin averaged 3N potential. (More precisely the force is repulsive whenever one angle within the triangle formed by the three nucleons is larger than 90° and attractive otherwise). In how far that expectation is realized we shall discuss in Section 6.2.

In Fig. 31 we display the loci of three special configurations (FSI, QFS, Coll) in the space of the lab. angles θ_1 and θ_2 ($\phi_{12} \equiv \phi_2 - \phi_1 = 180^\circ$).

Clearly there is a continuum of angular positions of the two detectors and the still nameless ones might carry surprises and even more information about the potential energy of the three nucleons than the above mentioned traditional ones. Therefore a full 4π study, covering all possible configurations,

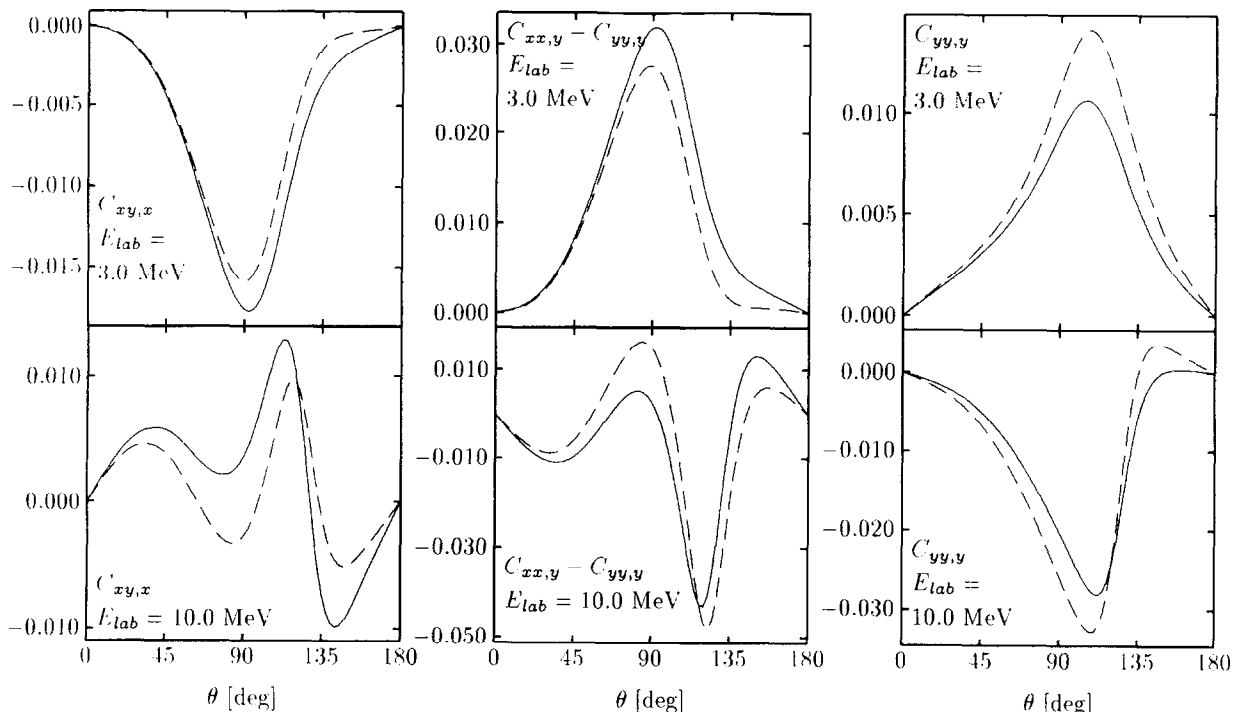


Fig. 30. The dependence of the spin correlation coefficients $C_{xy,x}$, $C_{xx,y} - C_{yy,y}$ and $C_{yy,y}$ on the 3P_j NN force components: (—) Bonn B and (---) 3P_j pp-np modified Bonn B [517].

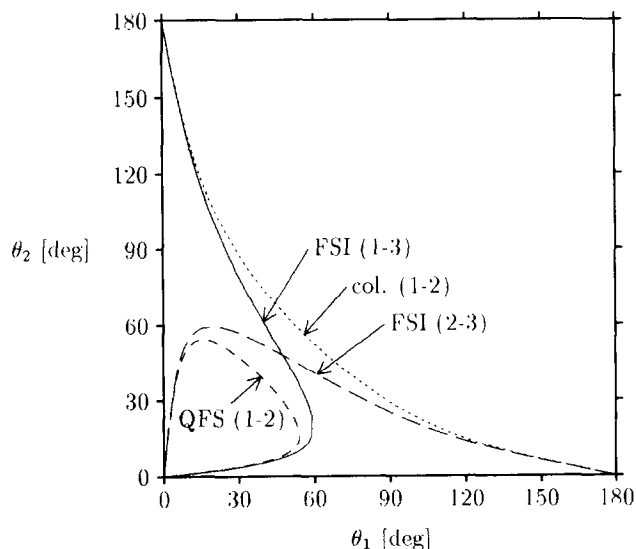


Fig. 31. Loci in the θ_1 - θ_2 -plane ($\phi_{12} = 180^\circ$) of the breakup configurations at $E_{lab} = 13$ MeV for the FSI(1-3), FSI(2-3), QFS(1-2) and collinear(1-2) conditions.

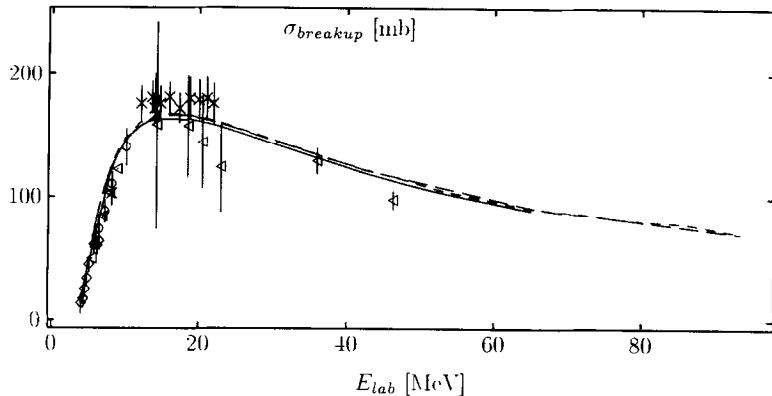


Fig. 32. The total nd breakup cross section. Comparison of data ((○): [77], (◇): [229], (×): [367], (△): [436]) and theory (—): AV18, (---): Paris, (- - -): Bonn B.

would be highly welcome.

Besides the kinematically complete measurements there are also incomplete ones, where for instance only one's particle momentum is detected. Clearly such measurements carry less information than kinematically complete ones, since one has to sum over all underlying configurations, which accompany that special event of the singled out momentum of one nucleon. Because of its relative simplicity quite a few measurements of that type exist in the literature. We mention [469,441,213,305,290,443,291], [37]. See also [487] for a recent theoretical analysis.

Let us now come to results, first just for cross sections; later we shall also regard spin observables. The situation will be seen to be rather controversial. There are cases of spectacular agreement and cases of striking disagreement. Certainly what is missing, is a well established and confirmed data basis and right now nearly always only one measurement for a certain breakup configuration exists.

The total breakup cross section

We compare in Fig. 32 data for the total breakup cross section to theory. The quality of the data is not satisfactory and one might see at energies below 10 MeV a discrepancy, which, however, we think does not reflect the real situation. We saw that the differential cross sections in elastic scattering are very well described at all the angles at which they have been measured. Unfortunately, the data do not cover the full angular range well enough to determine the total elastic cross section correspondingly well. Otherwise we think that the total breakup cross section, which is the difference between the total cross section and the one of elastic scattering, both of which are perfectly well described by theory, should also coincide very well with theory. Stronger efforts on the experimental side would be very welcome to nail down at least the total breakup cross section much more precisely.

Quasi free scattering

The approximation lowest order in t neglecting any rescattering is according to Eq. (154)

$$T \approx tP \quad (218)$$

Then the breakup amplitude is

$$\langle \phi_0 | (1 + P) T | \phi \rangle \approx \langle \phi_0 | (1 + P) tP | \phi \rangle$$

$$= \langle \phi_0 | t_1 | \phi \rangle_2 + \langle \phi_0 | t_1 | \phi \rangle_3 + \langle \phi_0 | t_2 | \phi \rangle_3 + \langle \phi_0 | t_2 | \phi \rangle_1 + \langle \phi_0 | t_3 | \phi \rangle_1 + \langle \phi_0 | t_3 | \phi \rangle_2 \quad (219)$$

The indices at the ket vectors denote the singled out nucleon which carries the relative momentum \mathbf{q}_0 in the channel state $|\phi\rangle = |\varphi_d\rangle |\mathbf{q}_0\rangle$.

Because of the antisymmetry of $|\varphi_d\rangle$ this can be written more compactly as

$$\langle \phi_0 | (1 + P) t P | \phi \rangle = \langle \phi_0 | (1 - P_{23}) t_1 | \phi \rangle_2 + \langle \phi_0 | (1 - P_{13}) t_2 | \phi \rangle_3 + \langle \phi_0 | (1 - P_{12}) t_3 | \phi \rangle_1 \quad (220)$$

It is also a fairly easy exercise to evaluate that further with the result

$$\begin{aligned} \langle \phi_0 | (1 + P) t P | \phi \rangle &= \sum_{m'_3 \nu'_3} {}_a \langle \mathbf{p} m_2 m_3 \nu_2 \nu_3 | t \left(E - \frac{3}{4m} \mathbf{q}^2 \right) | \mathbf{q}_0 + \frac{1}{2} \mathbf{q} m_N m'_3 \nu_N \nu'_3 \rangle \\ &\times \langle -\frac{1}{2} \mathbf{q}_0 - \mathbf{q} m'_3 m_1 \nu'_3 \nu_1 | \varphi_d \rangle \\ &+ \sum_{m'_1 \nu'_1} {}_a \langle -\frac{1}{2} \mathbf{p} - \frac{3}{4} \mathbf{q} m_1 m_3 \nu_1 \nu_3 | t \left(E - \frac{3}{4m} (\mathbf{p} - \frac{1}{2} \mathbf{q})^2 \right) | \frac{1}{2} \mathbf{p} + \mathbf{q}_0 - \frac{1}{4} \mathbf{q} m'_1 m_N \nu'_1 \nu_N \rangle \\ &\times \langle -\mathbf{p} + \frac{1}{2} \mathbf{q} - \frac{1}{2} \mathbf{q}_0 m'_1 m_2 \nu'_1 \nu_2 | \varphi_d \rangle \\ &+ \sum_{m'_2 \nu'_2} {}_a \langle -\frac{1}{2} \mathbf{p} + \frac{3}{4} \mathbf{q} m_1 m_2 \nu_1 \nu_2 | t \left(E - \frac{3}{4m} (\mathbf{p} + \frac{1}{2} \mathbf{q})^2 \right) | -\frac{1}{2} \mathbf{p} + \mathbf{q}_0 - \frac{1}{4} \mathbf{q} m_N m'_2 \nu_N \nu'_2 \rangle \\ &\times \langle \mathbf{p} + \frac{1}{2} \mathbf{q} - \frac{1}{2} \mathbf{q}_0 m'_2 m_3 \nu'_2 \nu_3 | \varphi_d \rangle \end{aligned} \quad (221)$$

where $|\mathbf{p} m_2 m_3 \nu_2 \nu_3\rangle_a \equiv (1 - P_{23}) |\mathbf{p} m_2 m_3 \nu_2 \nu_3\rangle$, etc. Let us choose QFS conditions, assuming for instance $\mathbf{k}_1^{\text{lab}} = 0$. This is equivalent to $\mathbf{q} = -\frac{1}{2} \mathbf{q}_0$, which puts the argument of the deuteron state in the first term of Eq. (221) to zero. Under this condition the accompanying two-nucleon t-matrix is on shell, except for a negligible ϵ_d correction. Namely

$$E - \frac{3}{4m} \mathbf{q}^2 = \frac{3}{4m} \mathbf{q}_0^2 + \epsilon_d - \frac{3}{4m} \frac{1}{4} \mathbf{q}_0^2 = \frac{(\frac{3}{4} \mathbf{q}_0)^2}{m} + \epsilon_d \quad (222)$$

is the energy related to the initial momentum $\mathbf{q}_0 + \frac{1}{2} \mathbf{q} = \frac{3}{4} \mathbf{q}_0$ and this is also the energy related to the final momentum \mathbf{p} since $E - (3/4m) \mathbf{q}^2 = (1/m) \mathbf{p}^2$. Thus the first term under QFS condition is the product of an on-shell two-nucleon t-matrix (except for ϵ_d corrections) and the deuteron state at zero momentum. In the other two terms the two-nucleon t-matrices are off-shell under this condition and also the argument of the deuteron state is different from zero. Of course choosing $\mathbf{k}_2^{\text{lab}} (\mathbf{k}_3^{\text{lab}}) = 0$ the second (third) term in (221) would take over the corresponding role. If q_0 is sufficiently large either the off-shell decrease of t or decrease of φ_d with increasing momentum or both render the contributions of the second and third term in (221) and the first one sticks out.

It is advisable and for higher energies (100 MeV and above) much more economic not to expand the arguments in the t-matrix and the deuteron wave function into spherical harmonics with respect to \hat{p} , \hat{q} , and \hat{q}_0 , but to calculate the terms in Eq. (221) which involves no integration, exactly. Thus we put

$$\begin{aligned} T|\phi\rangle &= t P |\phi\rangle_{\text{wpw}} + (T - t P) |\phi\rangle_{\text{pw}} \\ \langle \phi_0 | U_0 | \phi \rangle &= \langle \phi_0 | (1 + P) T | \phi \rangle = \langle \phi_0 | (1 + P) t P | \phi \rangle_{\text{wpw}} + \langle \phi_0 | (1 + P) (T - t P) | \phi \rangle_{\text{pw}} \end{aligned} \quad (223)$$

The index wpw stands for "without partial wave decomposition", whereas pw means the treatment based on partial wave decomposition as described in Section 3. Of course the t-matrix t is still built up by partial wave contributions up to a certain j_{max} . Also note that in the last term in Eq. (223) the partial wave representation refers only to $(T - tP)|\phi\rangle$ and not to the permutation operator P in $(1 + P)$, which of course is applied to the left and thus treated without truncation.

Now varying q around the QFS point the argument of φ_d differs from zero and the first term decreases in magnitude. Thus we expect to see a peak. This first term in (221) $\langle\phi_0|tP|\phi\rangle$ alone is often referred to [83,293] as the impulse approximation. The corresponding breakup cross sections are displayed in Fig. 33 for various energies and indeed reveal a characteristic peak. In this figure we did not fix p and vary just q but we fixed two detector angles and varied the energy distribution around the QFS condition. This leads to changes in both, p and q .

Now we add the other two terms corresponding altogether to

$$\langle\phi_0|U_0|\phi\rangle_{FIA} \equiv \langle\phi_0|(1 + P)tP|\phi\rangle \quad (224)$$

Here in this article we shall call that whole term full impulse approximation (FIA). This causes only a small shift (see Fig. 33). At 65 MeV and higher it is negligible. Then we add (without using Padé) rescattering terms of first order in t , which amounts to

$$T\phi \rightarrow tP\phi + tPG_0tP\phi, \quad (225)$$

then rescattering terms including the integral kernel twice etc. Always all the permutations are carried out as usual according to the j_{max} chosen (see Fig. 33). Clearly that multiple scattering series diverges at 19 and 65 MeV. At the two higher energies shown it converges essentially after the first order rescattering term (except in the wings for 140 MeV, where the second order effect is visible). The correct final value, as given by the solution of Eq. (154), exhibits also a peak, but its height and width is different from the one of the impulse approximation at 19 and 65 MeV. Even at 140 and 220 MeV the impulse approximation overshoots the correct result by about 20%, which is due to the first order rescattering term. We quantify the contributions of the first few terms in the rescattering series (not using Padé) on top of the impulse approximation in Fig. 34. There we show the corresponding QFS peak heights as a function of energy. Already at around 100 MeV the second order rescattering contribution can be neglected, but the first order one remains significant till the highest energy considered. The reason for the strong divergence at 19 and 65 MeV lies solely in the amplitude for $J'' = 1/2^+$. If one drops the $1/2^+$ amplitude the wild behavior disappears and it is only in the wings at 19 MeV that the higher orders contribute significantly. Moreover the $1/2^+$ contribution gets less important with increasing energy [515] already around 65 MeV. At 140 and 220 MeV the $1/2^+$ contribution can be safely neglected. Nevertheless it should be noted that the multiple scattering series for $J'' = 1/2^+$ diverges also at the higher energies 65, 140 and even 220 MeV. However correctly summed up by Padé its value is negligible in comparison to the sum of all other amplitudes for $J'' \neq 1/2^+$. The dominant contributions shift to higher J 's with increasing energy.

Let us now analyze a series of measurements we are aware of. They are displayed in Fig. 35 for energies between 10 and 65 MeV. It is again interesting to see the agreement among the different NN force predictions. Except for 65 MeV theory is always too high. Since these are all pd data the discrepancies at the lower energies might be due to Coulomb force effects [11]. We shall come back to that point in Section 8.5.

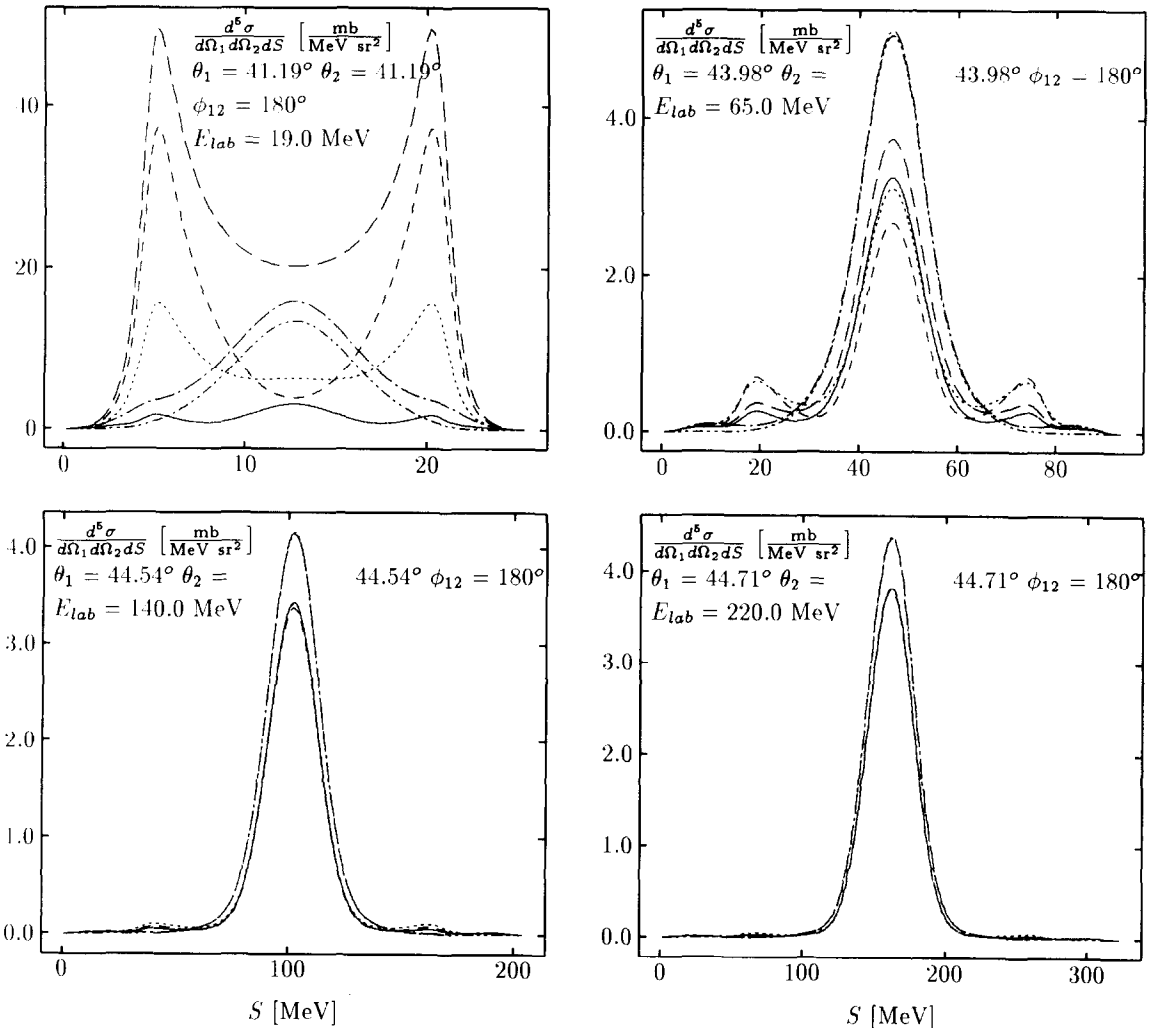


Fig. 33. Comparison of different approximations to the full calculation for nn QFS breakup cross sections: impulse approximation (· · · · ·), full impulse approximation (FIA) (— · — ·), with rescattering correction up to first order (····), second order (·····) and third order (·····) in t in comparison to the full calculation (——).

Final state interaction peaks

Now let us regard final state interaction peaks. This has always been an important issue, since it is considered to provide information on the nn scattering length. We shall come back to that aspect in Section 7.2.

A quantitative description of the FSI peak requires not only s-wave interactions but also higher angular momenta force components. This is demonstrated in Fig. 36. We see that s-wave forces alone are totally insufficient. At 10 MeV $j \leq 2$ forces suffice, however not at 65 MeV where $j \leq 3$ force effects are quite noticeable and reduce the peak height.

From the expression for T which ends to the left with $t(z)$ it is obvious that with the two-body energy z going to zero T has a characteristic energy variation $\mathcal{O}(1/\sqrt{z} + i\kappa)$, where $\kappa^2 = |E_V|$ is

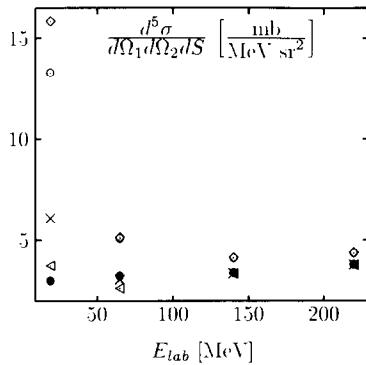


Fig. 34. The energy dependence of the nn QFS peak heights in impulse approximation (\circ), in full impulse approximation (\diamond), with rescattering correction of first order (\times) and second order (\square) in t in comparison to the full calculation (\bullet).

about 100 keV. That wave number κ is inversely proportional to the scattering length. Therefore the larger the scattering length the larger the peak height. It seems therefore obvious that nn and np t-matrices should be distinguished if one is interested in seeing differences between np and nn scattering lengths. Therefore in the isospin formalism a full treatment has to be undertaken as described in Section 3, namely on top of the total isospin $T = 1/2$ also $T = 3/2$ states have to be included. We show in Fig. 37 results of four calculations based on Bonn B for nn and np FSI peak heights as a function of the lab. production angle of the pair interacting in the final state. One just uses Bonn B, which has been fitted to the np system, thus has a scattering length $a(^1S_0) = a_{np}$. The second uses a modified Bonn B with $a(^1S_0) = a_{pp}^{\text{strong}}$. The third allows for different np and nn t-matrices in the state 1S_0 but neglects a $T = 3/2$ admixture and uses just the effective t-matrix

$$t_{eff} = \frac{2}{3}t_{nn} + \frac{1}{3}t_{np} \quad (226)$$

following from (160). The fourth calculation is based on a full and correct treatment allowing for a $T = 3/2$ admixture. All the four curves are clearly distinguishable, with the exception of small angular regions. In any case it is clearly seen how important it is to use the full treatment ($T = 3/2$) to extract from the peak height the value of a_{nn} (see Section 7.2 for more quantitative details).

In the past often a Watson–Migdal approximation [496,341,190] has been used to extract the nn scattering length from FSI peaks in the nd breakup process. In that approximation, based on a representation of the Jost function [256], one factorizes the absolute square of the breakup amplitude into an energy independent constant N and an enhancement factor. Thus the breakup cross section has the form

$$\frac{d\sigma}{d\hat{k}_1 d\hat{k}_2 dS} = k_s N (\frac{1}{2}r_0)^2 \frac{p^2 + (1/r_0 + \sqrt{1/r_0^2 - 2/r_0 a})^2}{p^2 + (-1/a + \frac{1}{2}r_0 p^2)^2} \quad (227)$$

where r_0 and a are the effective range and scattering length parameters for the nn system and p is the relative momentum of the two neutrons. This form has been fitted to the experimental cross sections in the FSI peak area with the aim to extract a and r_0 .

We investigated the reliability of that procedure in the following manner. Pseudodata were generated in a Faddeev calculation using the Nijm93 potential and allowing for different np and nn forces in the state 1S_0 . For nn we choose $a_{nn} = -17.58$ fm and $r_0 = 2.81$ fm. Then we generated nn FSI peaks at

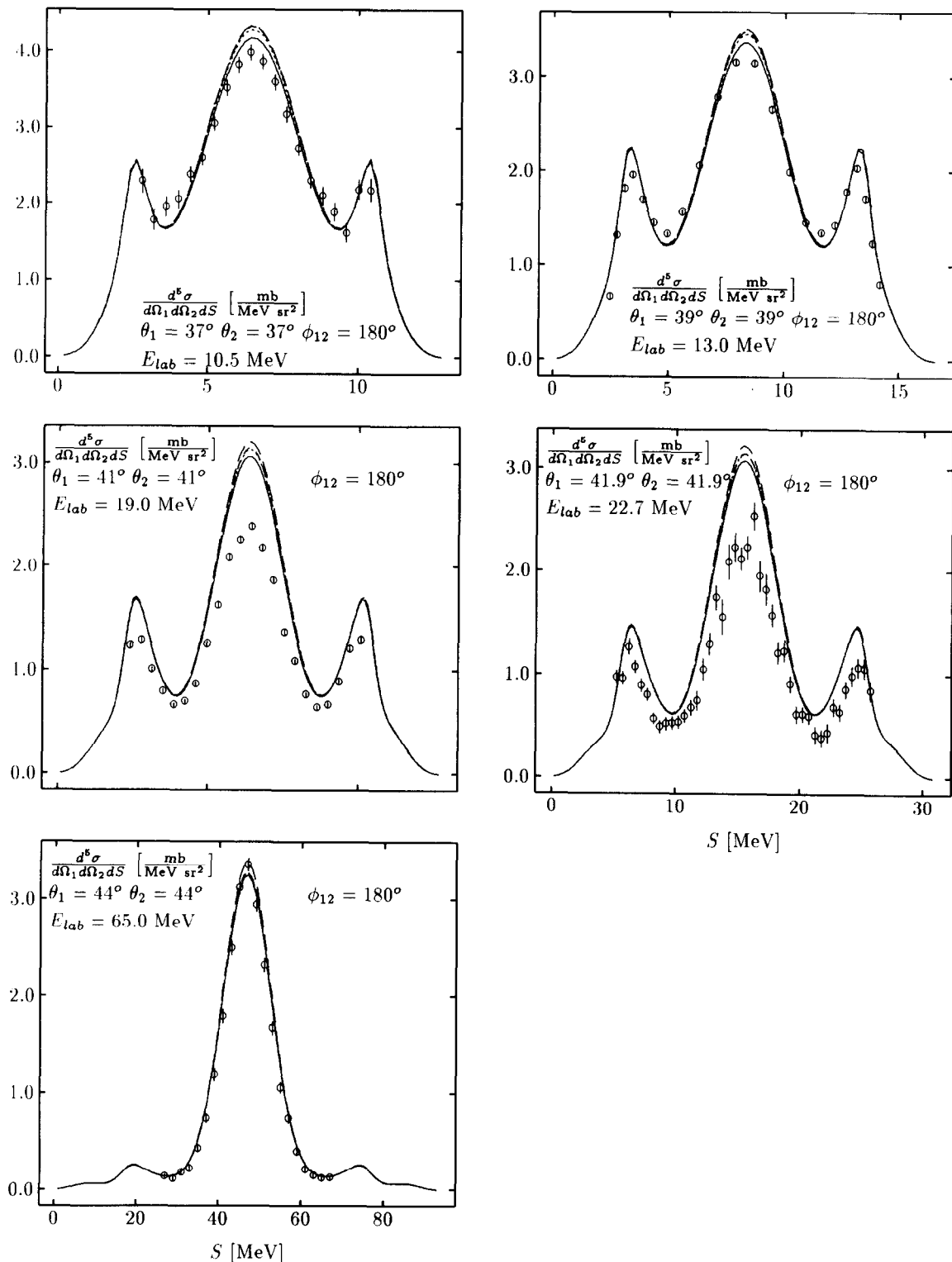


Fig. 35.

Table 10

The Watson–Migdal formula fits to FSI peaks generated at 22.7 MeV with the Nijm93 NN force for various production angles θ . ΔE denotes the maximal relative energy up to which the fit has been performed, a and r_0 the resulting optimal scattering length and range parameters (see text). The numbers in parenthesis results if r_0 is fixed at the correct value 2.81 fm.

θ [deg]	ΔE [MeV]	a [fm]	r_0 [fm]
5	1.0	−17.1(−17.1)	2.8
10	0.5	−17.2(−17.1)	2.7
15	2.0	−17.6(−17.5)	2.7
20	0.1	−17.7(−17.7)	2.7
25	0.3	−17.6(−17.6)	2.7
30	0.1	−17.6(−17.6)	2.7
35	0.2	−17.5(−17.5)	2.7
40	0.1	−17.5(−17.5)	2.6
45	0.1	−17.5(−17.4)	2.7
50	0.1	−17.4(−17.3)	2.7
55	0.1	−17.2(−17.2)	2.8
60	0.1	−17.1(−17.0)	2.8
65	0.1	−17.5(−17.5)	2.8

all lab. production angles θ of the nn pair in steps of 5°. For each angle the approximate form (227) was fitted to the FSI peaks allowing N , a and r_0 to vary. Within the peak area one can restrict the adjustment to different ranges of the maximal relative energy ΔE of the two neutrons. It should be restricted to small values of ΔE , since the form (227) contains a representation of the Jost function valid for $p \rightarrow 0$. On the other hand one cannot use a too small ΔE interval since in praxis there will be not sufficient data points due to the experimental energy resolution. Thus we investigated the adjustment within the range 100 keV $\leq \Delta E \leq$ 3 MeV. Within that range starting from $\Delta E = 3$ MeV downwards we determined for each ΔE the optimal fit by means of a χ^2 criterion. For most production angles the χ^2 reached a minimum within that interval, which we have chosen to be the optimal adjustment. As an example we display in Table 10 the results achieved at $E_{lab} = 22.7$ MeV. We see that at several angles the minimum in χ^2 is not reached for $\Delta E > 100$ keV. The extracted a_{nn} ranges between −17.1 and −17.7 fm and r_0 between 2.6 and 2.8 fm and are within 0.4 fm and 0.1 fm to the correct input values for a_{nn} and r_0 , respectively. We display in Fig. 38 the fits for the two extreme cases at $\theta_1 = 5^\circ$ and 20° , which look both equally good. If one fixes $r_0 = 2.81$ fm, which is the input value, the adjustment of a_{nn} leads to very similar results, as also shown in Table 10. We repeated that study also for $E_{lab} = 13$ MeV and 65 MeV and found the ranges −17.0 to −17.8 fm and −17.5 to −17.8 fm, respectively. The effective range parameters varied between 2.6–2.9 fm and 2.7–2.8 fm, respectively. Again one ends up with about 0.5 fm to 0.3 fm variations to the correct value of a_{nn} . Also the results turned out to be similar again when allowing r_0 to vary or keeping it fixed at the right value. From that study one can conclude that the Watson–Migdal analysis is not

Fig. 35. Breakup cross sections under QFS conditions. Comparison of $d(p, pp)n$ data (10.5 MeV: (○) [350]; 13 MeV: (○) [397]; 19 MeV: (○) [366]; 22.7 MeV: (○) [530]; 65 MeV: (○) [11]) to different NN potential predictions (AV18 (—), Nijm 93 (−−−), Nijm I (· · ·) and Nijm II (····)).

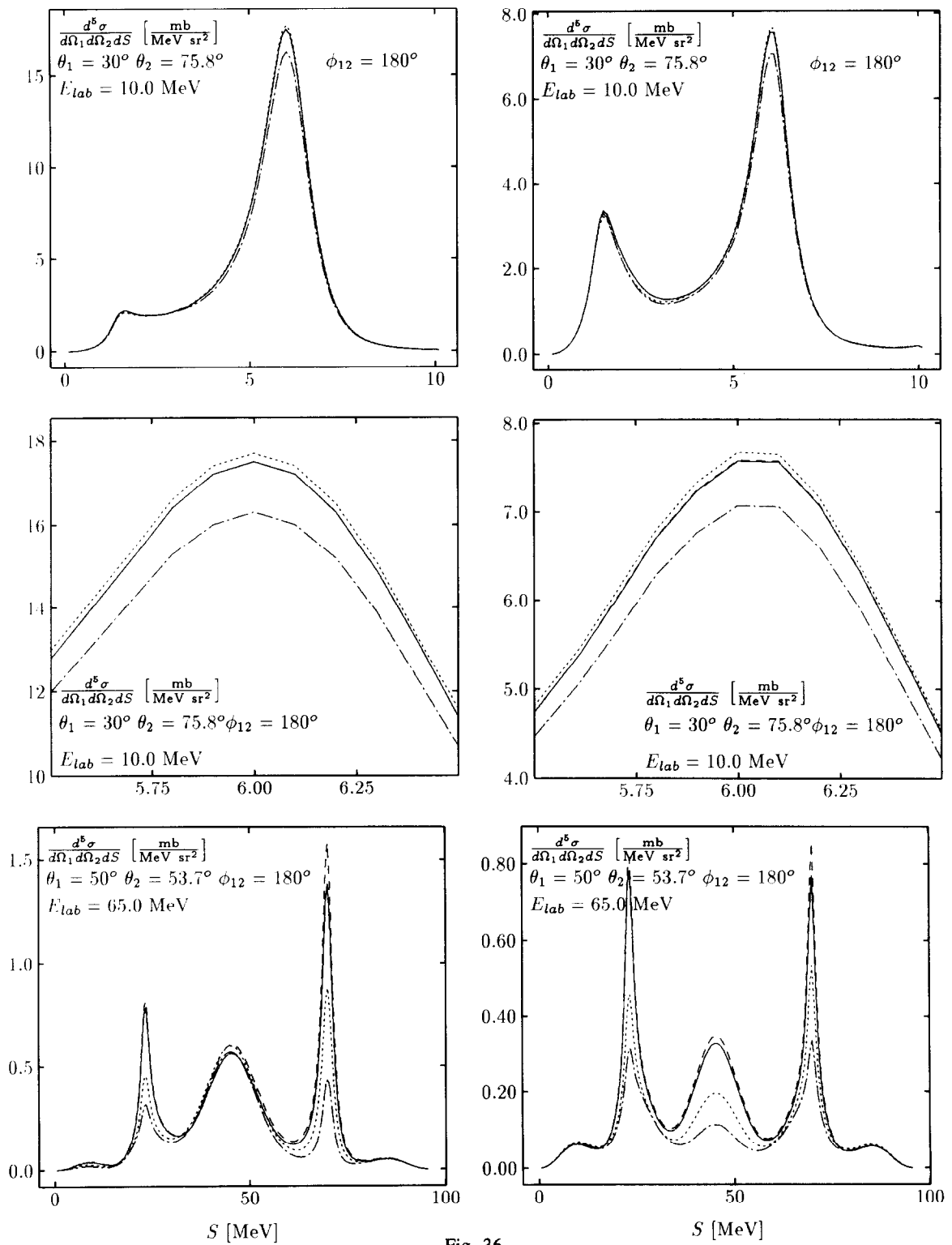


Fig. 36.

unreasonable, if one is satisfied with an inherent uncertainty of not better than about 0.5 fm. To contribute quantitatively to the question of CSB between a_{pp}^{strong} and a_{nn} one will, however, require smaller uncertainty and an analysis based on modern Faddeev calculations should be preferred.

Fig. 36. The contribution of various NN force components to the breakup cross section in a nn FSI peak (left side) and a np FSI peak (right side): s-waves ($\cdots\cdots$), $j \leq 1$ ($\cdot\cdot\cdot\cdot$), $j \leq 2$ ($- - -$), and $j \leq 3$ (—). The NN force is Bonn B. The pictures in the second row are zooms of the FSI peaks in the first row.

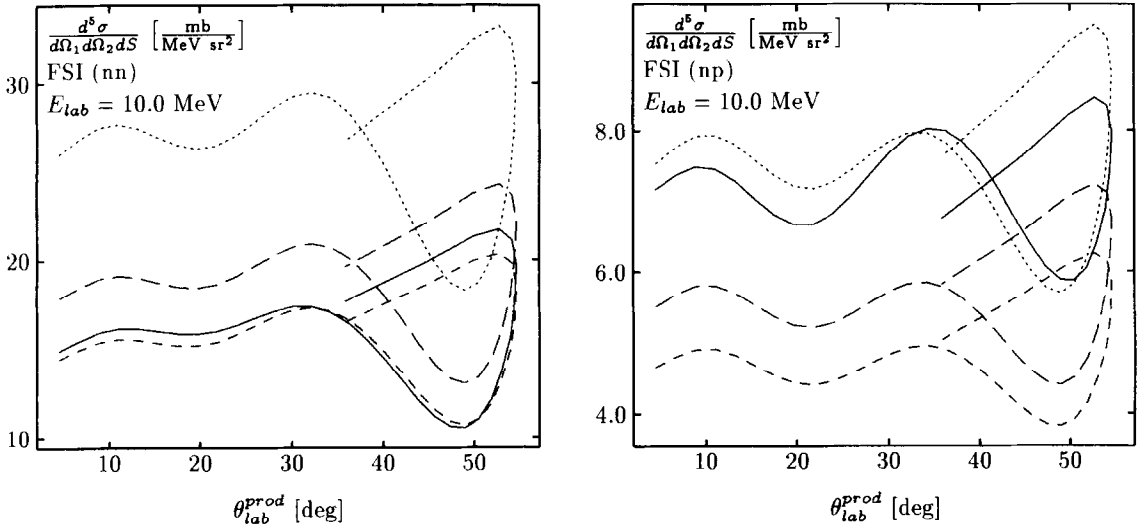


Fig. 37. Different treatments of CIB in the nn (a) and np (b) FSI peak: ($\cdot\cdot\cdot\cdot$) np 1S_0 force, ($- - - -$) nn 1S_0 force, ($- - -$) nn and np 1S_0 forces used via (226) without $T = 3/2$ admixture, (—) nn and np 1S_0 forces including $T = 3/2$ admixtures.

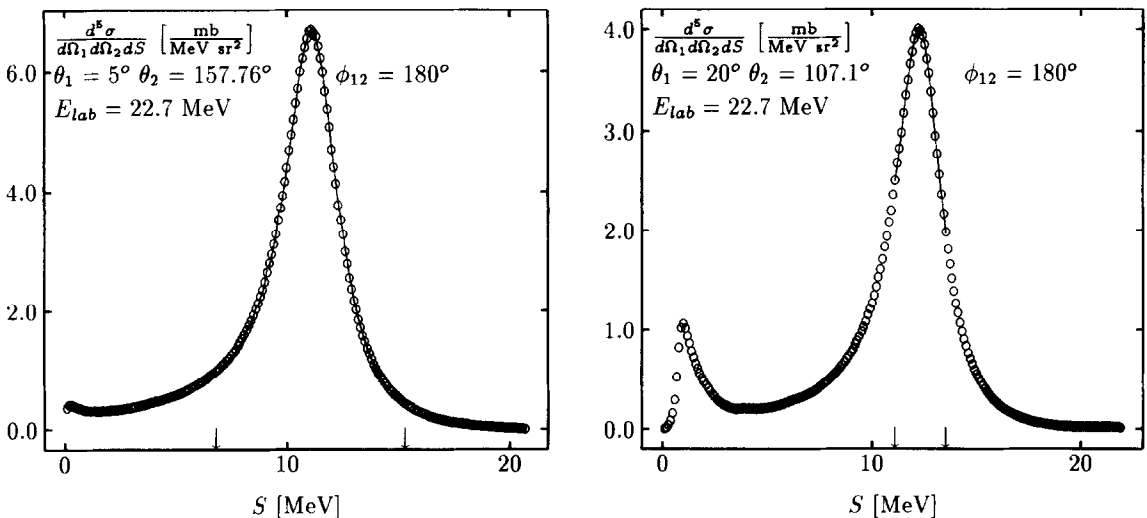


Fig. 38. Watson–Migdal approximations to nn FSI peaks for two production angles. The fits (solid curves) used all the pseudodata (open circles) located between the arrows.

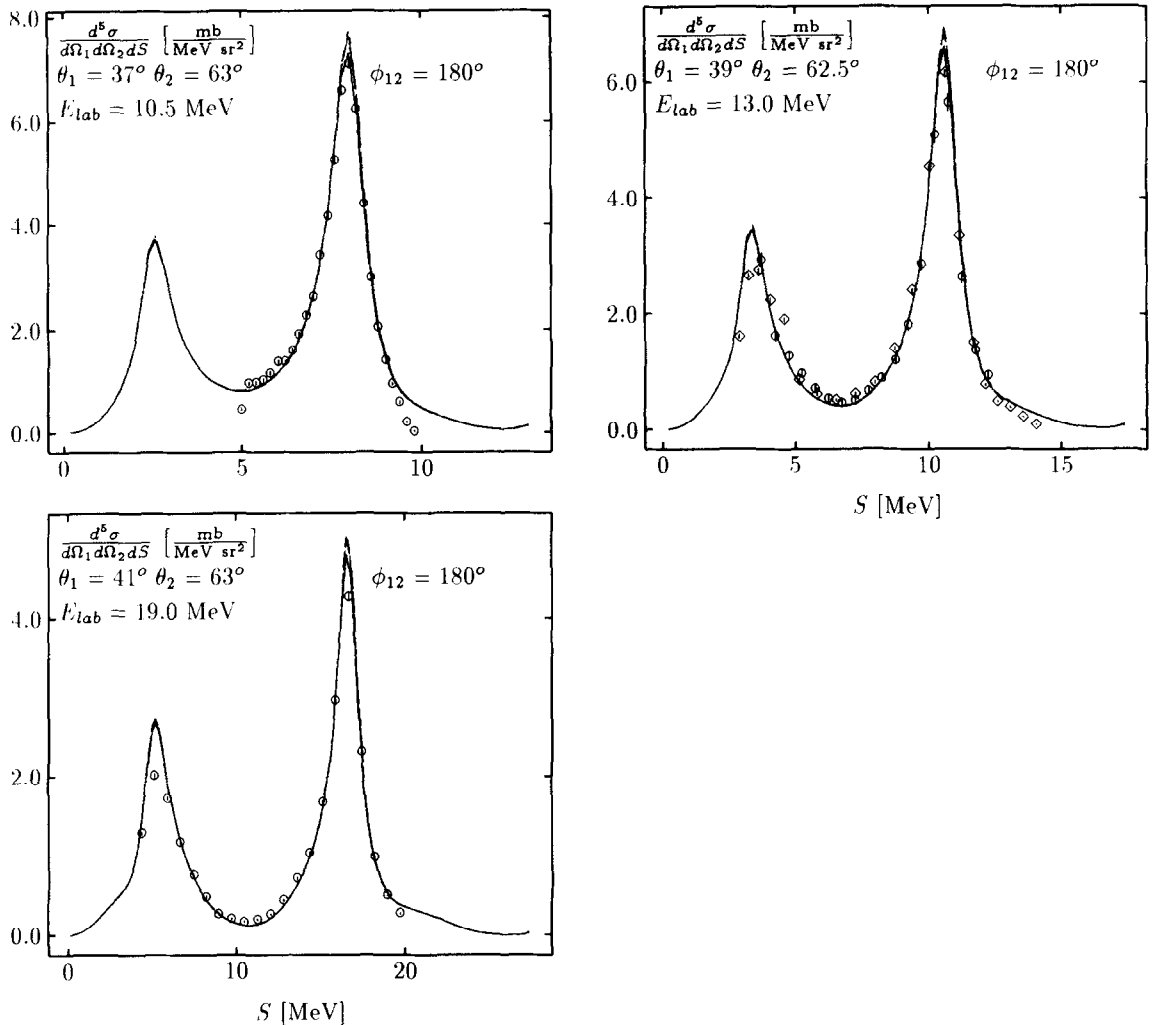


Fig. 39. Breakup cross sections under np FSI conditions (right peaks). Comparison of data (10.5 MeV: pd data (\circ) [203]; 13 MeV: nd data (\circ) [470,471], pd data (\diamond) [397]; 19 MeV: pd data (\circ) [366]) to NN force predictions (AV18 (—), Nijm 93 (---), Nijm I (- - -) and Nijm II (· · ·)).

Let us now compare theory to experimental pd and nd results containing np FSI peaks in Fig. 39. Since the np scattering length is known there is no adjustment possible (small variations in the nn 1S_0 force would have no effect on the np FSI peak). The agreement with the data is very good in the FSI peak area, especially if theory has been averaged according to the experimental conditions [397,203,366].

In case of nn FSI peaks highly involved projectings are required, which for measurements at 10.3 and 67 MeV [302] and at 13 MeV [485] are still in progress. We shall come back to another nd measurement at 13.0 MeV in Section 7.2. Quite a few of nn FSI peak measurements have been published in the past [534,59,65,535,509]. Unfortunately their documentation is so insufficient (no data given in tables and not sufficient information in order to set up a realistic simulation) that none of them can be analyzed by the modern Faddeev calculations using realistic NN forces. These old

data have been analyzed by highly insufficient tools and those results should be taken with great caution. We shall come back to that problem of analyzing the nn FSI peak in Section 7.2.

Collinear configurations

In the past [358] there arose interest whether or not any special effects occur under collinearity conditions. This question has been studied again more recently in [470,512,397,518,9,434]. These more recent data are compared to theory in Fig. 40. While the pd data like the theory show no peculiarity at all at and around the point of collinearity, the nd data show in one case a hump. In general the agreement between data and theory is quite good. There are however small deviations at all energies, the strongest one at 8 MeV and a final judgement has to wait until Coulomb force effects will be under control. Clearly the hump of the nd data at 13 MeV should be checked by another independent measurement. Preliminary data taken at TUNL for the same configuration show no hump [485]. Possible 3NF effects under the condition of collinearity will be discussed below in Section 6.2.

Star configurations

The space star configuration has been proposed in [275] as a promising place to search for 3NF effects. The argument was that the breakup cross section in that configuration is insensitive to the choice of NN forces, which however at that time were only simple s-wave interactions. In reality higher NN force components contribute significantly as is shown in Fig. 41. We see that s-wave forces are not sufficient and at the higher energies $j \leq 2$ forces must be included. Nevertheless the claim of [275] remains true also for all the present day realistic NN forces. This is seen in Fig. 42, where data are compared to the various NN force predictions. At 10.5 MeV theory agrees fairly well with one set of nd data [462], but disagrees strongly with the other one [136]. Also the pd data lie clearly below the nd data and the theory. Similarly at 13 MeV the situation appears controversial. The nd [470,512,471,516] and pd [397] data differ strongly and theory lies in between. The nd data have been remeasured [486] and support the older nd data. Thus there appears to be a problem with theory based on NN forces only. At 19 MeV [366] the pd data are slightly below theory. Finally the pd data at 65 MeV agree quite well with theory based on NN forces only. A very first estimation of Coulomb force effects for this particular configuration will be mentioned in Section 8.5. Another possible shift of theory caused by 3NF effects will be discussed in Section 6.2. A final judgement, however, is possible only if the pp Coulomb forces have been rigorously incorporated and well confirmed nd data will be available.

The plane for the star configuration can have any orientation with respect to the beam axis. Data in the nd and pd systems for coplanar configurations, which contain the beam axis, are shown in Fig. 43. The nd data at 13.0 MeV deviate strongly from theory [512], while the pd data at 22.7 MeV agree perfectly. The nd data at 13.0 MeV have been remeasured and are presently being analyzed [484]. Preliminary results show a good agreement with theory and consequently disagreement with the old data. This underlines that a solidly confirmed set of data is badly needed, in order to come to definite conclusions. At 65 MeV the pd data [536] and theory show some discrepancy, which possibly is related to Coulomb force effects.

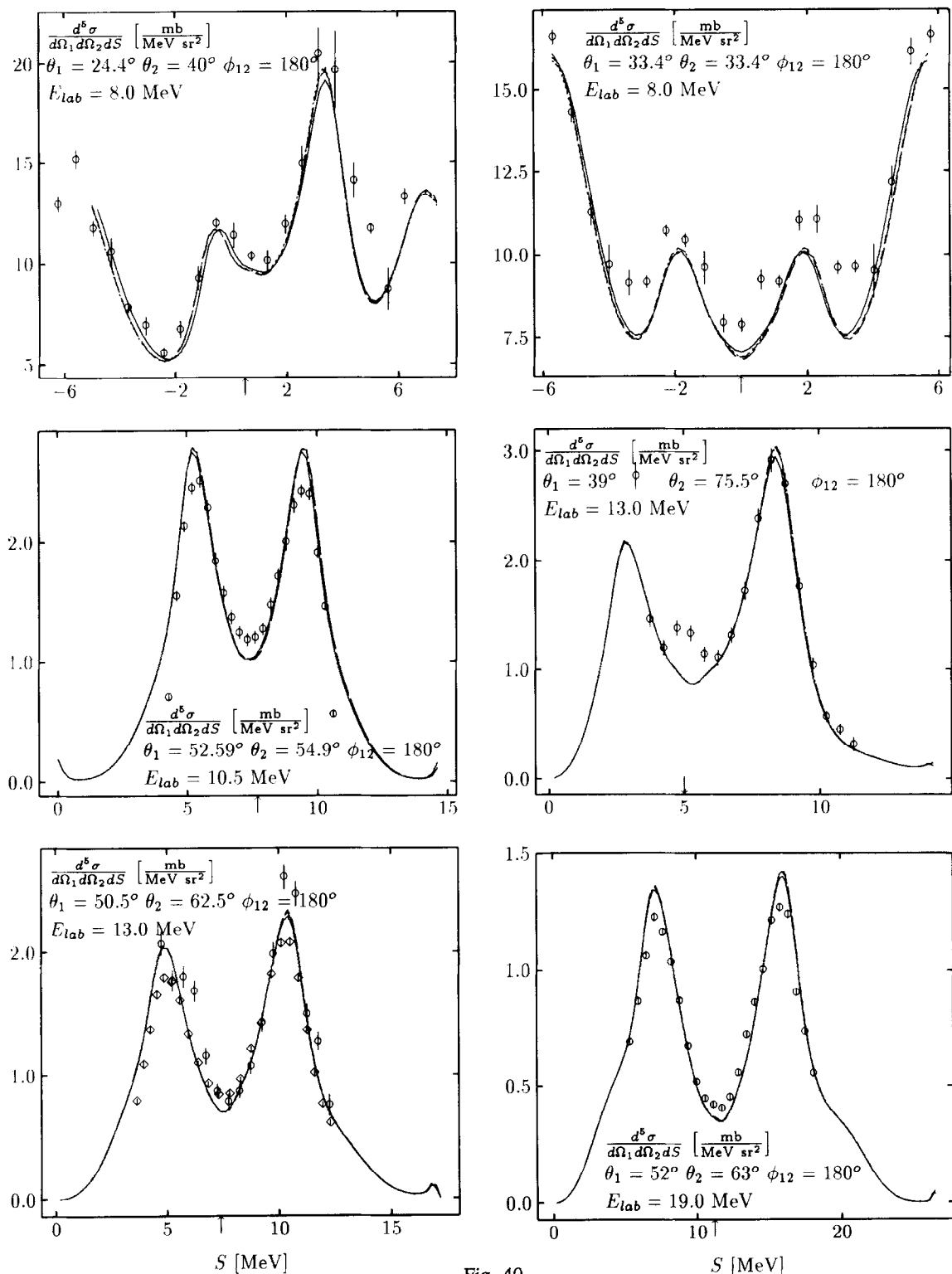


Fig. 40.

Other configurations

Breakup configurations have been proposed which exhibit destructive interference minima [323]. They are defined by fixed values of the final state NN relative energies and a fixed value of the momentum of one of the emerging nucleons. This defines an one-dimensional kinematical locus and the configurations are named "constant relative-energy-loci". For simple s-wave NN force models the breakup cross section was shown to be dominated by one of the two doublet state (total 3N spin $S = 1/2$) amplitudes in which the two identical nucleons are coupled to spin zero, if the relative energies and the fixed momentum is chosen in a particular way. Such configurations were at the same time claimed [275] to be most sensitive to various s-wave NN force models. A special

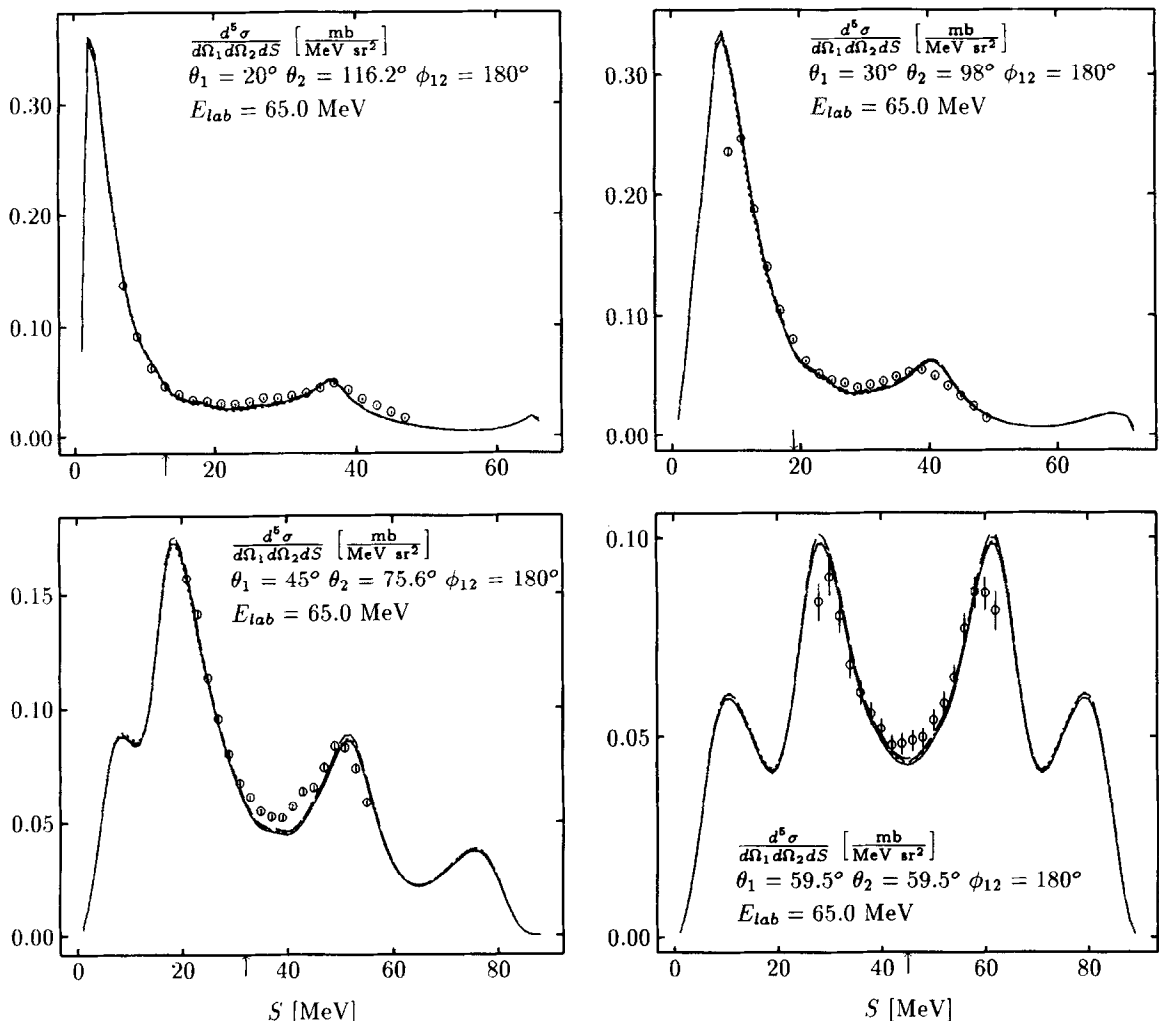


Fig. 40. Breakup cross sections including the condition of collinearity, indicated by an arrow. Comparison of data (8.0 MeV: pd data (\circ) [101]; 10.5 MeV: pd data (\circ) [203]; 13 MeV: nd data (\circ) [470,471], pd data (\diamond) [397]; 19 MeV: pd data (\circ) [366]; 65 MeV: pd data (\circ) [9]) with NN force predictions (AV18 (—), Nijm 93 (---), Nijm I (- - -) and Nijm II (· · ·)).

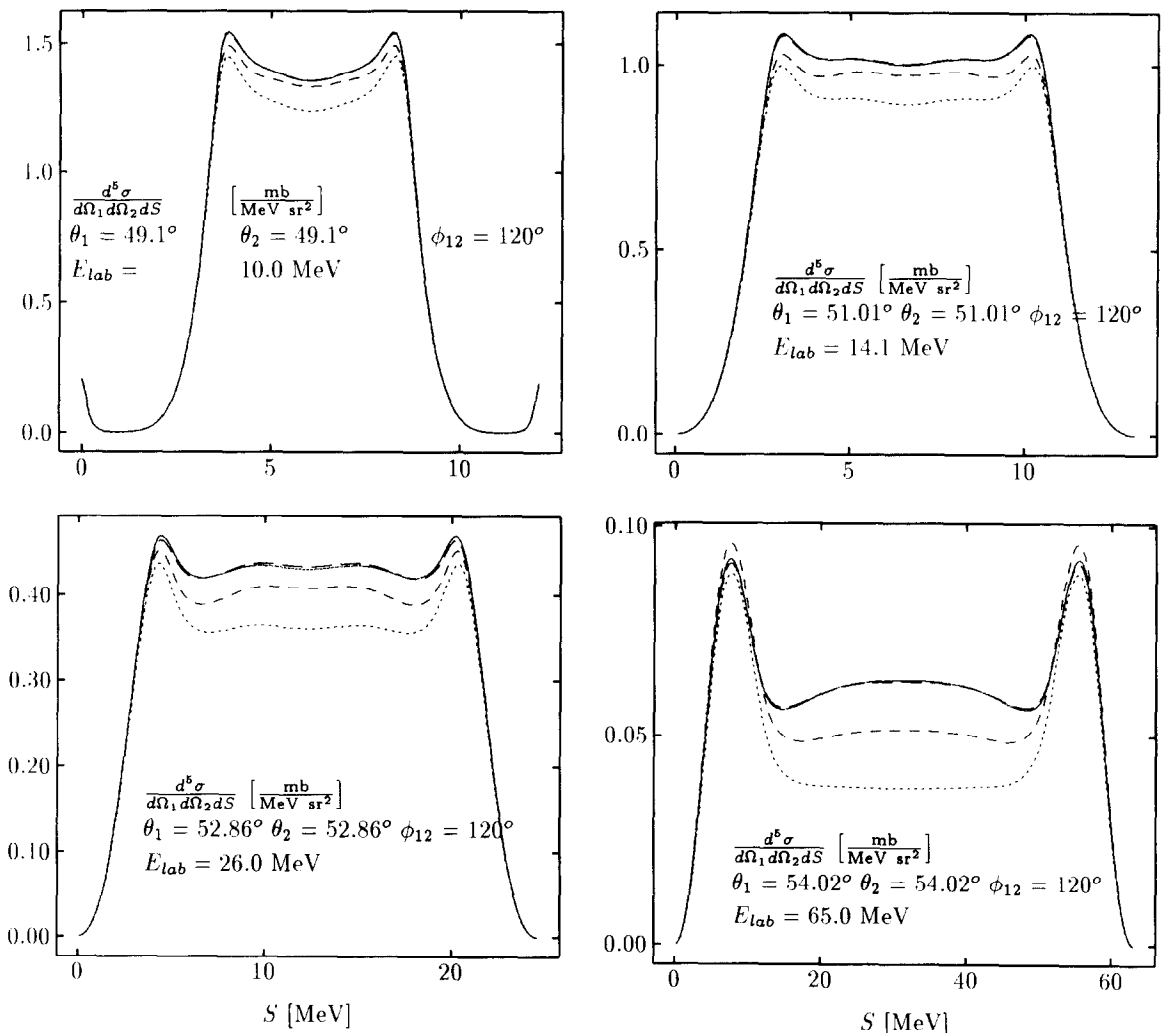


Fig. 41. The contribution of different NN force components to the breakup cross section in the space star configuration: s-waves (· · · · ·), $j \leq 1$ (- - -), $j \leq 2$ (---), and $j \leq 3$ (—).

case is, to have equal relative energies and symmetry with respect to the incident beam direction for the momenta of the two identical nucleons. Measurements for such configurations [330,355] have been performed and compared to simple s-wave NN force calculations. Severe discrepancies between theory and data in the minima have been found, which however might be due to the oversimplified forces (no tensor force, no $l = 1$ and 2 forces). Again, unfortunately the data cannot be reanalyzed using the present day realistic NN forces due to the lack of sufficient information on the experimental conditions. Renewed measurements would be very desirable. We shall come back in Section 7.1 to the question, whether the claim of [275] about the most sensitive configurations, among which are these constant relative energy loci, survives if modern phase-equivalent NN forces are being used.

More recently data have been taken under detector angles, which do not coincide with the four standard configurations mentioned up to now. We display some of them in Fig. 44. In some cases there

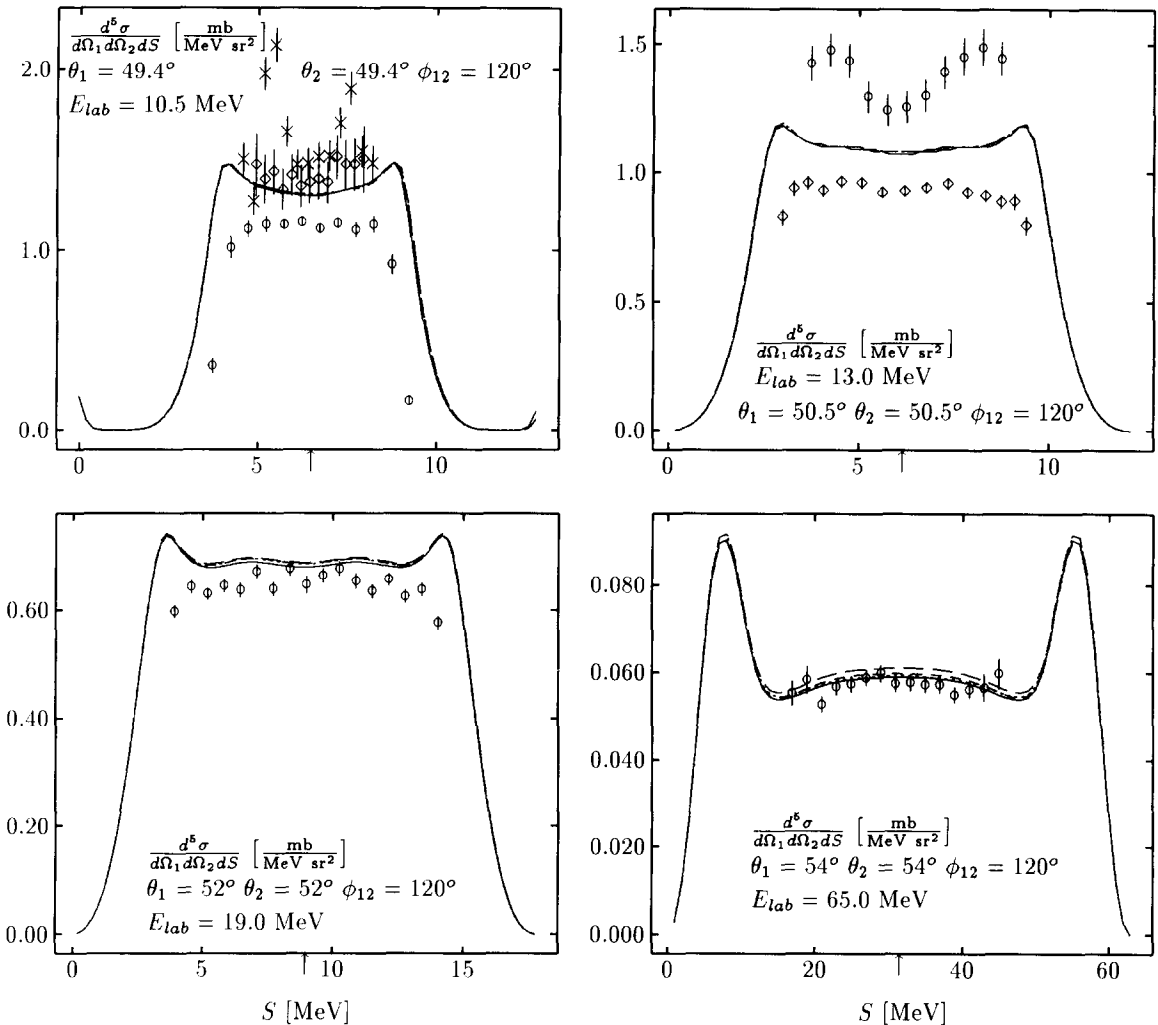


Fig. 42. Breakup cross sections including kinematics of the space star, indicated by an arrow. Comparison of data (10.5 MeV: pd data (\circ) [350], nd data (\diamond) [462], (\times) [460]; 13 MeV: nd data (\circ) [470,471], pd data (\diamond) [397]; 19 MeV: pd data (\circ) [366]; 65 MeV: pd data (\circ) [536]) with NN force predictions (AV18 (—), Nijm 93 (---), Nijm I (- - -) and Nijm II (· · ·)).

is strong disagreement to the theory. Especially at 13 and 65 MeV one faces a 100% discrepancy. At 65 MeV the cross section is rather low, which is not due to the phase space factor k_S given in Eq. (105), which is even somewhat larger than in the symmetric QFS configuration of Fig. 35, but due to the nuclear matrix element. Our results are stable with respect to different choices of NN forces. Therefore, assuming the experimental data to be correct, we face a problem. The pd data at 8 MeV, which have a kinematics close to the collinearity condition, agree relatively well with theory, though unknown Coulomb force effects introduce an uncertainty. Interesting is also the disagreement of theory to one set of pd data at 22.7 MeV and the very good agreement with the other set (see Fig. 43).

An experimental full 4π investigation covering all possible configurations would be very welcome.

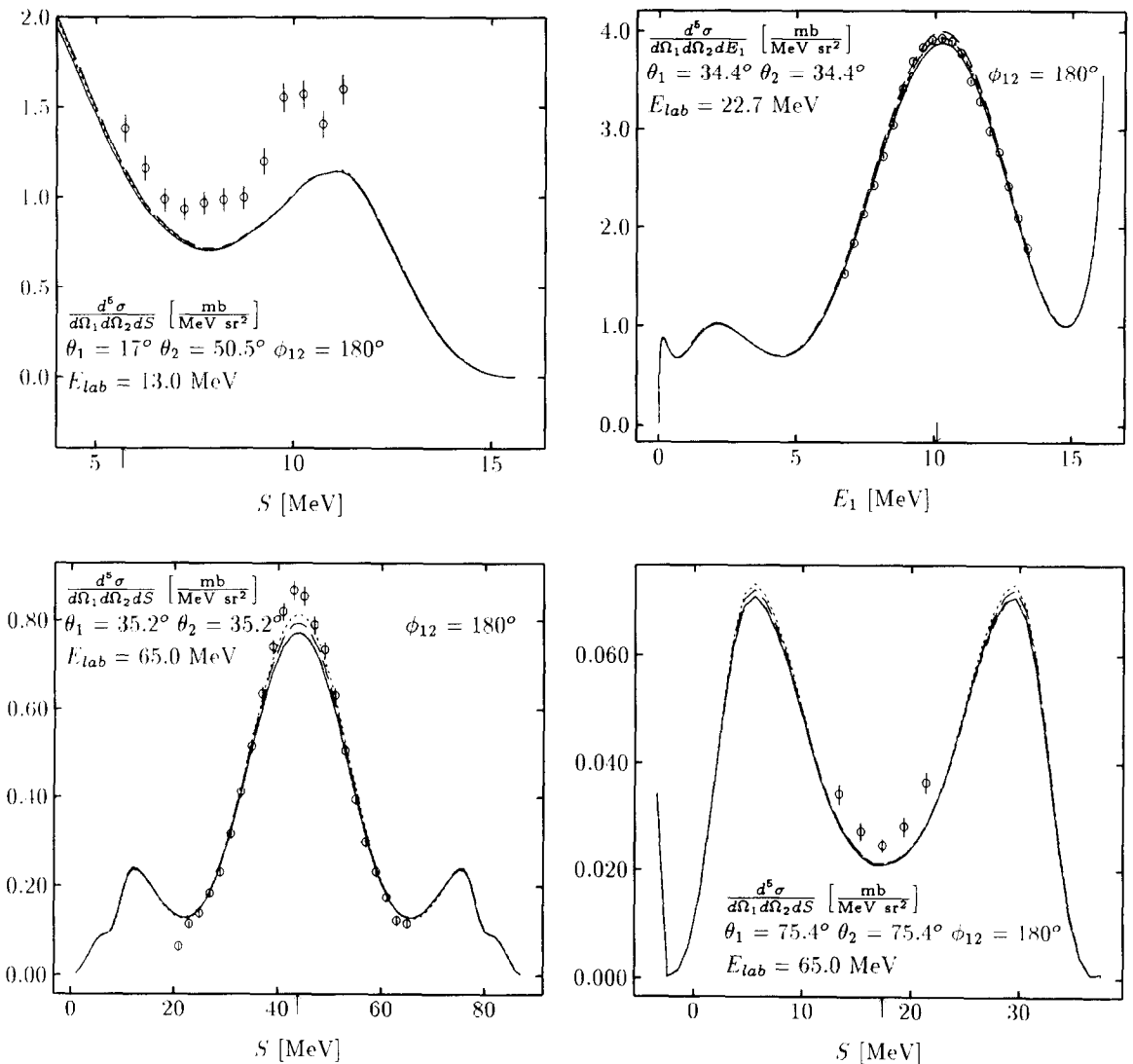


Fig. 43. Breakup cross sections including the kinematics of a coplanar star, indicated by an arrow. Comparison of data (13 MeV: nd data (\circ) [470,471]; 22.7 MeV: pd data (\circ) [146]; 65 MeV: pd data (\circ) [536]) with NN force predictions: AV18 (—), Nijm 93 (---), Nijm I (- - -) and Nijm II (· · · · ·). Note that for 22.7 MeV the cross section is plotted as a function of E_1 .

This would test the underlying 3N Hamiltonian in the most stringent manner. In the past “ 4π ” data have been recorded [502,56]; unfortunately they are not documented and no longer available.

Spin observables in the breakup process

Let us regard now spin observables in the breakup process. A first set of data are analyzing powers, where the projectile nucleon is polarized. Trials in kinematically incomplete setups were successful [233,273]. Recent data in kinematically complete arrangements [145,146,397,9–12,366,536] in comparison to the theory are displayed in Figs. 45–49. These are all pd data and the possible

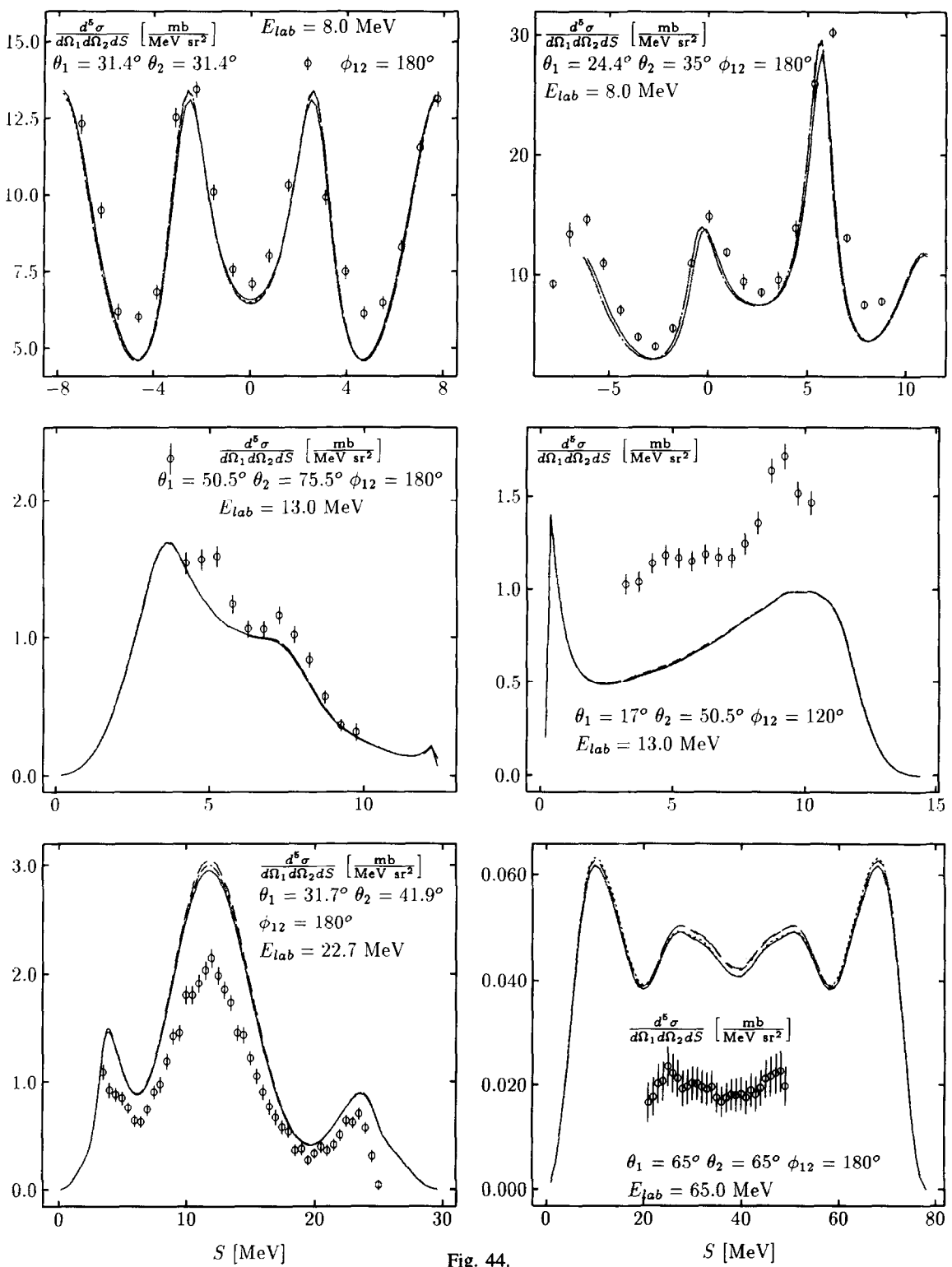


Fig. 44.

Coulomb force effects are unknown. The observables are grouped according to QFS (Fig. 45), FSI (Fig. 46), collinear (Fig. 47), space star (Fig. 48) and coplanar star (Fig. 49). The agreement is in general good, with some possible exceptions at 22.7 MeV (Fig. 45) and 65 MeV (Fig. 47). In the latter case there is a hump in the theory not so clearly present in the data and a slight shift of theory in comparison to experiment. In all cases the predictions of the most recent NN forces agree with each other with slight differences occurring at 65 MeV in Fig. 47.

Finally we show in Fig. 50 how A_y is built up out the NN force components for an example which includes FSI kinematics. Clearly the $j = 2$ forces are needed even at 10 MeV.

A second set of data are deuteron vector and tensor analyzing powers A_y , A_{yy} , A_{xx} at $E_d^{lab} = 16$, 52.1 and 95 MeV. The deuteron vector and tensor analyzing powers at 16 MeV, shown in Fig. 51, agree quite well with the data [101] taken under collinearity conditions or close to it, but the data have relatively large error bars.

At 52.1 MeV the symmetric collinear and coplanar star configurations have been chosen [394]. While for the deuteron vector analyzing power theory and data agree there are drastic discrepancies for A_{xx} and A_{yy} . This is shown in Fig. 52. The structures are much more pronounced in theory than in the data. It is interesting to see how the theoretical values are built up; this is displayed in Fig. 53. One sees that very important contributions come from the $j = 2$ NN force components. All the NN force predictions agree among each other and therefore we face a problem if the data will be confirmed by renewed measurements. At the deuteron lab energy of 95 MeV the A_{yy} data [319,524] have been taken at a special symmetric constant relative energy geometry, which has star geometry. The two protons are emerging symmetrically to a plane defined by the beam axis and the outgoing neutron. The data are shown as a function of the angle α between the direction of the neutron and the beam axis. Data and theory agree, see Fig. 54, except around $\alpha \approx 150^\circ$, where theory is rather smooth and does not show the peak seen in experiment. Since theory develops such a peak at an energy about 15 MeV lower it would be of interest, if that observable could be remeasured and then more systematically studied at several energies. In Fig. 55 the breakup data are shown along the S-curve for two fixed α -values, in the peak and outside the peak of Fig. 54. We see that the clear discrepancy is present for all energy distributions in the peak while theory agrees very well with the data for all values of S outside the peak.

From the examples shown we see that the spin data set for the breakup process is much poorer than for elastic scattering. What is really needed is a firmly established extensive data basis in order to be able to find out possible deficiencies in the nuclear 3N Hamiltonian.

6.2. 3N scattering including 3NF's

To the best of our knowledge the first time that Faddeev equations have been solved for the breakup process including a 3NF was in [333,334]. Restricted computer resources at that time imposed the use of only simplified two-nucleon forces and of a spin-isospin averaged 3NF [63]. The whole phase-space has been explored and the most promising configurations with the largest 3NF effects

Fig. 44. Breakup cross sections for nonstandard kinematics. Comparison of data (8 MeV: pd data (\circ) [101]; 13 MeV: nd data (\circ) [470,471]; 22.7 MeV: pd data (\circ) [530]; 65 MeV: nd data (\circ) [302]) with NN force predictions (AV18 (—), Nijm 93 (---), Nijm I (- - -) and Nijm II (· · ·)).

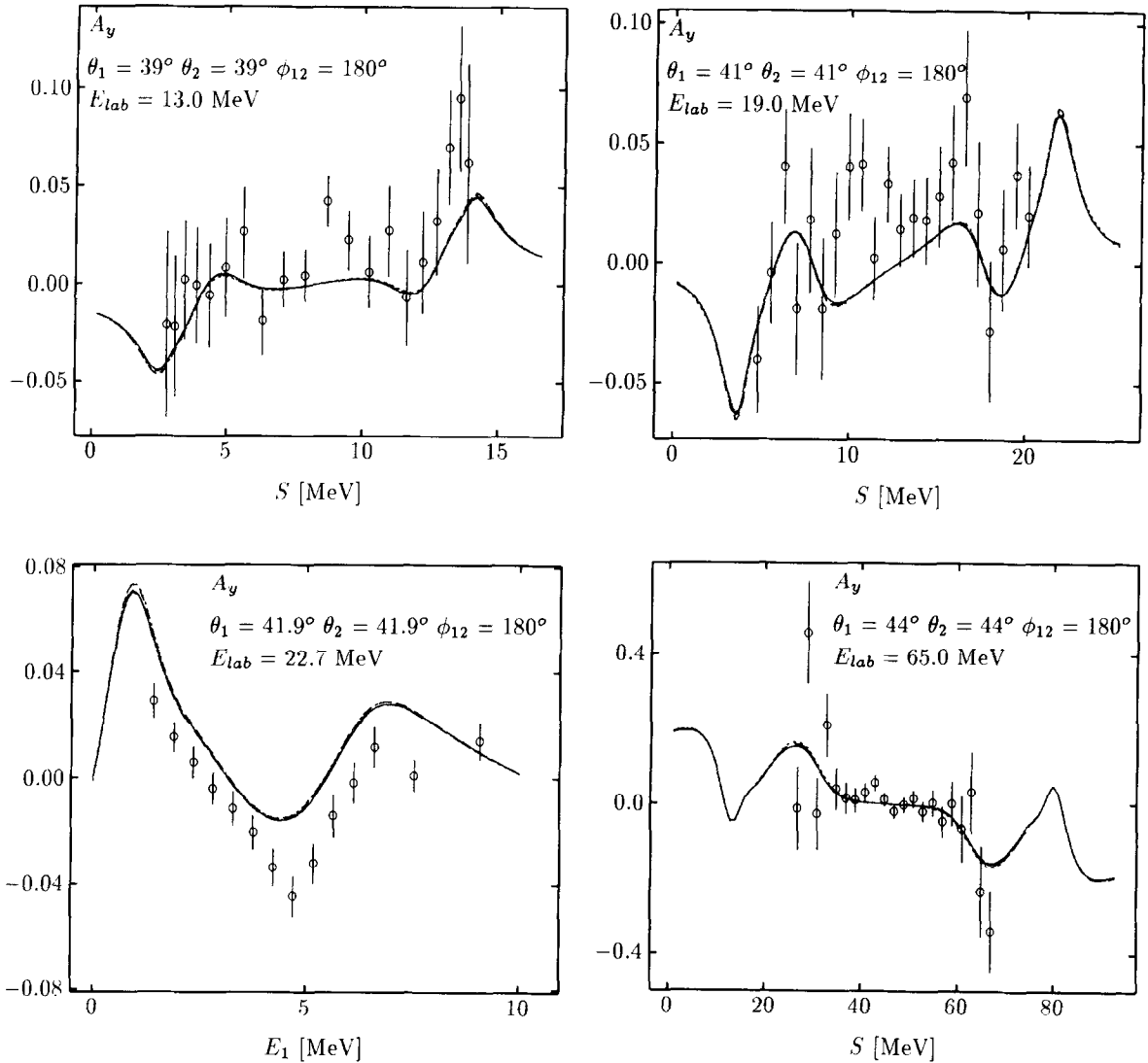


Fig. 45. The nucleon analyzing power including QFS kinematics. Comparison of data (13 MeV: pd data (\circ) [397]; 19 MeV: pd data (\circ) [366]; 22.7 MeV: pd data (\circ) [145]; 65 MeV: pd data (\circ) [11]) to NN force predictions (AV18 (—), Nijm 93 (---), Nijm I (- - -) and Nijm II (· · ·)). For the position of the QFS point see Fig. 33.

were pointed out. Now more powerful computers came up and it got possible to use NN forces in all their complexities including in addition 3NF's without further approximation.

The most obvious 3NF is the $\pi - \pi$ exchange among three nucleons with one intermediate Δ , the so-called Fujita-Miyazawa force [157]. This model ignores chiral constraints. The need for consistency with (broken) chiral symmetry for the πN scattering amplitude embedded in the processes of Fig. 2 has been emphasized by [67]. The Tucson-Melbourne (TM) $\pi - \pi$ exchange 3NF [96] was developed in that spirit taking into account the low-energy theorems of the current algebra-PCAC description of axial-vector nucleon amplitudes. On top it includes a term dominated by the Δ -isobar, which, however, does not outweigh the current algebra piece. Thereby the off-the-mass-shell π -

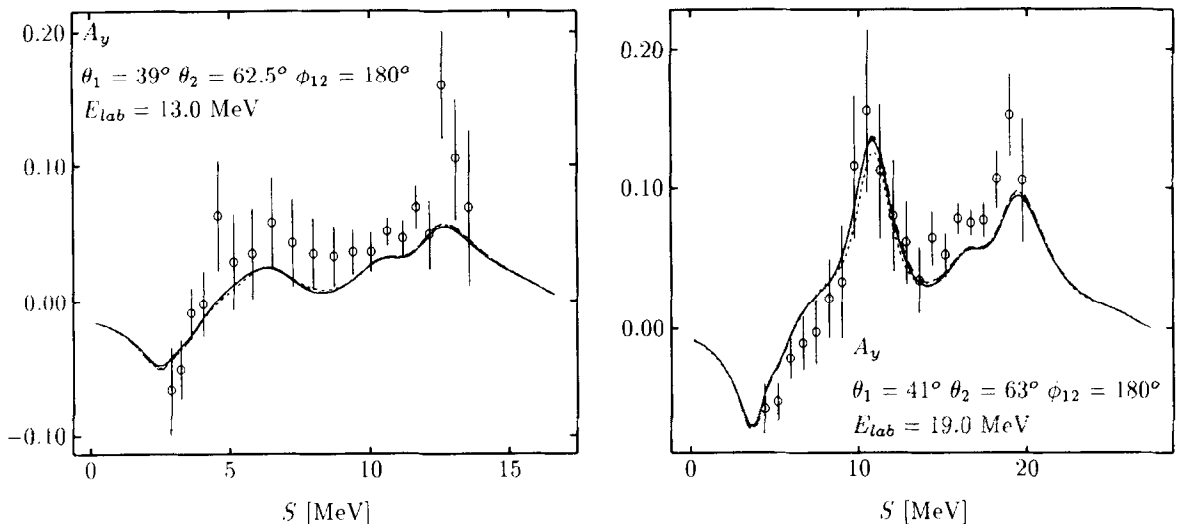


Fig. 46. The nucleon analyzing power including FSI kinematics. Comparison of data (13 MeV: pd data (\circ) [397]; 19 MeV: pd data (\circ) [366]) to NN force predictions (AV18 (—), Nijm 93 (---), Nijm I (- · -) and Nijm II (· · ·)). For the position of the FSI point see Fig. 39.

N amplitude is represented in a low momentum expansion, which for higher momenta obviously has to fail badly. That amplitude increases with momenta instead of decreasing. Since in realistic nuclear wave functions, momenta larger than the pion mass are significantly populated and not at all negligible, that wrong behavior has to be corrected by the strong form factors, which results in a severe cut-off dependence.

Extending the current algebra-PCAC approach the $\pi - \rho$ and $\rho - \rho$ exchange 3NF's have been constructed [122] and, including the $\pi - \pi$ exchange, all three run under the name TM model [331,98–100]. The Brazilian group [405–407,409] just took tree diagrams of effective Lagrangians (approximately) invariant under chiral transformations and gauge transformations, with π , ρ and σ 's to generate a model for the $\pi - \pi$, $\pi - \rho$ and $\rho - \rho$ exchanges. When the parameters were properly adjusted that force gave essentially very similar results in triton calculations [84,152,423] as the TM-model. For a recent application of the TM 3NF to ${}^3\text{H}$ see [458,460].

Then there is a purely phenomenological approach by the Urbana–Argonne collaboration [73,432], in the form of the UB 3NF, which has the $\pi - \pi$ long range features built in and a phenomenological short range part, which balances the attraction of the long range part. That force has been adjusted [506] together with the AV14 NN force to the triton and ${}^4\text{He}$ binding energies. Recently that force has been used in 3N scattering calculations below the breakup threshold [271].

If the Hilbert space includes in addition to 3N states also states with one, two or three nucleons being replaced by Δ 's, one has to establish transition potentials between nucleons and Δ 's. This has been done [199,505] and applied in the 3N bound state [219,220,371,375,376,459,377–380]. That formulation is equivalent to introducing certain types of 3NF's in the Hilbert space of nucleons only [425]. Interestingly, that formulation allows for a new dynamical feature, the so-called dispersive effects [199]. If two nucleons interact by a box diagram with one intermediate Δ , which is part of the two nucleon force, then the presence of a third nucleon modifies the intermediate propagator and consequently that part of the two-nucleon force. In case of the 3N bound state with a negative

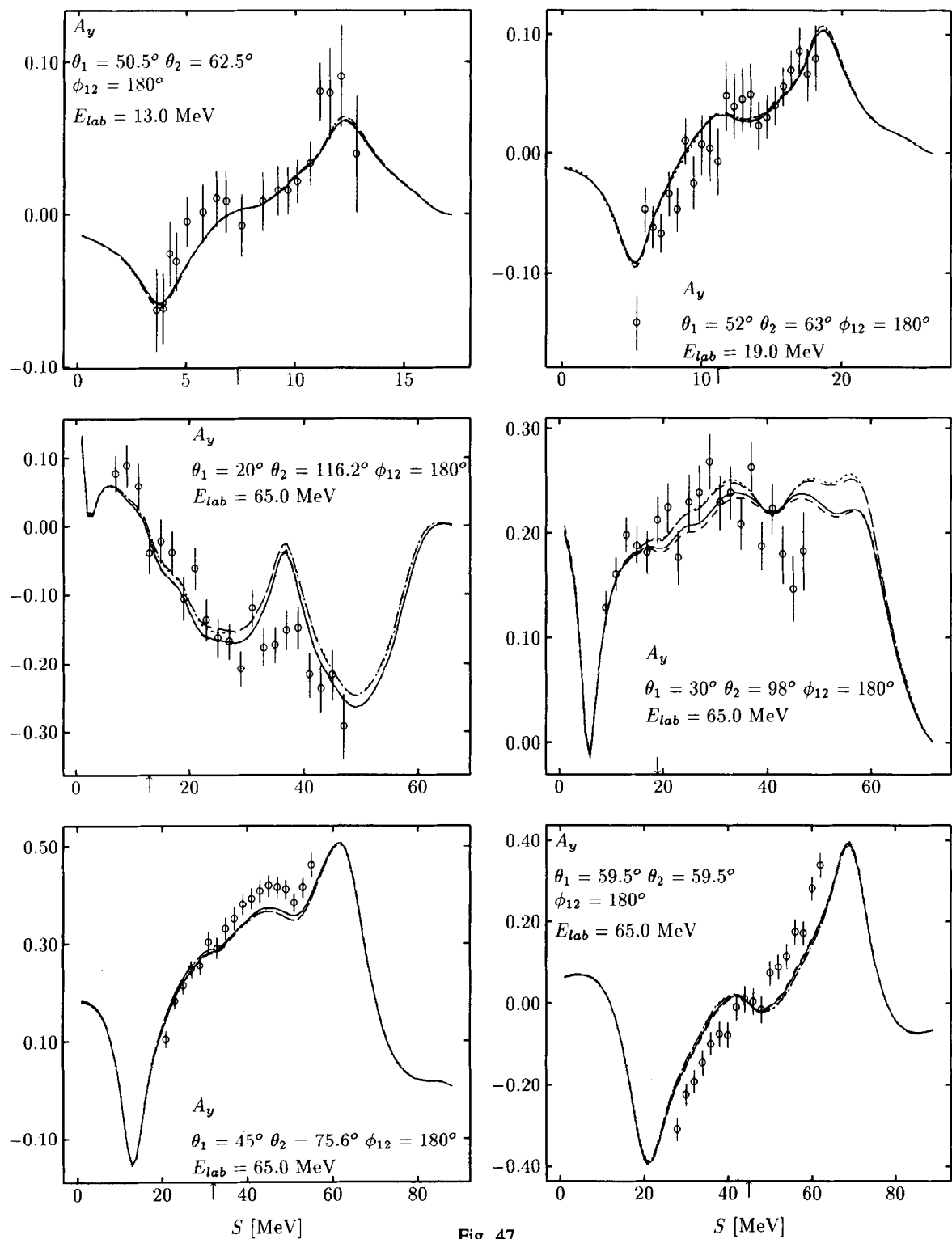


Fig. 47.

3N energy the presence of the additional kinetic energy of that third nucleon in the propagator makes that force weaker. That dispersive effect counteracts the attraction provided by the Fujita-Miyazawa force, mentioned above [157]. To the best of our knowledge that dynamics has not yet been applied in rigorous 3N scattering calculations, but appears to be worth the efforts. This would be a straightforward extension of what is being done now, just having more channels, and is quite feasible on present day computers.

Fig. 47. The nucleon analyzing power including collinearity conditions. Comparison of data (13 MeV: pd data (\circ) [397]; 19 MeV: pd data (\circ) [366]; 65 MeV: pd data (\circ) [9]) to NN force predictions (AV18 (—), Nijm 93 (---), Nijm I (- - -) and Nijm II (· · ·)). The position of the collinearity point is indicated by an arrow.

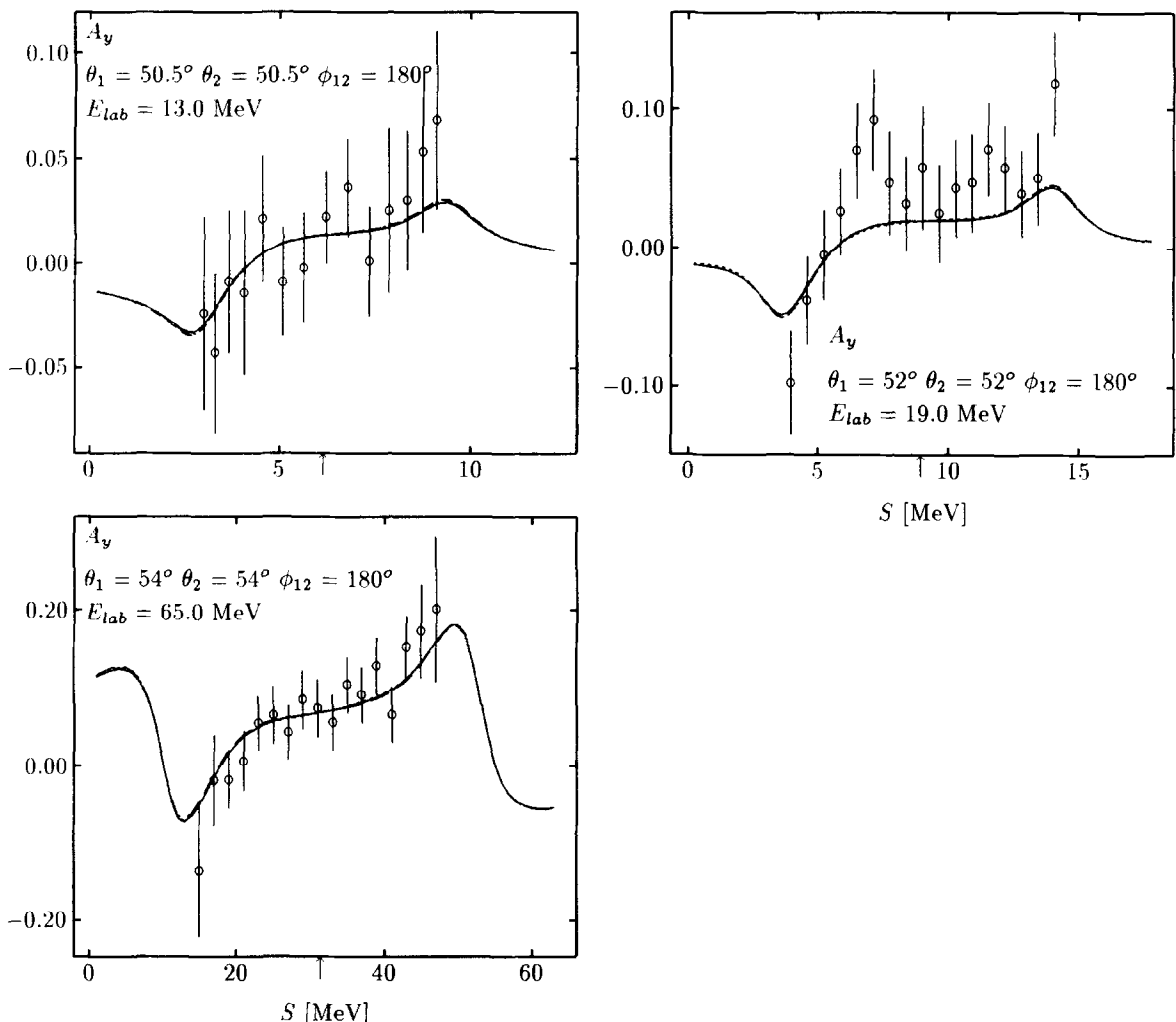


Fig. 48. The nucleon analyzing power including the space star configuration. Comparison of data (13 MeV: pd data (\circ) [397]; 19 MeV: pd data (\circ) [366]; 65 MeV: pd data (\circ) [536]) to NN force predictions (AV18 (—), Nijm 93 (---), Nijm I (- - -) and Nijm II (· · ·)). The position of the space star point is indicated by an arrow.

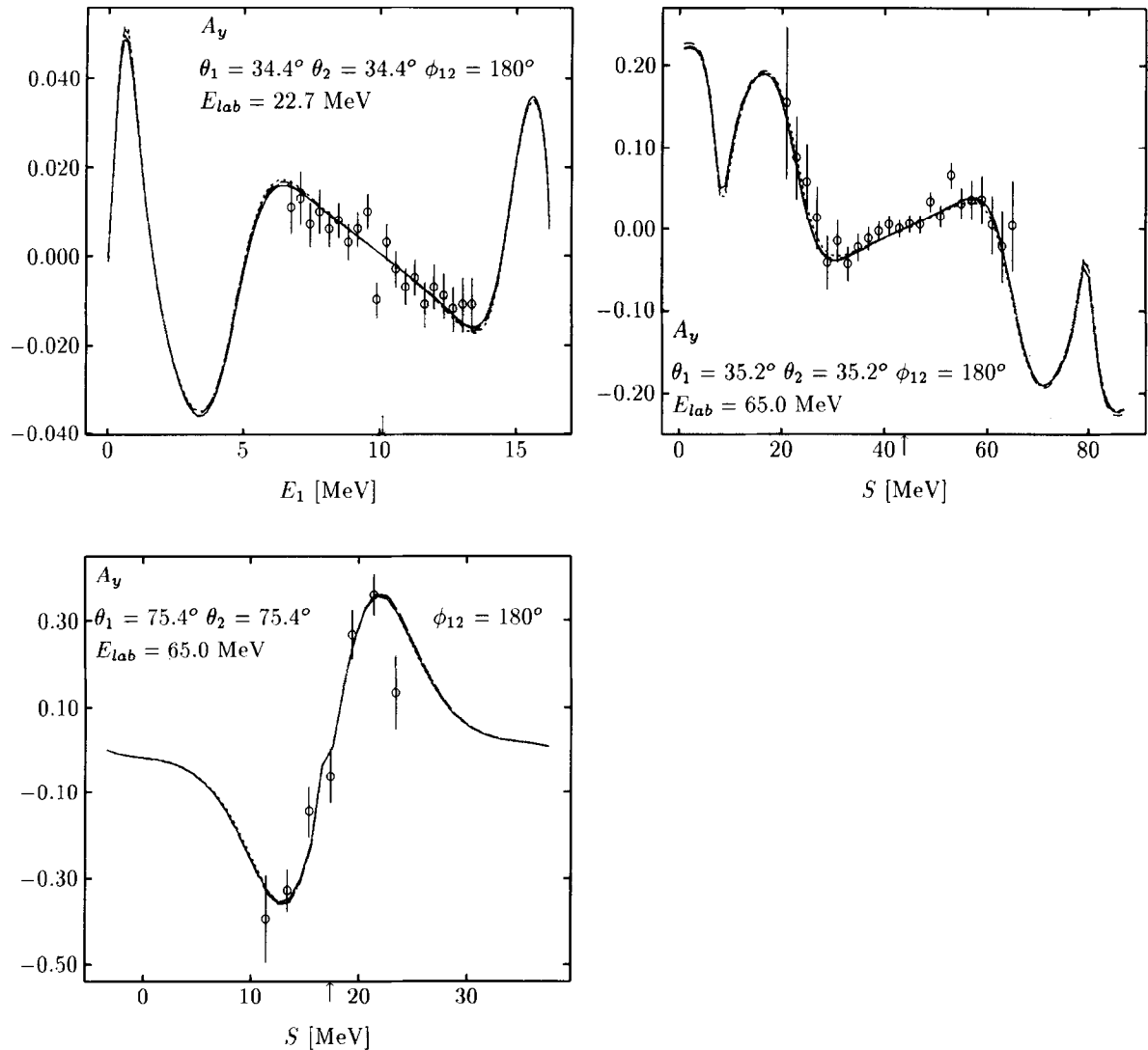


Fig. 49. The nucleon analyzing power including coplanar star configurations. Comparison of data (22.7 MeV: pd data (\circ) [146]; 65 MeV: pd data (\circ) [536]) to NN force predictions (AV18 (—), Nijm 93 (---), Nijm I (- - -) and Nijm II (· · ·)). The position of the coplanar star point is indicated by an arrow.

A very first scattering observable to be calculated is the doublet nd scattering length 2a . As already mentioned it is correlated to the triton binding energy. Since that observable is evaluated exactly at the nd threshold, the boundary conditions are very simple and one can reformulate the equations such that it is like solving a bound state problem. We refer to [86] for the configuration space and to [238] for the momentum space treatments. Examples for various combinations of 2N and 3N forces are shown in Table 11. In all cases (except Bonn B, $j_{max} = 3$) the 3N forces have been chosen such that the correct 3H binding energy results. We see that the scattering length 2a come thereby close to the experimental value of 0.65 fm. In agreement with experiences from other groups we see from the example of Bonn B, where we increased j_{max} to three, that partial waves beyond $j_{max} = 2$ are indeed

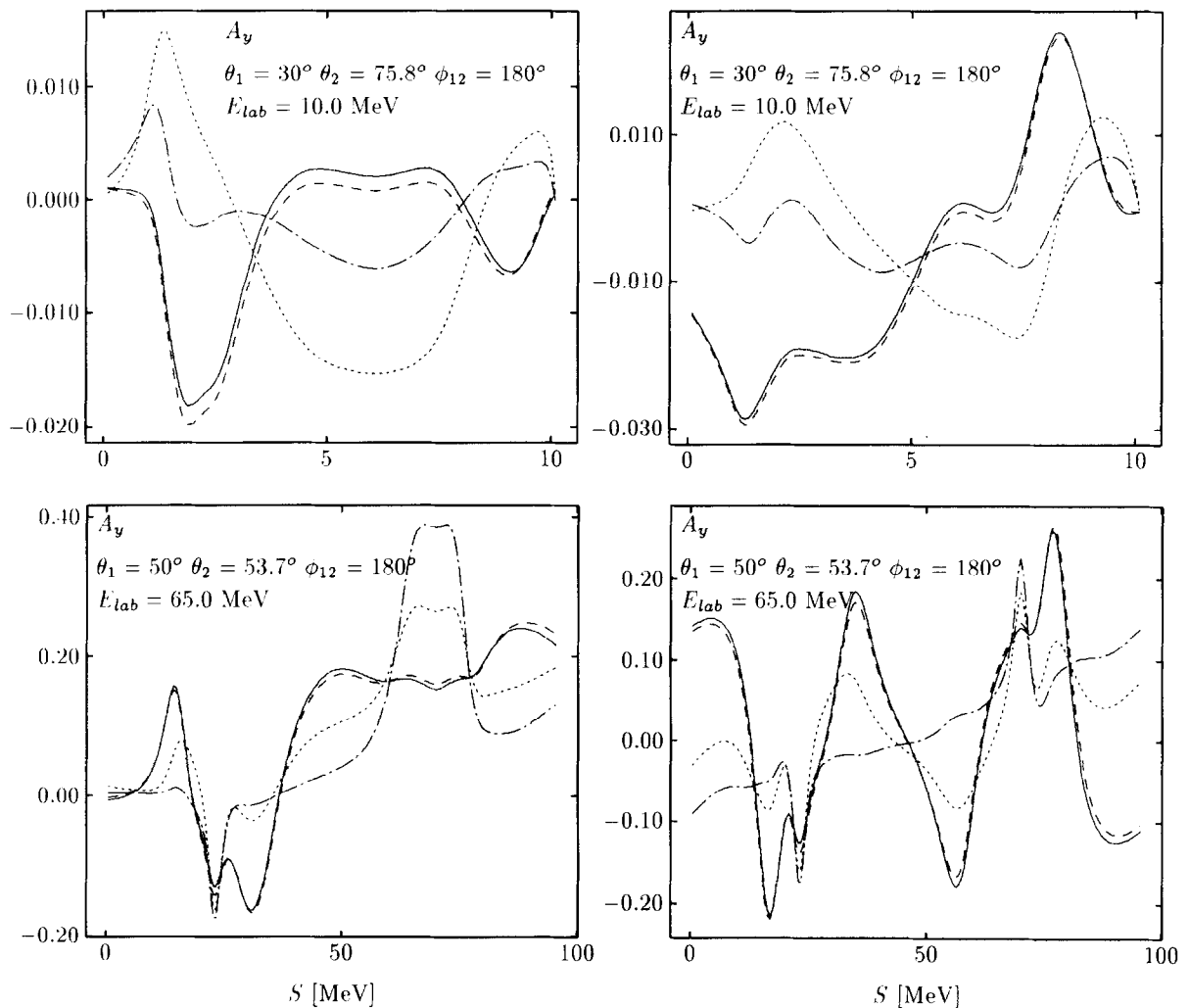


Fig. 50. The contribution of various NN force components to the analyzing power A_y along the S-curve for configurations including FSI conditions: s-waves ($\cdots\cdots$), $j \leq 1$ ($\cdot\cdot\cdot$), $j \leq 2$ ($-\cdot-\cdot$), and $j \leq 3$ ($-$). As NN force Bonn B is used. The figures on the left hand side show nn FSI configurations and on the right hand side np FSI configurations.

needed. The calculations based on $j_{max} = 4$ were carried through in configuration space [86]. Finally we display very recent results achieved by the pair correlated harmonic basis technique [271] using the AV18 NN force together with an Urbana 3NF. In that case the forces are not truncated.

Let us now regard possible 3NF effects in elastic Nd scattering and the breakup process. The calculations require substantial computer resources and we have up to now only results for the TM model, which can serve as a first orientation of what might be expected.

Similarly what has been found in 3N and 4N bound state calculations [181] the scattering results depend on which NN force is "married" to the TM 3NF. This is not surprising in view of the different short range repulsions for the different NN forces. Thus, since the 2N and 3N forces are not consistently derived within one scheme (with the exception of the Ruprecht [388]), one has to

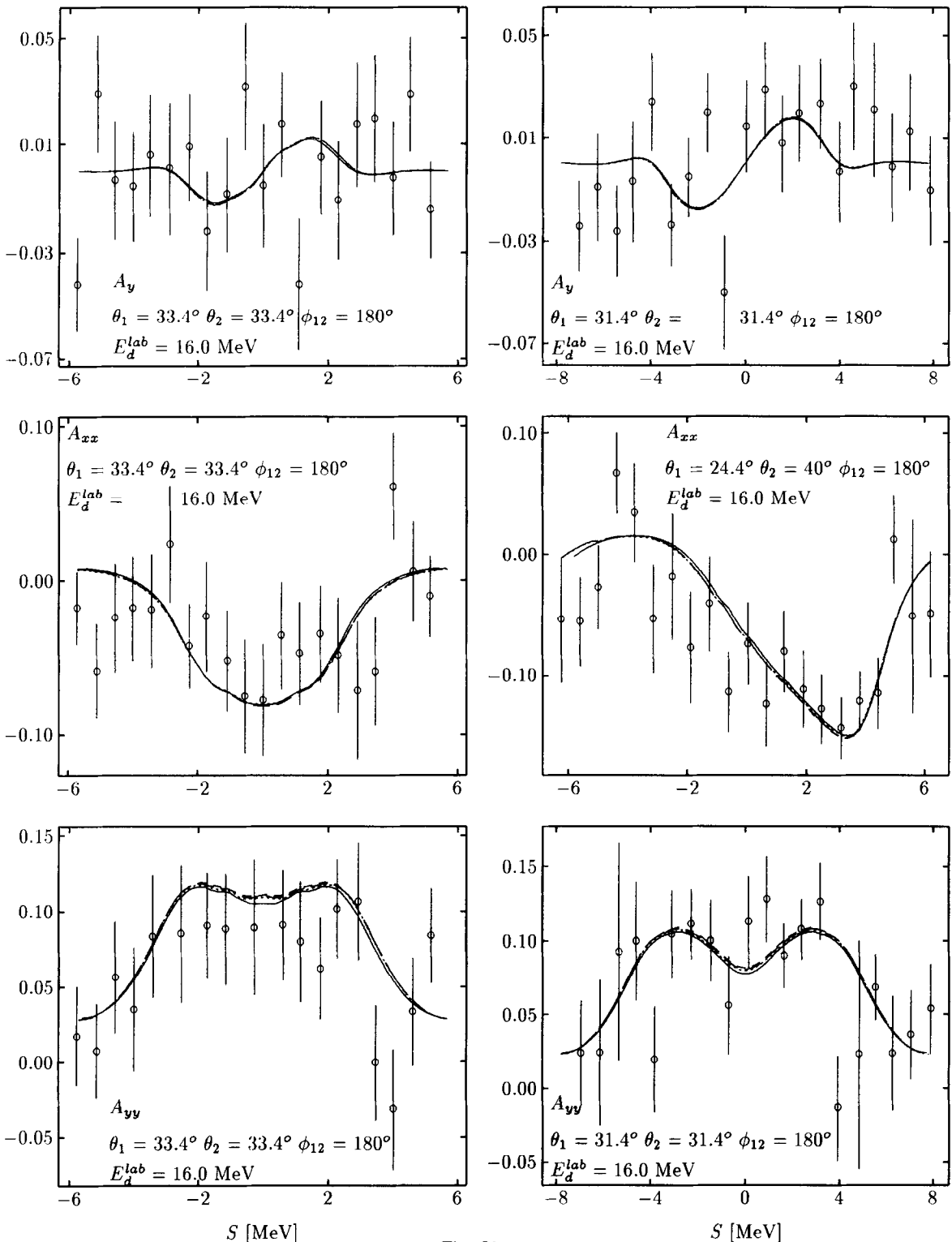


Fig. 51.

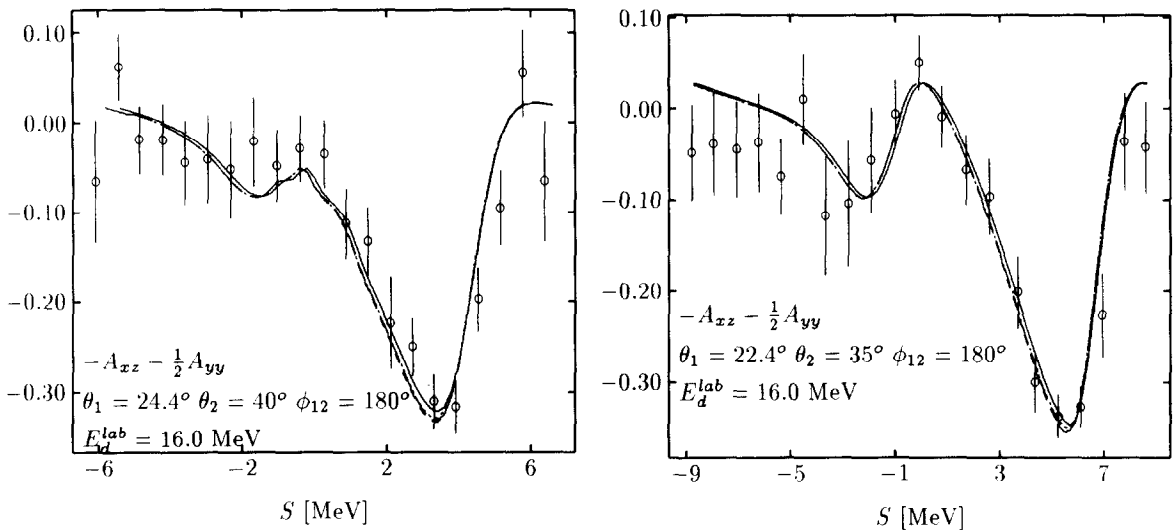


Fig. 51. The deuteron vector and tensor analyzing powers in various breakup configurations at $E_d^{lab} = 16$ MeV. pd data are taken from [101]. The two configurations with $\theta_1 = \theta_2 = 33.4^\circ$ and $\theta_1 = 24.4^\circ$, $\theta_2 = 40^\circ$ include collinearity at $S = 0$, the other two configurations are close to collinearity. The theoretical predictions are AV18 (—), Nijm 93 (---), Nijm I (- · - · -), and Nijm II (·····).

Table 11

nd doublet scattering lengths for NN and 3N forces: (a) Bochum, (b) [86], (c) [271].

2NF	j_{max}	3NF	Λ [m_π]	j_{max}	2a
Bonn B	2	TM	4.55	2	0.548 ^(a)
Bonn B	3	TM	4.55	3	0.638 ^(a)
AV18	2	TM	4.85	2	0.577 ^(a)
Nijm78	2	TM	5.15	2	0.509 ^(a)
AV14	4	BR	5.01	4	0.567 ^(b)
RSC	4	TM	5.49	4	0.657 ^(b)
AV18		UR			0.63 ^(c)

accept right now a certain width in the predictions. Also as in the bound state studies one encounters a strong dependence on the cut-off parameter of the strong form factors in the 3NF [235].

We shall display three studies, one where the $\pi - \pi$ exchange TM model is taken together with the Bonn B NN potential and a second one where the $\pi - \rho$ and $\rho - \rho$ exchanges are additionally taken into account, and a third one where the parameters of the TM model are adjusted in combination with different NN forces to give the correct triton binding energy. Since in the first two studies the triton will turn out to be overbound, the resulting 3NF effects in 3N scattering are thus presumably overestimated. In the third case one expects smaller effects and possible scaling with the triton binding energy. That means, certain observables might be predicted with the same values, independent which NN force is paired with the properly adjusted 3NF.

In the first study we pair the Bonn B NN potential with the $\pi - \pi$ exchange TM 3NF. We restrict the calculation to $j_{max} = 2$ and have chosen the lab. energies 3, 13, 14.1, 19, 65, and 140 MeV. Adding

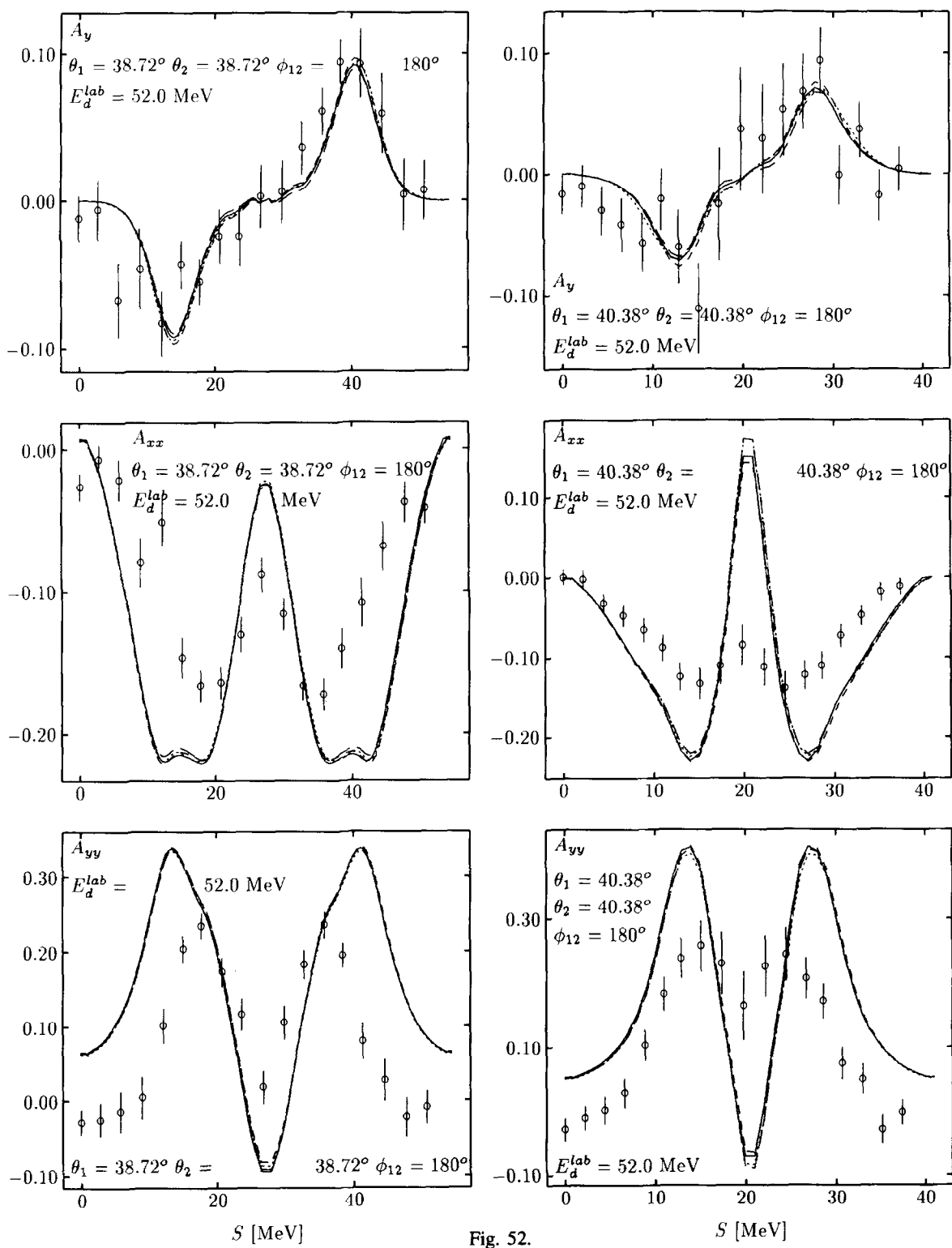


Fig. 52.

the TM 3NF generated with $A_\pi = 5.8m_\pi$ ($m_\pi = 139.6$ MeV) changes the triton binding energy from 8.14 MeV to 10.32 MeV. That strong overbinding leads presumably to an overestimation of the resulting 3NF effects. The elastic differential cross section is essentially unaffected at all energies. On the other hand essentially all spin observables in elastic scattering show effects, which however are energy dependent. Thus for instance C_{yy} shows large effects only at 3 MeV, the nucleon to nucleon spin-transfer coefficient K_y^y (n) up to 19 MeV, the nucleon to deuteron transfer K_y^y (d) at 3 MeV and 65 MeV but little in between. We display a few examples in Fig. 56. Note that the 3NF effects lowers the minimum in K_y^y (n), which theoretically is a bit too high compared to data using the most modern forces NijmI, II, 93, and AV18. Only the CD Bonn prediction passes through the data. In contrast to the other potentials it has a rather low deuteron D-state probability and also leads to the largest triton binding energy. That feature appears to be an example of a theorem that off-shell effects can act in the same manner as 3NF effects [390]. At 140 MeV our $j_{max} = 2$ calculation is certainly not fully converged and is shown to demonstrate that possibly large effects at these higher energies might occur.

In the breakup process we looked into all np and nn FSI, QFS, Star and Collinear configurations between 14.1 and 140 MeV. Only at 14.1 MeV relatively significant effects in the cross sections of up to about 10% showed up. This is exemplified in Fig. 57 for the nn FSI's and QFS's. Shown are the FSI peak heights and QFS maxima as a function of the angle between a neutron momentum and the beam axis. In both cases the effects are angle dependent. For future experiments aiming at the extraction of the nn scattering length (and also the np one for testing purposes), the fact that at some specific angle the 3NF effects are zero, here at $\approx 45^\circ$ for 14.1 MeV, should be of interest. A measurement at that angle would certainly lower the theoretical uncertainty of the extracted scattering length. On the other hand measurements at larger and smaller angles could verify the systematics of that specific 3NF effect in the FSI peak heights. At the higher energies studied, 65 and 140 MeV, the corresponding effects are essentially zero for the FSI cross sections. In case of QFS the analyzing power behaves similarly as the cross section: interesting effects at 14.1 MeV (where however the analyzing power is very small) and essentially vanishing effects at 65 and 140 MeV. This is displayed in Fig. 58. The fact that under QFS conditions the 3NF effects under study are essentially absent at the higher energies is very interesting, since at least it does not oppose the hope to use the deuteron as a neutron target at higher energies. We shall come back to that issue in Section 7.5. For the analyzing power under FSI conditions the situation is reversed: small effects at small energies and increasingly strong effects at the higher energies, as seen in Fig. 59. However, we would also like to express a warning on the outcome of the specific 3NF effects under study. For instance in the space star configuration at 13 MeV the discrepancy to the data is increased adding this 3NF. Also the description of the analyzing power under collinearity condition at 65 MeV worsens. Both cases are displayed in Fig. 60.

In the second study [525] we added the $\pi - \rho$ and $\rho - \rho$ exchange TM 3N forces in addition to the $\pi - \pi$ exchange. The influence of the $\pi - \rho$ exchange was generally found to be smaller than for the $\pi - \pi$ exchange and to act in opposite direction. The effect of the $\rho - \rho$ 3NF was found

Fig. 52. The deuteron analyzing powers A_y , A_{xx} and A_{yy} in the symmetric collinear (left hand side) and coplanar star (right hand side) configurations. Comparison of pd data [394] and theory (AV18 (—), Nijm 93 (---), Nijm I (- - -) and Nijm II (· · ·)).

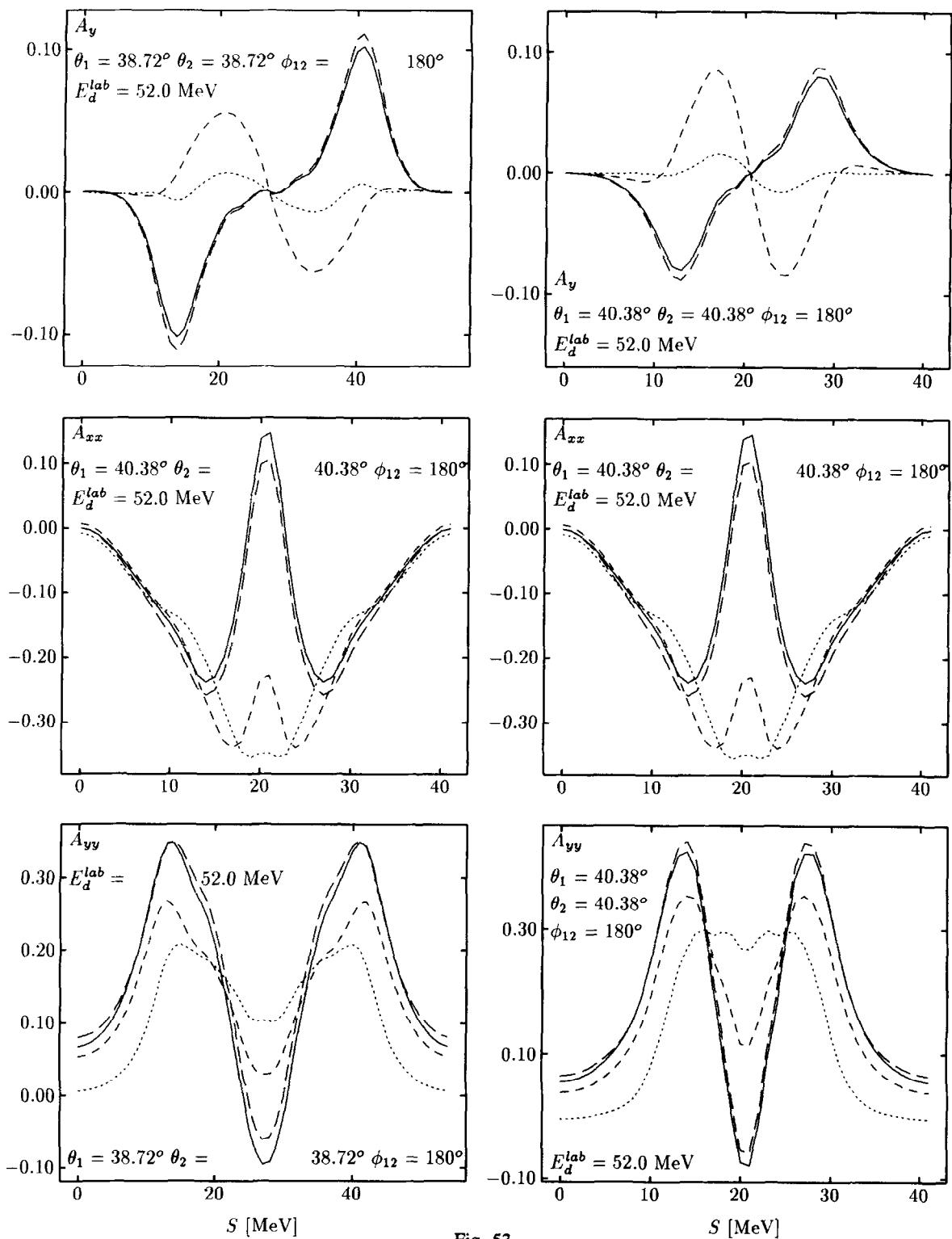


Fig. 53.

to be always negligible. The study was carried through at 3 and 14.1 MeV. For C_{yy} and 3 MeV the effect for the $\pi - \pi$ exchange is now reduced to about half its size, the same is true for $K_y^{yy}(n)$, see Fig. 56. Nevertheless the effect of lowering the minimum is interesting, since it is also generated by weakening the $^3S_1 - ^3D_1$ tensor force or the 1P_1 NN force component. Thus this minimum in the 3N

Fig. 53. The NN force contributions to the deuteron analyzing powers of Fig. 52: s-waves ($\cdots\cdots$), $j \leq 1$ ($- - -$), $j \leq 2$ ($- - -$), and $j \leq 3$ (—).

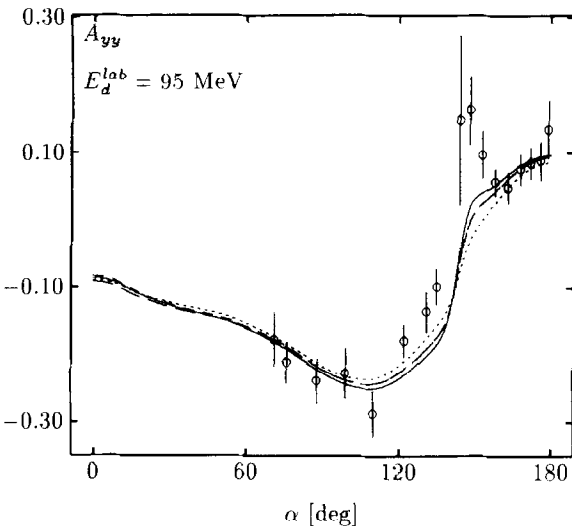


Fig. 54. The deuteron analyzing power A_{yy} under symmetric constant relative energy geometry (see text). α is the angle between the outgoing neutron and the beam axis. Comparison of pd data [319] to theory (AV18 (—), Nijm 93 (---), Nijm I (- - -) and Nijm II (· · ·)).

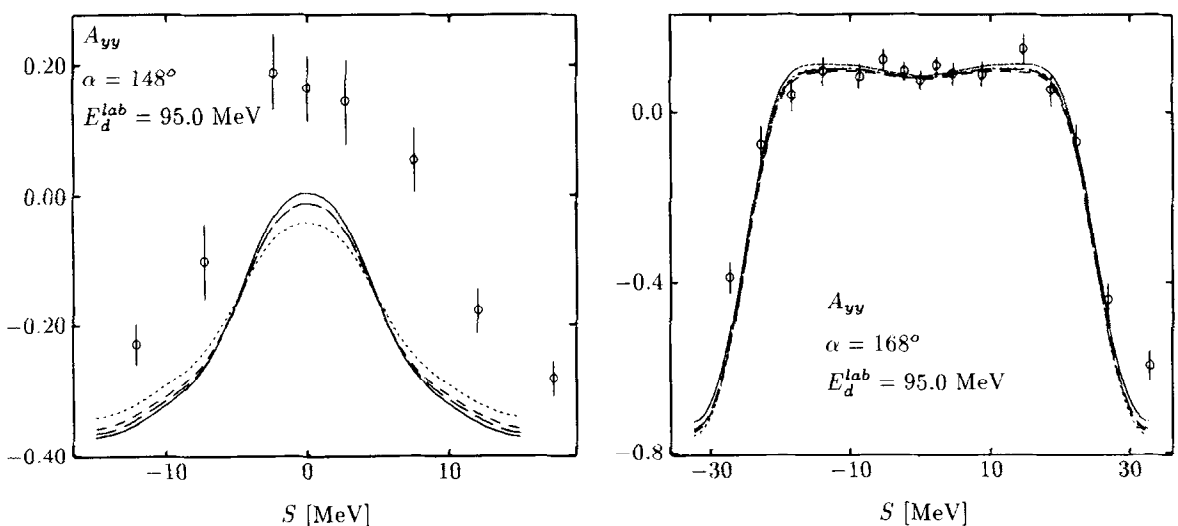


Fig. 55. The deuteron analyzing power A_{yy} along the S -curve for two angles α from Fig. 54. The theoretical predictions are AV18 (—), Nijm 93 (---), Nijm I (- - -) and Nijm II (· · ·). pd data (\circ) are from [319].

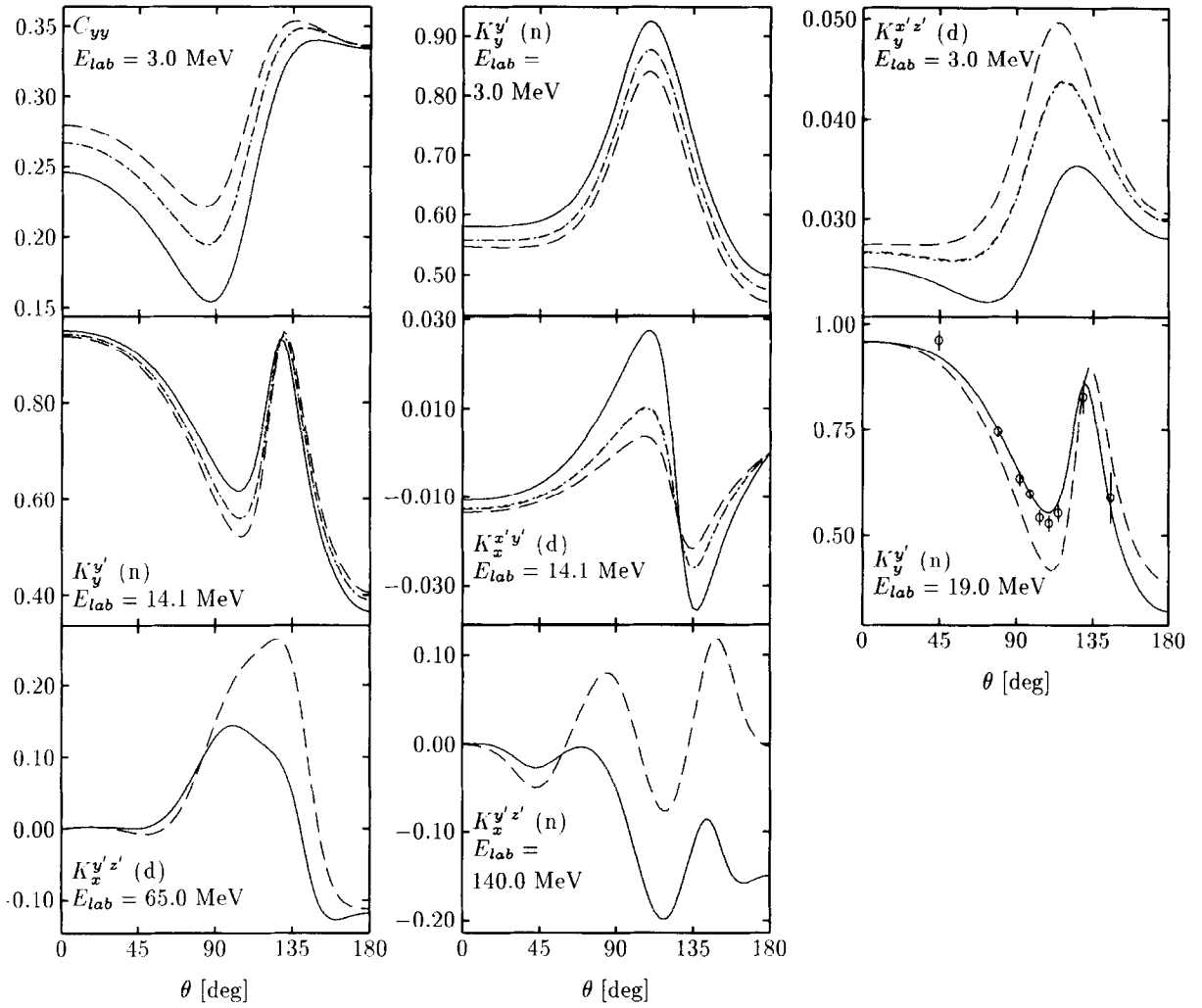


Fig. 56. Examples for TM 3NF effects in elastic nd scattering, $\pi\text{-}\pi$ exchange (---), $\pi\text{-}\pi + \pi\text{-}\rho$ exchange (- - -) and $\pi\text{-}\pi + \pi\text{-}\rho + \rho\text{-}\rho$ exchange (· · · · ·), in conjunction with Bonn B (—). pd data at 19 MeV are from [474].

observable $K_y^{y'}(n)$ provides an example, where certain 2NF and 3NF effects are similar. Therefore not taking 3NF effects into account and drawing conclusions about 2NF properties might be misleading.

The analyzing power A_y is an example, where the discrepancy to the data based on two-nucleon forces only does not get cured by including that TM 3NF model [522]. This is clearly seen in Fig. 61, where the TM 3NF effect even increases the discrepancy. Obviously if the NN forces and the underlying 3P phases would be basically correct, then that TM 3NF model would have to be outweighed by a strong 3NF of different nature. Of course there is also always the possibility that the off-shell features of the NN forces might be different. According to [390] off-shell properties of NN forces are mathematically equivalent to 3NF effects and vice versa. We shall come back to that A_y puzzle in Section 7.3 below.

In case of the breakup cross section the already relatively small effects found for the $\pi\text{-}\pi$ exchange

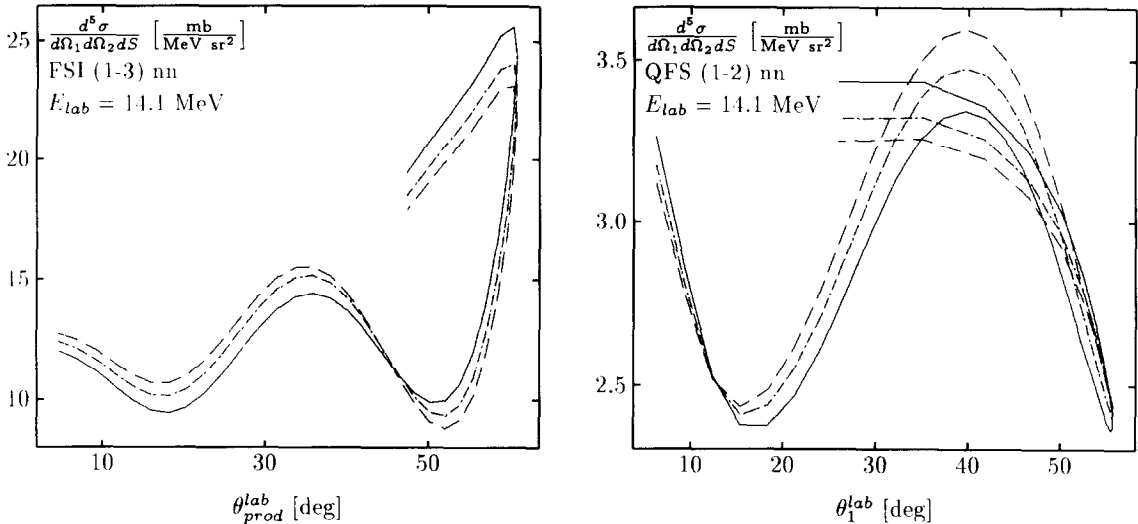


Fig. 57. TM 3NF effects, $\pi\pi$ exchange (---), $\pi\pi + \pi\rho$ exchange (- - -) and $\pi\pi + \pi\rho + \rho\rho$ exchange (· · · · ·), in conjunction with Bonn B (—) for the nn FSI and the nn QFS peak heights as a function of a neutron lab angle.

alone are further reduced by adding $\pi - \rho$ exchanges. Especially the still controversial situation for the space star configuration, mentioned in Section 6.1, is not changed by the negligible effect of the TM 3NF. See also Fig. 58–59 for the small shifts caused by addition of the $\pi - \rho$ exchange in the analyzing power under FSI and QFS conditions. For more detailed information we refer to [525].

Let us now come to the third study, the question whether different 3N Hamiltonians give for certain 3N scattering observables the same prediction when the corresponding triton binding energy is correct. It has been claimed in [61] that this is true in general at low energies and nothing new can be learned from scattering. This claim has been already criticized some time ago [472] by providing counter examples in model calculations of the breakup process. We took up that question again using the modern AV18 NN force, the Bonn B and Nijmegen78 NN potential, and adjusted to each force the TM $\pi - \pi$ exchange 3NF such that one gets in each case the correct triton binding energy. As parameter to be adjusted we took the Λ -value of the strong form factors in that TM model. The resulting values for Λ are 4.55, 4.85 and 5.15 m_π for the NN forces Bonn B, AV18 and Nijmegen 78, respectively, which reflects the different binding energies of -8.10, -7.72 and -7.54 MeV, for the NN forces only. In this manner we generated three different Hamiltonians yielding all the same triton binding energy. Now we looked into observables for elastic Nd scattering and the breakup process, between 3 and 19 MeV using either only the different NN forces or the corresponding full Hamiltonians supplemented by the adjusted 3NF's. Whenever the individual NN force predictions differ but coincide for the full Hamiltonians we call that phenomena "scaling with the triton binding energy". We found observables, which do scale and others which do not. With increasing energy scaling dies out and already at 10 MeV it is essentially gone. Thus it is a clear low energy phenomena.

Let us first regard elastic scattering. As already mentioned the differential cross section shows essentially no 3NF effect. The observables which scale at 3 MeV are the vector spin correlation coefficients C_{xx} and C_{yy} and all nucleon to nucleon and nucleon to deuteron vector polarization transfer coefficients; on the other hand all analyzing powers and nucleon to deuteron tensor spin transfer and tensor spin correlation coefficients (S, T) do not scale. In the latter nonscaling group

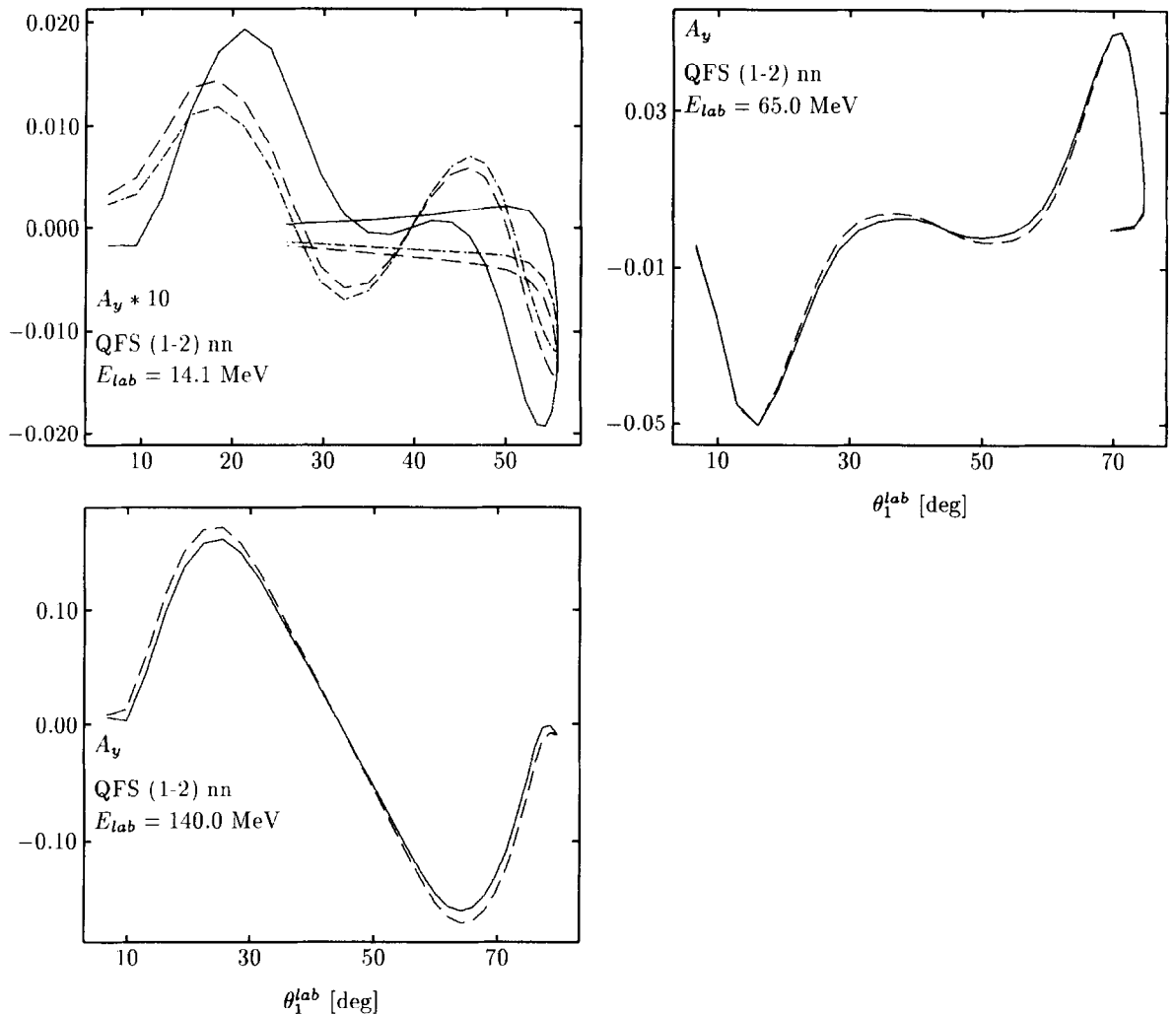


Fig. 58. TM 3NF effects, $\pi\pi$ exchange (---), $\pi\pi + \pi\rho$ exchange (- · - · -) and $\pi\pi + \pi\rho + \rho\rho$ exchange (· · · · ·), in conjunction with Bonn B (—) for the analyzing power A_y under nn QFS condition as a function of a neutron lab angle.

the predictions with and without 3NF deviate from each other for different choices of the forces. Some prominent examples for scaling observables and nonscaling observables are shown in Fig. 62 and Fig. 63, respectively.

In the breakup process we also found scaling and non-scaling behavior for the cross section. We performed an angular search in the space of all angles of the two nucleon detector positions. Only at small energies close to the breakup threshold scaling was present. For instance at 4.5 MeV there is a very small phase space region around $\theta_1 = 45^\circ$, $\theta_2 = 22^\circ$ and $\Delta\phi_{12} \leq 50^\circ$ where the individual NN force predictions deviate by more than 10% and agree within 3% when the corresponding 3NF's are switched on. An example is shown in Fig. 64. There are also domains which are extremely insensitive and all NN force predictions agree with each other and the additionally 3NF effects are negligible.

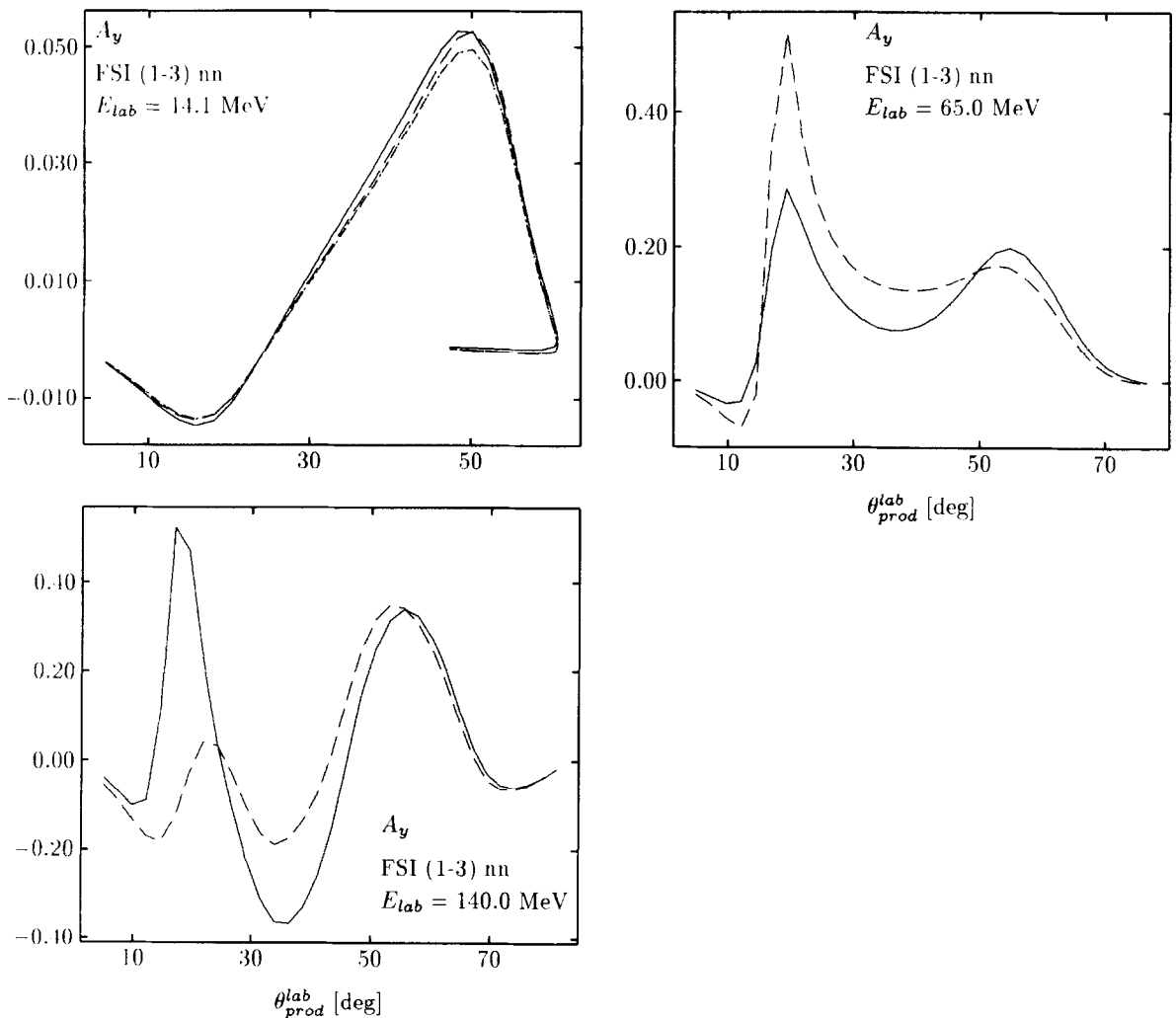


Fig. 59. TM 3NF effects, $\pi\text{-}\pi$ exchange (---), $\pi\text{-}\pi + \pi\text{-}\rho$ exchange (- - -) and $\pi\text{-}\pi + \pi\text{-}\rho + \rho\text{-}\rho$ exchange (· · · · ·), in conjunction with Bonn B (—) for the analyzing power A_y under nn FSI condition as a function of a neutron lab angle.

This is also exemplified in Fig. 64. At the higher energies studied, 6.5 and 10.5 MeV, the effects of the 3NF become smaller and scaling is much less pronounced.

For the breakup cross section scaling occurs unfortunately only at rather low energies, where measurements are presumably very difficult. The domains which are very insensitive to the choice of the nuclear forces (2N and 3N forces) occur at all energies and are equally challenging. We shall devote the special Section 7.1 to that subject.

It might be added that several 3N bound state properties are already well established to scale with the triton binding energy. These are the charge radii and the D/S ratios of the asymptotic normalization constants of ${}^3\text{He}$ and ${}^3\text{H}$ and the ${}^3\text{He}$ binding energy. For a recent review see [527].

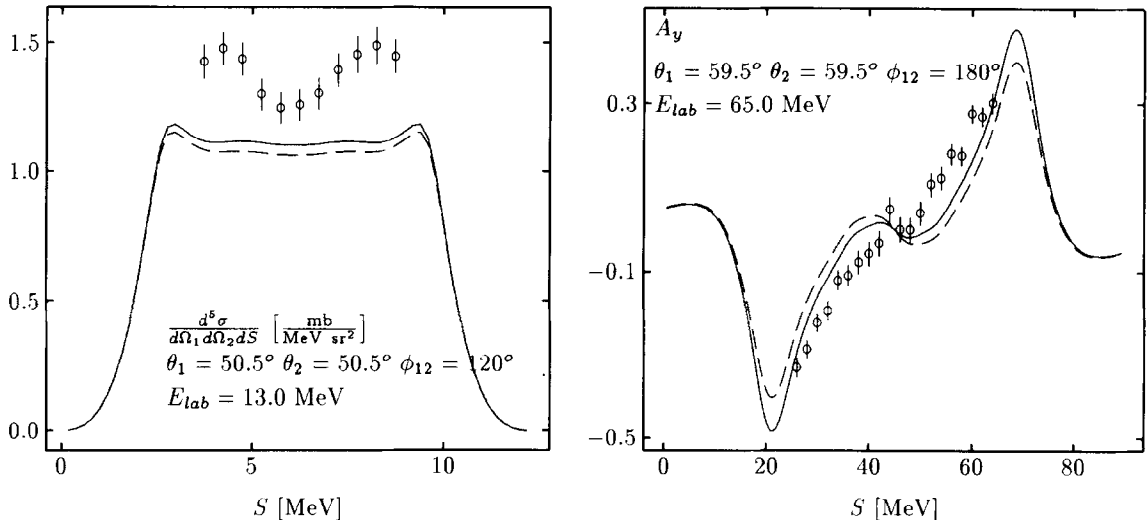


Fig. 60. TM 3NF effects, $\pi\pi$ exchange (---), on top of Bonn B predictions (—) for the space star configuration (left part) and the analyzing power A_y under collinearity condition (right part).

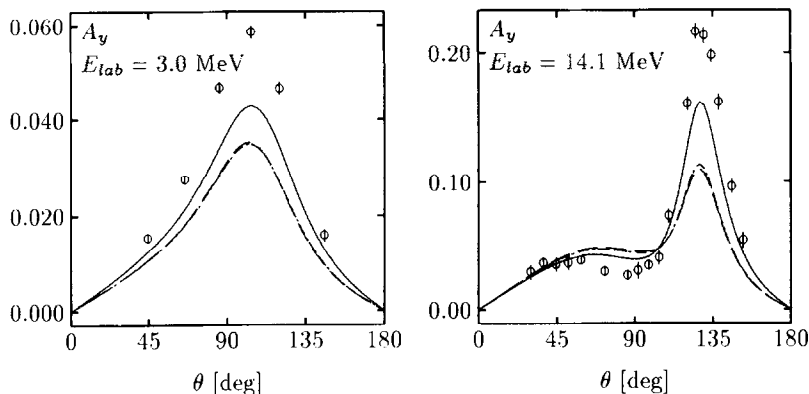


Fig. 61. TM 3NF effects, $\pi\pi$ exchange (---), $\pi\pi + \pi\rho$ exchange (----) and $\pi\pi + \pi\rho + \rho\rho$ exchange (.....), in conjunction with the Bonn B prediction (—) for the analyzing power A_y in elastic nd scattering at 3.0 and 14.1 MeV. The nd data are from [328,329] (3 MeV) and [232] (14.1 MeV).

7. Special topics

7.1. Survey of breakup cross sections

Up to now we concentrated mainly on the four types of breakup configurations, briefly called FSI, QFS, Collinear and Star. But already for some configurations discussed in Section 6.1 (Fig. 44) we encountered a surprise. Thus it might well be that outside of these specific configurations one can find even more sensitive cases to probe the 3N potential energy. In the context of simple forces sensitivity studies have been performed in [502,472,56], with the result, that certain configurations were identified, where different NN forces gave quite different results. We evaluated in steps of 5° in the angles θ_1 and θ_2 and in steps of 10° in the relative azimuthal angle $\phi_{12} = \phi_2 - \phi_1$ of two

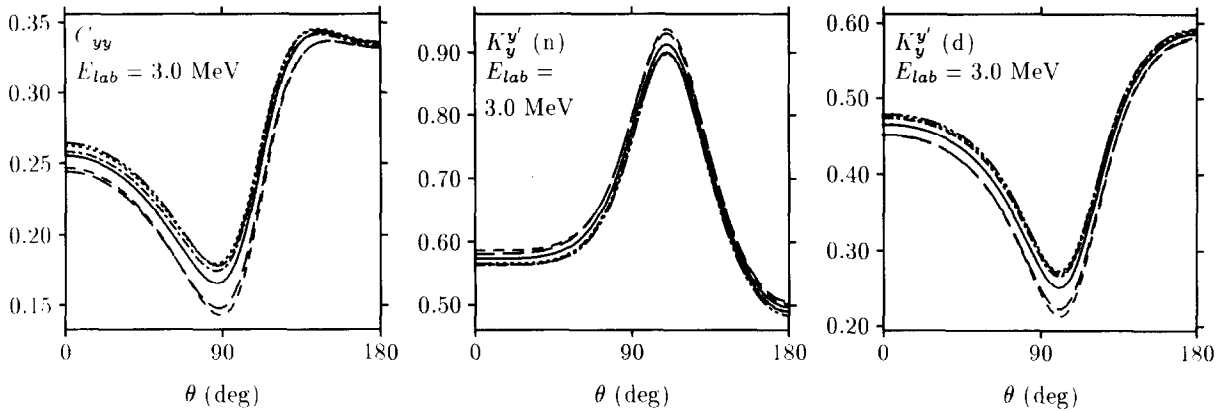


Fig. 62. Examples for Nd spin observables at 3 MeV, which scale with the triton binding energy. The theoretical predictions for the NN forces: Bonn B (—), AV18 (---) and Nijm78 (- - -) deviate from each other, the predictions for NN and 3NF's Bonn B + TM 3NF ($\Lambda = 4.55m_\pi$) (· · · ·), AV18 + TM 3NF ($\Lambda = 4.85m_\pi$) (····) and Nijm78 + TM 3NF ($\Lambda = 5.15m_\pi$) (·····) essentially coincide.

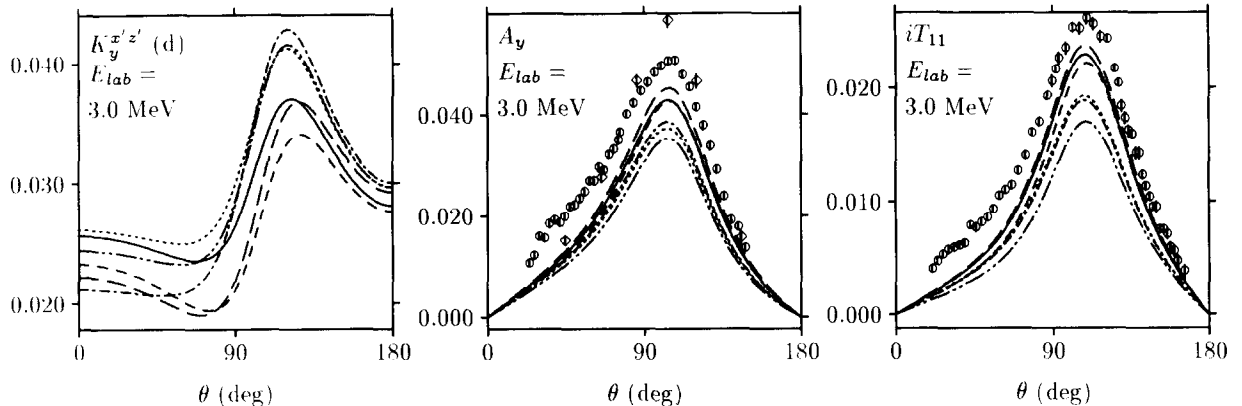


Fig. 63. Examples for Nd spin observables at 3 MeV, which do not scale with the triton binding energy. Description of curves as in Fig. 62. The pd data (○) are from [416] and the nd data (◊) from [328,329].

nucleon detectors the breakup cross sections over all phase space. We used Bonn B and the recently updated NN forces AV18, Nijm93, NijmI and NijmII. The resulting cross sections were compared to each other and those regions in that three-dimensional angular domain were identified, where the cross sections did not deviate from each other by more than 3%. Let us call these configurations insensitive ones with respect to the choice of the NN force. Then we looked whether there are angular configurations under which the cross sections for the various NN forces (at least one of them) deviate among themselves by more than 8%. They will be called the sensitive domains. Both are realised.

We show in Fig. 65 the sensitive domains projected into the θ_1 - θ_2 , θ_1 - ϕ_{12} and θ_2 - ϕ_{12} planes for four energies: $E = 10.3, 13.0, 19.0$ and 65 MeV. We find that at 10.3 and 13 MeV all the sensitive configurations are just nn and np FSI peaks or configurations close to them. Thereby the deviations do not surpass 10.5%. The lines under which nn and np FSI's occur are displayed in the respective θ_1 - θ_2 planes. That result is not surprising since the a_{nn} and a_{np} values of the potentials used in that

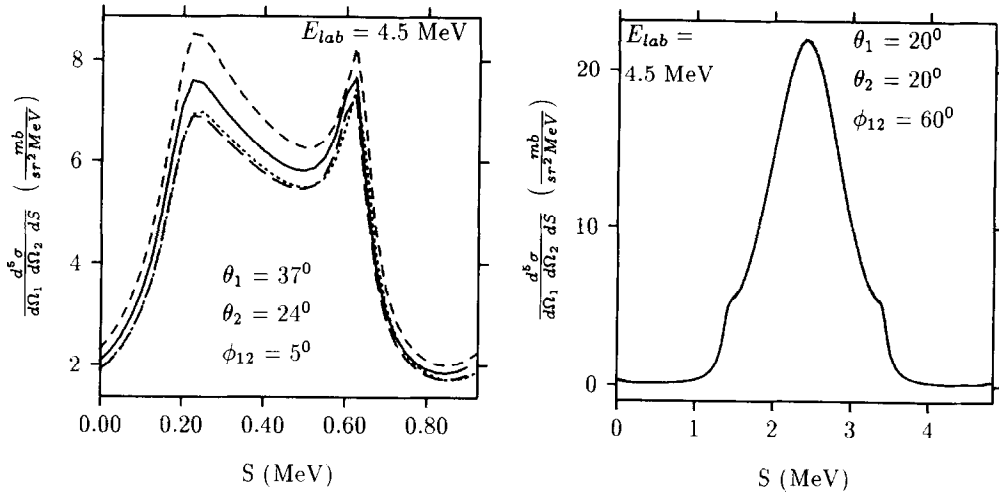


Fig. 64. An example for the breakup cross section at 4.5 MeV which shows scaling (left side) and an example for utmost insensitivity to nuclear dynamics (right side). Theoretical predictions are: Bonn B (—), AV18 (---), Bonn B + TM 3NF ($\Lambda = 4.55m_\pi$) (- · -), and AV18 + TM 3NF ($\Lambda = 4.85m_\pi$) (· · ·).

study deviate slightly from each other and this is reflected in a magnified manner in the FSI peak heights. Therefore that sensitivity is mostly a consequence of "bad" force properties. They are not well enough adjusted in that specific on-shell property. We left out a few cases around $\theta_2 = 60^\circ$, where the deviations are larger than 10.5% but where the arclength is quite short (about 1–2 MeV) and therefore hardly accessible experimentally. At 19 MeV additional sensitive configurations show up, which when plotted against the arclength S have a deep minimum, where the sensitive dependence on the choice of the NN force is located. There the deviations among the different force predictions are up to 15%. Finally at 65 MeV the sensitive domain is strongly enlarged and more different types of cross section patterns appear, which display sensitivity up to 20% (this latter result does not include the NijmII interaction). We show two examples in Fig. 66. Note that the shapes of the cross sections are quite different and the largest spread is 15% in both cases.

Regarding Fig. 65 we see that the sensitive domain in the θ_1 – θ_2 – ϕ_{12} space is gradually changing with energy.

In the literature [251] breakup configurations have been cited which are claimed to be extremely sensitive to the choice of NN forces (oversimplified forces on present day standards). Since in our search with a step size of 5° in θ_1 and θ_2 and 10° in ϕ_{12} we might have overlooked them we looked into one case, the symmetric constant relative energy locus at 19 MeV. The constant relative energy loci are defined by constant relative energies of the three outgoing nucleon pairs. In the symmetric choice one has the additional condition, that the relative energies between the two np pairs are equal. Then the cross section as a function of the energy E_3 of that outgoing nucleon, which is different from the other two, shows a deep minimum. We found that the cross section in this deep minimum is indeed sensitive to the choice of the NN force. At 19 MeV that minimum is located at $E_3 = 1.015$ MeV and the corresponding detector angles are $\theta_1 = 41.19^\circ$, $\theta_2 = 47.62^\circ$ and $\phi_{12} = 152.20^\circ$. Using the modern NN potentials the largest discrepancy was between Bonn B and NijmII and has the value 14.9%. Replacing Bonn B by CD Bonn, which has a perfect χ^2 like NijmII, the discrepancy shrinks to 9.3%. Thus indeed that specific configuration is sensitive, but it is not too special, since it is

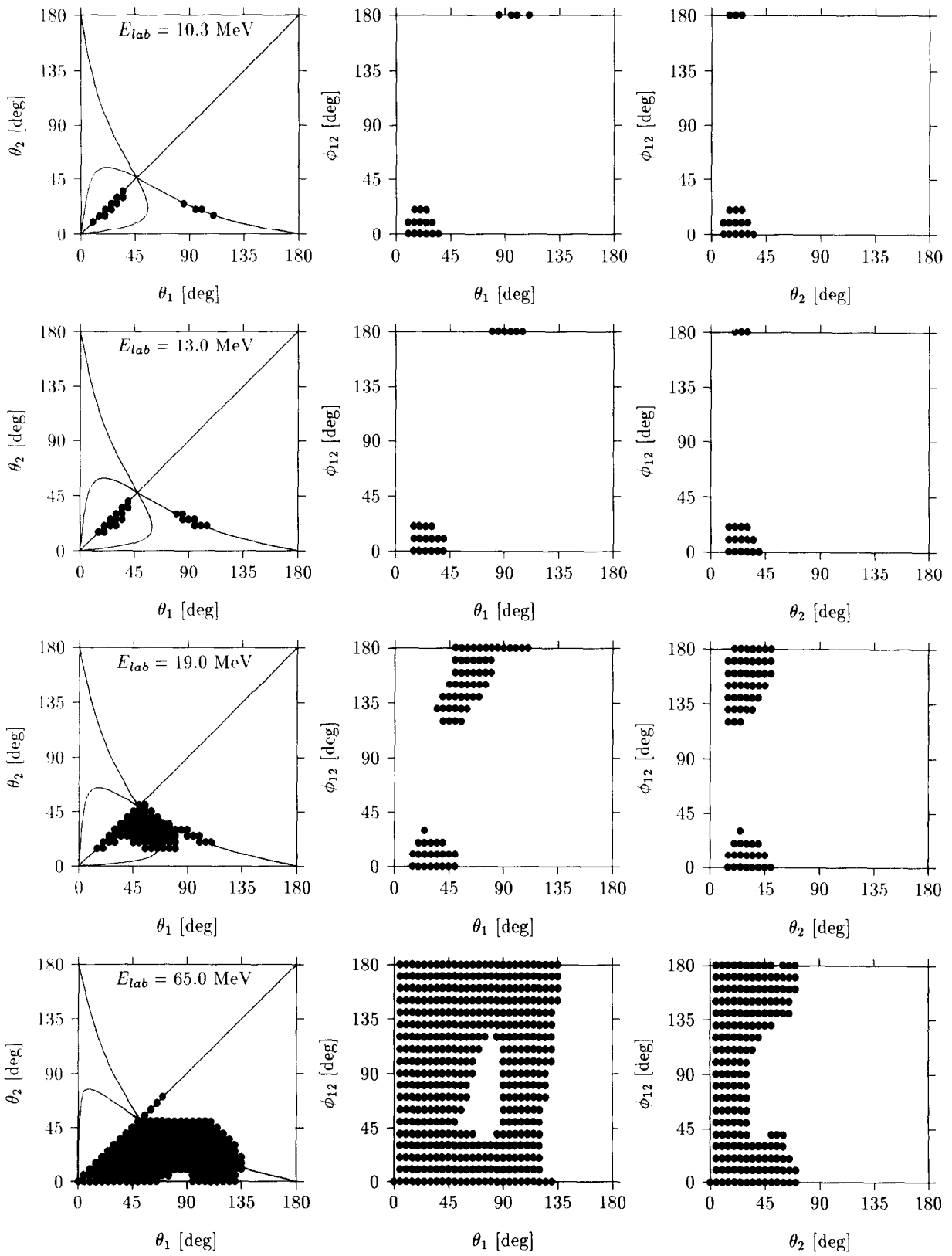


Fig. 65.

surrounded by equally sensitive configurations as seen from Fig. 65. It is located in the sensitive domain and with our grid we came anyhow close to it.

We searched for this minimum also at $E_{lab} = 13$ MeV and found it located at $E_3 = 0.808$ MeV with the corresponding detector angles $\theta_1 = 39.04^\circ$, $\theta_2 = 46.74^\circ$ and $\phi_{12} = 148.16^\circ$. However, at this energy the minimum is not very deep. This is in accordance with what has been found at 14.4 MeV by [251]. In our calculation at 13 MeV the largest discrepancy of 6% was between Bonn B and Nijm93. Since these 6% stay below our ad hoc chosen threshold value of 8% for sensitive configurations it is not included in Fig. 65. Again replacing Bonn B by CD Bonn that discrepancy of 6% shrinks to 3.9%.

Since at 65 MeV the sensitive domain has significantly broadened an extensive set of experimental data there would be very useful to test the theory. The continuation of that study to higher energies is planned.

The extremely insensitive domains, where all the NN force predictions agree among each other within < 3% appear to be also of great interest, since there deviations of the data to theory would seriously question all the present day NN forces. The corresponding domains are shown in Fig. 67. We restricted ourselves to show only cases where the cross sections are larger than 1 mb/(MeV sr²) except at 65 MeV, where all the insensitive cross sections stayed below that value. Again the domains change gradually with energy. We propose that measurements in those most insensitive domains should be performed.

Since an exact treatment of the pp Coulomb force problem together with realistic NN forces is still not yet under control, nd measurements would be preferable. But pd measurements would be

Fig. 65. Domains projected into the $\theta_1-\theta_2$, $\theta_1-\phi_{12}$ and $\theta_2-\phi_{12}$ planes, in which the different NN force predictions (see text) deviate among each other by more than 8%. The four rows are for 10.3, 13.0, 19.0 and 65.0 MeV, respectively.

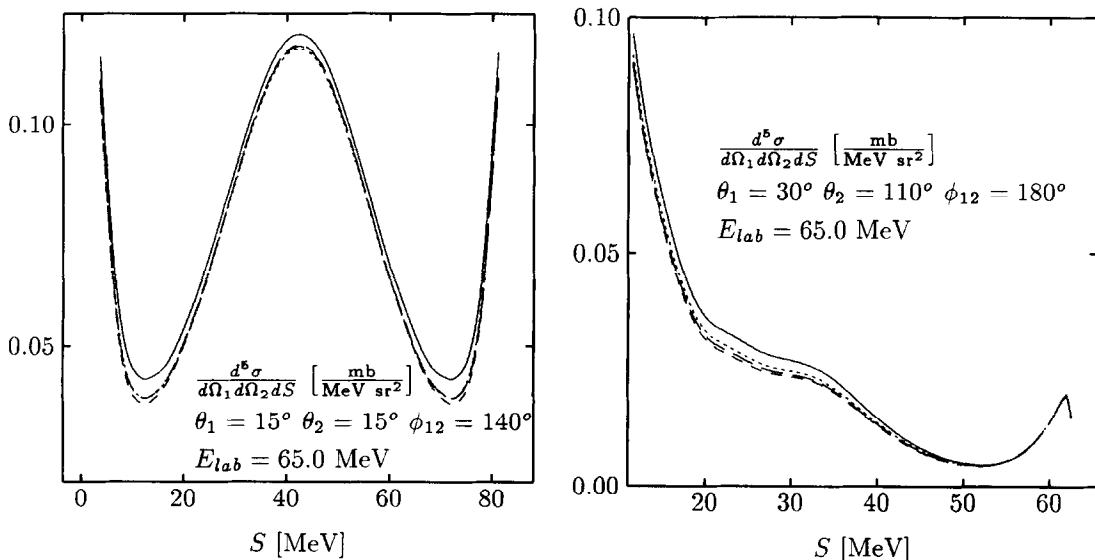


Fig. 66. Two examples out of the sensitive domains at 65.0 MeV. The deviations among the NN force predictions are up to 15%. We used Bonn B (—), AV18 (---), Nijm93 (- - -) and Nijm I (· · · ·).

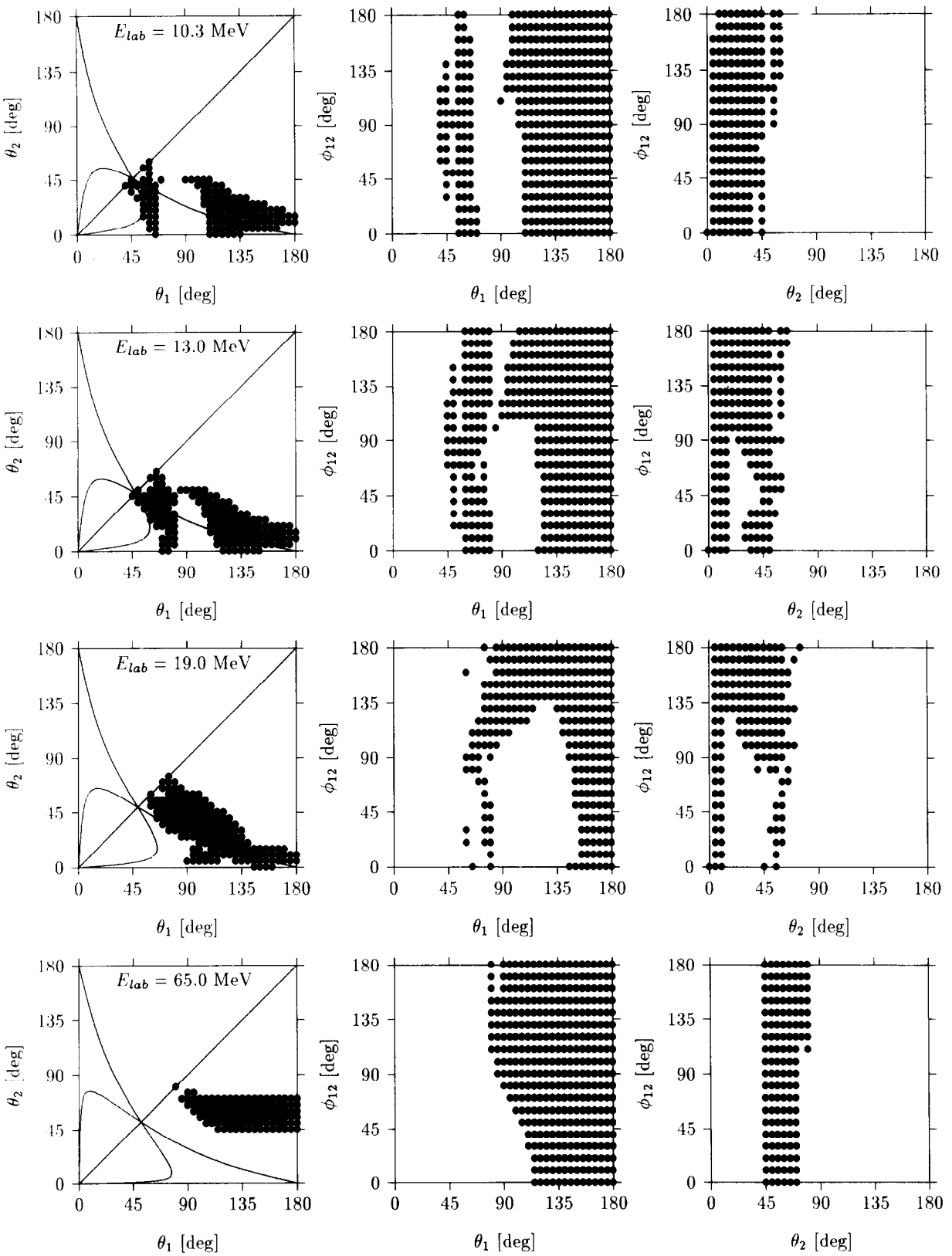


Fig. 67.

also welcome, since they might have smaller error bars and would stimulate that finally one group would solve that technically very challenging theoretical problem of Coulomb forces in 3N scattering in conjunction with realistic forces.

Looking into breakup data known to us we found at 13 MeV a few cases, which lie in the insensitive domain. They are shown in Fig. 39, where we have very good agreement, in Fig. 40, where we agree quite well with the pd data, but not with the nd data (they are presently remeasured [485]), in Fig. 42, where our theory lies between the nd and pd data, and in Fig. 44, where our theory deviates drastically from the nd data. If the cases with strong disagreement would be reconfirmed experimentally, one would have caught hot candidates to see 3NF effects in the 3N breakup process.

In Fig. 68 we show two example of cross sections taken from those insensitive domains. The first one is close to a FSI condition for particles 2 and 3. The second case is rather far away from FSI conditions.

7.2. Extraction of the nn scattering length a_{nn} from the 3N breakup process

We already mentioned that values for the nn scattering length extracted in the past from the nn FSI peak area in the nd breakup process have to be taken with some caution. The use of the Watson–Migdal parametrization introduces additional theoretical uncertainties on top of the experimental errors as has been demonstrated in Section 6.1. In the past also simple finite rank NN forces have been

Fig. 67. Domains projected into the $\theta_1-\theta_2$, $\theta_1-\phi_{12}$ and $\theta_2-\phi_{12}$ planes, in which the different NN force predictions (see text) agree among each other within less than 3% and where the cross sections are larger than $1 \text{ mb MeV}^{-1} \text{ sr}^{-2}$, except at 65 MeV, where the cross sections stay below $1 \text{ mb MeV}^{-1} \text{ sr}^{-2}$. The four rows are for 10.3, 13.0, 19.0 and 65.0 MeV, respectively.

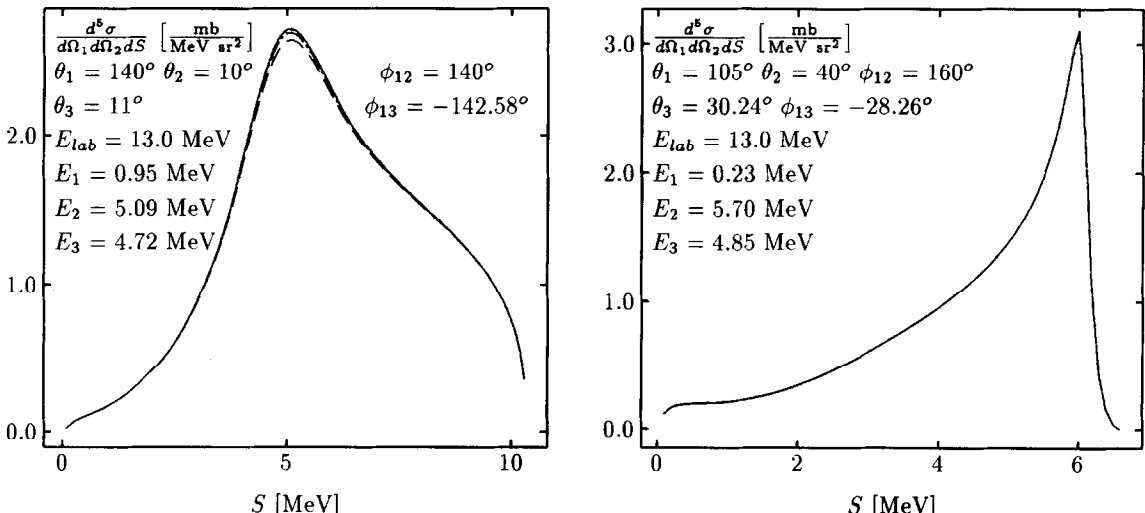


Fig. 68. Two breakup cross sections from the insensitive domains in Fig. 67, see text. The five potential predictions essentially coincide. The left figure refers to a configuration which is close to a 2-3 FSI condition and the relative angle between the momenta k_2 and k_3 is 13.11° ; in the right figure the corresponding angle is 70.03° . The energies E_1 , E_2 , and E_3 together with the angles θ_3 and ϕ_{13} refer to the maxima in the cross sections.

used, often only s-wave forces, and the solution of the Faddeev equations have been compared to the data [535]. Again this can lead to inaccurate results, since as we already pointed out, higher NN force components give a nonnegligible contribution to the FSI peak cross section. Also these simplified old forces certainly do not describe the NN data in a sufficiently accurate manner, which induces further uncertainties. Furthermore as we pointed out in Section 7.1 the FSI peak areas in general belong to the sensitive domains and cross sections evaluated even with the most modern NN forces can deviate from each other, which has consequences for the a_{nn} values extracted. We shall come back to that point below.

In the past [446] also several kinematical incomplete nd measurements have been performed, where only the outgoing proton has been detected in forward direction. The cross section around the highest possible proton energies exhibits a peak, which is due to the nn pair interacting most strongly if its relative energy tends towards zero. Recently in [483] the most reliable data sets have been reanalyzed using various realistic NN forces in fully charge dependent calculations (including T=3/2 states). Thereby the nn force in the state 1S_0 was allowed to vary according to different nn scattering lengths.

The reanalysis of published data between 11 and 62.8 MeV led to a range of extracted a_{nn} values between -12 to -22 fm. They are clustered around -15 fm, which is significantly different from the central value -19.7 ± 1.8 fm [446] achieved by the old analysis. The large spread of that newly found interval is quite disturbing and poses questions about the reliability of the data - and possible 3NF effects, which might be energy dependent. For instance two data sets around 14 MeV are clearly incompatible and require a remeasurement [483]. As an example we display in Fig. 69 a proton spectrum at 11 MeV [306] in comparison to Bonn B predictions with three choices of nn 1S_0 forces supporting $a_{nn} = -15, -17.67$ and -20 fm. The data are normalized by a factor 1.17 in order to agree with theory in the energy range 6.55 to 7.91 MeV to the left of the FSI peak. In that energy range there is a negligible dependence of the theory on the value of a_{nn} . In this case an optimal value of $a_{nn} = -18.54 \pm 2.22$ fm results. See also [526] for possible 3NF effects. A very thorough review on that issue can be found in [484].

Since the np scattering length a_{np} in the state 1S_0 is very precisely known from np scattering, it seems most natural to firstly extract that number from the nd breakup process before attacking the nn problem. Since there are no well documented np FSI peaks from nd breakup known to us we analyzed the three pd breakup data displayed in Fig. 39. First of all theory has to be averaged over the opening angles of the detectors, which has quite a significant influence on the peak heights, whose values are decisive for the extraction of the scattering length. According to [398], [203,366] we used the angular openings of the detectors ($\Delta\theta_1 = 0.3^\circ$, $\Delta\phi_1 = 1.0^\circ$, $\Delta\theta_2 = 1.0^\circ$, $\Delta\phi_2 = 1.5^\circ$), ($\Delta\theta_i = 0.5^\circ$, $\Delta\phi_i = 1.5^\circ$), ($\Delta\theta_1 = 1.0^\circ$, $\Delta\phi_1 = 2.7^\circ$, $\Delta\theta_2 = 0.7^\circ$, $\Delta\phi_2 = 2.9^\circ$) for the three measurements at 10.5, 13.0 and 19.0 MeV, respectively, and assumed equal response probabilities over those $\Delta\theta_i$ and $\Delta\phi_i$ ranges. Then we allowed for variations in the 1S_0 np scattering lengths between -20 fm and -26 fm. The corresponding variations of the potential parameters were installed for us for the Nijmegen and CD Bonn potentials by the respective authors [322,468]. As an example for the dependence of the theoretical cross section (already averaged over the detector opening angles) on the a_{np} value we display in Fig. 70 the np FSI peak at 13.0 MeV. Performing a χ^2 fit based on NijmI(cd), Nijm93(cd) and CD Bonn predictions we found the following results shown in Table 12. We see the results at each energy are only very slightly dependent on the choice of the potential, however vary with energy. At

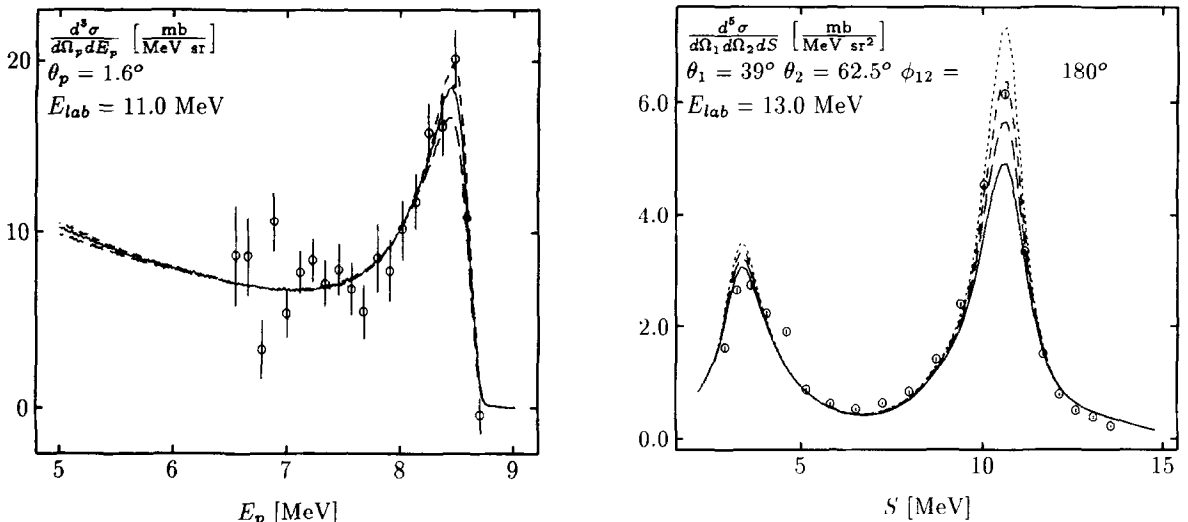


Fig. 69. Renormalized proton spectra (see text) of [306] in comparison with Monte-Carlo simulations using the Bonn B NN potential corresponding to $a_{nn} = -17.67$ fm (—) and modified versions of Bonn B with $a_{nn} = -15$ fm (---) and $a_{nn} = -20$ fm, (- · - · -).

Fig. 70. The a_{np} -dependence of a np FSI peak at 13.0 MeV: (—) $a_{np} = -20$ fm, (---) $a_{np} = -22$ fm, (- · - · -) $a_{np} = -23.74$ fm from CD-Bonn, (· · · ·) $a_{np} = -26$ fm. pd data are from [397].

Table 12

Optimally adjusted a_{np} values to np FSI peaks in the pd breakup process.

E_{lab} (MeV)	$a_{np} \pm \Delta a_{np}$ (fm)		
	CD-Bonn	Nijm 93	Nijm I
10.5	-22.98 ± 0.28	-23.05 ± 0.29	-22.92 ± 0.28
13.0	-23.30 ± 0.22	-23.47 ± 0.23	-23.32 ± 0.22
19.0	-23.98 ± 0.26	-24.44 ± 0.27	-24.20 ± 0.26

13 MeV one is closest to the correct value of $a_{np}^{exp} = -23.74$ fm. Obvious reasons for the discrepancy can be: on the theoretical side unknown Coulomb force and 3NF effects and uncontrolled systematic errors on the experimental side. Also the simulation of the experimental conditions (opening angles of the detectors, detector geometry, etc.) has to be performed with great care. For instance repeating the theoretical analysis using CD Bonn and half (twice) the angular openings given above, the optimal a_{np} values change from -23.3 ± 0.22 fm to -22.83 ± 0.21 fm (-23.8 ± 0.24 fm) for $E = 13.0$ MeV. Thus apparently a sophisticated averaging procedure has to be performed reproducing precisely the experimental conditions.

We also evaluated the np FSI peak heights for all production angles and the three potentials, to see whether there exists a dependence on the choice of the NN force and whether at some angles that possible dependence vanishes. This would be a phenomena like the "magic" angle found for 3NF effects in Section 6.2. Indeed it turned out that there are very small angular ranges at which the predictions of the forces nearly coincide: $\theta = 37^\circ, 43^\circ$ and 51° for $E = 10.5, 13.0$ and 19.0 MeV, respectively. The spreads of FSI peak heights among the different force predictions at angles different

from these "magic" ones can be up to 5%. The above np FSI experiments have been performed under the angles 37° , 39° and 41° for $E = 10.5$, 13.0 and 19.0 MeV, respectively. Since the first two are very close to the magic angles the dependence on the choice of the force is very small, only in the third case there is some dependence, see Table 12. In future experiments one should try always to measure at or close to the magic angles.

The specific 3NF effects generated by the TM 3NF and studied up to now are such that they increase the FSI peak height to the left of the magic angles. Now for the first two cases we are on or very close to the magic angles and should therefore not expect much effects. For the third case, however, we are significantly to the left of the magic angle and based on that 3NF effect should expect that the extracted a_{np} based on NN forces only should be too large. Indeed it turned out to be too large. Right now, however, it is premature to draw quantitative conclusions, since possible Coulomb force effects have not yet been taken into account. That theoretical hindrance would be absent in the analysis of np FSI peaks in the nd breakup process. A measurement is presently being performed at TUNL [484].

The above results prompted us to investigate the model dependence in the analysis of a recently measured nn FSI peak at 13.0 MeV [160]. The model data spanning a band around a kinematical curve corresponding to point geometry have been simulated by theory taking into account the finite geometry effects. Theory in that case was a W-matrix approximation [41] to the Paris potential. With the help of that model the data were projected onto a kinematical curve situated in the middle of the band. According to the authors of [160] those projected data can be analyzed in future studies like "experimental data for point geometry". This has been done in [523] and we update that study now in the following way. We used the Nijm93, NijmI and the CD Bonn potentials, which can be varied with respect to the a_{nn} values similarly as described above for the np FSI case. The optimal adjusted a_{nn} values turned out to be: -14.40 ± 0.40 fm for Nijm93, -14.44 ± 0.39 fm for NijmI and -14.31 ± 0.30 fm for CD Bonn. In Fig. 71 we show the dependence of the FSI cross section on the nn scattering length in the case of the CD Bonn potential. In no case there is a satisfactory description of the shape of the data. We notice that there is negligible force dependence of the extracted a_{nn} values, though the experiment has been performed at a nn production angle of 25° , which is far away from the specific angle of 43° mentioned in [523], only at which the model dependence should vanish. This apparent contradiction results from the fact, that in [523] older potentials have been used, which are much less phase equivalent and which do not describe NN data as well as the new ones. This is another example which shows that it is extremely important to use only NN forces which describe properly NN data in order not to introduce artificial sensitivities to the choice of NN forces, which are not real ones but just a result of insufficient parameter tuning.

The optimally adjusted a_{nn} value of about -14.4 fm is far away from the value -18.6 ± 0.3 fm extracted from π -absorption on the deuteron [159,433]. To clarify the experimental situation a renewed nn FSI measurement at this energy is presently being performed at TUNL [484].

In view of the small NN force dependence we also updated the study presented in [523] on the nn FSI peak heights as a function of the production angles, now for the most modern NN forces. We also added the shifts caused by the π - π exchange TM 3NF ($A_\pi = 5.8 m_\pi$) in conjunction with Bonn B. The result is displayed in Fig. 72. We see that there is indeed an angular range close to 43° , where all predictions come very close together, but the dependence of the FSI peak heights on the new NN force predictions alone is now much weaker than in [523]. Nevertheless that angular range seems to be the place where FSI peaks should be measured in order to extract a_{nn} with the least

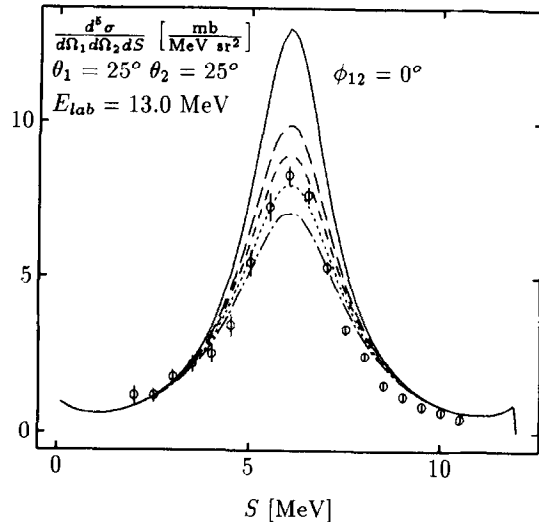


Fig. 71. The a_{nn} -dependence of a nn FSI peak at 13.0 MeV: (—) $a_{nn} = -18.0 \text{ fm}$ from CD-Bonn, (---) $a_{nn} = -16 \text{ fm}$, (- · -) $a_{nn} = -15 \text{ fm}$, (···) $a_{nn} = -14 \text{ fm}$, (- · · -) $a_{nn} = -13 \text{ fm}$. Data are from [160].

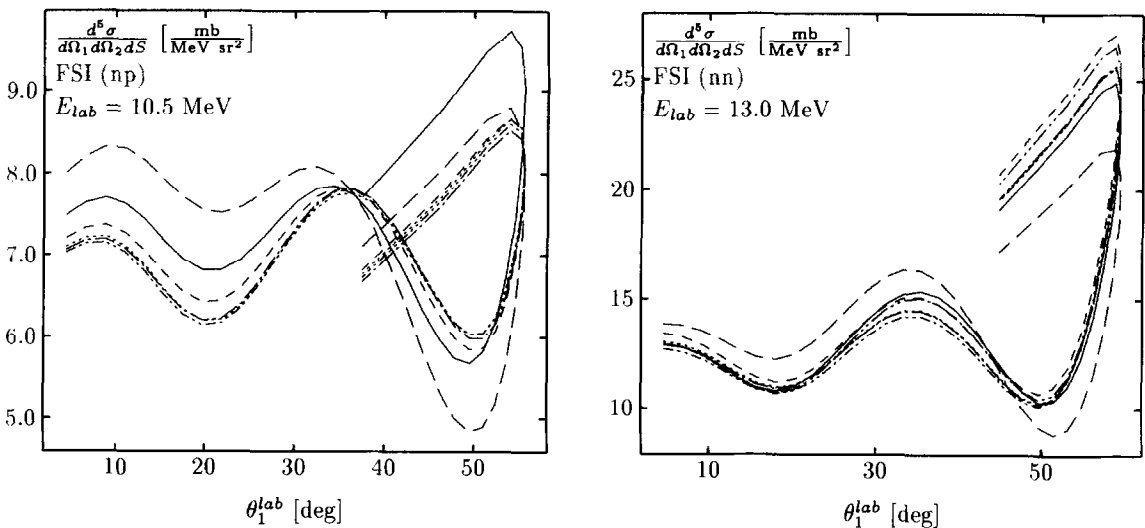


Fig. 72. The "magic" angle at 10.5 and 13 MeV for np and nn FSI peak heights, respectively, as function of lab. angles of nucleon 1. Theoretical predictions are for np FSI at 10.5 MeV: (—) Bonn B, (---) Bonn B + TM 3NF ($\Lambda = 5.8m_\pi$), (- · -) CD-Bonn, (···) Nijm93, (- · · -) NijmI and (- · · · -) NijmII. For nn FSI at 13 MeV: (—) Bonn B, (---) Bonn B + TM 3NF ($\Lambda = 5.8m_\pi$), (- · -) Nijm78, (···) Nijm93, (- · · -) NijmI, (- · · · -) NijmII and (- · - · -) AV14.

possible theoretical uncertainty. It is interesting to note that in the context of very simple forces the existence of such an angle has also been found [472]. Unfortunately none of the experiments done so far and we are aware of have been performed under such an angle. Of course the cross sections at the crossing point of all the curves in Fig. 72 should still vary with a_{nn} . This is demonstrated in [523]. Thus based on the above results a measurement of a_{nn} with an accuracy of $\pm 0.5 \text{ fm}$ would require the experimental error of the cross section to be less than about 5%, which appears to be not

unrealistic.

7.3. The A_y puzzle

We saw the nagging discrepancy between nd and pd data for the low energy analyzing power in elastic scattering on one side and the predictions of all modern NN forces, even including 3NF's (of the TM type) on the other side. We also saw the strong sensitivity of A_y to the 3P_0 , 3P_1 and $^3P_2 - ^3F_2$ NN force components. We also would like to point to the small difference between the pd and nd data, shown as an example in Fig. 14. The pd data around $\theta = 120^\circ$ are a bit smaller than nd data. A qualitative explanation of that effect based on a slow-down hypothesis of the proton in the Coulomb field of the deuteron was tried in [481]. Assuming that the proton will loose some energy (of the order of a few hundred keV) before interacting strongly the pd A_y -values should be smaller around $\theta = 120^\circ$, since the maximum of A_y decreases with decreasing energy. But there is also a change of slope below $\theta = 45^\circ$, whose explanation requires presumably a full treatment of the pp Coulomb force problem. Calculations [51] within the framework of finite rank potentials and including the Coulomb force show indeed such enhancements and at the same time a lowering of the maximum (see Section 8.5). Whether the difference between pd and nd data also requires CSB effects in the 3P_j NN forces [517] can only be decided, if the Coulomb force problem is treated correctly in conjunction with the best present day NN forces.

Now the PSA of Nijmegen and Arndt do not fully agree with each other; furthermore each one has error bars. In the Nijmegen case they are explicitly given, in Arndt's case they are recommended to be the deviations between the results of the single energy and the multi energy analysis. Also the NN phases of the newest potentials can be considered as results of independent PSA's, since the forces have been fitted to the NN data and the χ^2 per datum is as good as in the Nijmegen PSA. If we regard the 3P_j phases in Table 8 we see a spread of about 3%, which has therefore to be taken as a typical uncertainty in PSA values of that type. What influence has this uncertainty onto the 3N analyzing power A_y ? Let us first regard the np and pp system. We modified the 3P_0 , 3P_1 and $^3P_2 - ^3F_2$ phases by 3% in such a direction, that the corresponding NN force predictions increase the maximum in the 3N A_y . This requirement is that the 3P_0 force has to be weakened and the 3P_1 and $^3P_2 - ^3F_2$ forces strengthened. In this study we used the NijmI potential. The effect on the pp analyzing power is hardly visible as shown in Fig. 73 in one example at $E_{lab} = 9.85$ MeV. The reason is that the pp A_y results from an interference of a very small nuclear and a dominating Coulomb amplitude. In the np case however the nuclear amplitude is much stronger and the effect of the 3% variation is clearly visible, see also Fig. 73. In fact the 3% variations in the np system are somewhat too strong, while in the pp system, based on A_y alone, even larger variations appear to be possible. The outcome for the 3N A_y is also displayed in Fig. 73. We see a significant increase in the maximum towards the experimental data, but it is not sufficient to solve that puzzle.

We would like to emphasize that only NN forces, which describe the NN system sufficiently well, should be used to deal with the 3N analyzing power puzzle [520].

Finally we would like to mention an explanatory purely phenomenological study [517], where we allowed for a much stronger CIB breaking in the 3P NN force components. The only constraint was to describe the np and pp A_y data about as well as the so called realistic NN potentials. It turned out that there are very many ways to choose the 3P NN phases. We chose one of them, which at the same time of course should favor the description of the 3N analyzing power A_y . In this manner a

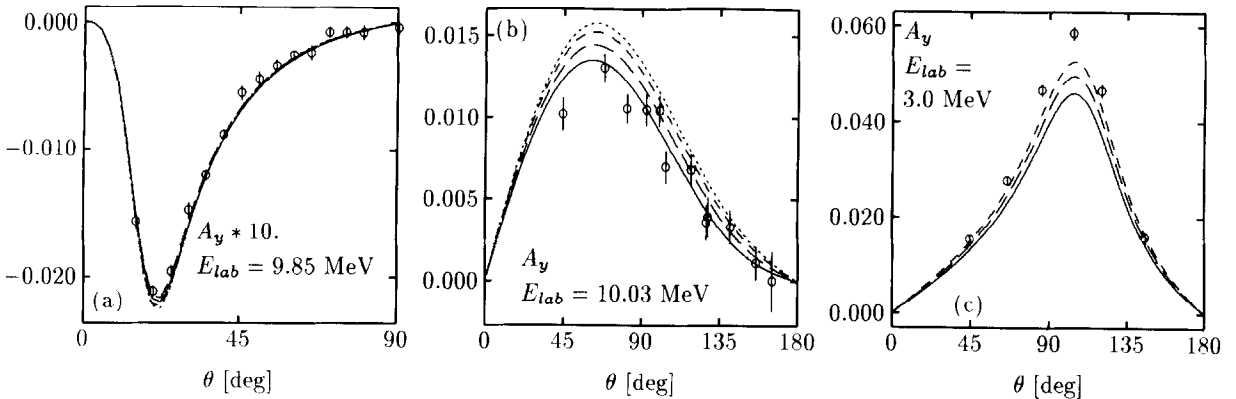


Fig. 73. Analyzing power A_y for pp (a), np (b) and nd (c) scattering. Comparison of the Nijmegen prediction (—) to ones with modified 3P_j forces, which lead to changes in the 3P_j phases by 3%: 3P_0 alone (---), 3P_0 and 3P_1 (- - -), 3P_0 , 3P_1 and 3P_2 – 3F_2 (.....) for (a) and (b). In (c) 3% in 3P_j np and 1% in 3P_j pp channels (---), 3% in 3P_j np and pp channels (- - -).

significant reduction of the old discrepancy could be achieved [517]. Also we think that this study can be refined to reach a very low χ^2 . Unfortunately that phenomenological CIB is quite opposite to what the meson theoretical study tells [322].

Right now the puzzle remains. If the 3P_j phases of the Nijmegen PSA will turn out to be final, then in view of the experience gained up to now with the adjusted NN forces it seems unlikely that the experimental A_y can be described with NN forces only. Three-nucleon force effects will thus be required, where however the first trial with the TM force totally failed.

7.4. Eigen phase shifts and mixing parameters for elastic nd scattering above the breakup threshold

In the past there have been several trials [429,279] to work out a PSA for elastic Nd scattering below and above the breakup threshold. With not sufficient theoretical guidance at that time some unrealistic simplistic assumptions were made, as we know now, not expecting that all possible complexities are indeed realised. In a channel spin representation (the channel spin Σ being the sum of spins of two colliding nuclei, here the deuteron and a nucleon) all possible transitions between the two Σ 's ($1/2$ and $3/2$) and the relative orbital angular momenta (here called λ) really occur, the only restriction being the conserved total 3N angular momentum and the parity. The resulting 3×3 S-matrix has been already displayed in Section 5. Now above the breakup threshold all quantities in (209)–(214), the eigen phases and the three mixing parameters ϵ , ξ and η can in principle be complex and they are. The spin and momentum dependencies of the NN force acting between the projectile nucleon and the constituents of the deuteron are transformed in the full 3N dynamics into effective forces between the projectile nucleon and the deuteron as a whole. These effective forces contain information about the coupling between elastic scattering and the breakup process. We used several NN forces and evaluated the phase shift and mixing parameters defined in Section 5. Though the 3N scattering observables are quite stable with respect to replacing one NN force by another some phase shift and mixing parameters change thereby significantly. This is displayed in Table 13 for 13 MeV. We notice that the predictions for η in the state $1/2^+$ have a spread of up to 20%. Also mixing parameters for higher J^π -values vary up to 4–5%. Among the eigen phases especially

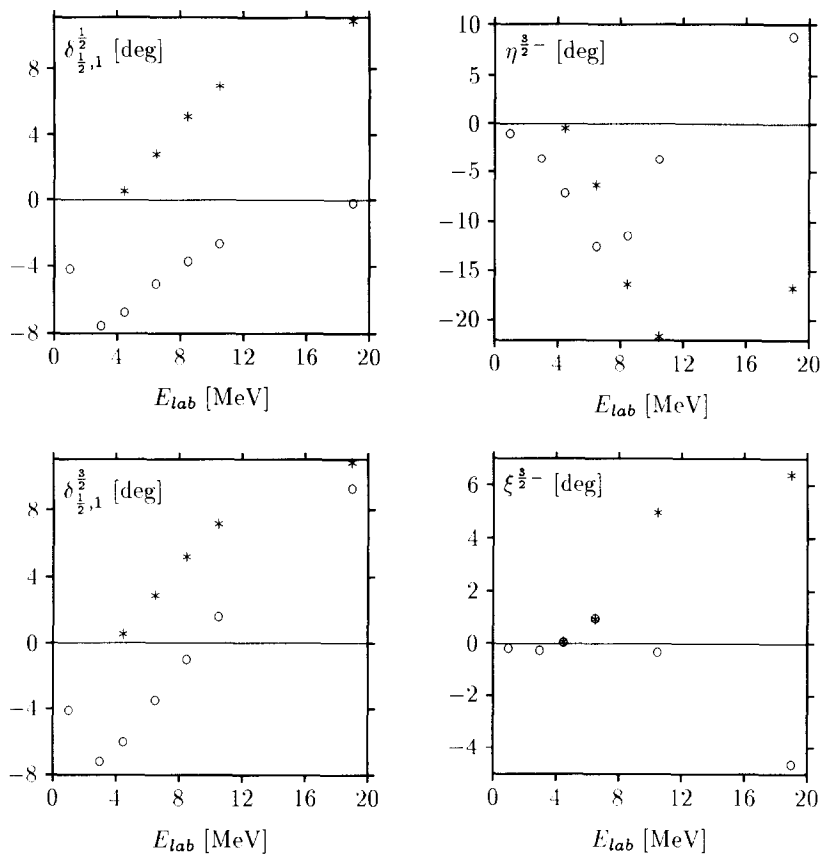


Fig. 74. Examples for eigen phases and mixing parameters for elastic nd scattering above the breakup threshold. Their real and imaginary parts are indicated by (○) and (*), respectively.

$\delta_{1/2}^{1/2}$ for $J'' = 1/2^+$ and $\delta_{1/2}^{3/2}$ for $J'' = 3/2^-$ stick out with variations of up to 5%. Apparently the 3N observables studied up to now are influenced by many of these S-matrix parameters and the variations seen in Table 13 are averaged out.

As example for the energy variations we display two eigen phase shift and two mixing parameters in Fig. 74 based on the Bonn B NN force. We notice imaginary parts which are comparable in magnitude to the real parts and which reflect the strong transitions between different Σ 's and λ 's through the loss of flux into the breakup channel. It might be worthwhile to evaluate the scalar coefficients in a "Wolfenstein parametrization" of the elastic scattering amplitude, quantifying the different types of spin and momentum dependencies. As worked out in [438] there are 12 independent scalar combinations built out of the two spin vectors and the momentum vectors in the initial and final state. In the NN case there are only five (on shell).

Regarding Fig. 74 one notices a strong variation of the $\eta^{3/2-}$ in the energy around 8–10 MeV. Does that signify some special dynamical event? We looked into the energy dependence of the underlying S-matrix elements, which govern the observables and found them to be smooth. Thus that strong energy variation of the $\eta^{3/2-}$ is just an artifact of the specific parametrization and seems to have no physical meaning. For more details see [239,240].

Finally we come back to the 3N analyzing power A_y . Using its representation in terms of the eigen

Table 13

Eigen phase shift and mixing parameters for elastic nd scattering at 13 MeV for various recent NN forces. The format is (real part, imaginary part). Notice the strong variations in $\delta_{\frac{1}{2}0}$ and η for $1/2^+$.

J^π	$\delta_{\Sigma\lambda}$	CD Bonn	AV18	Nijm 93	Nijm I	Nijm II
$\frac{1}{2}^+$	$\delta_{\frac{1}{2}2}$	(-7.69, .57)	(-7.65, .56)	(-7.58, .57)	(-7.67, .57)	(-7.70, .57)
	$\delta_{\frac{1}{2}0}$	(-70.97, 19.31)	(-75.46, 18.39)	(-74.21, 18.77)	(-73.03, 18.76)	(-74.99, 18.63)
	η	(1.27, .13)	(.94, .09)	(1.06, .12)	(1.10, .11)	(1.03, .09)
$\frac{1}{2}^-$	$\delta_{\frac{1}{2}1}$	(-.73, 8.30)	(-.86, 8.11)	(-.47, 8.24)	(-.83, 8.22)	(-.83, 8.25)
	$\delta_{\frac{3}{2}1}$	(36.66, 3.42)	(36.71, 3.27)	(36.86, 3.38)	(36.73, 3.41)	(36.34, 3.36)
	ϵ	(23.01, 4.98)	(22.49, 4.67)	(22.89, 4.89)	(22.88, 4.89)	(22.66, 4.89)
$\frac{3}{2}^+$	$\delta_{\frac{3}{2}0}$	(75.09, .29)	(75.24, .28)	(75.42, .29)	(75.67, .29)	(75.08, .29)
	$\delta_{\frac{1}{2}2}$	(6.84, 1.57)	(6.83, 1.52)	(6.86, 1.55)	(6.84, 1.56)	(6.82, 1.55)
	$\delta_{\frac{3}{2}2}$	(-8.17, .57)	(-8.15, .56)	(-8.05, .57)	(-8.15, .57)	(-8.17, .57)
	η	(-1.65, -.22)	(-1.68, -.21)	(-1.66, -.21)	(-1.67, -.22)	(-1.65, -.22)
	ϵ	(2.08, .51)	(1.97, .51)	(2.02, .52)	(2.03, .51)	(2.04, .50)
	ξ	(4.57, -.11)	(4.55, -.10)	(4.57, -.11)	(4.57, -.11)	(4.53, -.11)
$\frac{3}{2}^-$	$\delta_{\frac{1}{2}3}$	(2.45, 1.11)	(2.49, 1.14)	(2.45, 1.10)	(2.47, 1.12)	(2.49, 1.11)
	$\delta_{\frac{1}{2}1}$	(4.99, 8.62)	(4.66, 8.30)	(5.21, 8.55)	(4.82, 8.52)	(4.72, 8.53)
	$\delta_{\frac{3}{2}1}$	(30.58, 2.90)	(30.78, 2.83)	(31.00, 2.90)	(30.87, 2.91)	(30.66, 2.87)
	η	(4.16, -19.33)	(3.80, -20.21)	(4.67, -19.11)	(3.95, -19.65)	(3.62, -19.60)
	ϵ	(-15.15, -4.59)	(-14.77, -4.20)	(-14.94, -4.46)	(-15.04, -4.42)	(-14.82, -4.35)
	ξ	(-2.31, 4.88)	(-2.14, 4.98)	(-2.37, 4.72)	(-2.24, 4.94)	(-2.14, 4.89)
$\frac{5}{2}^+$	$\delta_{\frac{3}{2}4}$	(-1.00, .02)	(-1.00, .02)	(-1.00, .02)	(-1.00, .02)	(-1.00, .02)
	$\delta_{\frac{1}{2}2}$	(6.69, 1.55)	(6.65, 1.50)	(6.68, 1.52)	(6.67, 1.53)	(6.65, 1.52)
	$\delta_{\frac{3}{2}2}$	(-9.32, .59)	(-9.32, .58)	(-9.23, .59)	(-9.30, .58)	(-9.32, .58)
	η	(-4.37, .74)	(-4.30, .70)	(-4.32, .71)	(-4.35, .72)	(-4.34, .72)
	ϵ	(-.63, -.24)	(-.63, -.24)	(-.66, -.25)	(-.62, -.24)	(-.63, -.24)
	ξ	(-3.14, -.11)	(-3.11, -.11)	(-3.15, -.12)	(-3.13, -.11)	(-3.12, -.11)
$\frac{5}{2}^-$	$\delta_{\frac{3}{2}1}$	(37.51, 2.39)	(37.31, 2.36)	(37.38, 2.39)	(37.55, 2.41)	(37.21, 2.38)
	$\delta_{\frac{1}{2}3}$	(-1.18, .23)	(-1.18, .22)	(-1.17, .22)	(-1.18, .22)	(-1.18, .22)
	$\delta_{\frac{3}{2}3}$	(2.99, .08)	(3.00, .08)	(3.01, .08)	(2.99, .08)	(2.99, .08)
	η	(-.70, .09)	(-.68, .08)	(-.69, .09)	(-.71, .09)	(-.71, .09)
	ϵ	(.29, .45)	(.33, .43)	(.33, .44)	(.30, .44)	(.29, .44)
	ξ	(1.96, -.03)	(1.92, -.03)	(1.94, -.03)	(1.98, -.03)	(1.98, -.03)
$\frac{7}{2}^+$	$\delta_{\frac{3}{2}2}$	(-7.63, .57)	(-7.64, .56)	(-7.57, .57)	(-7.62, .56)	(-7.64, .57)
	$\delta_{\frac{1}{2}4}$	(.61, .04)	(.61, .03)	(.61, .04)	(.61, .04)	(.61, .04)
	$\delta_{\frac{3}{2}4}$	(-.98, .02)	(-.98, .01)	(-.98, .02)	(-.98, .02)	(-.98, .02)
	η	(-2.73, -.19)	(-2.69, -.19)	(-2.73, -.20)	(-2.71, -.19)	(-2.70, -.19)
	ϵ	(-.45, -.08)	(-.44, -.08)	(-.47, -.08)	(-.45, -.08)	(-.44, -.08)
	ξ	(6.10, .35)	(6.02, .35)	(6.10, .36)	(6.06, .35)	(6.03, .35)

Table 13—continued

J^P	$\delta_{\Sigma\lambda}$	CD Bonn	AV18	Nijm 93	Nijm I	Nijm II
$\frac{7}{2}^-$	$\delta_{\frac{5}{2},5}$	(.40, .01)	(.40, .01)	(.40, .01)	(.40, .01)	(.40, .01)
	$\delta_{\frac{3}{2},3}$	(−1.12, .22)	(−1.12, .21)	(−1.12, .21)	(−1.12, .21)	(−1.12, .21)
	$\delta_{\frac{5}{2},1}$	(3.45, .08)	(3.45, .08)	(3.46, .08)	(3.45, .08)	(3.45, .08)
	η	(−9.42, −1.40)	(−9.26, −1.33)	(−9.35, −1.38)	(−9.37, −1.38)	(−9.31, −1.36)
	ϵ	(.14, −.24)	(.13, −.23)	(.15, −.24)	(.14, −.24)	(.14, −.24)
	ξ	(−2.24, .06)	(−2.19, .05)	(−2.21, .05)	(−2.22, .05)	(−2.21, .05)

phase shift and mixing parameters, one can search for those of them, which rule that observable in the most sensitive manner. The clear result is that these are the eigen phase shifts $\delta_{3/2,1}^{1/2}$, $\delta_{3/2,1}^{3/2}$ and $\delta_{3/2,1}^{5/2}$. The next question then appears, is there a close connection between specific NN force components and these three eigen phases. Thus we varied all NN force components individually by 10% in strength and looked for those eigen phase shifts and mixing parameters which were affected most strongly. It turned out in a very clear cut manner that just the 3P NN force components are mostly responsible for the three eigen phases, which again determine A_y . Thus we rediscovered again what one has known before without using the language of eigen phases and mixing parameters, namely that the 3P forces govern A_y at low energies. This opens now a door to possibly solve the A_y -puzzle. If a Nd PSA would succeed to extract these three eigen phases their values would put constraints on the underlying 3P NN forces. The NN forces presently existing certainly generate incorrect values for those eigen phases, the reason being either on- or off-shell defects or action of 3NF's of a new type.

7.5. High energy limit

At high projectile energies the deuteron binding energy can be neglected and one might expect that the deuteron can be considered to be a nucleon target with the other nucleon just a spectator. Thus a simple scattering process (first order in t) should finally emerge. But on the other hand the second nucleon, though very weakly bound, is rather close by and this might necessarily lead to some rescattering effects. We investigated that question already in Section 6.1 for the QFS breakup configuration and found that first order rescattering was present even at 220 MeV. This is presumably due to the fact that the de Broglie wave length $\lambda = h/q_0$ at this energy is still 2.9 fm, larger than the typical distance of np in the deuteron. Now we repeat that study for all breakup configurations. Thus we solve Eq. (154) exactly and compare its solution to the first order term, tP , the sum of the first order and second order term in t , etc. We used AV18 as the working vehicle and studied 65 and 140 MeV. As in the sensitivity study of Section 7.1 we went through all the phase space in steps of 5° or 10° for $E = 65$ MeV and 140 MeV, respectively, in the angles θ_1 , θ_2 and in steps of 10° in ϕ_{12} and compared the breakup cross sections evaluated in first order, up to second, third and fourth order in t to the exact results. As a measure we used

$$\Delta^{(i)} = \sqrt{\frac{\int (\sigma(S)^{(i)} - \sigma(S)^{full})^2 dS}{\int (\sigma(S)^{full})^2 dS}} \quad (228)$$

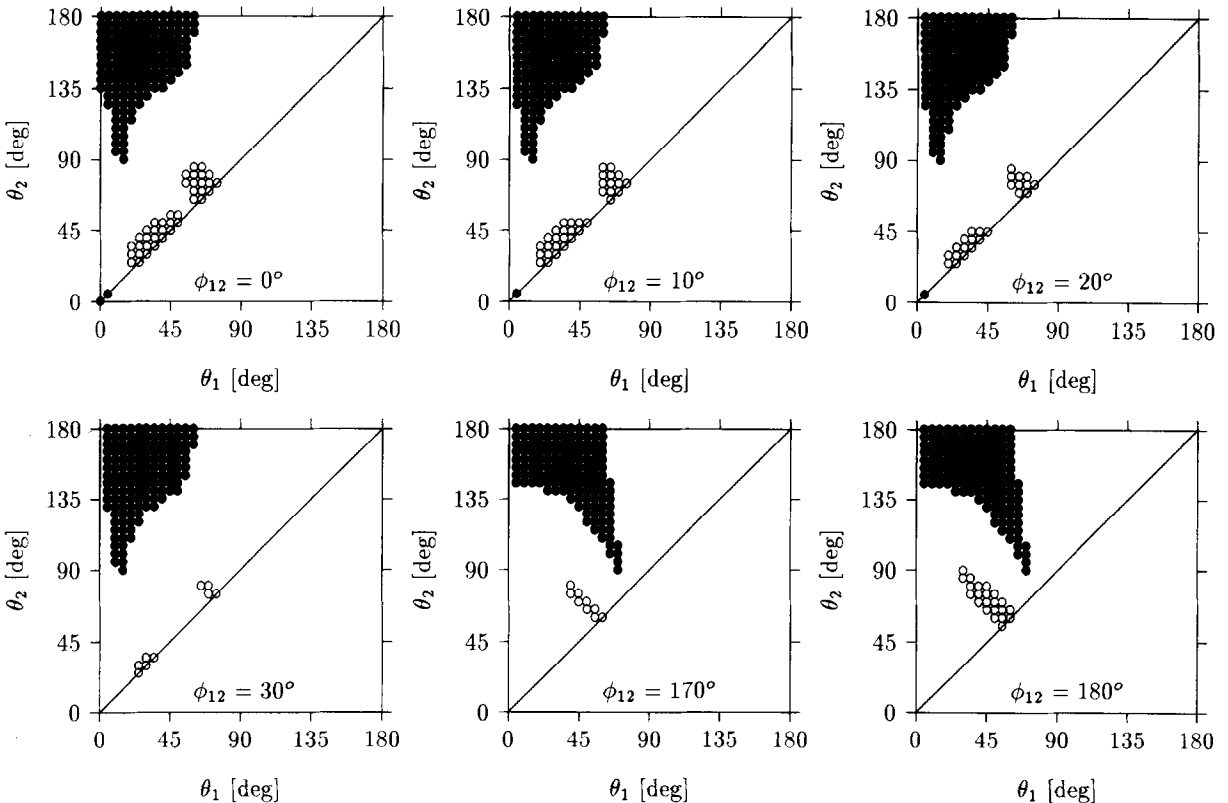


Fig. 75. The locations (open circles) for strong rescattering (second group, see text) in the θ_1 - θ_2 planes for fixed ϕ_{12} 's. The events of the first group reaching the exact result within 5% after the fourth order in t are shown as solid circles. The remaining events lie in between. This refers to 65 MeV.

where $\sigma(S)^{(i)}$ is the fivefold differential breakup cross section evaluated up to the i th order in the t -matrix t , $\sigma(S)^{full}$ is the cross section to all orders in t and S the arclength on the kinematically allowed locus in the E_1 - E_2 plane.

At 65 MeV we decomposed all the events into three groups, a first one where after the fourth order in t one reaches the exact result within 5%, a second one, where after the fourth order rescattering one is still away from the exact result by more than 100% and the remaining cases, which are in between, but require more than the fourth order in t . Since the events of the second group are located either at or near $\phi_{12} = 0^\circ$ or $\phi_{12} = 180^\circ$ we show their location in θ_1 - θ_2 planes for various fixed values of ϕ_{12} . As we see from Fig. 75 the domains of strong rescattering (second group) are mostly at $\phi_{12} = 0^\circ$ and die out near $\phi_{12} = 30^\circ$ and then again another region occurs for $\phi_{12} = 180^\circ$ and close to it. Representative cross sections out of these domains are displayed in Fig. 76. The structures seen are all caused by FSI's (also nearby ones). We see strong divergencies. As one example out of the third group Fig. 76 shows also a space star configuration, where after fourth order in t one is still off by 20% from the exact result.

It is also interesting to note that in first order in t the smallest Δ -value among all the configurations considered was 0.13 and the largest one 10.5, up to second, third, fourth orders the corresponding numbers were 0.09 and 3.8, 0.02 and 5.54 and finally 0.018 and 5.09, respectively. This shows both,

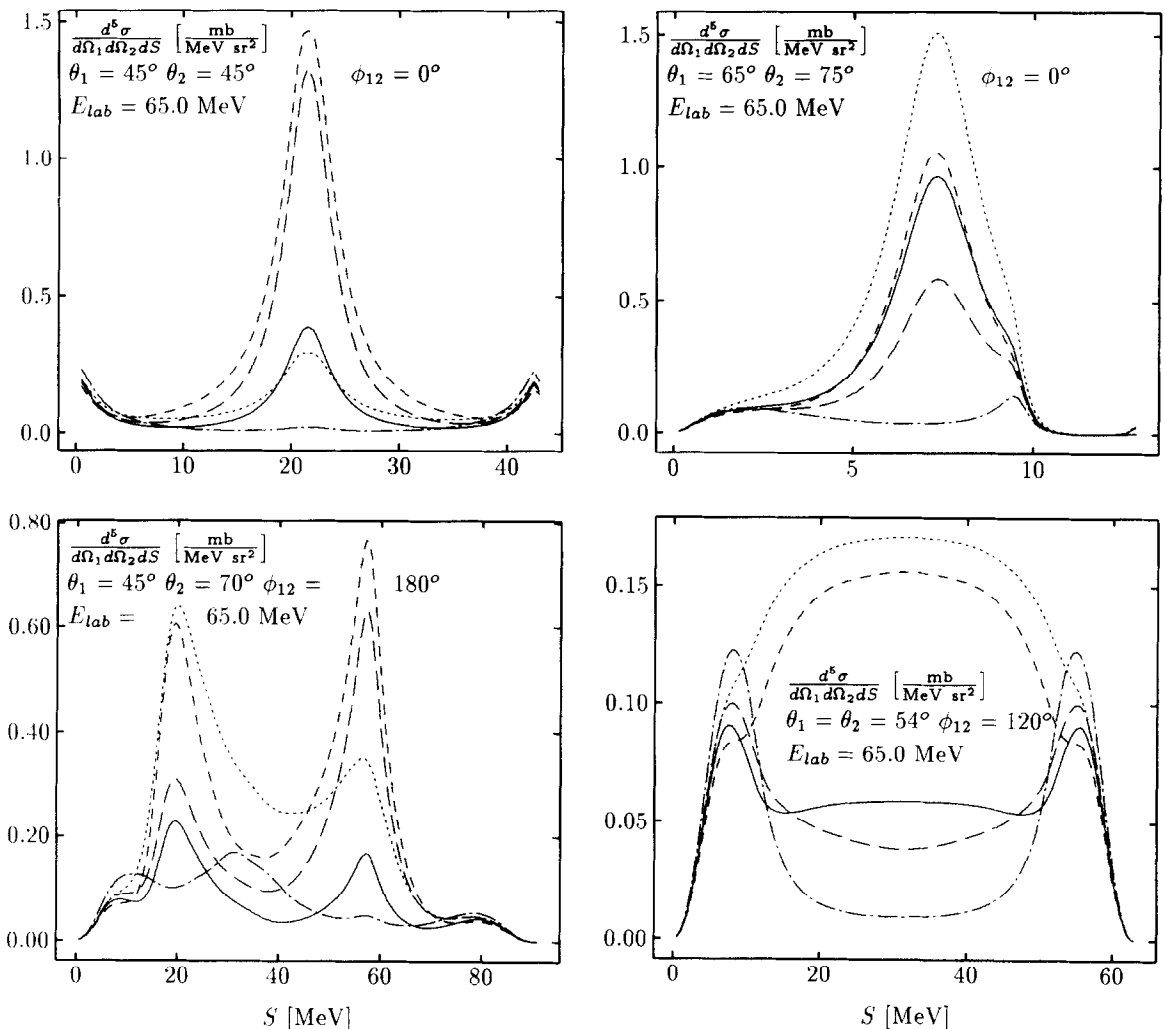


Fig. 76. Three representative cross sections out of the second group in Fig. 75 for $\phi_{12} = 0^\circ$ and 180° . The cross sections evaluated up to the first, second, third and fourth order in t (not using Pade) are given as $(\cdots \cdots)$, $(\cdot \cdot \cdot \cdot)$, $(- - -)$, and $(- - - -)$, respectively, the fully converged result as $(—)$. The cross section for $\phi_{12} = 120^\circ$ is a space star configuration out of the third group, where rescattering is less strong, but even after the fourth order one is still 20% off the exact result.

convergence and severe divergence.

Now at 140 MeV the corresponding numbers are 0.094 and 8.32, 0.012 and 1.54, 0.008 and 0.84 and finally 0.0016 and 0.51, respectively. Thus even the worst case in relation to the number of rescatterings appears to converge.

At 140 MeV we have chosen again 3 groups of events, one with $\Delta < 5\%$ and one with $\Delta > 20\%$ after the fourth order in t , and the rest. The angular regions spanned by the events of the second group are now much smaller and occur only for $\phi_{12} = 0^\circ$ and 180° . This is displayed in Fig. 77 together with the regions for the events of the first group. Finally Fig. 78 shows two cross sections out of the two separated regions for the second group. Again the structures are linked to FSI's or nearby FSI's.

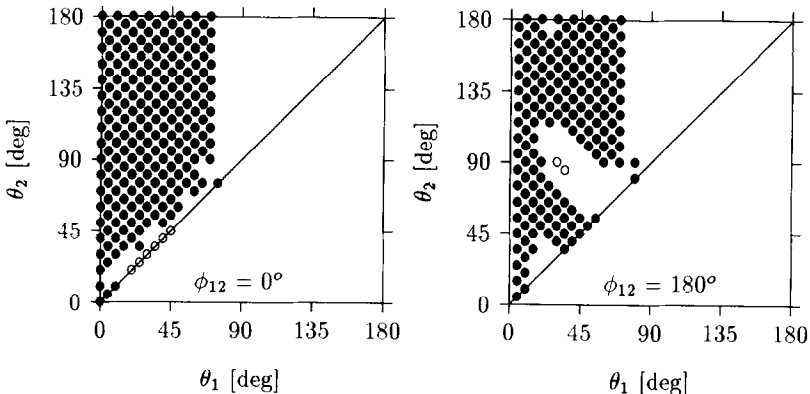


Fig. 77. The locations of the second group (open circles) and the first group (solid circles) at 140 MeV (see text). The few events of the second group are still off by at least 20% from the exact result even after the fourth order in t , while all the events of the first group reach the exact result within 5% after the fourth order in t .

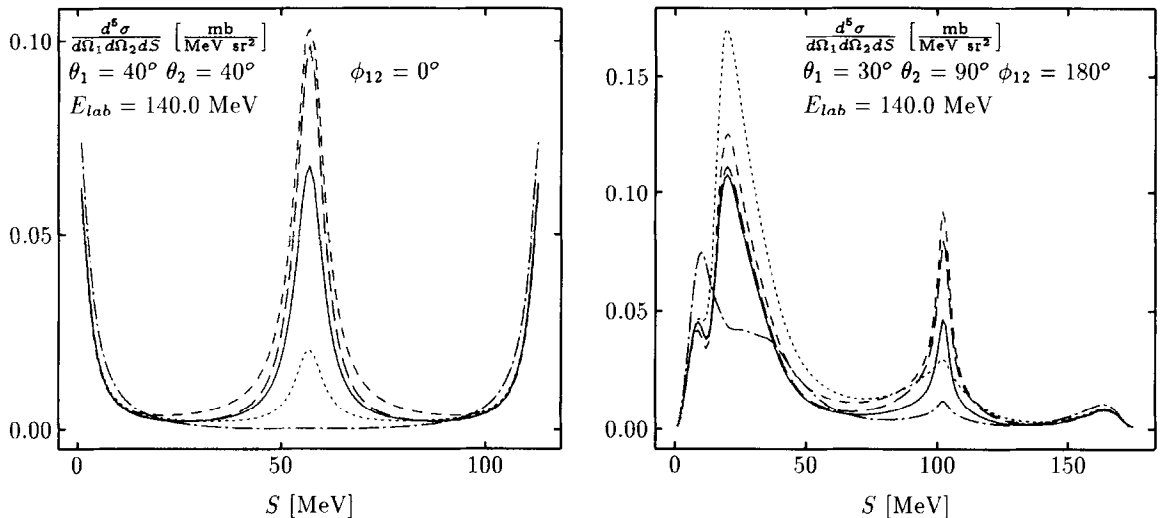


Fig. 78. Two representative cross sections out of the second group in Fig. 77. Description of the curves as in Fig. 76.

Now from a practical point of view, calculating the first order rescattering process (second order in t) is as difficult as calculating a process of an arbitrary order in t . It requires the full integral kernel with all its singularities. The only advantage is, that working only to second or third order saves computer time in comparison to evaluate processes as high as the 10th order, say.

Using the extreme impulse approximation in the breakup cross section formula (Eq. (99)), the first term in Eq. (221), and strict QFS condition (note that the D-wave part of the deuteron state does not contribute, since it vanishes for zero argument) – one easily finds

$$\frac{d^5\sigma}{d\hat{p}d\hat{q}dq}\Big|_{\text{QFS}}^{\text{IA}} = \frac{1}{8}\pi^3 m^2 q_0^2 \sqrt{1 + \frac{m\epsilon_d}{(\frac{3}{4}q_0)^2}} \varphi_0^2(0) \frac{1}{4} \sum_{m_2 m_3} \sum_{m_N m}$$

$$\times \left| {}_a \left\langle \frac{3}{4} q_0 \sqrt{1 + \frac{m \epsilon_d}{(\frac{3}{4} q_0)^2}} \hat{p} m_2 m_3 \nu_2 \nu_3 \left| t \left(\frac{(\frac{3}{4} q_0)^2}{m} + \epsilon_d \right) \left| \frac{3}{4} q_0 m_N m \nu_N - \nu_1 \right. \right\rangle \right| \right|^2 \quad (229)$$

Besides known factors we see the momentum space deuteron wave function at zero argument and the spin averaged NN off-shell differential cross section. Depending on the isospin quantum numbers ν we have np, pp, or nn scattering.

For practical purposes it might be more convenient to formulate Eq. (229) in the lab. system. It results from Eq. (106)

$$\begin{aligned} \frac{d^5 \sigma}{d \hat{k}_2 d \hat{k}_3 d S} \Big|_{\text{QFS}}^{1A} &= \frac{1}{4} \sum_{m_2} \sum_{m_3} \sum_{m_N} \left| {}_a \langle \mathbf{p} m_2 m_3 \nu_2 \nu_3 | t \left(\frac{(\frac{3}{4} q_0)^2}{m} + \epsilon_d \right) | \frac{3}{4} q_0 m_N m \nu_N - \nu_1 \rangle \right|^2 \\ &\times \frac{2\pi^3 \varphi_0^2(0) m^3 k_2^2 k_3^2 \frac{2}{3q_0}}{\sqrt{k_2^2 (2k_3 - \hat{k}_3 \cdot (\mathbf{k}_{lab} - \mathbf{k}_2))^2 + k_3^2 (2k_2 - \hat{k}_2 \cdot (\mathbf{k}_{lab} - \mathbf{k}_3))^2}} \end{aligned} \quad (230)$$

with

$$\mathbf{p} = \frac{1}{2} (\mathbf{k}_2 - \mathbf{k}_3), \quad \mathbf{q}_0 = \frac{2}{3} \mathbf{k}_{lab} \quad (231)$$

and the QFS condition $k_1 = 0$.

The NN t-matrix is off-shell. For higher energies, above 100 MeV say, the ϵ_d term causing the t-matrix being off-shell will loose importance, as will be demonstrated.

We compared the breakup cross section under np and nn QFS conditions for the full solution of the Faddeev equations to the expression (230), which is valid only in the extreme impulse approximation and to the full impulse approximation, which includes the remaining two terms in Eq. (221). Shown is also the expression (230), where the off-shell NN t-matrix is replaced by the on-shell one (neglection of the two ϵ_d corrections). This is displayed in Fig. 79 for the energies 65, 140 and 220 MeV. All the calculations are just based on $j_{max} = 3$, which is certainly not sufficient at the two highest energies, but we expect no principal change with an increase of j_{max} .

We see a very strong deviation between the IA and the full calculation at 65 MeV, but even at 220 MeV there remains a gap of $\approx 20\%$. This is of course consistent to what we already discussed in Section 6.1. There we found that the rescattering terms of first order in t are not negligible even at the highest energy of 220 MeV.

It is interesting to note that there are energy dependent angular domains, different for np and nn QFS, with angle independent factors between the full calculation and the IA. As an example at 140 MeV the angular regions are between 34° and 53° (43° and 75°) where the factors are 1.2 (1.1) for nn (np) QFS, respectively. This is just a numerical result and we have not yet any deeper insight. It appears very interesting to check that angular independent factor experimentally by comparing the 3N breakup cross section under np QFS conditions with the corresponding angular distribution for np scattering. A positive result would allow to measure the deuteron quantity

$$\varphi_0(p = 0) = \sqrt{\frac{2}{\pi}} \int dr r^2 \varphi_0(r) \quad (232)$$

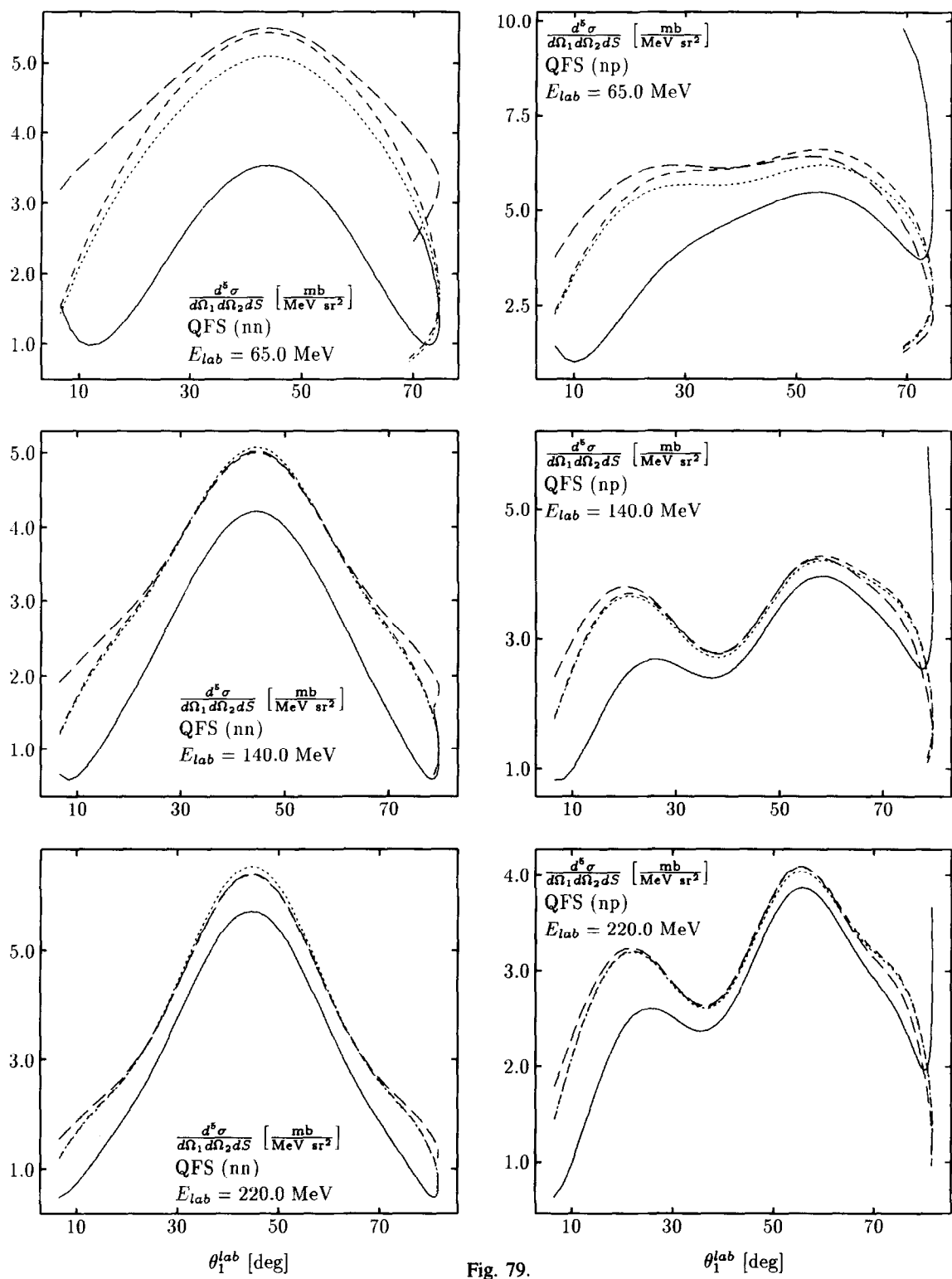


Fig. 79.

A positive check of the 3N reaction theory in the np QFS might also lend credit to believe in the reaction theory for the nn QFS, which would then allow to extract the nn differential cross section from nd quasi free scattering.

Let us now regard spin observables in the nd breakup process. Let us first consider the question whether two-nucleon spin observables can be extracted. If at all one has to work under QFS conditions. We assume the extreme IA to be valid, whence

$$\langle \phi_0 | U_0 | \phi \rangle \rightarrow \frac{(-)^{\frac{1}{2} + \nu_1}}{\sqrt{2}} \frac{\varphi_0(0)}{\sqrt{4\pi}} C(\frac{1}{2}\frac{1}{2}1, m_d - m_1, m_1) \\ \times_a \langle \mathbf{p}m_2 m_3 \nu_2 \nu_3 | t \left(E - \frac{3}{4m} q^2 \right) | \frac{3}{4} \mathbf{q}_0 m_N m_d - m_1 \nu_N - \nu_1 > \quad (233)$$

Can that be used to extract for instance the NN analyzing power? Inserting (233) into (132) one arrives immediately at

$$A_y = A_y^{NN} (\mathbf{p} \nu_2 \nu_3, \frac{3}{4} \mathbf{q}_0 \nu_N - \nu_1) \quad (234)$$

where A_y^{NN} is the on-shell NN analyzing power (except for the ϵ_d correction) for the scattering of nucleons from the initial to the final quantum numbers as indicated. Thus as for the cross section np, pp, and nn analyzing powers can be gained.

The same applies to the nucleon spin transfer $K_y^{y'}$ as is easily verified,

$$K_y^{y'} = K_y^{y'NN} (\mathbf{p} \nu_2 \nu_3, \frac{3}{4} \mathbf{q}_0 \nu_N - \nu_1) \quad (235)$$

NN spin correlation coefficients work exactly the same way if in the 3N breakup process the spin directions of the two nucleons are detected in the final state in coincidence. Then this outgoing polarization

$$P_{kl} \equiv \frac{\text{Tr}(NN^\dagger \sigma_k \sigma_l)}{\text{Tr}(NN^\dagger)} \quad (236)$$

boils down to

$$P_{kl} = C_{kl}^{NN} (\mathbf{p} \nu_2 \nu_3, \frac{3}{4} \mathbf{q}_0 \nu_N - \nu_1) \quad (237)$$

Note we used the notation N from Eq. (146) for the breakup amplitude, as described in Section 2.4.

In case when the nucleon and the deuteron are polarized in the initial state linear combinations of NN correlation coefficients arise. This is simply seen from

$$C_{k,l} \equiv \frac{\text{Tr}(N \sigma_k \mathcal{P}_l N^\dagger)}{\text{Tr}(NN^\dagger)} \quad (238)$$

For N be chosen as given in Eq. (233) the trace in the numerator of Eq. (238) is up to a factor, which cancels against the one in the denominator

Fig. 79. nn and np QFS breakup cross sections at 65, 140 and 220 MeV as a function of the neutron lab. angle. Comparison of the full Faddeev calculation (—), $U_0 = tP$ (---), $U_0 = (1 + P)tP$ (—), among each other and to expression (229) without the ϵ_d correction in the NN t-matrix (····).

$$\text{Tr}(N\sigma_k \mathcal{P}_l N^\dagger) \propto \sum_{m_1 m_2 m_3} \sum_{m_d m_N m'_d m'_N} C\left(\frac{1}{2}\frac{1}{2}1, m_d - m_1, m_1\right) C\left(\frac{1}{2}\frac{1}{2}1, m'_d - m_1, m_1\right) \\ \times t_{m_2 m_3, m_N m_d - m_1}(\sigma_k)_{m_N m'_N} (\mathcal{P}_l)_{m_d, m'_d} t^*_{m_2 m_3, m'_N m'_d - m_1} \quad (239)$$

Now we can define

$$\Gamma_{\mu\mu'}^{(l)} \equiv \sum_{m_d, m_1} \delta_{m_d - m_1, \mu} \sum_{m'_d} \delta_{m'_d - m_1, \mu'} C\left(\frac{1}{2}\frac{1}{2}1, \mu, m_1\right) C\left(\frac{1}{2}\frac{1}{2}1, \mu', m_1\right) (\mathcal{P}_l)_{m_d, m'_d} \quad (240)$$

Thus

$$\text{Tr}(N\sigma_k \mathcal{P}_l N^\dagger) \propto \sum_{m_2 m_3} \sum_{m_N \mu m'_N \mu'} t_{m_2 m_3, m_N \mu}(\sigma_k)_{m_N m'_N} \Gamma_{\mu\mu'}^{(l)} t^*_{m_2 m_3, m'_N \mu'} \quad (241)$$

Since $\Gamma_{\mu\mu'}^{(l)}$ can be decomposed into Pauli matrices

$$\Gamma^{(l)} = \sum_m \alpha_{lm} \sigma_m \quad (242)$$

one finds

$$C_{k,l} = \sum_m \alpha_{lm} C_{km}^{\text{NN}}(p\nu_2\nu_3, \frac{3}{4}q_0\nu_N - \nu_1) \quad (243)$$

This again appears to be an interesting case to verify experimentally that reaction theory.

We exemplify these predictions in Fig. 80. There we display A_y and K_y' for np and nn QFS's and compare the full calculation to the impulse approximation (evaluated off-shell) and the corresponding NN spin observable. While at 65 MeV impulse approximation and thus also the direct NN observable deviates strongly from the full 3N scattering result, at 140 and 220 MeV the situation is much more favorable. For some observables impulse approximation (evaluated off-shell), the on-shell NN observable and the full calculation (which includes all rescattering processes) agree very well in a certain range of the lab. angle of nucleon 1. On the other hand for np A_y at 140 MeV off-shell effects remain noticeable and this is also true for nn K_y' at 140 and even 220 MeV. Thus a careful analysis is required. Again only a $j_{max} = 3$ calculation is shown, but we expect taking larger j_{max} no basic change in these results. Quasielastic scattering of nucleons on the deuteron can therefore be used with proper care to extract NN spin observables under QFS conditions at the two highest energies considered. Therefore we propose for instance to measure in this manner nn spin observables after it has been verified experimentally that corresponding np observables can be extracted correctly from the 3N breakup process under QFS conditions.

QFS configurations are especially suited for this aim due to the fact that as we pointed in Section 6.2 the 3NF effects are practically negligible for these configurations at high energies. We shall come back to that point in Section 7.8.

In the literature several data sets under QFS conditions exist, which were interpreted as NN data. As examples we mention [303,477,495,313], whose pd QFS data were used in Arndt's PSA for np data.

In [313] for instance spin transfer coefficients were extracted at 140 MeV in an angular range, which starts at 20° . At least for K_y' shown in Fig. 80 this would require substantial corrections which can also be true for the other spin transfer coefficients discussed in [313]. If that would be

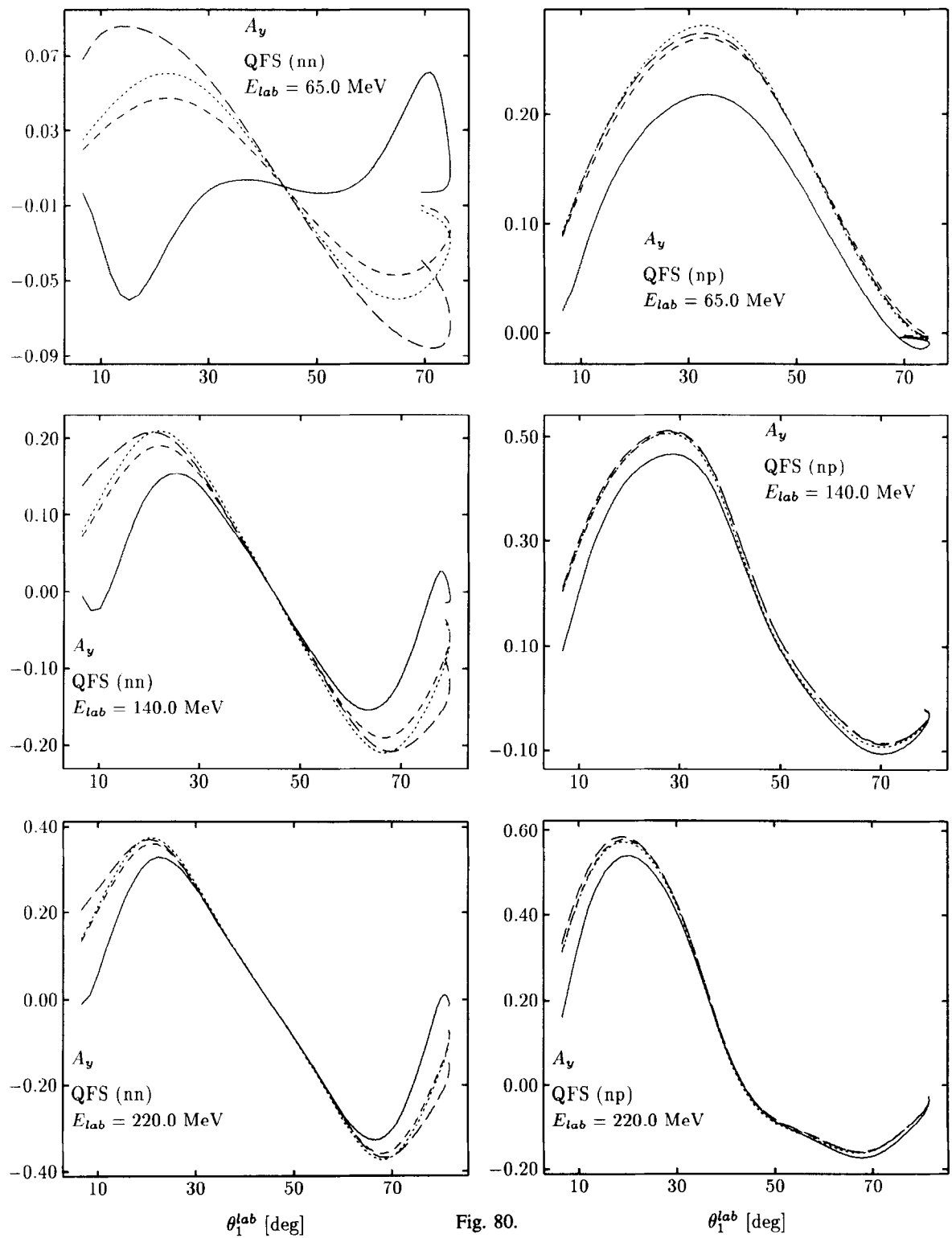


Fig. 80.

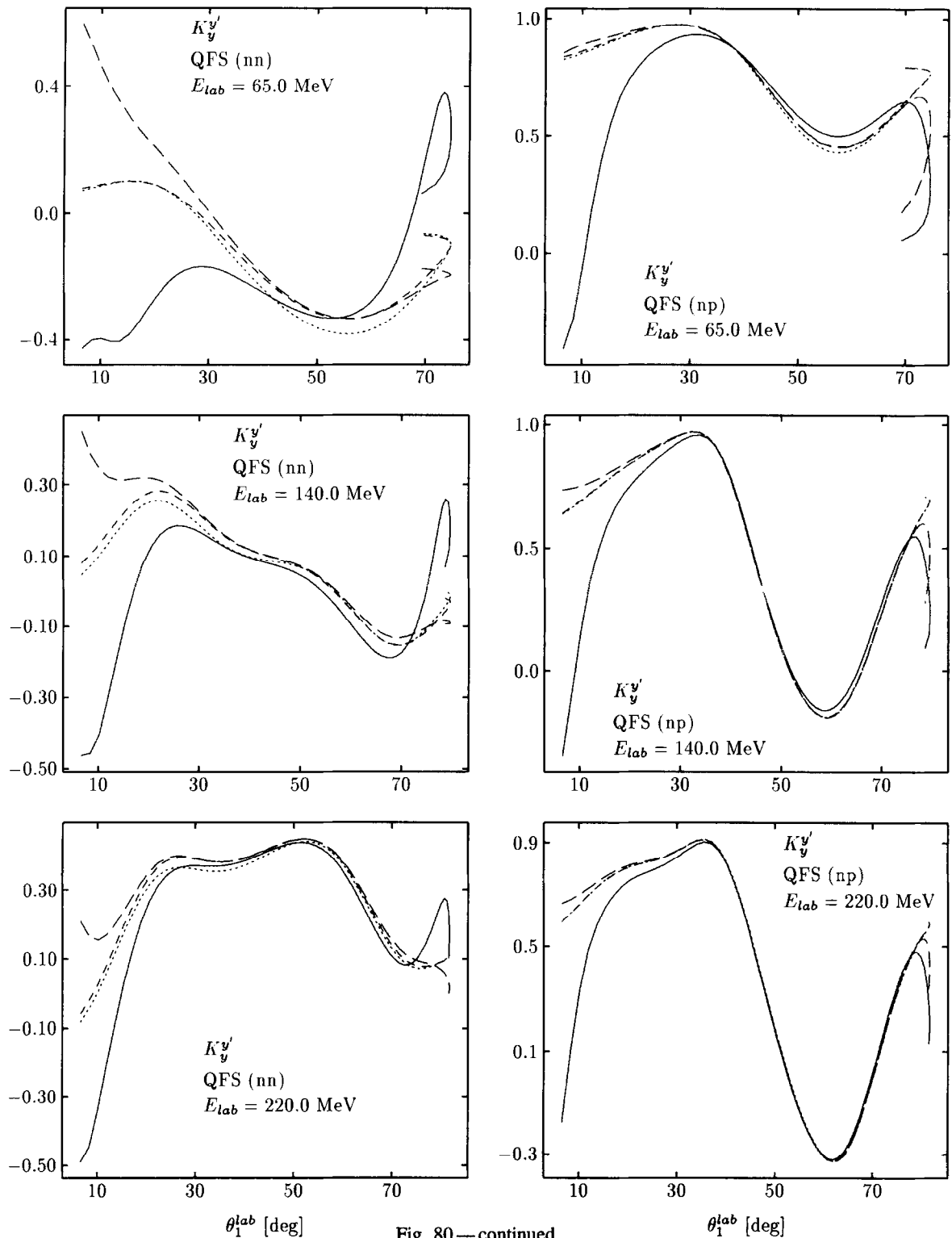


Fig. 80—continued.

the case they should not be included in a np data set. In [495] np K_y^y' has directly been extracted from quasielastic pd scattering at 212 MeV. The angles chosen were between 19.5° and 40° , which according to Fig. 80 lie outside the safe region and where substantial rescattering corrections are needed.

We would recommend to rely only on data which lie in an angular range, where the four curves in Fig. 80 fully overlap. Another example which appears to be very doubtful is the np analyzing power extracted under QFS conditions at 140 MeV in [303]. As already mentioned off-shell effects are not negligible and moreover at the angles chosen rescattering corrections are substantial. A pd experiment [477] carried through at 217 MeV under pp and pn quasielastic conditions is more favorable as Fig. 80 shows. In that study A_y was measured in the free pp system and compared to the quasielastic pp data. The agreement is quite good, which motivated the authors to have confidence also in the pn quasielastic data. Except for the smallest angles the remaining ones are in the safe angular range and thus acceptable according to our present study. A more detailed investigation is planned.

In order to verify this reaction theory more completely also the other extreme configurations with strong rescattering in FSI's or configurations near FSI's should be measured.

Does elastic neutron-deuteron scattering also simplify at high energies? This will be studied in the next section.

7.6. The nucleon-deuteron optical potential and its high energy limit

Since one can calculate nucleon-deuteron scattering exactly, including the breakup process, the question of introducing the auxiliary concept of an optical potential into that scheme is perhaps artificial. Also there is obviously too little nuclear medium, only two nucleons, which could serve to build up a mean field for the projectile nucleon. Nevertheless this is a system whose optical model properties can be determined precisely, with its inherently nonlocal nature and complicated spin and momentum dependencies. To that aim we would like to write down the defining equations and their high energy limit.

As shown in Sections 2.1 and 2.2, the operator for elastic scattering U obeys the Faddeev type equation

$$U = PG_0^{-1} + PtG_0U \quad (244)$$

This is not yet the equation searched for, since the kernel also includes intermediate breakup states. We separate tG_0 as

$$tG_0 = V \frac{1}{E + i\epsilon - H_0 - V} \equiv VG_d + VG_c \quad (245)$$

where G_d is the deuteron and G_c the continuum contribution in the spectral decomposition of the two-body Hamiltonian. Then it is a simple exercise to see that Eq. (244) is equivalent to

Fig. 80. A_y and K_y^y' under nn and np QFS conditions at 65, 140 and 220 MeV as a function of the neutron lab. angle. Comparison of the full Faddeev calculation (—), $U_0 = tP$ (---), $U_0 = (1 + P)tP$ (- · -) among each other and to the NN on-shell quantities (·····).

$$\begin{aligned} U &= \mathcal{V} + \mathcal{V}G_dU \\ \mathcal{V} &= PV + PVG_c\mathcal{V} \end{aligned} \quad (246)$$

We replaced $P\mathcal{G}_0^{-1}$ by PV , which is the same if applied onto the initial (on-shell) channel state ϕ . In the first of the two Eqs. (246), however, \mathcal{V} is applied onto arbitrary off-shell states. Thus by that replacement we modified the operator U off-shell, but not on-shell.

Now the first equation of (246) is just appropriate to describe elastic nd scattering. Applied to the initial channel state $\phi \equiv |\varphi_d\rangle|\mathbf{q}_0\rangle$ and acting by $\langle\mathbf{q}|\langle\varphi_d|$ from the left we get

$$\begin{aligned} \langle\mathbf{q}|\langle\varphi_d|U|\varphi_d\rangle|\mathbf{q}_0\rangle &= \langle\mathbf{q}|\langle\varphi_d|\mathcal{V}|\varphi_d\rangle|\mathbf{q}_0\rangle \\ &+ \int d\mathbf{q}' \langle\mathbf{q}|\langle\varphi_d|\mathcal{V}|\varphi_d\rangle|\mathbf{q}'\rangle \left(E + i\epsilon - \epsilon_d - \frac{3}{4m}q'^2 \right)^{-1} \langle\mathbf{q}'|\langle\varphi_d|U|\varphi_d\rangle|\mathbf{q}_0\rangle \end{aligned} \quad (247)$$

This is an equation describing potential scattering and the optical potential can be read off to be

$$\mathcal{V}(\mathbf{q}, \mathbf{q}') \equiv \langle\mathbf{q}|\langle\varphi_d|\mathcal{V}|\varphi_d\rangle|\mathbf{q}'\rangle \quad (248)$$

How do we get \mathcal{V} ? The second equation in (246) is not suitable for a numerical treatment and we rewrite it into a more convenient form. Define

$$t_c G_0 \equiv VG_c \quad (249)$$

and

$$VG_c\mathcal{V} \equiv T_c \quad (250)$$

then

$$T_c = t_c G_0 PV + t_c G_0 PT_c \quad (251)$$

which is the equation to be solved. Knowing T_c one can read off \mathcal{V} from the second equation in (246) as

$$\mathcal{V} = PV + PT_c \quad (252)$$

Finally the breakup operator U_0 given as

$$U_0 = (1 + P)T \quad (253)$$

can be put into the identical form

$$U_0 = \frac{1}{2}(1 + P)U \quad (254)$$

using the identity

$$\frac{1}{2}(P - 1)P = 1 \quad (255)$$

Evaluating U_0 via that second form in Eq. (254) one has obviously to solve first U projected from the left onto the deuteron state and then Eq. (247) is used again, now projected from the left onto free states. This last step is just a quadrature. This scheme is an alternative to solve nd scattering to

what has been described and used up to now. Let us go into more details. Comparing the definitions of t in Eq. (245) and t_c in Eq. (249) one finds

$$t_c = t - VG_d G_0^{-1} \quad (256)$$

Thus t_c has no deuteron pole, what is anyhow evident from its very definition (249). Eq. (256) also shows that t_c is not symmetric in contrast to t and obeys the Lippman–Schwinger equation

$$t_c = V - V|\phi_d\rangle\langle\phi_d| + t_c G_0 V \quad (257)$$

The solution of Eq. (251) is as difficult as the solution of the Faddeev Eq. (154), even if it has no deuteron pole. The difficulty arises because of the driving term. On top of that Eq. (251) has to be solved quite often according to the different \mathbf{q}' values needed in (247). In our present way of solving the Faddeev equations, the central Eq. (154) has to be solved only once for the initial momentum \mathbf{q}_0 . For future parallel computers this might be, however, no obstacle.

The optical potential $\mathcal{V}(\mathbf{q}, \mathbf{q}')$ of Eq. (248) can be decomposed into the various scalars formed out of the deuteron and nucleon spin vectors and the nucleon momenta \mathbf{q} and \mathbf{q}' . Each of those scalars will be multiplied by a scalar function in \mathbf{q} and \mathbf{q}' . This appears to be a worthwhile exercise including its transformation into configuration space in order to see the complexity of the optical potential, even for such a simple target as the deuteron. Instead of pursuing that further we would like to regard only the high energy limit of that optical potential.

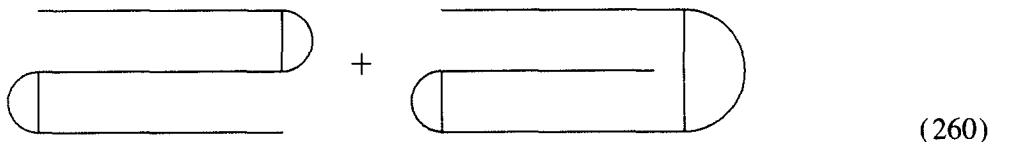
Assuming the first term, PV , in (252) and the lowest order one for T_c to be the leading ones at high energies the optical potential will be

$$\mathcal{V}(\mathbf{q}', \mathbf{q}) = \langle \mathbf{q}' | \langle \varphi_d | PV + Pt_c PG_0 V | \varphi_d \rangle | \mathbf{q} \rangle \quad (258)$$

Using the Schrödinger equation of the deuteron this can be easily rewritten into

$$\begin{aligned} \mathcal{V}(\mathbf{q}', \mathbf{q}) &= \langle \mathbf{q}' | \langle \varphi_d | P(E - H_0) | \varphi_d \rangle | \mathbf{q} \rangle + \langle \mathbf{q}' | \langle \varphi_d | Pt_c P | \varphi_d \rangle | \mathbf{q} \rangle \\ &\quad + \frac{3}{4m}(q^2 - q_0^2) \langle \mathbf{q}' | \langle \varphi_d | P | \varphi_d \rangle | \mathbf{q} \rangle + \frac{3}{4m}(q^2 - q_0^2) \langle \mathbf{q}' | \langle \varphi_d | Pt_c PG_0 | \varphi_d \rangle | \mathbf{q} \rangle \end{aligned} \quad (259)$$

The first term has often been regarded in the past [88,23] in the treatment of elastic nd scattering. It is called the nucleon-exchange term. Because of the cyclic and anticyclic permutations contained in P the deuteron in the ket vector is composed either of nucleons 1,3 or 1,2 whereas the deuteron in the bra vector contains nucleons 2,3. Those processes are often depicted as



The second term on the right hand side of Eq. (259), when explicitly written out is

$$\begin{aligned} \langle \mathbf{q}' | \langle \varphi_d | Pt_c P | \varphi_d \rangle | \mathbf{q} \rangle &= {}_1\langle \mathbf{q}' | \langle \varphi_d | t_{c,2} + t_{c,3} | \varphi_d \rangle | \mathbf{q} \rangle_1 \\ &\quad + {}_1\langle \mathbf{q}' | \langle \varphi_d | t_{c,2} | \varphi_d \rangle | \mathbf{q} \rangle_3 + {}_1\langle \mathbf{q}' | \langle \varphi_d | t_{c,3} | \varphi_d \rangle | \mathbf{q} \rangle_2 \end{aligned} \quad (261)$$

We added indices to the bra and ket vectors to show which pair forms the deuteron and which nucleon is the free one. Thus for instance the free nucleon 1 goes with the deuteron formed out of particles 2 and 3, etc. The first term on the right hand side has obvious physical meaning: nucleon 1 interacts with the two constituents of the deuteron via the NN t-matrix t_c (in t_c the deuteron contribution is taken out in the states ${}^3S_1 - {}^3D_1$). The last two terms can be rewritten as $-{}_1\langle \mathbf{q}' | \langle \varphi_d | t_{c,2} P_{13} | \varphi_d \rangle | \mathbf{q} \rangle_1 - {}_1\langle \mathbf{q}' | \langle \varphi_d | t_{c,3} P_{12} | \varphi_d \rangle | \mathbf{q} \rangle_1$, using the antisymmetry of the deuteron state in the particle numbers 2 and 3. Thus Eq. (261) can be given the form

$$\langle \mathbf{q}' | \langle \varphi_d | P t_c P | \varphi_d \rangle | \mathbf{q} \rangle = {}_1\langle \mathbf{q}' | \langle \varphi_d | t_{c,2} (1 - P_{13}) + t_{c,3} (1 - P_{12}) | \varphi_d \rangle | \mathbf{q} \rangle_1 \quad (262)$$

which nicely shows the effect of antisymmetrization between projectile nucleon and target nucleon. Now $t_{c,2}$ and $t_{c,3}$ act of course in antisymmetric states leading to $t_{c,2} (1 - P_{13}) = 2t_{c,2}$ and similarly for $t_{c,3}$. Finally because of the antisymmetry of $|\varphi_d\rangle$ we end up with

$$\langle \mathbf{q}' | \langle \varphi_d | P t_c P | \varphi_d \rangle | \mathbf{q} \rangle = 4 {}_1\langle \mathbf{q}' | \langle \varphi_d | t_{c,2} | \varphi_d \rangle | \mathbf{q} \rangle_1 \quad (263)$$

It remains to be seen at which energy the optical potential as given in Eq. (259) is a valid and quantitative limiting form.

Finally let us regard the channel-spin representation introduced in Section 5 for the optical potential, $\mathcal{V}_{\lambda' \Sigma' \lambda \Sigma}(q', q)$. Like in Eq. (208) it follows from

$$\begin{aligned} \mathcal{V}_{\lambda' \Sigma' \lambda \Sigma}(q', q) &\equiv \sum_{l'l} \int dp' p'^2 \varphi_{l'}(p') \int dp p^2 \varphi_l(p) \\ &\times \langle p' q'(l'1) 1(\lambda'_1) I' JM | \mathcal{V} | p q(l1) 1(\lambda_1) IJM \rangle \end{aligned} \quad (264)$$

Numerical studies of that whole issue appear to be very interesting, since it would be the only case where all the properties of the optical potential could be determined starting from first principles.

7.7. Connection between total nd and nn and np cross sections in the high energy limit

An interesting issue at high energies has been pointed out long time ago [403]. The total cross section for nd scattering at high energies should be equal to the sum of the total cross sections for nn and np scattering. This has been verified at that time to the extent that the nn forces were assumed to be known. Let us see under which conditions that result can be derived. Assuming Born approximation in Eq. (247) it follows for $\mathbf{q} = \mathbf{q}_0$

$$\begin{aligned} \langle \mathbf{q}_0 | \langle \varphi_d | U | \varphi_d \rangle | \mathbf{q}_0 \rangle - \langle \mathbf{q}_0 | \langle \varphi_d | U | \varphi_d \rangle | \mathbf{q}_0 \rangle^* \\ = \langle \mathbf{q}_0 | \langle \varphi_d | \mathcal{V} | \varphi_d \rangle | \mathbf{q}_0 \rangle - \langle \mathbf{q}_0 | \langle \varphi_d | \mathcal{V} | \varphi_d \rangle | \mathbf{q}_0 \rangle^* \end{aligned} \quad (265)$$

Taking into account Eq. (259) one finds, using the optical theorem on the left hand side

$$\begin{aligned} 2i \text{Im} \langle \mathbf{q}_0 | \langle \varphi_d | U | \varphi_d \rangle | \mathbf{q}_0 \rangle &= -2i \frac{1}{(2\pi)^3} \frac{3}{4} q_0 \frac{1}{m} \sigma_{tot} \\ &= \langle \mathbf{q}_0 | \langle \varphi_d | P(t_c - t_c^\dagger) P | \varphi_d \rangle | \mathbf{q}_0 \rangle = 2 ({}_2\langle \phi | t_c - t_c^\dagger | \phi \rangle_2 + {}_2\langle \phi | t_c - t_c^\dagger | \phi \rangle_3) \end{aligned} \quad (266)$$

Again the indices indicate the choice of two-nucleon subsystems and t_c (t_c^\dagger) refers as before to the 23 subsystem. According to Eq. (256) t_c is equal to t minus a term which contains the deuteron

states (acting to both sides) for the subsystem 23. Thus that second term does not contribute for large q_0 's, since deuterons are formed of different pairs. It is an easy exercise to verify that. Thus we are left to regard the right hand side of (266) with t_c replaced by t . This also follows directly from Eq. (57). Inserting complete basis states in momentum, spin and isospin spaces and using the recoupling between different sets of Jacobi momenta one arrives after some algebra at

$$\begin{aligned} {}_2\langle \phi | t - t^\dagger | \phi \rangle_2 = & \sum_{m_1 m_3} \sum_{m'_3} \sum_{\nu_1 \nu_3} \sum_{\nu'_3} \int d\mathbf{q} \langle \varphi_d | -\frac{1}{2}\mathbf{q}_0 - \mathbf{q} m_3 m_1 \nu_3 \nu_1 \rangle \\ & \times \langle \mathbf{q}_0 + \frac{1}{2}\mathbf{q} m_N m_3 \nu_N \nu_3 | t - t^\dagger | \mathbf{q}_0 + \frac{1}{2}\mathbf{q} m_N m'_3 \nu_N \nu'_3 \rangle \langle -\frac{1}{2}\mathbf{q}_0 - \mathbf{q} m'_3 m_1 \nu'_3 \nu_1 | \varphi_d \rangle \end{aligned} \quad (267)$$

For q_0 significantly larger than the dominant momenta in the deuteron state $|\mathbf{q}|$ has to be close to $|\frac{1}{2}\mathbf{q}_0|$ in order to keep the argument of φ_d sufficiently small. Then the initial and final momenta for the t-matrix are large. Since the t-matrix for small variations around large values of the momenta is fairly constant it can be taken outside the integral evaluated at $\mathbf{q} = -\frac{1}{2}\mathbf{q}_0$ and we get

$$\begin{aligned} {}_2\langle \phi | t - t^\dagger | \phi \rangle_2 \xrightarrow{|\mathbf{q}_0| \rightarrow \infty} & \sum_{m_1 m_3} \sum_{m'_3} \sum_{\nu_1 \nu_3} \sum_{\nu'_3} \langle \frac{3}{4}\mathbf{q}_0 m_N m_3 \nu_N \nu_3 | t - t^\dagger | \frac{3}{4}\mathbf{q}_0 m_N m'_3 \nu_N \nu'_3 \rangle \\ & \int d\mathbf{q} \langle \varphi_d | -\frac{1}{2}\mathbf{q}_0 - \mathbf{q} m_3 m_1 \nu_3 \nu_1 \rangle \langle -\frac{1}{2}\mathbf{q}_0 - \mathbf{q} m'_3 m_1 \nu'_3 \nu_1 | \varphi_d \rangle \end{aligned} \quad (268)$$

The deuteron state is

$$\begin{aligned} \langle p m_3 m_1 \nu_3 \nu_1 | \varphi_d \rangle = & \frac{(-)^{1/2-\nu_3}}{\sqrt{2}} \delta_{\nu_3, -\nu_1} \\ & \times \sum_{l=0,2} \varphi_l(p) \sum_{\mu} Y_{l\mu}(\hat{p}) C(l11, \mu, m_d - \mu) C(\frac{1}{2}\frac{1}{2}1, m_3, m_1, m_d - \mu) \end{aligned} \quad (269)$$

Now we neglect the small d-wave admixture leading to

$$\langle p m_3 m_1 \nu_3 \nu_1 | \varphi_d \rangle \rightarrow \frac{(-)^{1/2-\nu_3}}{\sqrt{2}} \delta_{\nu_3, -\nu_1} \varphi_0(p) \frac{1}{\sqrt{4\pi}} C(\frac{1}{2}\frac{1}{2}1, m_3, m_1, m_d) \quad (270)$$

Thus

$$\begin{aligned} & \int d\mathbf{q} \langle \varphi_d | -\frac{1}{2}\mathbf{q}_0 - \mathbf{q} m_3 m_1 \nu_3 \nu_1 \rangle \langle -\frac{1}{2}\mathbf{q}_0 - \mathbf{q} m'_3 m_1 \nu'_3 \nu_1 | \varphi_d \rangle \\ & \rightarrow \frac{1}{2} \delta_{\nu_3, \nu'_3} \delta_{\nu_3, -\nu_1} \delta_{m_3, m'_3} C(\frac{1}{2}\frac{1}{2}1, m_3 m_1 m_d)^2 \end{aligned} \quad (271)$$

Altogether we are left with

$$\begin{aligned} {}_2\langle \phi | t - t^\dagger | \phi \rangle_2 \longrightarrow & \frac{1}{2} \sum_{m_1} \sum_{\nu_1} C(\frac{1}{2}\frac{1}{2}1, m_d - m_1 m_1)^2 \\ & \times \langle \frac{3}{4}\mathbf{q}_0 m_N m_d - m_1 \nu_N - \nu_1 | t - t^\dagger | \frac{3}{4}\mathbf{q}_0 m_N m_d - m_1 \nu_N - \nu_1 \rangle \end{aligned} \quad (272)$$

The energy argument of t is $(1/m)(\frac{3}{4}q_0)^2$ neglecting again ϵ_d . Thus we have on-shell NN t-matrices. The second term in (266) with $|\phi\rangle_2$ replaced by $|\phi\rangle_3$ leads automatically to the necessary antisymmetrization and we get

$$2(2\langle\phi|t-t^\dagger|\phi\rangle_2 + 2\langle\phi|t-t^\dagger|\phi\rangle_3) \longrightarrow \sum_{m_1} \sum_{\nu_1} C(\frac{1}{2}\frac{1}{2}1, m_d - m_1 m_1)^2 \\ \times \langle \frac{3}{4}q_0 m_N m_d - m_1 \nu_N - \nu_1 | t - t^\dagger | \frac{3}{4}q_0 m_N m_d - m_1 \nu_N - \nu_1 \rangle_a, \quad (273)$$

where $| \rangle_a \equiv (1 - P_{23})| \rangle$. Since t is symmetric we can also antisymmetrize the bra vector. Then using the unitarity relation for t we get

$$2(2\langle\phi|t-t^\dagger|\phi\rangle_2 + 2\langle\phi|t-t^\dagger|\phi\rangle_3) \longrightarrow \frac{1}{2} \sum_{m_1} \sum_{\nu_1} C(\frac{1}{2}\frac{1}{2}1, m_d - m_1 m_1)^2 (-2\pi i) \frac{3}{4} q_0 \frac{1}{2} m \\ \times \sum_{m_2 m_3} \int d\hat{p}' |_a \langle \frac{3}{4}q_0 m_N m_d - m_1 \nu_N - \nu_1 | t | \frac{3}{4}q_0 \hat{p} m_2 m_3 \nu_2 \nu_3 \rangle_a|^2 \quad (274)$$

The total cross section for NN scattering initiated by fixed spin and isospin magnetic quantum numbers is

$$\sigma_{NN}^{\text{tot}}(m_2 m_3 \nu_2 \nu_3) = (2\pi)^4 (\frac{1}{2}m)^2 \frac{1}{2} \sum_{m'_2 m'_3 \nu'_2 \nu'_3} \int d\hat{p}' | \langle p \hat{p}' m'_2 m'_3 \nu'_2 \nu'_3 | t | p m_2 m_3 \nu_2 \nu_3 \rangle_a |^2 \quad (275)$$

(Note the factor 1/2 is due to the identity of the particles).

Thus neglecting the D-wave admixture of the deuteron Eq. (266) leads to

$$\sigma_{\text{tot}}^{\text{Nd}}(m_N m_d \nu_N) \xrightarrow{q_0 \rightarrow \infty} \sum_{m_1 \nu_1} C(\frac{1}{2}\frac{1}{2}1, m_d - m_1 m_1)^2 \sigma_{\text{tot}}^{\text{NN}}(m_N m_d - m_1 \nu_N - \nu_1) \quad (276)$$

Except for that this is an exact result within that nonrelativistic scheme. We are not aware of a proof given in the literature before.

Finally we average over the initial nucleon and deuteron spin magnetic quantum numbers to arrive at the usual definition of the total Nd cross section. After a simple algebra and introducing also the usual spin averaged NN cross section we get

$$\sigma_{\text{tot}}^{\text{Nd}}(\nu_N) \equiv \frac{1}{6} \sum_{m_N m_d} \sigma_{\text{tot}}^{\text{Nd}}(m_N m_d \nu_N) = \sigma_{\text{tot}}^{\text{NN}}(\nu_N, -\frac{1}{2}) + \sigma_{\text{tot}}^{\text{NN}}(\nu_N, \frac{1}{2}) \quad \text{for } q_0 \rightarrow \infty \quad (277)$$

For instance choosing $\nu_N = -\frac{1}{2}$ we have nd scattering and then the right hand side contains $\sigma_{nn}^{\text{tot}} + \sigma_{np}^{\text{tot}}$.

We checked the validity of that relation evaluating exactly the total nd, np and nn cross sections. We restricted the NN force to act up to $j_{\max} = 3$ and used Bonn B as representative NN potential. To our surprise we see in Fig. 81 that already around 30 MeV that relation is fulfilled within about 5%. Thus there have to occur cancellations in rescattering terms, which were not considered in our most simplifying steps leading to Eq. (277). This calls for a deeper theoretical consideration.

Can that result be used to determine the total nn cross section? Since that nn cross section is much smaller than the np cross section the 5% deviation leads to a rather inaccurate estimate for σ_{nn}^{tot} at least for the energies considered in Fig. 81. This might change at higher energies, where however a relativistic framework is required in order to arrive at quantitatively meaningful results.

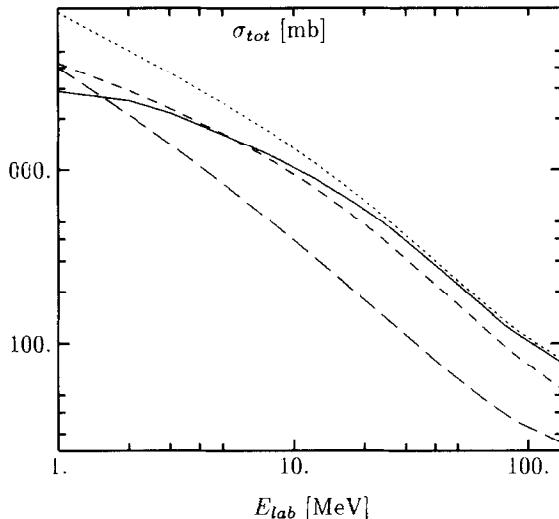


Fig. 81. Comparison of the total cross section for nd scattering (—) to the ones for nn scattering (---), np scattering (- · -) and their sum (····). As NN potential Bonn B with $j_{max} = 3$ was used.

7.8. 3NF effects at higher energies

We saw that the TM 3NF effects at low energies were not favorable for observables, where a discrepancy to data existed using NN forces only. The 3NF effects increased the discrepancy like for A_y in QFS and FSI configurations. The only observable which improved was the nd doublet scattering length, which, however, is correlated to the triton binding energy. Observables scaling with the triton binding energy might also improve, unfortunately the ones we mentioned previously have not yet been measured.

Since 3NF effects in scattering are an essentially virgin land, it might be justified to point out also the TM 3NF effects at higher energies of 65 and 140 MeV as examples. Our results might change however in future since, because of limited computer resources, we could include the 3NF only up to two-body angular momenta $j_{max} = 2$. Also the two-nucleon force was kept up to $j_{max} = 2$ in the presented cases. With stronger computer resources coming up these investigations have to be pushed to a higher number of partial waves. Nevertheless we would like to exhibit some results which show very dramatic effects and optimistically one might expect that they will survive the future improved studies at least to some degree.

We investigated all our standard elastic scattering observables and many breakup configurations including spin observables. We also considered in addition all nonzero spin correlation coefficients, where in the initial state nucleon and deuteron are polarized. The study was based on the Bonn B NN force and the TM 3NF restricted to $\pi - \pi$ exchange. For the cut-off parameter we choose two cases, $\Lambda_\pi = 4.55m_\pi$, which together with Bonn B leads to the correct ${}^3\text{H}$ binding energy, and $\Lambda_\pi = 5.8m_\pi$, the "recommended value" which, however, leads to overbinding. In Fig. 82 we show elastic scattering observables at 65 and 140 MeV for which we found especially big 3NF effects.

In the breakup process we restricted ourselves in a first survey to the standard four configurations, QFS, FSI, Coll, and Star. It turns out that the nn and np FSI peak heights are totally unaffected by such 3NF effects. This is also true for np and nn QFS cross sections. Some small effects were

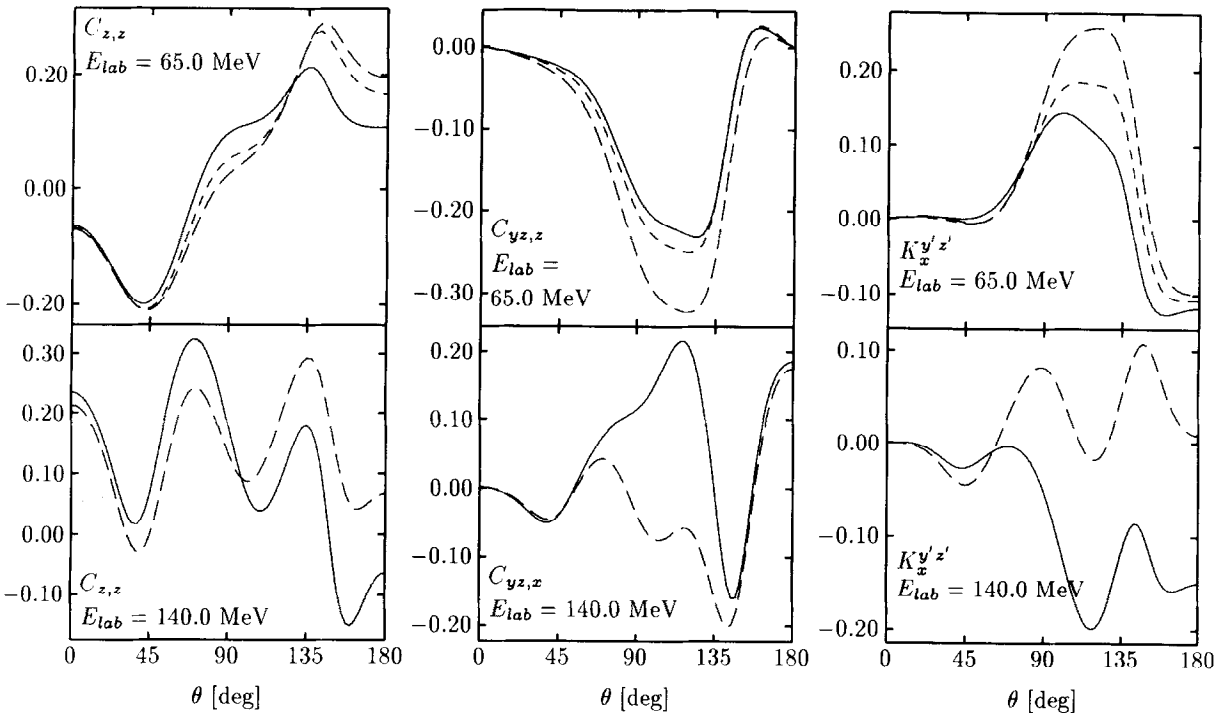


Fig. 82. TM 3NF effects with cut off parameters $\Lambda = 5.8m_\pi$ (---) and $\Lambda = 4.55m_\pi$ (- - -) at 65 and 140 MeV for various spin observables in elastic nd scattering. The underlying NN force is Bonn B (—).

observed in case of Coll and Star configurations. Let us regard now spin observables. For QFS conditions they are very little affected, while the other configurations show for some spin observables very dramatic effects. Examples are displayed in Fig. 83. Though the calculations have definitely not yet reached the final degree of convergence these observables might be interesting candidates to start an experimental search for 3NF effects.

8. Other rigorous techniques and open questions

8.1. Configuration space treatment

Like for the 3N bound state [312,44] also for 3N scattering the Grenoble group pioneered [167, 338] the configuration space treatment of the Faddeev equations. In configuration space the integral formulation is only good for extracting the proper asymptotic behavior [169,338,172] in the elastic and the breakup channels, but not for the actual calculations. One has to use the differential form, which is often called the Faddeev–Noyes equation [352]. For identical particles it reads

$$(H_0 + V - E)\psi = -VP\psi \quad (278)$$

where the total state Ψ is built out of the three Faddeev components

$$\Psi = (1 + P)\psi \quad (279)$$

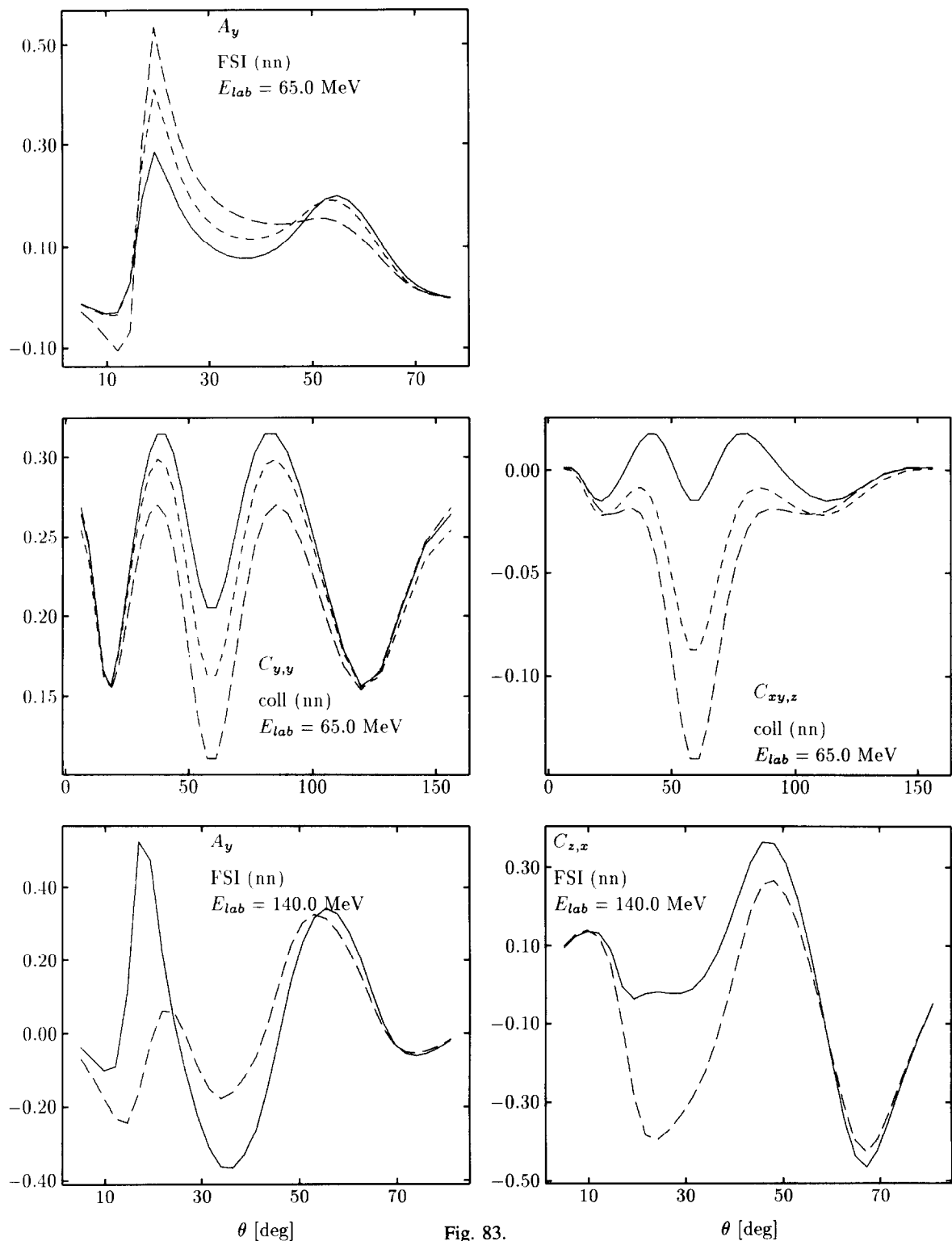


Fig. 83.

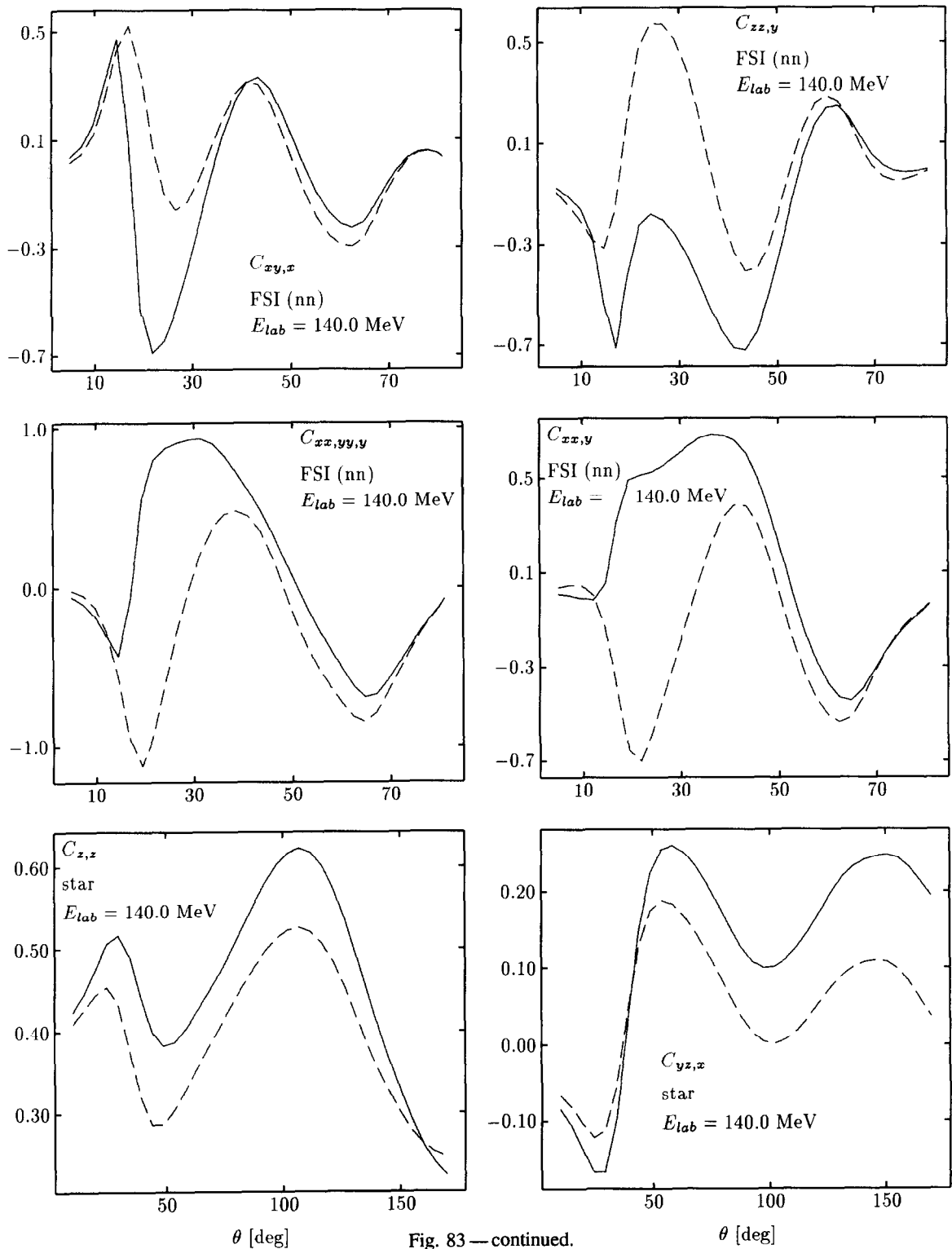


Fig. 83 — continued.

The partial wave decomposition is analogous to the one in momentum space and we refer the reader to [34,222,151,368,369]. In the standard Jacobi coordinates introduced in Section 2.4 Eq. (278) is a second order partial differential equation in the two vectors \mathbf{r} and \mathbf{R} . In fact because of the permutation operator on the right hand side, skew arguments show up in that ψ and the equation, partial wave decomposed, picks up an integral on the right hand side. Thus one gets a coupled set of integro-partial differential equations in the two variables r and R . From a numerical point of view it can be advantageous to use polar coordinates ρ and θ instead of r and R .

For scattering processes the reduced Faddeev component $\tilde{\psi}(r, R) \equiv rR\psi(r, R)$, assuming s-waves for simplicity, behaves asymptotically as [169,185]

$$\tilde{\psi}(r, R) \longrightarrow \varphi_d(r)(\sin q_0 R + e^{iq_0 R} f) + O\left(\frac{1}{R^{3/2}}\right) \quad (280)$$

for r fixed and $R \rightarrow \infty$. This describes the elastic channel and f is the elastic scattering amplitude. The correction term gets contributions from the breakup process [169,185]. For r and R getting large at a constant ratio

$$\frac{r}{R} = \sqrt{\frac{4}{3}} \cot \theta, \quad 0 < \theta < \frac{1}{2}\pi \quad (281)$$

$$\tilde{\psi}(r, R) \longrightarrow \frac{e^{i\sqrt{mE}\rho}}{(\sqrt{mE}\rho)^{1/2}} A(\theta) + O\left(\frac{1}{\rho^{3/2}}\right) \quad (282)$$

where $A(\theta)$ is part of the full breakup amplitude. The total breakup amplitude is built coherently [169] out of the contributions from the three Faddeev components, see Eq. (279). It is the long ranged source term on the right hand side of (278) decreasing only like $O(1/\rho^{1/2})$, which is responsible that the leading term in (282) by itself represents ψ only at unexpected large ρ -values, a few hundreds to thousands of fm [176,179]. Adding however correction terms, like

$$\frac{e^{i\sqrt{mE}\rho}}{(\sqrt{mE}\rho)^{1/2}} \left(A(\theta) + \frac{B(\theta)}{\sqrt{mE}\rho} + \frac{C(\theta)}{(\sqrt{mE}\rho)^2} + \dots \right) \quad (283)$$

helps significantly to match to that form at much smaller ρ -values, 100 fm or even below [179,185].

As we have mentioned in Section 5, a first application [156] using s-wave NN forces and keeping the two relative orbital angular momenta zero, carried through at 14.1 MeV and 42 MeV worked out very well and the agreement with our momentum space treatment was very good. Both the elastic amplitude f and the breakup amplitude $A(\theta)$ were in perfect agreement. It is therefore quite predictable that this method will also work using NN forces in all their complexities and solving typically 60 coupled equations for each conserved total angular momentum and parity. But this is still to be worked out.

An interesting technical step forward in the formulation of scattering (as well as bound states) has been done in [292,309]. The orientation of the plane spanned by the three nucleons has been described by three Euler angles and the motion inside the plane by r and R together with the angle

Fig. 83. Various spin observables in various breakup configurations at 65 and 140 MeV. TM 3NF effects are shown (see Fig. 82 for description of curves) on top of the underlying Bonn B prediction. θ denotes θ_1^{lab} in case of FSI, θ_{cm}^{plane} in case of space star and θ_1^{cm} in case of collinear configuration.

between the two Jacobi vectors \mathbf{r} and \mathbf{R} . In this manner one arrives at a coupled set of integro-partial differential equations in three variables, once the projection on the Wigner D-functions has been done. Also the appropriate boundary conditions for the 3N scattering processes have been given [292]. This formulation might be especially useful for treating the Coulomb force problem, since partial wave decomposition might be slowly converging.

8.2. The method of continued fractions

The method of continued fractions has been applied very successfully to fully realistic 3N bound state calculations (including 3NF's) [527] and also to 3N scattering calculations in the context of pd capture [245] and elastic nd scattering [244,248]. It appears to be very flexible and applicable to many problems, see [230,231,422,424].

Here it is briefly sketched. The Faddeev equation in integral form

$$\psi = \psi_0 + GVP\psi \quad (284)$$

is rewritten by splitting the kernel into two parts. One introduces

$$\tilde{G} = G - GVP|\psi_0\rangle \frac{1}{\langle\psi_0|VP|\psi_0\rangle} \langle\psi_0| \quad (285)$$

Inserted into (284) yields

$$\psi = \psi_0 + \tilde{G}VP\psi + GVP\psi_0 \frac{1}{\langle\psi_0|VP|\psi_0\rangle} \langle\psi_0|VP|\psi\rangle \quad (286)$$

One defines

$$\tilde{\psi} = GVP\psi_0 + \tilde{G}VP\tilde{\psi} \quad (287)$$

and can thus rewrite (286) as

$$\psi = (1 - \tilde{G}VP)^{-1}\psi_0 + \tilde{\psi} \frac{1}{\langle\psi_0|VP|\psi_0\rangle} \langle\psi_0|VP|\psi\rangle \quad (288)$$

Since from the very definition (285)

$$\tilde{G}VP\psi_0 = 0 \quad (289)$$

one gets

$$\psi = \psi_0 + \tilde{\psi} \frac{1}{\langle\psi_0|VP|\psi_0\rangle} \langle\psi_0|VP|\psi\rangle \quad (290)$$

The kernel is separable, thus one can proceed and easily finds

$$\psi = \psi_0 + \tilde{\psi} \frac{\langle\psi_0|VP|\psi_0\rangle}{\langle\psi_0|VP|\psi_0\rangle - \langle\psi_0|VP|\tilde{\psi}\rangle} \quad (291)$$

and

$$\langle\psi_0|VP|\psi\rangle = \frac{\langle\psi_0|VP|\psi_0\rangle^2}{\langle\psi_0|VP|\psi_0\rangle - \langle\psi_0|VP|\tilde{\psi}\rangle} \quad (292)$$

This is the first step of a recursive procedure. The amplitude ψ is expressed in terms of a new amplitude $\tilde{\psi}$ defined in (287) and the quantity $\langle \psi_0 | VP | \psi \rangle$, which is the elastic scattering amplitude, is expressed in terms of $\langle \psi_0 | VP | \tilde{\psi} \rangle$.

Now one defines

$$\psi^{(0)} \equiv \psi \quad (293)$$

$$\phi^{(0)} \equiv \psi_0 \quad (294)$$

$$G^{(0)} \equiv G \quad (295)$$

and

$$\psi^{(1)} \equiv \tilde{\psi} \quad (296)$$

$$\phi^{(1)} \equiv G^{(0)} VP \phi^{(0)} \quad (297)$$

$$G^{(1)} \equiv \tilde{G} = G^{(0)} - \phi^{(1)} \frac{1}{\langle \phi^{(0)} | VP | \phi^{(0)} \rangle} \langle \phi^{(0)} | \quad (298)$$

Then again Eqs. (284), (288), (290), (292) and (293) read

$$\psi^{(0)} = \phi^{(0)} + G^{(0)} VP \psi^{(0)} \quad (299)$$

$$\psi^{(1)} = \phi^{(1)} + G^{(1)} VP \psi^{(1)} \quad (300)$$

$$G^{(1)} VP \phi^{(0)} = 0 \quad (301)$$

$$\psi^{(0)} = \phi^{(0)} + \psi^{(1)} \frac{\langle \phi^{(0)} | VP | \phi^{(0)} \rangle}{\langle \phi^{(0)} | VP | \phi^{(0)} \rangle - \langle \phi^{(0)} | VP | \psi^{(1)} \rangle} \quad (302)$$

$$\langle \phi^{(0)} | VP | \psi^{(0)} \rangle = \frac{\langle \phi^{(0)} | VP | \phi^{(0)} \rangle^2}{\langle \phi^{(0)} | VP | \phi^{(0)} \rangle - \langle \phi^{(0)} | VP | \psi^{(1)} \rangle} \quad (303)$$

This transition from Eq. (299) to (302) and (303) can be repeated starting now from Eq. (300) for $\psi^{(1)}$ with the obvious result

$$\psi^{(1)} = \phi^{(1)} + \psi^{(2)} \frac{\langle \phi^{(0)} | VP | \phi^{(1)} \rangle}{\langle \phi^{(0)} | VP | \phi^{(1)} \rangle - \langle \phi^{(0)} | VP | \psi^{(2)} \rangle} \quad (304)$$

$$\langle \phi^{(0)} | VP | \psi^{(1)} \rangle = \frac{\langle \phi^{(0)} | VP | \phi^{(1)} \rangle^2}{\langle \phi^{(0)} | VP | \phi^{(1)} \rangle - \langle \phi^{(0)} | VP | \psi^{(2)} \rangle} \quad (305)$$

Thereby

$$\phi^{(2)} = G^{(1)} VP \phi^{(1)} \quad (306)$$

$$G^{(2)} = G^{(1)} - \phi^{(2)} \frac{1}{\langle \phi^{(0)} | VP | \phi^{(1)} \rangle} \quad (307)$$

and

$$G^{(2)} VP \phi^{(1)} = 0 \quad (308)$$

have been used.

Apparently the general step is

$$\psi^{(i)} = \phi^{(i)} + \psi^{(i+1)} \frac{\langle \phi^{(0)} | VP | \phi^{(i)} \rangle}{\langle \phi^{(0)} | VP | \phi^{(i)} \rangle - \langle \phi^{(0)} | VP | \psi^{(i+1)} \rangle} \quad (309)$$

$$\langle \phi^{(0)} | VP | \psi^{(i)} \rangle = \frac{\langle \phi^{(0)} | VP | \phi^{(i)} \rangle^2}{\langle \phi^{(0)} | VP | \phi^{(i)} \rangle - \langle \phi^{(0)} | VP | \psi^{(i+1)} \rangle} \quad (310)$$

Thus $\psi \equiv \psi^{(0)}$ and $\langle \psi_0 | VP | \psi \rangle \equiv \langle \phi^{(0)} | VP | \psi^{(0)} \rangle$ are expressed in the form of a continued fraction expansion. The idea is that the higher order kernels get smaller and smaller and therefore for i sufficiently large (typically 10–20), $i = n$

$$\psi^{(n)} \approx \phi^{(n)} \quad (311)$$

$$\langle \phi^{(0)} | VP | \psi^{(n)} \rangle \approx \langle \phi^{(0)} | VP | \phi^{(n)} \rangle \quad (312)$$

Working backwards one ends up with the solution of the original Faddeev Eq. (284). Technically the equations are treated in a hybrid manner using momentum space for the relative motion of the third particle with respect to the pair and configuration space for the relative motion within the pair.

8.3. The pair correlated hyperspherical harmonic basis method

Expansions of three-body states into hyperspherical harmonics have a long tradition [108,109,448, 449,42,118,314,537,31,445]. In nuclear physics they met only with very modest success, because the strong short range repulsion of the NN forces induces strong variations into the wave function in its dependence on the hyperspherical angle, which for three particles is just the polar angle in the r - R plane. In order to describe these strong variations in that angular dependence for fixed hyperradius ρ hyperspherical harmonics of very high order are needed (see [325,326] and references therein).

The system of three charged particles interacting by Coulomb forces only poses a similar problem with respect to cusp effects, when two particle positions coincide. That problem was brilliantly solved [325,326] by extracting the analytically known form of the cusp effects from the wave function and expanding only the remainder part into hyperspherical harmonics. The convergence is then relatively fast and the accuracy achieved for the electronic motion in atoms is extremely good.

The Pisa group [268,270] took up similar ideas. First, they decomposed the short range part of the 3N scattering state into three parts like a Faddeev decomposition and partial wave decomposed each part in the usual manner. The resulting amplitudes depending only on r and R were then factored into a two-body correlation part, essentially determined by the two-nucleon system alone, and a remainder. Only the remainder was expanded into hyperspherical harmonics, which for three particles are just Jacobi polynomials. The unknown radial functions depending on the hyperradius ρ and the K-matrix elements of the outer part of the wave function are determined by means of the Kohn-variational principle. This technique has been used up to now for 3N scattering below the breakup threshold [270]. As already mentioned in Section 5 handling a fully realistic case, for example the AV14 NN potential, their results in form of eigen phase shifts and mixing parameters turned out to be in perfect agreement [238] with our momentum space results. In this method one can also easily include the pp Coulomb force and 3N forces as well, but up to now it has been applied only below the deuteron breakup threshold [269–271]. The step above the breakup threshold will require a safe

handling of the asymptotic breakup behavior, which, having the experience of the configuration space treatment of the Faddeev equations, mentioned before, appears feasible.

8.4. Finite rank expansions

Faddeev equations were originally solved mostly using NN forces of finite rank, often just rank 1 separable forces. Finite rank forces reduce the Faddeev equations to a set of coupled one-dimensional equations for the motion of the third particle with respect to the remaining pair and this for all arrangements. These finite rank forces were mostly chosen ad hoc with little or no physical background behind. Therefore the interpretation of the results remained somewhat open (see Section 1 for references).

Therefore the idea came up to approximate two-nucleon t-matrices, based on realistic NN forces, by a series of separable terms, like the unitary pole expansion (UPE) method [221], the Adhikari–Sloan expansion [4], a generalized separable expansion by Oryu [362–364], which is an extension of the Kowalski–Noyes method [296,351] and the Gamow Separable Approximation [36,134]. Another systematic procedure is the Ernst–Shakin–Thaler (EST) method [125], for which we sketch briefly the idea. For a separable force $V_s = |g\rangle\langle g|$ the two-nucleon LSE for the scattering state can be solved algebraically with the result

$$|\phi^{(+)}\rangle = |k\rangle + \frac{\lambda G_0^{(+)}(s)|g\rangle\langle g|k\rangle}{1 - \lambda\langle g|G_0^{(+)}(s)|g\rangle} \quad (313)$$

where $G_0^{(+)}(s)$ is the free Green operator at the energy s . We compare that result to the LSE for the scattering state generated by the general potential V

$$|\psi^{(+)}\rangle = |k\rangle + G_0^{(+)}(s)V|\psi^{(+)}\rangle \quad (314)$$

One requires $|\phi^{(+)}\rangle = |\psi^{(+)}\rangle$, thus

$$G_0^{(+)}(s)V|\psi^{(+)}\rangle \propto G_0^{(+)}(s)|g\rangle \quad (315)$$

If we choose (315) to be an equality, then

$$|g\rangle = V|\psi^{(+)}\rangle \quad (316)$$

and

$$\lambda = \langle\psi^{(+)}|V|\psi^{(+)}\rangle^{-1} \quad (317)$$

This can be generalized to n different energies. Then

$$V_s = \sum_{ij} V|\psi_i\rangle\langle\psi_i|M|\psi_j\rangle\langle\psi_j|V \quad (318)$$

where $|\psi_i\rangle$ stands for $|\psi^{(+)}(s)\rangle$ or $|\psi_{bi}\rangle$ in the case of scattering or bound states, respectively, and the matrix M is defined by the relation

$$\delta_{im} = \sum_j \langle\psi_i|M|\psi_j\rangle\langle\psi_j|V|\psi_m\rangle = \sum_j \langle\psi_i|V|\psi_j\rangle\langle\psi_j|M|\psi_m\rangle \quad (319)$$

Then by construction

$$V_s|\psi_i\rangle = V|\psi_i\rangle \quad (320)$$

which means that the half-shell t-matrices are identical at the n chosen energies. Of course this is also applicable to coupled channel cases [214]. Applications to present realistic NN forces, like the Paris or Bonn potentials were pushed forward by the Graz–Osaka collaboration [215–218,387,283].

Relatively high ranks (up to 8) are needed to achieve a good representation of the half-shell and full off-shell NN t-matrices for some given realistic NN force. Such finite rank forces were also used in the accuracy study [102] mentioned in Section 5. But that study had also another aim. It was shown by comparing to the exact results that these high rank approximations gave a good representation of the Paris potential.

A more recent development in representing given realistic NN forces by expressions of finite rank has been pushed forward in [285]. Thereby the Adhikari–Sloan expansion and the EST method are combined and the original potential is decomposed into a short and long range part, which then are separately expanded.

A test case determining nd model phase shifts of elastic scattering [153] was perfectly successful, another application to the 3N bound state [285] worked equally well. Thus it appears that this new type of finite rank expansion can just be considered as a sort of quadrature, a discretization of the continuum problem, and this technique may turn out to be very economical.

8.5. The Coulomb problem in pd scattering

There is a vast literature on that subject reviewed in [18,19,82], which has by far not been realised in terms of real numbers. It is a very tough problem and we cite important first steps: [15,307,17,48,49,85], [20]. In configuration space one faces complicated boundary conditions in the asymptotic breakup configurations [339,292,130] and in momentum space nontrivial singularities [209,286].

It can be questioned whether a partial wave expansion is very economical and the treatment [292] mentioned in Section 8.1 keeping r , R and the angle between r and R as variables might be safer.

With the first strides performed successfully in solving a scattering problem in configuration space [156] the additional inclusion of the pp Coulomb force appears feasible.

At the energy of the pd threshold a full-fledged realistic 3N calculation with Coulomb forces and even including a 3NF has been already performed in configuration space [86]. The two Phillips lines [86] between the doublet scattering length and the 3N binding energies for the nd and the pd systems are displayed in Fig. 84. While the nd line goes through the experimental point, the $^2a_{pd}$ datum falls well off the theoretical curve. Very likely the reason is the strong curvature in the effective range function below 300 keV which inables the extrapolation to zero energy from incident experimental energies above 400 keV. Renewed efforts to measure below 400 keV would be very worthwhile.

The pair correlated hyperspherical harmonic basis method, which works in configuration space, has been already applied to pd scattering below the deuteron breakup threshold [269–271]. This appears to be very promising. First results based on realistic NN forces and even 3N forces have been achieved. This is the first time that the Coulomb force problem was exactly solved with realistic nuclear forces. The Coulomb force effects turn out to be large below the deuteron breakup threshold. The comparison with pd data revealed good agreement for the differential cross section and the tensor analyzing power T_{20} , however, for the tensor analyzing powers T_{21} and T_{22} as well as for A_y ,

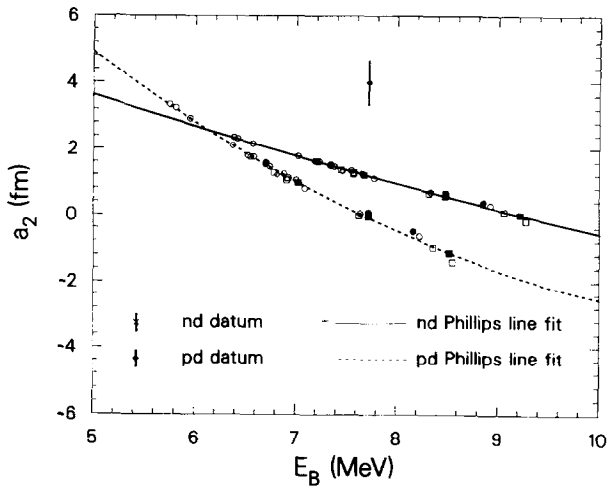


Fig. 84. The doublet scattering lengths 2a against 3N binding energies for the nd and pd systems (Phillips lines) [86]. The various symbols refer to different 2N and 3N forces.

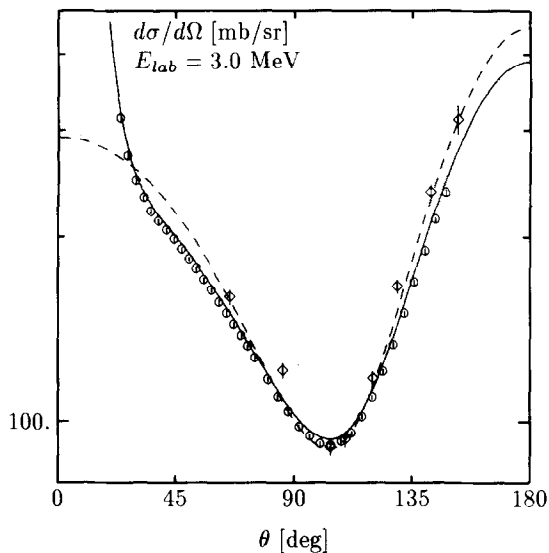


Fig. 85. pd (○) [416] and nd (◇) [431] differential cross section data at 3 MeV in comparison to theory [271] based on AV18 and an Urbana 3NF; (—) with Coulomb, (---) without Coulomb.

significant discrepancies are visible. In Fig. 85 their results for the differential cross section based on AV18 together with an Urbana 3NF and with and without Coulomb interaction are shown in comparison to data. As can be seen Coulomb force effects appear mainly at forward angles and to a smaller extend at backward angles, too. The agreement with the data is essentially perfect. Very precise pd data [444] at low energies appeared recently; their theoretical analysis poses a challenge.

In momentum space a scheme starting with a screened pp Coulomb force and taking the limit of vanishing screening has been investigated theoretically to quite some extent [16,18,19]. The asymptotic Coulomb distortion in the elastic channel is generated by the Coulomb force between the

proton and the center of mass of the deuteron, which is taken care of by adding and subtracting that force. The 3-body transition amplitudes in the limit of no screening acquire violent oscillating phase factors which are known (analytically in the case of exponential screening) and which can be removed exactly (renormalization) leading to amplitudes independent of the screening radius.

A first semirealistic calculation in that scheme using a rank 1 approximation to the Paris potential appeared for elastic pd scattering below the breakup threshold [51]. The results are interesting and provide a first idea about the magnitudes of Coulomb force effects in conjunction with more or less realistic NN forces. Thus for instance the pd observable A_y has indeed a lower maximum in comparison to the nd case and there is a shoulder in the left side of the maximum, absent for the nd case. Also the tensor analyzing powers show significant Coulomb force effects.

Another more recent study in that scheme [395,20,21] is in the pd breakup process. Unfortunately the NN force is only a rank one separable Yamaguchi force, but even then the calculations were nevertheless already very involved and the analytical nature of that strong force of great help. The effects for the breakup cross sections were sometimes quite large (up to 20%), but questions remain, whether this will remain true in conjunction with realistic forces and the accompanying higher partial waves.

A direct attack on the pp Coulomb force problem in momentum space in conjunction with realistic forces, not using finite rank expansions, like we have succeeded to do without Coulomb forces, has not yet been performed to the best of our knowledge.

The solution of that long pending problem especially in the pd breakup process will be a very important step to remove the related Coulomb force effect uncertainties and to make 3N pd scattering to a wonderful quantitative tool for testing nuclear interactions.

8.6. Relativistic 3N equations

There are various approaches towards a relativistic description. One is relativistic quantum mechanics for N interacting particles, which is defined by having established a representation of the Poincaré algebra. In other words the ten generators of the Poincaré group have to be found as expressed in terms of the degrees of freedom of the N particles. There is a famous construction by Bakamjian and Thomas [32], achieving that, but it does not have the property of cluster separability for more than two particles. If subclusters of the N particle system are separated in space from each other, the generators should correspondingly reduce to the sum of the generators belonging to the isolated clusters [139]. A cure of that defect has been also found [451–453], [93,389], but the actual realization is a heavy task. That scheme can be formulated in the instant, light front and point forms, which have been proposed by Dirac [111]. An excellent display of the concepts and the techniques are given in [266]. To the best of our knowledge that scheme has not yet been applied to 3N scattering, but it has been used in a 3N bound state model calculation [174].

Another very natural approach is via field theory. An obvious scheme are the 3N Bethe–Salpeter equations [149]. Even in the ladder approximation (with respect to the exchanged mesons) they are quite heavily stuffed with singularities in the two energy variables, which come now on top of the usual two three-momenta. As far as we know no solution has been achieved so far for 3N scattering. For the 3N bound state first trials [414] employing finite rank potentials are underway. That approach with the Bethe–Salpeter equation has the clear advantage of manifest covariance.

Related to that approach are quasipotential equations. Among them are the spectator or Gross equations [200], which represent an approximation to field theory and might be superior to the bookkeeping of the Bethe-Salpeter equation insofar that certain cancellations between crossed and uncrossed box graphs (with "on-shell" propagations taken out) are taken into account. However whether those cancellations do occur depend on the type of meson-nucleon coupling [201]. In the spectator approach for three particles in all intermediate states two particles always are set on the mass-shell by hand, which reduces the four-dimensional integrations to three-dimensional ones. Though this formulation keeps manifestly covariance it necessarily introduces spurious singularities [202] coming from meson propagators. Their effect in the two-nucleon system appears to be minor [204]. Presently this scheme is applied to the 3N bound state problem [461]. We are not aware of applications to 3N scattering.

Blankenbecler-Sugar equations for three particles [55,249,419] suffer definitely from the formal defect of violating cluster separability. The quantitative importance or negligence thereof appears to be hardly touched upon. The cited references refer to the 3N bound state, where that defect will play a minor role.

An approximate realization of the Poincaré algebra for N particles has been proposed by Foldy [140,141]. The generators of the Poincarè group are expanded around the Galilean limit ($c \rightarrow \infty$) in a $1/c^2$ expansion. When inserted into the algebra, conditions on the correction terms to the interaction in the Hamiltonian and on the interaction in the boost operator (we refer here to the instant form) arise, and this in each order in $1/c^2$. Special solutions can be found expressed in terms of the interaction in the Galilean invariant input Hamiltonian. They lead to two-body interactions, which depend on the total two-body momentum, to 3NF's depending on the total 3N momentum, etc. Quite a few applications thereof to the 3N bound state have appeared [208,52,250,288,75]. As far as we know there are not yet applications to 3N scattering.

Finally we would like to mention another approximate scheme for the Hamiltonian by Okubo [360]. Starting from a field theoretical Hamiltonian it is block diagonalized by a unitary transformation into two parts. One part acts only on states with N nucleons and the other on all remaining states. Thus the coupling between the states of N nucleons and the states with mesons for instance is eliminated. One ends up with an effective Hamiltonian in the space of N nucleons which contains then meson-mediated nuclear interactions. This cannot be carried through exactly but only in a perturbative expansion in the strong coupling constant g . In [170] that idea was taken up again and applied to all the ten generators of the Poincarè group. It was shown that one and the same unitary operator block diagonalizes all ten generators. Thus the commutation relations among the effective generators are the same as for the original ones and therefore the effective generators in the space of N nucleons would fulfill the Poincarè algebra if the perturbation expansion could be carried through to infinite order. In practice it is truncated and because of the nonlinear nature of the Poincarè algebra errors creep in which are pushed to higher orders by increasing the order in g in which the effective generators are calculated. This scheme can at least be very useful in getting experience about generators for N interacting particles and moreover they are then linked to field theory. Applications to the 3N bound state exist in model calculations [346,347]. 3N scattering calculations have not yet been undertaken, as far as we know.

The demand for a relativistic framework will get more and more urgent in the near future, because of the new accelerators like COSY, CEBAF, MAMI, etc. and more theoretical efforts will be required than invested up to now.

9. Applications

Whenever there is a reaction with three final nucleons final state interactions among them are likely to occur and can have a strong influence on the observables. Without knowing them, conclusions about the processes generating the final nucleons, in which one is mainly interested, are plagued by uncomfortable uncertainties. We shall sketch a few of these applications: inclusive and exclusive electron scattering on ^3He and ^3H , photodisintegration of ^3He and ^3H or pd capture, pion absorption on ^3He and ^3H and nonmesonic decays of the hypertriton.

9.1. Inclusive and exclusive electron scattering on ^3He and ^3H

Inelastic electron scattering on 3N bound states has various aims [494,361]: to learn about properties of ^3He and ^3H like momentum distributions, two-nucleon correlation functions, large and small parts of the 3N wave function, to learn about the hadronic current operator, especially two-body and possibly even three-body currents, and last not least about the electromagnetic nucleon form factors in the nuclear medium. Will the latter ones be different or rather close to the free ones? Also the neutron form factors have to be extracted from a nucleus like the deuteron or ^3He (^3H) [274]. These are all questions to which we would like to have quantitative answers and therefore the control of the final state interactions is mandatory. First steps were laid quite some time ago (for a compilation of references see [193]) using simple separable forces. More recently the Utrecht group [335–337] employed spin-dependent s-wave MT forces, which was a step forward. The Euclidean response method [74] suitable for inclusive scattering is able to determine exactly the Laplace transformed responses including nuclear interactions in the initial 3N bound state and the final 3N scattering state equally well. Our contributions [182,246,247,193–195] were in the same spirit as the one of the Utrecht group, but using now fully realistic forces. This will now be sketched briefly.

The nuclear matrix element for inelastic electron scattering has the form:

$$N_\mu = \langle \Psi_f^{(-)} | j_\mu(Q) | \Psi_{\text{bound}} \rangle \quad (321)$$

where $|\Psi_{\text{bound}}\rangle$ and $|\Psi_f^{(-)}\rangle$ are the 3N bound and scattering states, respectively. The asymptotic quantum number f stands either for the momenta of a nucleon and a deuteron or for the momenta of three nucleons. In a nonrelativistic framework, which we use, the hadronic current operator $j_\mu(Q)$ depends on the three-momentum transfer Q carried by the virtual photon. Now $|\Psi_f^{(-)}\rangle$ is Faddeev decomposed as

$$|\Psi_f^{(-)}\rangle = (1 + P)\psi \quad (322)$$

and the Faddeev amplitude ψ obeys the Faddeev equation

$$\psi = \psi_0 + G_0^{(-)} t^{(-)} P \psi \quad (323)$$

The driving term ψ_0 is different for two- and three- body fragmentations. All that inserted into N_μ yields

$$N_\mu = \langle \psi_0 | (1 + P) j_\mu(Q) | \Psi_{\text{bound}} \rangle + \langle \psi | P t G_0 (1 + P) j_\mu(Q) | \Psi_{\text{bound}} \rangle \quad (324)$$

For pd breakup for instance ψ_0 is just the product of a deuteron state and a momentum eigenstate of the free motion of the proton against the deuteron. Thus the first term is the symmetrized plane

wave impulse approximation, carrying no final state interaction. The second term, N_μ^{rescatt} , incorporates all the final state interactions. By simple algebraic manipulations [182,193,194] it can be identically rewritten into

$$N_\mu^{\text{rescatt}} = \langle \psi_0 | (1 + P) | U_\mu \rangle \quad (325)$$

where $|U_\mu\rangle$ obeys the Faddeev-type integral equation

$$|U_\mu\rangle = tG_0(1 + P)j_\mu(Q)|\Psi_{\text{bound}}\rangle + tG_0P|U_\mu\rangle \quad (326)$$

The kernel in Eq. (326) is exactly the same as for 3N scattering in Eq. (154), only the driving term is different and contains now the current operator applied to the target state. Iterating Eq. (326) and inserting it into Eq. (325) displays the physics of the multiple rescattering processes in a very nice and transparent manner. The forms are very similar also for the full three-nucleon breakup case (see [182,193,194]).

In this manner we analyzed [246,247,193–195] already several data taken at NIKHEF [265,253], Bates [117,401] and Saclay [327]. In every case analyzed up to now, final state interactions turned out to be very important. Applications to processes with polarized electrons and targets are underway.

9.2. Photodisintegration and pd capture in the 3N system

Again the first steps [38,40,164,165] were laid using simple separable forces and the importance of final state interactions were clearly visible. These reactions can be treated in much the same manner as outlined above in Section 9.1 just replacing the off-shell virtual photon by a real photon and applications are already underway [194]. In [245] and [142–144] first calculations have already been performed, one group [245] using the method of continued fractions in the treatment of 3N scattering as described in Section 8.2 and the other [142–144] using finite rank approximations to realistic NN forces. Thermal and radiative capture including the full nuclear dynamics has been treated in [153]. Also spin observables in the pd capture process are being studied [257]. In photon disintegration it is also expected to see processes where three nucleons are involved [415] in an irreducible manner.

9.3. Pion absorption on ${}^3\text{He}$ and ${}^3\text{H}$

Several series of experiments [30,25,29,450,499,501,348,500,418,22,196] have been performed in order to study the absorption mechanism of pions at rest and in flight on the light nuclei ${}^3\text{He}$ and ${}^3\text{H}$. Some of them are kinematically complete, measuring all the independent degrees of freedom for the final nucleons. Due to kinematical reasons there is little absorption on one nucleon. Mostly it occurs on two nucleons, but there seems to be also indication of three nucleons being involved [30, 25, 450, 348, 500, 418, 66, 243, 22]. To clarify that more reliably the effects of final state interactions have to be under control. Obviously the nuclear matrix element will have the same structure like for inelastic electron scattering with an appropriate “current operator” describing the absorption processes. Therefore making certain assumptions on that operator the matrix element can be calculated taking all the final state interactions into account as described above. Applications are underway [262].

9.4. Nonmesonic decay of the hypertriton

The hypertriton has been investigated by variational techniques and using models for the ΛN interaction and even including $\Lambda-\Sigma$ conversion [228,58,225,226,428,227,106,105,163,166,356,6,7]. Very recently the Faddeev equations have been solved [344,345] with the interactions among nucleons and hyperons (Λ or Σ) of meson exchange nature [402,404,468]. The Jülich interaction [402] did not bind the hypertriton [344] but the Nijmegen one [468] did [345], even at the correct binding energy without any further adjustments. This might be fortuitous, though, since still little experimental information is available on ΛN data [123,8,437,120,260]. Thereby the $\Lambda-\Sigma$ conversion played a very decisive role. To learn more about the hypertriton its decays should be studied. Especially interesting ones are the nonmesonic decays [94], where a Λ emits a pion, turns into a nucleon and the pion is reabsorbed. There are of course more processes possible. The three final nucleons undergo final state interactions, whose exact treatment is important in order not to blur the view on the pionic exchange current, which has both weak and strong vertices. The process goes by π^0 and π^+ exchanges. A first, somewhat schematic study neglecting all final state interactions appeared in [46]. Using the scheme displayed above the angular and energy distributions of the three final nucleons can be calculated taking all the final state interactions exactly into account. Data are very much needed.

10. Conclusions and outlook

Three-nucleon scattering has been always a vivid field of research both experimentally and theoretically in order to test nuclear forces in a first nontrivial context and to cultivate reaction theory. Nowadays the 3N scattering problem can be solved for any type of NN force far more accurately than the errors in present day data require and also the correct technical handling of 3NF's is on a good way. The most advanced calculations have been performed recently in the Faddeev formalism for energies below and above the nd breakup threshold; below the breakup threshold the variational pair correlated hyperspherical harmonic basis method is equally advanced and can even include the pp Coulomb forces in conjunction with realistic interactions. Above the breakup threshold that old Coulomb problem is still pending. Also recently several NN force parametrizations appeared, which describe NN data up to about 350 MeV to unprecedented accuracy and thus remove on-shell deficiencies, which plagued the interpretation of theoretical predictions in the past. Discrepancies to data could be due to those defects but also due to wrong off-shell properties or closely linked 3NF effects. Now with that set of newest force parametrizations on-shell deficiencies have shrunked to a minimum and differences in predictions, if present at all, are due to their different off-shell properties, like different radial shapes and/or nonlocalities. Equipped with these newest forces and the technical tools for solving the 3N equations precisely, very many data can now be compared to that theory. In general the agreement between theoretical and experimental 3N scattering observables is very good and in most cases there is no difference among the different force predictions. This refers to the NN force picture only and this tells that based on these forces there is very little room left for 3NF effects. A closer inspection, however, reveals, as discussed in detail in Section 6, that a few interesting discrepancies stick out and quite a few gaps in the data set exist, which should be filled in order to make the picture more complete and convincing.

The differential cross section in elastic Nd scattering above ≈ 100 MeV deviates from theory. Whether we see the onset of relativistic effects has to be clarified.

For spin observables in elastic Nd scattering one strong discrepancy sticks out, the low energy nucleon analyzing power A_y and the deuteron vector analyzing power iT_{11} , which is very similar in shape. It is well established that the 3P_j ($j = 0, 1, 2$) NN force components govern strongly these two observables. The modern NN forces adjusted to the present day NN PSA values in these states are not able to describe A_y and iT_{11} . At higher energies, above ≈ 30 MeV, where data are available, the agreement with theory is essentially perfect.

Data for tensor analyzing powers are only available up to now in the pd system and comparison to theory suffers in principle from unknown Coulomb force effects, which are clearly visible below 10 MeV at forward angles. At higher energies one would desire to have high precision data, like the ones at 22.7 MeV, where the agreement with theory (without Coulomb) is perfect.

Measurements of spin-transfer coefficients in elastic pd scattering are not too numerous and exist only at low energies. Data at higher energies would be very useful, however they should be quite accurate in order to test theory stringently.

Spin correlation coefficients, where both, nucleon and deuteron, in the initial state are polarized are hardly measured and data of high quality at low and also high energies would be equally useful to probe the 3N Hamiltonian.

In the 3N breakup process we can expect that the total cross section should be very well predicted by theory, since the total nd cross section as well as the elastic differential cross section agree very well with theory. Unfortunately the experimental total breakup data are old and presumably inaccurate and an experimental effort to provide new and accurate data would be very useful to form a consistent and well established picture.

Kinematically complete breakup data are numerous, but a well established data basis confirmed by independent measurements can not be claimed to exist. Overall we find cases of spectacular agreement between data and theory, but also cases of strong disagreement. Right now we can not point to breakup configurations with a well established agreement or disagreement like for observables in elastic Nd scattering. Breakup cross sections, however, where we face a serious discrepancy should be remeasured. At 13.0 MeV some of the old nd measurements, which strongly deviate from theory, are presently remeasured at TUNL and preliminary analysis already reveals that the data change. Some pd data at 22.7 MeV show also too strong deviations to theory to be caused by pp Coulomb force effects which are not taken into account in our theoretical treatment. A very interesting case is a nameless configuration shown in Fig. 44, where data from a nd measurement are a factor 2 below theory.

If one really wants to test the potential energy in a 3N system seriously – and this appears to be basic for nuclear physics – one should perform a full 4π investigation, probing the breakup process with respect to all angular and energy correlations of the three outgoing nucleons. This would provide the most comprehensive test of the 3N Hamiltonian and the outcome would constrain very much the degree to which 3NF's can be present in relation to the present day NN forces. In order to stimulate such an experimental investigation we performed a theoretical 4π study covering all phase space and searched for breakup configurations, where the most modern NN force predictions agree among each other with less than 3%, say, and those where they disagree by more than 8%, say. Both cases, the insensitive ones and the sensitive ones, would be of high interest to be measured. In the first case discrepancies to theory would quite seriously question present day NN forces or call for 3NF effects,

in the second case data could possibly differentiate between NN forces.

Spin observables in the breakup process deserve more attention in the future. While vector analyzing powers measured up to now agree quite well with our predictions, some tensor analyzing powers disagree strongly. This should definitely be remeasured. If those data would be confirmed this would pose a serious problem to theory.

Our first experience with 3NF's, specifically the Tucson–Melbourne $\pi - \pi$, $\pi - \rho$ and $\rho - \rho$ exchange forces, in 3N scattering was not encouraging. The effects are in general small and in case of the outstanding discrepancy in A_y they go into the wrong direction. Certainly a truly consistent theory for 2N and 3N forces is required, in order to approach that issue properly. Possible ways to go might be along recent work on chiral symmetry [287] and the systematic approach [388] advocated since many years.

We find that 3NF effects have possibly a good chance to be detectable at rather low energies where phenomena like the scaling of certain 3N observables with the triton binding energy and no scaling of certain other observables has been predicted. Precise data for all kind of spin observables would be needed, for instance spin correlation and spin transfer coefficients, in order to pin down 3NF effects. At high energies, above 100 MeV, our calculations including 3NF effects are not yet matured enough (too few partial waves), but on the present level we predict interesting and strong 3NF effects for the analyzing power under FSI conditions and for spin correlation coefficients.

In any case that regime of about 150 MeV is interesting also in other aspects. Under QFS conditions one might expect that the deuteron can be considered as a nucleon target. For the cross section this is not correct and rescattering corrections are present on the level of about 20%. But for spin observables in certain angular ranges that picture is true and NN spin observables can be extracted from the 3N scattering process. That prediction could be checked experimentally in the pp case and then np and even nn observables could be gained. On the other hand there are also plenty of breakup configurations, other than QFS, where rescattering processes are dominant, which should also be measured to verify the reaction theory.

With respect to reaction theory the concept of the optical potential can rigorously be studied in the 3N system. Though the "medium" is rather dilute, just one additional nucleon, one can calculate all the properties of the optical potential exactly, like its nonlocality, the effects of antisymmetrization, its spin dependencies, its leading form at high energies, etc. We only displayed some formalism and left the numerical investigation to the future.

With increasing energy, 150 MeV and higher, relativity can certainly be no longer neglected and its correct treatment poses a real challenge. We mentioned some possible first starting points discussed in the literature.

Relativity will also be unavoidable in the applications, where the 3N continuum appears mostly in the final state, like in inelastic electron scattering or pion absorption on ${}^3\text{He}$ (${}^3\text{H}$) or in the nonmesonic decay of the hypertriton. We were rather brief about these exciting subjects, since they all deserve a broad presentation by themselves. It is only if the final state interaction is well under control that one has a reliable view on the interesting processes like photon or pion absorption, on the form factors involved and the meson exchange currents.

We think [187–189] that the 3N continuum due to the enormous computational possibilities now available, will be an excellent laboratory in the future to make decisive steps forward in the understanding of nuclear dynamics.

Acknowledgements

This work was supported by the Deutsche Forschungsgemeinschaft, the European Economic Community under Grant No. CI1*-CTG1-0894, the Polish Committee for Scientific Research under Grant No. 2 P302 104 06 and the Polish-American Maria Skłodowska-Curie II FUND under Grant No. MEN/NSF-94-161. The numerical calculations have been performed on the CRAY Y-MP of the Höchstleistungsrechenzentrum in Jülich, Germany and of the North Carolina Supercomputing Center at Research Triangle Park, North Carolina, USA, and on the Convex 3820 of the Academic Computational Center (ACK) in Cracow, Poland. We acknowledge the important support of the Alexander von Humboldt Foundation in the initial stage of this work (H.W.). Special thanks are also to Dr. Th. Cornelius for computational help in the first calculations.

Appendix A. Cross sections

Here we supplement the derivation of the cross sections for elastic and scattering and the breakup process carried through in Section 2.4 in time independent scattering theory by using time dependent theory. We follow closely the steps laid out in [172]. We define an initial wave packet for the relative motion of nucleon 1 with respect to the deuteron composed of nucleons 2 and 3.

$$\psi_0(t) = \int d\mathbf{q} |\mathbf{q}\rangle e^{-iE_q t} f_0(\mathbf{q}) \quad (\text{A.1})$$

with $E_q \equiv (3/4m)\mathbf{q}^2$. The momentum distribution $f_0(\mathbf{q})$ will finally be peaked infinitely sharply at $\mathbf{q} = \mathbf{q}_0$, but because of the normalization condition for $\psi_0(t)$ it does not approach a δ -function. Using a Gaussian wave packet as an example one can choose as in [172]

$$f_0(\mathbf{q}) = b^{3/2} (2\pi)^{3/2} f_\delta(\mathbf{q}) \quad (\text{A.2})$$

where $f_\delta(\mathbf{q})$ is a sequence of functions, which approach $\delta(\mathbf{q} - \mathbf{q}_0)$ if b tends towards zero.

The complete initial channel state is

$$|\Psi_0(t)\rangle = |\varphi_d\rangle \int d\mathbf{q} |\mathbf{q}\rangle e^{-i(E_q + \epsilon_d)t} f_0(\mathbf{q}) \quad (\text{A.3})$$

where $|\varphi_d\rangle$ is the deuteron wave function. It obeys the time dependent Schrödinger equation with the Hamiltonian $H_d \equiv H_0 + V_{23}$. The proof for the existence of the Möller wave operator

$$\Omega^{(+)} = \lim_{t \rightarrow -\infty} e^{iHt} e^{-iH_dt} \quad (\text{A.4})$$

is essentially identical to the one presented for potential scattering in [172], the only difference being that the norm $\|V\|$ is replaced by $\|(V_{13} + V_{12})|\varphi_d\rangle\|$, which of course exists for short range interactions. Then rewriting the representation of the Möller wave operator in the usual manner the scattering state can be put into the form

$$|\Psi(t)\rangle = \int d\mathbf{q} |\Psi_q^{(+)}\rangle e^{-i(E_q + \epsilon_d)t} f_0(\mathbf{q}) \quad (\text{A.5})$$

where the stationary scattering state has been defined as

$$|\Psi_q^{(+)}\rangle = \lim_{\epsilon \rightarrow 0} \frac{i\epsilon}{E_q + \epsilon_d + i\epsilon - H} |\varphi_d\rangle |\mathbf{q}\rangle \quad (\text{A.6})$$

The antisymmetrization is easily achieved by applying $(1 + P)$, assuming as always that the deuteron state is already antisymmetrized. Thus

$$|\Psi^{(+)}\rangle_a = \int d\mathbf{q} (|\Psi_q^{(+)}\rangle_1 + |\Psi_q^{(+)}\rangle_2 + |\Psi_q^{(+)}\rangle_3) e^{-i(E_q + \epsilon_d)t} f_0(\mathbf{q}) \quad (\text{A.7})$$

where in $|\Psi_q^{(+)}\rangle_i$ the particle i is the initial projectile.

Let $A_{q_f}(t)$ be the probability amplitude to find the state

$$|\Psi_{q_f}^0(t)\rangle \equiv |\varphi_d\rangle |\mathbf{q}_f\rangle e^{-i(E_{q_f} + \epsilon_d)t} \equiv |\phi_{q_f}\rangle e^{-i(E_{q_f} + \epsilon_d)t} \quad (\text{A.8})$$

in the $|\Psi^{(+)}\rangle_a$:

$$A_{q_f}(t) \equiv \langle \Psi_{q_f}^0(t) | \Psi^{(+)}(t) \rangle_a = \int d\mathbf{q} e^{i(E_{q_f} - E_q)t} \langle \phi_{q_f} | \Psi_q^{(+)}(0) \rangle_a f_0(\mathbf{q}) \quad (\text{A.9})$$

with the stationary antisymmetrized state

$$|\Psi_q^{(+)}(0)\rangle_a \equiv |\Psi_q^{(+)}\rangle_a \equiv \sum_{i=1}^3 |\Psi_q^{(+)}\rangle_i \quad (\text{A.10})$$

It obeys the Lippmann–Schwinger equation

$$|\Psi_q^{(+)}\rangle_a = |\Psi_q^0\rangle + G_1(V_2 + V_3)|\Psi_q^{(+)}\rangle_a \quad (\text{A.11})$$

since $|\Psi_q^{(+)}\rangle_{2,3}$ fulfill the homogeneous equation corresponding to (A.11) and $|\Psi_q^{(+)}\rangle_1$ of course brings in the driving term in (A.11). (See Section 2.2). Thus

$$A_{q_f}(t) = f_0(\mathbf{q}_f) + \lim_{\epsilon \rightarrow 0} \int d\mathbf{q} e^{i(E_{q_f} - E_q)t} \frac{\langle \phi_{q_f} | V_2 + V_3 | \Psi_q^{(+)} \rangle_a}{E_q - E_{q_f} + i\epsilon} f_0(\mathbf{q}) \quad (\text{A.12})$$

Now we can follow literally [172], take the limit $b \rightarrow 0$ and easily find

$$\lim_{b \rightarrow 0} \frac{1}{b^3 (2\pi)^{3/2}} \frac{d}{dt} |A_{q_f}(t)|^2 = 2 \operatorname{Im} \langle \phi_{q_f} | U | \phi_{q_0} \rangle \delta(\mathbf{q}_f - \mathbf{q}_0) + 2\pi \delta(E_{q_0} - E_{q_f}) |\langle \phi_{q_f} | U | \phi_{q_0} \rangle|^2 \quad (\text{A.13})$$

where we switched to the notation introduced in Section 2

$$\langle \phi_{q_f} | U | \phi_{q_0} \rangle_a \equiv \langle \phi_{q_f} | V_2 + V_3 | \Psi_{q_0}^{(+)} \rangle_a \quad (\text{A.14})$$

Then the number of scattered particles into the volume element $d\mathbf{q}_f$ is

$$\begin{aligned} dN &= |\langle \phi_{q_f} | U | \phi_{q_0} \rangle_a|^2 \int d\mathbf{q}_f 2\pi \delta(E_{q_0} - E_{q_f}) \\ &= 2\pi^2 m |\mathbf{q}_0| |\langle \phi_{q_f} | U | \phi_{q_0} \rangle|^2 d\hat{q}_f \end{aligned} \quad (\text{A.15})$$

The initial current $|j|$ carries the same factor $b^3(2\pi)^{3/2}$ in the limit $b \rightarrow 0$ as follows from (A.3) and one has

$$|j| = b^3(2\pi)^{3/2} \frac{3}{2m} \frac{|\mathbf{q}_0|}{(2\pi)^3} \quad (\text{A.16})$$

We end up with the differential cross section

$$\frac{d\sigma}{d\hat{q}_f} = \left(\frac{2}{3}m\right)^2 (2\pi)^4 |\langle \phi_{q_f} | U | \phi_{q_0} \rangle|^2 \quad (\text{A.17})$$

which agrees with Eq. (86).

In case of the breakup cross section one asks for the overlap of $|\Psi^{(+)}(t)\rangle_a$ with

$$|\Psi_{p_f q_f}^0(t)\rangle \equiv |\mathbf{p}_f\rangle |\mathbf{q}_f\rangle e^{-iE_{p_f q_f} t} \equiv |\phi_{0,f}\rangle e^{-iE_{p_f q_f} t} \quad (\text{A.18})$$

where $E_{p_f q_f} \equiv (1/m)\mathbf{p}_f^2 + (3/4m)\mathbf{q}_f^2$. Thus

$$A_{p_f q_f}(t) \equiv \langle \Psi_{p_f q_f}^0(t) | \Psi^{(+)}(t) \rangle_a = \int d\mathbf{q} e^{i(E_{p_f q_f} - E_q - \epsilon_d)t} \langle \phi_{0,f} | \Psi_q^{(+)} \rangle_a f_0(\mathbf{q}) \quad (\text{A.19})$$

Since $|\Psi_q^{(+)}\rangle_a$ obeys the homogeneous Lippmann–Schwinger equation

$$|\Psi_q^{(+)}\rangle_a = G_0(V_1 + V_2 + V_3)|\Psi_q^{(+)}\rangle_a \quad (\text{A.20})$$

one finds

$$A_{p_f q_f}(t) = \lim_{\epsilon \rightarrow 0} \int d\mathbf{q} e^{i(E_{p_f q_f} - E_q - \epsilon_d)t} \frac{\langle \phi_{0,f} | V_1 + V_2 + V_3 | \Psi_q^{(+)} \rangle_a}{E_q + \epsilon_d - E_{p_f q_f} + i\epsilon} f_0(\mathbf{q}) \quad (\text{A.21})$$

The analogous steps then lead to

$$\lim_{b \rightarrow 0} \frac{1}{b^3(2\pi)^{3/2}} \frac{d}{dt} |A_{p_f q_f}(t)|^2 = 2\pi \delta(E_{q_0} + \epsilon_d - E_{p_f q_f}) |\langle \phi_{0,f} | U_0 | \phi_{q_0} \rangle|^2 \quad (\text{A.22})$$

for $b \rightarrow 0$ and we switched again to the notation for the breakup amplitude introduced in Section 2.2.

Thus the number of scattered particles per unit time into the volume elements $d\mathbf{p}_f$ and $d\mathbf{q}_f$ are

$$dN = |\langle \phi_{0,f} | U_0 | \phi_{q_0} \rangle|^2 \int d\mathbf{p}_f d\mathbf{q}_f 2\pi \delta(E_{q_0} + \epsilon_d - E_{p_f q_f}) \quad (\text{A.23})$$

Performing the integral for given q_f and directions $d\hat{p}_f$ and $d\hat{q}_f$ the breakup cross section results

$$d\sigma = \frac{dN}{(3/2m)|\mathbf{q}_0|/(2\pi)^3} = \frac{1}{3} \frac{m^2(2\pi)^4}{|\mathbf{q}_0|} p_f q_f^2 d\mathbf{q}_f d\hat{p}_f d\hat{q}_f |\langle \phi_{0,f} | U_0 | \phi_{q_0} \rangle|^2 \quad (\text{A.24})$$

which agrees with Eq. (99).

The optical theorem follows easily from noting that for $t \rightarrow \infty$

$$\frac{d}{dt} \left\{ \int d\mathbf{q}_f |A_{q_f}(t)|^2 + \int d\mathbf{p}_f d\mathbf{q}_f |A_{p_f q_f}(t)|^2 \right\} = 0 \quad (\text{A.25})$$

Inserting (A.13) and (A.22) and taking the elastic and breakup cross sections from (A.17) and (A.24) one gets directly

$$\text{Im}\langle\phi|U|\phi\rangle = -\frac{1}{(2\pi)^3} \frac{3}{4} q_0 \frac{1}{m} \sigma_{\text{tot}} \quad (\text{A.26})$$

Appendix B. Breakup kinematics

We start from Eq. (103) of Section 2.4 describing an ellipse in the k_1-k_2 plane. It can be put into the normal form by a rotation of the k_1-k_2 plane by $\pi/4$:

$$k_1 = \frac{1}{\sqrt{2}} (k'_1 + k'_2), \quad k_2 = \frac{1}{\sqrt{2}} (-k'_1 + k'_2) \quad (\text{B.1})$$

It results in

$$\begin{aligned} & (2 - \cos \theta_{12}) \left[k'_1 - \frac{k^{lab}}{\sqrt{2}} (\cos \theta_1 - \cos \theta_2) \frac{1}{2 - \cos \theta_{12}} \right]^2 \\ & + (2 + \cos \theta_{12}) \left[k'_2 - \frac{k^{lab}}{\sqrt{2}} (\cos \theta_1 + \cos \theta_2) \frac{1}{2 + \cos \theta_{12}} \right]^2 \\ & = \frac{k^{lab} 2}{2} \left(\frac{(\cos \theta_2 - \cos \theta_1)^2}{2 - \cos \theta_{12}} + \frac{(\cos \theta_1 + \cos \theta_2)^2}{2 + \cos \theta_{12}} \right) + 2m\epsilon_d \end{aligned} \quad (\text{B.2})$$

The ellipse shrinks to a point if the right hand side is zero, which leads to the condition

$$\cos^2 \theta_1 + \cos^2 \theta_2 - \cos \theta_1 \cos \theta_2 \cos \theta_{12} + \frac{m\epsilon_d}{k^{lab 2}} (4 - \cos \theta_{12}) = 0 \quad (\text{B.3})$$

Here $\cos \theta_{12} \equiv \hat{k}_1 \cdot \hat{k}_2 = \cos \theta_1 \cos \theta_2 + \sin \theta_1 \sin \theta_2 \cos(\phi_1 - \phi_2)$.

The curve defined by Eq. (B.3) is very close in form to a circle for $\phi_1 - \phi_2 = \pi/2$ and to an ellipse otherwise. Values for θ_1 and θ_2 lying inside that curve are mathematically forbidden. Otherwise one has an ellipse, which can lie totally or partially outside the first quadrant of the k_1-k_2 plane. The conditions for crossing the k_1 -axis ($k_2 = 0$) are read off from Eq. (103) to be

$$k_1^2 - k_1 k^{lab} \cos \theta_1 - m\epsilon_d = 0 \quad (\text{B.4})$$

which leads to

$$(k_1)_{1,2} = \frac{k^{lab} \cos \theta_1 \pm \sqrt{k^{lab 2} \cos^2 \theta_1 + 4m\epsilon_d}}{2} \quad (\text{B.5})$$

Consequently, the two crossing points of the ellipse with the k_1 -axis coincide for θ_1 equal $\theta^{(-)}$ and $\theta^{(+)}$ given by

$$\theta^{(-)} = \cos^{-1} \sqrt{\frac{4m|\epsilon_d|}{k^{lab 2}}} < \theta^{(+)} = -\cos^{-1} \sqrt{\frac{4m|\epsilon_d|}{k^{lab 2}}} \quad (\text{B.6})$$

For $\theta^{(-)} < \theta_1 < \theta^{(+)}$ the ellipse lies above the k_1 -axis. The corresponding applies for the k_2 -axis.

The resulting picture for the location of all possible ellipses depending on θ_1 , θ_2 and ϕ_{12} is displayed in Fig. 1.

Appendix C. Geometrical quantities related to permutation operators

The quantity $g_{\alpha\alpha'}^{kl_1l_2l'_1l'_2}$ from Eq. (164) is given by

$$\begin{aligned} g_{\alpha\alpha'}^{kl_1l_2l'_1l'_2} &= \sqrt{\hat{l} \hat{s} \hat{j} \hat{t} \hat{\lambda} \hat{I} \hat{l}' \hat{s}' \hat{j}' \hat{t}' \hat{\lambda}' \hat{I}'} (-) \left\{ \begin{array}{ccc} \frac{1}{2} & \frac{1}{2} & t \\ \frac{1}{2} & T & t' \end{array} \right\}} \\ &\times \sum_{LS} \hat{L} \hat{S} \left\{ \begin{array}{ccc} \frac{1}{2} & \frac{1}{2} & s \\ \frac{1}{2} & S & s' \end{array} \right\} \left\{ \begin{array}{ccc} l & s & j \\ \lambda & \frac{1}{2} & I \\ L & S & J \end{array} \right\} \left\{ \begin{array}{ccc} l' & s' & j' \\ \lambda' & \frac{1}{2} & I' \\ L & S & J \end{array} \right\} \\ &\times \hat{k} \left(\frac{1}{2} \right)^{l_2+l'_1} \sqrt{\frac{(2l+1)!}{(2l_1)!(2l_2)!}} \sqrt{\frac{(2l'+1)!}{(2l'_1)!(2l'_2)!}} \\ &\times \sum_{ff'} \left\{ \begin{array}{ccc} l_1 & l_2 & l \\ \lambda & L & f \end{array} \right\} \left\{ \begin{array}{ccc} l'_2 & l'_1 & l' \\ \lambda' & L & f' \end{array} \right\} C(l_2 \lambda f, 0 0 0) C(l'_1 \lambda' f', 0 0 0) \\ &\times \left\{ \begin{array}{ccc} f & l_1 & L \\ f' & l'_2 & k \end{array} \right\} C(k l_1 f', 0 0 0) C(k l'_2 f, 0 0 0) \end{aligned} \quad (\text{C.1})$$

The quantity \tilde{G} of Eq. (197) can be written as

$$\tilde{G}_{\alpha\alpha'}(pqx) = \sum_k P_k(x) \sum_{l_1+l_2=l'} \sum_{\lambda_1+\lambda_2=\lambda'} p^{l_1+\lambda_1} q^{l_2+\lambda_2} \tilde{g}_{\alpha\alpha'}^{kl_1l_2\lambda_1\lambda_2} \quad (\text{C.2})$$

with

$$\begin{aligned} \tilde{g}_{\alpha\alpha'}^{kl_1l_2\lambda_1\lambda_2} &= \sqrt{\hat{l} \hat{s} \hat{j} \hat{t} \hat{\lambda} \hat{I} \hat{l}' \hat{s}' \hat{j}' \hat{t}' \hat{\lambda}' \hat{I}'} (-) \left\{ \begin{array}{ccc} \frac{1}{2} & \frac{1}{2} & t \\ \frac{1}{2} & T & t' \end{array} \right\}} \\ &\times \sum_{LS} (-)^L \hat{L} \hat{S} \left\{ \begin{array}{ccc} \frac{1}{2} & \frac{1}{2} & s \\ \frac{1}{2} & S & s' \end{array} \right\} \left\{ \begin{array}{ccc} l & s & j \\ \lambda & \frac{1}{2} & I \\ L & S & J \end{array} \right\} \left\{ \begin{array}{ccc} l' & s' & j' \\ \lambda' & \frac{1}{2} & I' \\ L & S & J \end{array} \right\} \\ &\times (-)^{k+\lambda'+\lambda_1} \left(\frac{1}{2} \right)^{l_1+\lambda_2} \left(\frac{3}{4} \right)^{l_2} \sqrt{\frac{(2l'+1)!}{(2l_1)!(2l_2)!}} \sqrt{\frac{(2\lambda'+1)!}{(2\lambda_1)!(2\lambda_2)!}} \\ &\times \sum_{ff'} \sqrt{\hat{f} \hat{f}'} C(l_1 \lambda_1 f, 0 0 0) C(l f k, 0 0 0) C(l_2 \lambda_2 f', 0 0 0) C(\lambda f' k, 0 0 0) \\ &\times \left\{ \begin{array}{ccc} l & f & k \\ f' & \lambda & L \end{array} \right\} \left\{ \begin{array}{ccc} l_1 & l_2 & l' \\ \lambda_1 & \lambda_2 & \lambda' \\ f & f' & L \end{array} \right\} \end{aligned} \quad (\text{C.3})$$

Appendix D. List of international few-body conferences

- Nuclear Forces and the Few Nuclear Problem (Pergamon Press, London, 1959).

- Few-Body Problems, Light Nuclei, and Nuclear Interactions, Brela, 1967, eds. G. Paić, I. Slaus (Gordon and Breach, New York, 1968).
- Three-Particle Scattering in Quantum Mechanics, College Station, Texas 1968, eds. J. Gillespie, J. Nuttal (Benjamin, New York, 1968).
- Three-Body Problems in Nuclear and Particle Physics, Birmingham 1969, eds. J.S.C. McKee, P.M. Rolph (North-Holland, Amsterdam, 1970)
- The Nuclear Three-Body Problem and Related Topics, Budapest 1971, *Acta Phys. Acad. Sci. Hung.* 33 (1973) 102.
- Few-Particle Problems in the Nuclear Interaction, Los Angeles 1972, eds. I. Slaus, S.A. Moszkowski, R.P. Haddock, W.T.H. van Oers (North-Holland, Amsterdam, 1972).
- The Nuclear Many-Body Problem, Rome 1972, eds. F. Calogero, C. Ciofi (Atti Editrice Compositori, Bologna, 1973).
- Few-Body Problems in Nuclear and Particle Physics, Laval 1974, eds. R.J. Slobodrian, B. Cujec, K. Ramavataram (Les Presses de l'Université, Laval, 1975).
- Few-Body Dynamics, Dehli 1975/76, eds. A.N. Mitra, I. Slaus, V.S. Bhasin, V.K. Gupta (North-Holland, Amsterdam, 1976).
- Few-Body Nuclear Physics, Trieste 1978, eds. G. Pisent, V. Vanzani, L. Fonda (IAEA, Vienna, 1978).
- Few-Body Systems and Nuclear Forces I, II, Graz 1978, eds. H. Zingl, M. Haftel, H. Zankel, *Lecture Notes Phys.*, Vols. 82, 87 (Springer, Berlin, Heidelberg, New York, 1978).
- The Few-Body Problem, Eugene 1980, eds. F.S. Levin (North-Holland, Amsterdam, 1981).
- Few-Body Problems in Physics, Karlsruhe, Germany, 1983, eds. B. Zeitnitz, Vol I: *Nucl. Phys. A416* (1984), Vol II - Contributed Papers (Elsevier Science Publishers B.V., Amsterdam, 1984).
- The Three-Body Forces in the Three-Nucleon System, Washington DC, 1986, eds. B.L. Berman and B.F. Gibson, *Lecture Notes in Physics* 260 (1986).
- Few-Body Methods: Principles and Applications, Nanning, PRC, 1985, eds. T.K. Lim, C.C. Bao, D.P. Hou, S. Huber (World Scientific, Singapore, 1986).
- Theoretical and Experimental Investigations of Hadronic Few-Body Systems, Rome, 1986, eds. C.C. degli Atti, O. Benhar, E. Pace, G. Salme, *Few-Body Systems, Suppl. 1* (1986).
- Few-Body Systems in Particle and Nuclear Physics, Tokyo & Sendai, Japan, 1986, eds. T. Sasakawa, K. Nisimura, S. Oryu, S. Ishikawa, *Nucl. Phys. A* 463 (1987).
- Few-Body Problems in Particle, Nuclear, Atomic and Molecular Physics, Fontevraud, 1987, eds. J.L. Ballot, M. Fabre de la Ripelle, *Few-Body Systems, Suppl. 1* (1987).
- Few-Body Problems in Physics, Vancouver, 1989, eds. H.W. Fearing, *Nucl. Phys. A* 508 (1990).
- Few-Body Problems in Physics, Adelaide, 1992, eds. I.R. Afnan, R.T. Cahill, *Nucl. Phys. A* 543 (1992).
- Few-Body Problems in Physics, Marciana Marina, Isola d'Elba, Italy, 1991, eds. C.C. degli Atti, E. Pace, G. Salme, S. Simula, *Few-Body Systems, Suppl. 6* (1992).
- Few-Body Problems in Physics '93, Amsterdam, 1993, eds. B.L.G. Bakker, R. van Dantzig, *Few-Body Systems, Suppl. 7* (1994).
- Few-Body Problems in Physics, Williamsburg, USA, 1994, eds. F. Gross, *AIP Conference Proceedings* 334 (AIP Press, New York, 1995).

References

- [1] R. Aaron, R.D. Amado, Y.Y. Yam, Phys. Rev. **140** (1965) B1291.
- [2] R. Aaron, R.D. Amado, Phys. Rev. **150** (1966) 857.
- [3] J.C. Aarons, I.H. Sloan, Nucl. Phys. A **182** (1972) 369.
- [4] S.K. Adhikari, I.H. Sloan, Phys. Rev. C **11** (1975) 1133; Nucl. Phys. A **241** (1975) 429.
- [5] S.K. Adhikari, W. Glöckle, Phys. Rev. C **19** (1979) 616.
- [6] I.R. Afnan, B.F. Gibson, Phys. Rev. C **40** (1989) R7.
- [7] I.R. Afnan, B.F. Gibson, Phys. Rev. C **41** (1990) 2787.
- [8] G. Alexander, U. Karshon, A. Shapira, G. Yekutieli, R. Engelmann, A. Filthuth, W. Lughofer, Phys. Rev. **173** (1968) 1452.
- [9] M. Allet, K. Bodek, W. Hajdas, J. Lang, R. Müller, O. Naviliat-Cunic, J. Sromicki, J. Zejma, L. Jarczyk, St. Kistryn, J. Smyrski, A. Strzałkowski, W. Glöckle, J. Golak, H. Witała, B. Dechant, J. Krug, P.A. Schmelzbach, Phys. Rev. C **50** (1994) 602.
- [10] M. Allet, K. Bodek, W. Hajdas, J. Lang, R. Müller, S. Navert, O. Naviliat-Cunic, J. Sromicki, J. Zejma, L. Jarczyk, St. Kistryn, J. Smyrski, A. Strzałkowski, W. Glöckle, J. Golak, H. Witała, D. Dechant, J. Krug, Few-Body Systems Suppl. **7** (1994) 243.
- [11] M. Allet, K. Bodek, W. Hajdas, J. Lang, R. Müller, S. Navert, O. Naviliat-Cunic, J. Sromicki, J. Zejma, L. Jarczyk, St. Kistryn, J. Smyrski, A. Strzałkowski, H. Witała, W. Glöckle, J. Golak, D. Hüber, H. Kamada, accepted for publication in Few-Body Systems.
- [12] M. Allet, K. Bodek, W. Glöckle, J. Golak, L. Jarczyk, St. Kistryn, J. Lang, R. Müller, S. Navert, O. Naviliat-Cunic, J. Smyrski, J. Sromicki, E. Stephan, A. Strzałkowski, H. Witała, J. Zejma, Few-Body Systems, Suppl. **8** (1996) 49.
- [13] E.O. Alt, P. Grassberger, W. Sandhas, Nucl. Phys. B **2** (1967) 167.
- [14] E.O. Alt, P. Grassberger, W. Sandhas, JINR Report E4-6688 (1972).
- [15] E.O. Alt, W. Sandhas, H. Zankel, H. Ziegelmann, Phys. Rev. Lett. **37** (1976) 1537.
- [16] E.O. Alt, W. Sandhas, H. Ziegelmann, Phys. Rev. C **17** (1978) 1981.
- [17] E.O. Alt, W. Sandhas, H. Ziegelmann, Nucl. Phys. A **445** (1985) 429.
- [18] E.O. Alt in: Few-Body Methods: Principles and Applications, eds. T.K. Lim, C.-G. Bao, D.-P. Hou, H.S. Huber, (World Scientific, Singapore, 1986) p. 239.
- [19] E.O. Alt, Few-Body Systems, Suppl. **1** (1986) 79.
- [20] E.O. Alt, M. Rauh, Few-Body Systems, Suppl. **7** (1994) 160.
- [21] E.O. Alt, M. Rauh, Phys. Rev. C **49** (1994) R2285.
- [22] T. Alteholz et al., Phys. Rev. Lett. **73** (1994) 1336.
- [23] R.D. Amado, Phys. Rev. **132** (1963) 485.
- [24] L. Amten, L. Goenozi, A. Johansson, L. Nilsson, B. Sundquist, Report TLU-52 (1977); NNDC, Entry 20994.
- [25] K.A. Aniol et al., Phys. Rev. C **33** (1986) 1714.
- [26] R.A. Arndt, L.D. Roper, R.A. Bryan, R.B. Clark, B.J. VerWest, P. Signell, Phys. Rev. D **28** (1983) 97.
- [27] R.A. Arndt, J.S. Hysby III, L.D. Roper, Phys. Rev. D **35** (1987) 128.
- [28] R.A. Arndt, L.D. Roper, R.L. Workman, M.W. McNaughton, Phys. Rev. D **45** (1992) 3995.
- [29] D. Ashery, I.P. Schiffer, Ann. Rev. Nucl. Part. Sci. **36** (1986) 207.
- [30] G. Backenstoss et al., Phys. Rev. Lett. **55** (1985) 2782.
- [31] A.M. Badalyan, Yu. A. Simonov, Sov. J. Nucl. Phys. **3** (1966) 755.
- [32] B. Bakamjian, L.H. Thomas, Phys. Rev. **92** (1953) 1300.
- [33] G.A. Baker Jr, in Advances in Theoretical Physics, Vol. 1, ed. K.A. Brueckner (Academic Press, New York, London, 1965) p. 1.
- [34] B. Balian, E. Brezin, Nuovo Cim. **2** (1969) 403.
- [35] J.L. Ballot, M. Fabre de la Ripelle, Int. School of Intermediate Energy Nuclear Physics, Arriccio, June 1979 (Harwood Academic Publishers, London).
- [36] M. Baldo, L.S. Ferreira, L. Streit, Phys. Rev. C **32** (1985) 685.
- [37] J. Balewski, K. Bodek, L. Jarczyk, B. Kamys, St. Kistryn, A. Strzałkowski, W. Hajdas, R. Müller, B. Dechant, J. Krug, W. Lübcke, H. Rühl, G. Spangardt, M. Steinke, M. Stephan, D. Kamke, R. Henneck, H. Witała, W. Glöckle, J. Golak, Nucl. Phys. A **581** (1995) 131.

- [38] I.M. Barbour, A.C. Phillips, Phys. Rev. Lett. **19** (1967) 1388.
- [39] H.H. Barshall, W. Haeberli, eds., Polarization phenomena in nuclear reactions (University of Wisconsin, Madison, 1970) p. xxv.
- [40] I.M. Barbour, A.C. Phillips, Phys. Rev. C **1** (1970) 165.
- [41] E.A. Bartnik, H. Haberzettl, Th. Januschke, U. Kerwarth, W. Sandhas, Phys. Rev. C **36** (1987) 1678.
- [42] M.A.B. Beg, H. Ruegg, J. Math. Phys. **6** (1965) 677.
- [43] Gy. Bencze, Nucl. Phys. A **210** (1973) 568.
- [44] J.J. Benayoun, J. Chauvin, C. Gignoux, A. Laverne, Phys. Rev. Lett. **36** (1976) 1438.
- [45] Gy. Bencze, C. Chandler, Phys. Lett. **90A** (1982) 162.
- [46] C. Bennhold, A. Ramos, D.A. Aruliah, U. Oelfke, Phys. Rev. C **45** (1992) 947.
- [47] A.C. Berick, R.A.J. Riddle, C.M. York, Phys. Rev. **174** (1968) 1105.
- [48] G.H. Berthold, H. Zankel, Phys. Rev. C **34** (1986) 1203.
- [49] G.H. Berthold, A. Stadler, H. Zankel, Phys. Rev. Lett. **61** (1988) 1077.
- [50] J.R. Bergervoert, P.C. van Campen, R.A.M. Klomp, J.L. de Kok, T.A. Rijken, V.G.J. Stoks, J.J. de Swart, Phys. Rev. C **41** (1990) 1435.
- [51] G.H. Berthold, A. Stadler, H. Zankel, Phys. Rev. C **41** (1990) 1365.
- [52] V.S. Bhasin, H. Jacob, A.N. Mitra, Phys. Lett. **32B** (1970) 15.
- [53] J. Birchall, J.P. Svenne, M.S. de Jong, J.S.C. McKee, W.D. Ramsey, M.S.A.L. Al-Ghazi, N. Videla, Phys. Rev. C **20** (1979) 1585.
- [54] J.M. Blatt, V.F. Weisskopf, Theoretical Nuclear Physics (John Wiley and Sons, New York, 1952).
- [55] R. Blankenbecler, R. Sugar, Phys. Rev. **142** (1966) 1051.
- [56] G.J.F. Blommestijn, R. van Dantzig, Y. Haitsma, R.B.M. Mooy, I. Slous, Nucl. Phys. A **365** (1981) 202.
- [57] A. Bömelburg, W. Glöckle, W. Meier, in: Few-Body Problems in Physics, Vol. II, Contributed Papers, B. Zeitnitz, ed. (Elsevier Science Publishers B.V., Amsterdam, 1984) p. 483.
- [58] J. Borysowicz, J. Dabrowski, Phys. Lett. **B 24** (1967) 549.
- [59] R. Bouchez, S. Desreumaux, J.C. Gondrand, C. Perrin, P. Perrin, R.T. Cahill, Nucl. Phys. A **185** (1972) 166.
- [60] A. Bratenahl, J.M. Peterson, J.P. Stoering, Phys. Rev. **110** (1958) 927.
- [61] D.D. Brayshaw Phys. Rev. Lett. **32** (1974) 382.
- [62] F.P. Brady, W.B. Broste, J.C. Wang, J.L. Romero, P. Martens, Phys. Rev. C **9** (1974) 1784.
- [63] R. Brandenburg, W. Glöckle, Nucl. Phys. A **377** (1982) 379.
- [64] R.A. Brandenburg, Few-Body Systems **3** (1987) 59.
- [65] W.H. Breunlich, S. Tagesen, W. Bartl, A. Chalupka, Nucl. Phys. A **221** (1974) 269.
- [66] W.I. Briscoe et al., Nucl. Phys. A **553** (1993) 585c.
- [67] G.E. Brown, A.M. Green, W.J. Gerace, Nucl. Phys. A **115** (1968) 435.
- [68] H. Brueckmann, V. Kluge, H. Mattaey, L. Schaenzler, K. Wick, Nucl. Phys. A **157** (1970) 209.
- [69] J. Bruinsma, W. Ebenhoeh, J.H. Stuivenberg, R. van Wageningen, Nucl. Phys. A **228** (1974) 52.
- [70] J. Bruinsma, R. van Wageningen, Nucl. Phys. A **282** (1977) 1.
- [71] S.N. Bunker, J.M. Cameron, R.F. Carlson, J. Reginald Richardson, P. Tomas, W.T.H. Van Oers, J.W. Verba, Nucl. Phys. A **113** (1968) 461.
- [72] R.T. Cahill, I.H. Sloan, Nucl. Phys. A **165** (1971) 161.
- [73] J. Carlson, V.R. Pandharipande, R.B. Wiringa, Nucl. Phys. A **401** (1983) 59.
- [74] J. Carlson, R. Schiavilla, Phys. Rev. Lett. **68** (1992) 3682.
- [75] J. Carlson, V.R. Pandharipande, R. Schiavilla, Phys. Rev. C **47** (1993) 484.
- [76] J. Carlson, R. Schiavilla, Phys. Rev. C **49** (1994) R2880.
- [77] H.C. Catron, M.D. Goldberg, R.W. Hill, J.M. Le Blanc, J.P. Stoering, C.J. Taylor, M.A. Williamson, Phys. Rev. **123** (1961) 218.
- [78] G. Cattapan, V. Vanzani, Phys. Rev. C **19** (1979) 1168.
- [79] O. Chamberlain, M.O. Stern, Phys. Rev. **94** (1954) 666.
- [80] J. Chauvin, D. Garreta, M. Fruneau, Nucl. Phys. A **247** (1975) 335.
- [81] C. Chandler, Nucl. Phys. A **301** (1978) 1.
- [82] C. Chandler, Nucl. Phys. A **463** (1987) 181c.
- [83] G.F. Chew Phys. Rev. **80** (1950) 196.

- [84] C.R. Chen, G.L. Payne, J.L. Friar, J.L. Gibson, Phys. Rev. C 33 (1986) 1740.
- [85] C.R. Chen, G.L. Payne, J.L. Friar, B.F. Gibson, Phys. Rev. C 39 (1989) 1261.
- [86] C.R. Chen, G.L. Payne, J.L. Friar, B.F. Gibson, Phys. Rev. C 44 (1991) 50.
- [87] C.R. Chinn, Ch. Elster, R.M. Thaler, Phys. Rev. C 48 (1993) 2956.
- [88] R.S. Christian, J.L. Gammel, Phys. Rev. 91 (1953) 100.
- [89] M. Clajus, P.M. Egun, W. Grüebler, P. Hautle, I. Slaus, B. Vuaridel, F. Sperisen, W. Kretschmer, A. Rauscher, W. Schuster, R. Weidmann, M. Haller, M. Bruno, D. Cannata, M. D'Agostino, H. Witała, Th. Cornelius, W. Glöckle, P.A. Schmelzbach, Phys. Lett. B 245 (1990) 333.
- [90] M. Clajus, P.M. Egun, W. Grüebler, P. Hautle, W. Kretschmer, A. Rauscher, W. Schuster, R. Weidmann, M. Haller, M. Bruno, D. Cannata, M. D'Agostino, I. Slaus, P.A. Schmelzbach, B. Vuaridel, F. Sperisen, H. Witała, Th. Cornelius, W. Glöckle, Nucl. Phys. A 508 (1990) 261c.
- [91] T.B. Clegg, W. Haeberli, Nucl. Phys. A 95 (1967) 608.
- [92] J.M. Clement, P. Stoler, C.A. Goulding, R.W. Fairchild, Nucl. Phys. A 183 (1972) 51.
- [93] F. Coester, W.N. Polyzou, Phys. Rev. D 26 (1982) 1348.
- [94] J. Cohen, Prog. Part. Nucl. Phys. 25 (1990) 139.
- [95] C.F. Cook, T.W. Bonner, Phys. Rev. 94 (1954) 651.
- [96] S.A. Coon, M.D. Scadron, P.C. McNamee, B.R. Barrett, D.W.E. Blatt, B.H.J. McKellar, Nucl. Phys. A 317 (1979) 242.
- [97] S.A. Coon, W. Glöckle, Phys. Rev. C 23 (1981) 1790.
- [98] S.A. Coon, Lecture Notes in Physics 260 (1986) 92.
- [99] S.A. Coon, Few-Body Systems, Suppl. 1 (1986) 41.
- [100] S.A. Coon, M.T. Peña, Phys. Rev. C 48 (1993) 2559.
- [101] F.D. Correll, R.E. Brown, G.G. Ohlsen, R.A. Hardekopf, N. Jarmie, J.M. Lambert, P.A. Treado, I. Slaus, P. Schwandt, P. Doleshall, Nucl. Phys. A 475 (1987) 407.
- [102] Th. Cornelius, W. Glöckle, J. Haidenbauer, Y. Koike, W. Plessas, H. Witała, Phys. Rev. C 41 (1990) 2538.
- [103] Th. Cornelius, PhD-thesis, Bochum 1990, unpublished.
- [104] V. Culler, R.W. Wanek, Phys. Rev. 99 (1955) 740.
- [105] J. Dabrowski, E. Fedorynska, Nucl. Phys. A 210 (1973) 509.
- [106] R.H. Dalitz, R.C. Herndon, Y.C. Tang, Nucl. Phys. B 47 (1972) 109.
- [107] J.C. Davis, H.H. Barschall, Phys. Rev. C 3 (1971) 1798.
- [108] L.M. Delves, Nucl. Phys. 9 (1958/59) 391.
- [109] L.M. Delves, Nucl. Phys. 20 (1960) 275.
- [110] W. Dilg, L. Koester, W. Nistler, Phys. Lett. B 36 (1971) 208.
- [111] P.A.M. Dirac, Rev. Mod. Phys. 21 (1949) 392.
- [112] H. Dobiasch, R. Fischer, B. Haesner, H.O. Klages, P. Schwarz, B. Zeitnitz, R. Maschuw, K. Sinram, K. Wick, Phys. Lett. B 76 (1978) 195.
- [113] P. Doleshall, Phys. Lett. B 38 (1972) 298; B 40 (1972) 443.
- [114] P. Doleshall, Nucl. Phys. A 201 (1973) 264.
- [115] P. Doleshall, Nucl. Phys. A 220 (1974) 491.
- [116] P. Doleshall, W. Grüebler, V. Koenig, P.A. Schmelzbach, F. Sperisen, B. Jenny, Nucl. Phys. A 380 (1982) 72.
- [117] K. Dow et al., Phys. Rev. Lett. 61 (1988) 1706.
- [118] A.J. Dragt, J. Math. Phys. 6 (1965) 533.
- [119] W. Ebenhoeh, Nucl. Phys. A 191 (1972) 97.
- [120] F. Eisele, H. Filthuth, W. Föhlisch, V. Hepp, G. Zech, Phys. Lett. B 37 (1971) 204.
- [121] H. Ekstein, Phys. Rev. 101 (1956) 880.
- [122] R.G. Ellis, S.A. Coon, B.H.J. McKellar, Nucl. Phys. A 438 (1985) 631.
- [123] R. Engelmann, H. Filthuth, V. Hepp, E. Kluge, Phys. Rev. Lett. 21 (1966) 587.
- [124] S.T. Epstein, Phys. Rev. 106 (1957) 598.
- [125] D.J. Ernst, C.M. Shakin, R.M. Thaler, Phys. Rev. C 8 (1973) 46.
- [126] A. Everett, Phys. Rev. 126 (1962) 831.
- [127] P. Extermann, Nucl. Phys. A 95 (1967) 615.
- [128] L.D. Faddeev, Sov. Phys. JETP 12 (1961) 1014.

- [129] L.D. Faddeev, Mathematical Aspects of the three body problem in quantum scattering theory (Davey, New York, 1965).
- [130] L.D. Faddeev, S.P. Merkuriev, Quantum Scattering Theory for Several Particle Systems (Kluwer Academic Publishers, Dordrecht, 1993).
- [131] P.G. Federbush, Phys. Rev. **148** (1966) 1551.
- [132] E. Feenberg, Phys. Rev. **47** (1935) 850.
- [133] E. Feenberg, S.S. Share, Phys. Rev. **50** (1936) 253.
- [134] L.S. Ferreira, Lecture Notes in Physics **273** (1987) 100.
- [135] E. Finckh, K. Geissdörfer, R. Lin, S. Schindler, J. Strate, Nucl. Instrum. Methods A **262** (1987) 441.
- [136] E. Finckh, private communication.
- [137] J. Flender, M.F. Gari, to appear in Phys. Rev. C (1995)
- [138] L.L. Foldy, W. Tobocman, Phys. Rev. **105** (1957) 1099.
- [139] L.L. Foldy, Phys. Rev. **122** (1961) 275.
- [140] L.L. Foldy, R.A. Krajcik, Phys. Rev. Lett. **32** (1974) 1025.
- [141] L.L. Foldy, R.A. Krajcik, Phys. Rev. D **12** (1975) 1700.
- [142] A.C. Fonseca, D.R. Lehman, Phys. Lett. B **267** (1991) 159.
- [143] A.C. Fonseca, D.R. Lehman, Few-Body Systems, Suppl. **6** (1992) 279.
- [144] A.C. Fonseca, D.R. Lehman, Phys. Rev. C **48** (1993) R503.
- [145] F. Foroughi, Ch. Nussbaum, H. Vuilleme, B. Vuilleumer, Nucl. Phys. A **346** (1980) 139.
- [146] F. Foroughi, H. Vuilleme, P. Chatelain, Ch. Nussbaum, B. Favier, J. Phys. G: Nucl. Phys. **11** (1985) 59.
- [147] R. Fox, C. Leith, L. Wouters, K.R. MacKenzie, Phys. Rev. **80** (1950) 23.
- [148] N.C. Francis, K.M. Watson, Phys. Rev. **92** (1953) 291.
- [149] D.Z. Freedman, C. Lovelace, J.M. Namysłowski, Nuovo Cimento **XLIII A** (1966) 258.
- [150] T. Frederico, I.D. Goldman, S.K. Adhikari, Phys. Rev. C **37** (1988) 949.
- [151] J.L. Friar, B.F. Gibson, E.L. Tomusiak, G.L. Payne, Phys. Rev. C **24** (1981) 665.
- [152] J.L. Friar, Few-Body Systems, Suppl. **1** (1986) 94.
- [153] J.L. Friar, B.F. Gibson, G.L. Payne, Phys. Lett. B **251** (1990) 11.
- [154] J.L. Friar, B.F. Gibson, G.L. Payne, C.R. Chen, Phys. Lett. B **247** (1990) 197.
- [155] J.L. Friar, B.F. Gibson, G. Berthold, W. Glöckle, Th. Cornelius, H. Witała, J. Haidenbauer, Y. Koike, G.L. Payne, J.A. Tjon, W.M. Kloet, Phys. Rev. C **42** (1990) 1838.
- [156] J.L. Friar, G.L. Payne, W. Glöckle, D. Hüber, H. Witała, Phys. Rev. C **51** (1995) 2356.
- [157] J. Fujita, H. Miyazawa, Prog. Theor. Phys. **17** (1957) 360.
- [158] N. Fujiwara, E. Hourany, H. Nakamura-Yokota, F. Reide, T. Yuasa, Phys. Rev. C **15** (1977) 4.
- [159] B. Gabiou, J.-C. Alder, C. Joseph, J.-F. Loude, N. Morel, A. Perrenoud, J.-P. Perroud, M.T. Tran, E. Winkelmann, W. Dahme, H. Panke, D. Renker, C. Zupancic, G. Strassner, P. Truöl, Phys. Rev. Lett. **42** (1979) 1508.
- [160] K. Gebhardt, W. Jaeger, C. Jeitner, M. Vitz, E. Finckh, T.N. Frank, Th. Januschke, W. Sandhas, H. Haberzettl, Nucl. Phys. A **561** (1993) 232.
- [161] E. Gerjuoy, Phys. Rev. **109** (1958) 1806.
- [162] E. Gerjuoy, Ann. Phys. **5** (1958) 58.
- [163] B.F. Gibson, D.R. Lehman, Phys. Rev. C **10** (1974) 888.
- [164] B.F. Gibson, D.R. Lehman, Phys. Rev. C **11** (1975) 29.
- [165] B.F. Gibson, D.R. Lehman, Phys. Rev. C **13** (1976) 477.
- [166] B.F. Gibson, D.R. Lehman, Phys. Rev. C **22** (1980) 2024.
- [167] C. Gignoux, A. Laverne, S.P. Merkuriev, Phys. Rev. Lett. **33** (1974) 1350.
- [168] W. Glöckle, Nucl. Phys. A **141** (1970) 620.
- [169] W. Glöckle, Z. Phys. **271** (1974) 31.
- [170] W. Glöckle, L. Müller, Phys. Rev. C **23** (1981) 1183.
- [171] W. Glöckle, G. Hasberg, A.R. Neghabian, Z. Phys. A **305** (1982) 217.
- [172] W. Glöckle, The Quantum-Mechanical Few-Body Problem (Springer Verlag, Berlin, Heidelberg, 1983).
- [173] W. Glöckle, R. Brandenburg, Phys. Rev. C **27** (1983) 83.
- [174] W. Glöckle, T.S.H. Lee, F. Coester, Phys. Rev. C **33** (1986) 709.
- [175] W. Glöckle, Lecture Notes in Physics **273** (1987) 3.

- [176] W. Glöckle, Phys. Rev. C 37 (1988) 6.
- [177] W. Glöckle, H. Witała, Th. Cornelius, Nucl. Phys. A 508 (1990) 115c.
- [178] W. Glöckle, H. Witała, Th. Cornelius, Proc. 25th Zakopane School on Physics, Vol. 2: Selected topics in nuclear structure, eds. J. Styczeń, Z. Stachura (World Scientific, Singapore, 1990) p. 300.
- [179] W. Glöckle, G.L. Payne, Phys. Rev. C 45 (1992) 974.
- [180] W. Glöckle, H. Kamada, H. Witała, Physicalla Mag. 14 (1992) 271.
- [181] W. Glöckle, H. Kamada Nucl. Phys. A 560 (1993) 541.
- [182] W. Glöckle, J. Golak, H. Kamada, S. Ishikawa, H. Witała, Proceedings of Workshop on Electron-Nucleus Scattering (EIPC, Italy, July 1993), eds. O. Benhar, A. Fabrocini, R. Schiavilla (World Scientific, Singapore, 1994) p. 64.
- [183] W. Glöckle, H. Kamada, H. Witała, in: Proceedings of the National Conference in Physics of Few-Body and Quark-Hadronic Systems, Kharkov, Ukraine, 1992, eds. V. Boldyshev, V. Kotlyar, A. Shebeko (KFTI Kharkov, 1994) p. 75.
- [184] W. Glöckle, H. Kamada, H. Witała, in Contemporary Topics in Medium Energy Physics, eds. K. Goeke, W.-Y. Pauchy Hwang, J. Speth (Plenum-Press, New York, 1994) p. 243.
- [185] W. Glöckle, G.L. Payne, in preparation.
- [186] A. Glombik et al., AIP Conference Proceedings 334 on Few Body Problems in Physics, Williamsburg 1994, ed. F. Gross (AIP Press, New York, 1995) p. 486.
- [187] W. Glöckle, H. Witała, H. Kamada, D. Hüber, J. Golak, AIP Conference Proceedings 334 on Few Body Problems in Physics, Williamsburg 1994, ed. F. Gross (AIP Press, New York, 1995) p. 45.
- [188] W. Glöckle, H. Witała, H. Kamada, D. Hüber, J. Golak, Few-Body Systems, Suppl 8 (1996) 9.
- [189] W. Glöckle, H. Kamada, H. Witała, D. Hüber, J. Golak, K. Miyagawa, S. Ishikawa, Few-Body Systems, Suppl 9 (1996) 384.
- [190] M.L. Goldberger, K.M. Watson, Collision Theory (Wiley, New York, 1964) p. 270.
- [191] D. Gola, W. Bretfeld, W. Burgmer, H. Eichner, Ch. Heinrich, H.J. Helten, H. Kretzer, K. Prescher, H. Oswald, W. Schnorrenberg, H. Paetz gen. Schieck, Phys. Rev. C 27 (1983) 1394.
- [192] D. Gola, Ch. Heinrich, Nucl. Instr. Meth. A 243 (1986) 424.
- [193] J. Golak, H. Kamada, H. Witała, W. Glöckle, S. Ishikawa, Phys. Rev. C 51 (1995) 1638.
- [194] J. Golak, PhD Thesis, Jagellonian University 1994, unpublished, and private communication.
- [195] J. Golak, H. Witała, H. Kamada, D. Hüber, S. Ishikawa, W. Glöckle, Phys. Rev C 52 (1995) 1216.
- [196] D. Gotta, M. Dörr, W. Fettscher, G. Schmidt, G. Ulrich, G. Backenstoss, M. Izzycki, W. Kowald, I. Schwanner, P. Weber, H.D. Weyer, Phys. Rev. C 51 (1995) 469.
- [197] M. Gouanere, M. Chemarin, G. Nicolai, J-P. Burg, Nucl. Phys. A 144 (1970) 607.
- [198] P. Grassberger, W. Sandhas, Nucl. Phys. B 2 (1967) 181.
- [199] A.M. Green, in: Mesons in Nuclei, M. Rho and D. Wilkinson, eds. (North-Holland, Amsterdam, 1979) p. 227.
- [200] F. Gross, Phys. Rev. C 26 (1982) 2203.
- [201] F. Gross, Phys. Rev. C 26 (1982) 2226.
- [202] F. Gross, J.W. van Orden, K. Holinde, Phys. Rev. C 45 (1992) 2094.
- [203] R. Großmann, Diplom Thesis, Köln, 1993.
- [204] F. Gross, private communication.
- [205] W. Grüebler, V. Koenig, P.A. Schmelzbach, B. Jenny, H.R. Buergl, P. Doleshall, G. Heidenreich, H. Roser, F. Seiler, W. Reichart, Phys. Lett. B 74 (1978) 173.
- [206] W. Grüebler, V. König, P.A. Schmelzbach, F. Sperisen, B. Jenny, R.E. White, F. Seiler, H.W. Roser, Nucl. Phys. A 398 (1983) 445.
- [207] W. Grüebler, Nucl. Phys. A 353 (1981) 31c.
- [208] V.K. Gupta, B.S. Bhakar, A.N. Mitra, Phys. Rev. Lett. 15 (1965) 974.
- [209] H. van Haeringen, R. van Wageningen, J. Math. Phys. 16 (1975) 1441.
- [210] H. van Haeringen, Charged-Particle Interactions (Coulomb Press, Leyden, 1985).
- [211] M.I. Hafel, I. Slaus, D.L. Shannon, M.B. Epstein, W.T.H. van Oers, G. Anzelon, E.L. Petersen, W. Breunlich, Nucl. Phys. A 269 (1976) 359.
- [212] Y. Hahn, D.J. Kouri, F.S. Levin, Phys. Rev. C 10 (1974) 1615.
- [213] R.C. Haight, S.M. Grimes, J.D. Anderson, Phys. Rev. C 16 (1977) 97.
- [214] J. Haidenbauer, W. Plessas, Phys. Rev. C 27 (1983) 63.

- [215] J. Haidenbauer, W. Plessas, Phys. Rev. C 30 (1984) 1822.
- [216] J. Haidenbauer, W. Plessas, Phys. Rev. C 32 (1985) 1424.
- [217] J. Haidenbauer, Y. Koike, W. Plessas, Phys. Rev. C 33 (1986) 439.
- [218] J. Haidenbauer, Y. Koike, Phys. Rev. C 34 (1986) 1187.
- [219] Ch. Hajduk, P.U. Sauer, W. Struve, Nucl. Phys. A 405 (1983) 581.
- [220] Ch. Hajduk, P.U. Sauer, S.N. Yang, Nucl. Phys. A 405 (1983) 605.
- [221] E. Harms, Phys. Rev. C 1 (1970) 1667.
- [222] E.P. Harper, Y.E. Kim, A. Tubis, Phys. Rev. C 6 (1972) 126.
- [223] K. Hatanaka, N. Matsuoka, H. Sakai, T. Saito, K. Hosono, Y. Koike, M. Kondo, K. Imai, H. Shimizu, T. Ichihara, K. Nismura, A. Okihana, Nucl. Phys. A 426 (1984) 77.
- [224] R. Henneck, Phys. Rev. C 47 (1993) 1859.
- [225] R.C. Herndon, Y.C. Tang, Phys. Rev. 153 (1967) 1091.
- [226] R.C. Herndon, Y.C. Tang, Phys. Rev. 159 (1967) 853.
- [227] R.C. Herndon, Y.C. Tang, Phys. Rev. 165 (1968) 1093.
- [228] J.H. Hetherington, L.H. Schick, Phys. Rev. B 139 (1965) 1164.
- [229] M. Holmberg, Nucl. Phys. A 129 (1969) 327.
- [230] J. Horacek, T. Sasakawa, Phys. Rev. A 28 (1983) 2151.
- [231] J. Horacek, T. Sasakawa, Phys. Rev. A 30 (1985) 2274; C 32 (1985) 70.
- [232] C.R. Howell, W. Tornow, K. Murphy, H.G. Pfützner, M.L. Roberts, Anli Li, P.D. Felsher, R.L. Walter, I. Slaus, P.A. Treado, Y. Koike, Few-Body Systems 2 (1987) 19.
- [233] C.R. Howell, W. Tornow, I. Slaus, P.D. Felsher, M.L. Roberts, H.G. Pfützner, Anli Li, K. Murphy, R.L. Walter, J.M. Lambert, P.A. Treado, H. Witała, W. Glöckle, Th. Cornelius, Phys. Rev. Lett. 61 (1988) 1565.
- [234] C.R. Howell, W. Tornow, H.R. Setze, R.T. Braun, D.E. Gonzalez Trotter, C.D. Roper, R.S. Pedroni, S.M. Grimes, C.E. Brient, N. Al-Niemi, F.C. Goeckner, G. Mertens, Few-Body Systems 16 (1994) 127.
- [235] D. Hüber, H. Witała, W. Glöckle, Few-Body Systems 14 (1993) 171.
- [236] D. Hüber, PhD Thesis, Bochum 1993, unpublished.
- [237] D. Hüber, H. Kamada, H. Witała, W. Glöckle, Few-Body Systems 16 (1994) 165.
- [238] D. Hüber, W. Glöckle, J. Golak, H. Witała, H. Kamada, A. Kievsky, S. Rosati, M. Viviani, Phys. Rev. C 51 (1995) 1100.
- [239] D. Hüber, J. Golak, H. Witała, W. Glöckle, H. Kamada, accepted for publication in Few-Body Systems.
- [240] D. Hüber, J. Golak, H. Witała, W. Glöckle, H. Kamada, in Few-Body Systems, Suppl 9 (1996) 399.
- [241] J. Hunziker, in: Lectures in Theoretical Physics, ed. A.O. Barut, W.E. Brittin (Gordon and Breach, New York, 1968) p. 1.
- [242] G. Igo, J.C. Fong, S.L. Verbeck, M. Goitein, D.L. Hendrie, J.C. Carroll, B. McDonald, A. Stetz, M.C. Makino, Nucl. Phys. A 195 (1972) 33.
- [243] C.H.Q. Ingram, Nucl. Phys. A 553 (1993) 573c.
- [244] S. Ishikawa, Nucl. Phys. A 463 (1987) 145c.
- [245] S. Ishikawa, T. Sasakawa, Phys. Rev. C 45 (1992) R1428.
- [246] S. Ishikawa, H. Kamada, W. Glöckle, J. Golak, H. Witała, Nuovo Cimento 107A (1994) 305.
- [247] S. Ishikawa, H. Kamada, W. Glöckle, J. Golak, H. Witała, Phys. Lett. B 339 (1994) 293.
- [248] S. Ishikawa, Y. Wu, T. Sasakawa, in: AIP Conference Proceedings 334 on Few-Body Problems in Physics, Williamsburg 1994, ed. F. Gross (AIP Press, New York, 1995) p. 840.
- [249] A.D. Jackson, J.A. Tjon, Phys. Lett. 32 B (1970) 9.
- [250] H. Jacob, V.S. Bhasin, A.N. Mitra, Phys. Rev. D 1 (1970) 3496.
- [251] M. Jain, J.G. Rogers, D.P. Saylor, Phys. Rev. Lett. 31 (1973) 838.
- [252] G. Janson, L. Glantz, A. Johansson, I. Koersner, in Few-Body Problems in Physics, Vol. II, ed. B. Zeitnitz (Amsterdam, North-Holland, 1984) p. 529.
- [253] E. Jans, private communication.
- [254] J.N. Jauch, Helv. Phys. Acta 31 (1958) 127; 31 (1958) 66.
- [255] A.R. Johnston, W.R. Gibson, J.H.P.C. Megaw, R.J. Griffiths, R.M. Eisberg, Phys. Lett. 19 (1965) 289.
- [256] R. Jost, Helv. Phys. Acta 20 (1947) 356.

- [257] J. Jourdan, M. Baumgartner, S. Burzynski, P. Egelhoff, R. Henneck, A. Klein, M.A. Pickar, G.R. Plattner, W.D. Ramsay, H.W. Roser, I. Sick, J. Torre, Nucl. Phys. A 453 (1986) 220.
- [258] J. de Juren, N. Knable, Phys. Rev. 77 (1950) 606.
- [259] J. de Juren, Phys. Rev. 80 (1950) 27.
- [260] J.A. Kadyk, G. Alexander, J.H. Chan, P. Gaposchkin, G.H. Trilling, Nucl. Phys. B 27 (1971) 13.
- [261] H. Kamada, H. Witała, W. Glöckle, Journal of Nuclear Physics 56 (1993) 29.
- [262] H. Kamada, private communication.
- [263] M. Karus, M. Bubulla, J. Helten, B. Laumann, R. Melzer, P. Niessen, H. Oswald, G. Rauprich, J. Schulte-Uebbing, H. Paetz gen. Schieck, Phys. Rev. C 31 (1985) 1112.
- [264] J. Kecskemeti, T. Czibok, B. Zeitniz, Nucl. Phys. A 254 (1975) 110.
- [265] P.H.M. Keizer, PhD Thesis (Amsterdam 1986), unpublished.
- [266] B.D. Keister, W.N. Polyzou, Advanc. in Nucl. Phys. 20 (1991) 225.
- [267] A.K. Kerman, M. McManus, R.M. Thaler, Ann. Phys. 8 (1959) 551.
- [268] A. Kievsky, M. Viviani, S. Rosati, Nucl. Phys. A 551 (1993) 241.
- [269] A. Kievsky, M. Viviani, S. Rosati, Few-Body Systems, Suppl. 7 (1994) 278.
- [270] A. Kievsky, M. Viviani, S. Rosati, Nucl. Phys. A 577 (1994) 511.
- [271] A. Kievsky, M. Viviani, S. Rosati, Phys. Rev. C 52 (1995) R15.
- [272] N.S.P. King, J.L. Romero, J. Ullmann, H.E. Conzett, R.M. Larimer, R. Roy, Phys. Lett. B 69 (1977) 151.
- [273] St. Kistryn, W. Hajdas, J. Lang, R. Müller, J. Balewski, K. Bodek, L. Jarczyk, B. Kamys, A. Strzalkowski, D. Dechant, J. Krug, W. Lübeck, H. Rühl, G. Spangardt, M. Steinke, M. Stephan, D. Kamke, R. Henneck, H. Witała, Th. Cornelius, W. Glöckle, J. Golak, Nucl. Phys. A 548 (1992) 49.
- [274] F. Klein et al in AIP Conference Proceedings 334 on Few-Body Problems in Physics, Williamsburg 1994, ed. F. Gross (AIP Press, New York, 1995) p. 146.
- [275] W.M. Kloet, J.A. Tjon, Nucl. Phys. A 210 (1973) 380.
- [276] W.M. Kloet, J.A. Tjon, Ann. Phys. 79 (1973) 407.
- [277] R.A.M.M. Klomp, J.L. de Kok, M.C.M. Rentmeester, Th. A. Rijken, J.J. de Swart, AIP Conference Proceedings 334 on Few-Body Problems in Physics, Williamsburg 1994, ed. F. Gross (AIP Press, New York, 1995) p. 367.
- [278] W. Kluge, R. Schlueter, W. Ebenhoeh, Nucl. Phys. A 228 (1974) 29.
- [279] L.D. Knutson, L.O. Lamm, J.E. McAninch, Phys. Rev. Lett. 71 (1993) 3762.
- [280] Y. Koike, Y. Taniguchi, Phys. Lett. B 118 (1982) 248.
- [281] Y. Koike, Y. Taniguchi, Few-Body Systems 1 (1986) 13.
- [282] Y. Koike, J. Haidenbauer, W. Plessas, Book of Contributions, 11th International IUPAP Conference in Few-Body Systems in Particle and Nuclear Physics, Tokyo and Sendai (1986) p. 346.
- [283] Y. Koike, J. Haidenbauer, Nucl. Phys. A 463 (1987) 365c.
- [284] Y. Koike, J. Haidenbauer, W. Plessas, Phys. Rev. C 35 (1987) 396.
- [285] Y. Koike, D.R. Lehman, L.C. Maximon, W.C. Parke, AIP Conference Proceedings 334 on Few-Body Problems in Physics, Williamsburg 1994, ed. F. Gross (AIP Press, New York, 1995) p. 836.
- [286] L.P. Kok, H. van Haeringen, Phys. Rev. C 21 (1980) 512.
- [287] U. van Kolck, Phys. Rev. C 49 (1994) 2932.
- [288] L.A. Kondratyuk, F.M. Lev, V.V. Soloviev, Few-Body Systems 7 (1989) 55.
- [289] N. Koori, Journ. of the Phys. Soc. of Japan 32 (1972) 306.
- [290] N. Koori et al., in Book of Contributions, Conference on Few-Body Systems in Particle and Nuclear Physics, eds. T. Sasakawa et al., Suppl. Res. Rep. Tohoku Univ. 19. (1986) 406.
- [291] N. Koori, M. Hyakutake, M. Matoba, H. Ijiri, Y. Fujita, Y. Uozumi, S. Shirato, T. Motobayashi, T. Ohsawa, K. Sagara, Nucl. Instr. Meth. A 278 (1989) 737.
- [292] V.V. Kostrykin, A.A. Kvitsinsky, S.P. Merkuriev, Few-Body Systems 6 (1989) 97.
- [293] H. Kottler, K.L. Kowalski, Phys. Rev. B 138 (1965) 619.
- [294] H.P. Kotz, Ch. Brandstaetter, W. Plessas, G. Berthold, AIP Conference Proceedings 334 on Few-Body Problems in Physics, Williamsburg 1994, ed. F. Gross (AIP Press, New York, 1995) p. 482.
- [295] D.J. Kouri, F.S. Levin, Phys. Lett. B 50 (1974) 421.
- [296] K.L. Kowalski, Phys. Rev. Lett. 15 (1965) 798.
- [297] K.L. Kowalski, Phys. Rev. D 7 (1973) 1806.

- [298] K.L. Kowalski, Nucl. Phys. A 264 (1976) 173.
- [299] K.L. Kowalski, Lett. Nuovo Cimento 22 (1978) 531.
- [300] W. Kretschmer, private communication.
- [301] W. Kretschmer et al., AIP Conference Proc. 339 (1995) 335. (Polarization Phenomena in Nuclear Physics, Bloomington, 1994).
- [302] J. Krug, private communication.
- [303] A.F. Kuckes, R. Wilson, Phys. Rev. 121 (1963) 1226.
- [304] A.F. Kuckes, R. Wilson, P.F. Cooper, Jr., Ann. Phys. 15 (1961) 193.
- [305] V. Kulkarni, PhD Thesis (1981).
- [306] V. Kulkarni, J. Rapaport, R.W. Finlay, G. Randers-Pehrson, R.D. Koshel, Nucl. Phys. A 367 (1981) 157.
- [307] Yu. A. Kuperin, S.P. Merkuriev, A.A. Kvitsinsky, Sov. J. Nucl. Phys. 37 (1983) 857.
- [308] K. Kuroda, A. Michalowicz, M. Poulet, Nucl. Phys. 88 (1966) 33.
- [309] A.A. Kvitsinsky, V.V. Kostrykin, S.P. Merkuriev, Sov. J. Part. Nucl. 21 (1990) 553.
- [310] M. Lacombe, B. Loiseau, J.M. Richard, R. Vinh Mau, J. Coté, P. Pirés, R. de Tourreil, Phys. Rev. C 21 (1980) 861.
- [311] J.M. Lambert, P.A. Treado, R.G. Allas, L.A. Beach, R.O. Bondelid, E.M. Diener, Phys. Rev. C 13 (1976) 43.
- [312] A. Laverne, C. Gignoux, Nucl. Phys. A 203 (1973) 597.
- [313] J. Lefrancois, R.A. Hoffman, E.H. Thorndike, R. Wilson, Phys. Rev. 131 (1963) 1660.
- [314] J.M. Levy-Leblond, M. Levy-Nahas, J. Math. Phys. 6 (1965) 1571.
- [315] F.S. Levin, W. Sandhas, Phys. Rev. C 29 (1984) 1617.
- [316] B.A. Lippmann, J. Schwinger, Phys. Rev. 79 (1950) 469.
- [317] B.A. Lippmann, Phys. Rev. 102 (1956) 264.
- [318] C. Lovelace, in: Lectures of the 1963 Edinburgh Summer School, ed. R.G. Moorhouse (1964).
- [319] D.A. Low, E.J. Stephenson, C. Olmer, A.K. Opper, B.K. Park, P. Schwandt, S.W. Wissink, Phys. Rev. C 44 (1991) 2276.
- [320] R. Machleidt, K. Holinde, Ch. Elster, Phys. Rep. 149 (1987) 1.
- [321] R. Machleidt, Adv. Nucl. Phys. 19 (1989) 189.
- [322] R. Machleidt, private communication.
- [323] Mahavir Jain, J.G. Rogers, D.P. Saylor, Phys. Rev. Lett. 31 (1973) 838.
- [324] R.A. Malfliet, J.A. Tjon, Nucl. Phys. A 127 (1969) 161.
- [325] V.B. Mandelzweig, Nucl. Phys. A 508 (1990) 63c.
- [326] V.B. Mandelzweig, Few-Body Systems, Suppl. 7 (1994) 371.
- [327] C. Marchand, P. Barreau, M. Bernheim, P. Bradu, G. Fournier, Z.E. Meziani, J. Miller, J. Morgenstern, J. Picard, B. Saghai, S. Turck-Chieze, P. Vernin, M.K. Brussel, Phys. Lett. B 153 (1985) 29.
- [328] J.E. McAninch, W. Haeberli, H. Witata, W. Glöckle, J. Golak, Phys. Lett. B 307 (1993) 13.
- [329] J.E. McAninch, L.O. Lamm, W. Haeberli, Phys. Rev. C 50 (1994) 589.
- [330] A.M. McDonald, D.I. Bonbright, W.T.H. van Oers, J.W. Watson, J.G. Rogers, J.M. Cameron, J. Soukup, W.M. Kloet, J.A. Tjon, Phys. Rev. Lett. 34 (1975) 488.
- [331] B.H.J. McKellar, Lecture Notes in Physics 260 (1986) 7.
- [332] D.F. Measday, J.N. Palmieri, Nucl. Phys. 85 (1966) 142.
- [333] W. Meier, Ph-D Thesis, Bochum 1983, unpublished.
- [334] W. Meier, W. Glöckle, Phys. Lett. 138B (1984) 329.
- [335] E. van Meijgaard, J.A. Tjon, Phys. Rev. C 42 (1990) 74.
- [336] E. van Meijgaard, J.A. Tjon, Phys. Rev. C 42 (1990) 96.
- [337] E. van Meijgaard, J.A. Tjon, Phys. Rev. C 45 (1992) 1463.
- [338] S.P. Merkuriev, C. Gignoux, A. Laverne, Ann Phys. 99 (1976) 30.
- [339] S.P. Merkuriev, Ann Phys. 130 (1980) 395.
- [340] D.I. Meyer, W. Nyer, Report LA-1279, 5107.
- [341] A.B. Migdal, Sov. Phys. JETP 1 (1955) 2.
- [342] G.A. Miller, B.M.K. Nefkens, I. Slaus, Phys. Rep. 194 (1990) 1.
- [343] A.N. Mitra, Nucl. Phys. 32 (1962) 529; Phys. Rev. 127 (1962) 1342.
- [344] K. Miyagawa, W. Glöckle, Phys. Rev. C 48 (1993) 2576.
- [345] K. Miyagawa, H. Kamada, W. Glöckle, V.C. Stoks, Phys. Rev. C 51 (1995) 2905.

- [346] L. Müller, Nucl. Phys. A 360 (1981) 331.
- [347] L. Müller, Nuovo Cimento **75A** (1983) 39.
- [348] S. Mukhopadhyya, S. Levenson, R.E. Segel, G. Garino, D. Geesaman, J.P. Schiffer, G. Stephans, B. Zeidman, E. Unguillet, H. Jackson, R. Kowalczyk, D. Ashery, E. Piaretsky, M. Moinester, I. Navon, L.S. Smith, R.S. Minehart, G.S. Das, R.R. Whitney, R. McKeown, B. Anderson, R. Madey, J. Watson, Phys. Rev. C 43 (1991) 957.
- [349] M.M. Nagels, T.A. Rijken, J.J. de Swart, Phys. Rev. D 17 (1978) 768.
- [350] G. Nitzsche, Diploma Thesis, Köln 1994, unpublished.
- [351] H.P. Noyes, Phys. Rev. Lett. **15** (1965) 538.
- [352] H.P. Noyes, in Three Body Problems in Nuclear and Particle Physics, eds. J.S.C. McKee and P.M. Rolph (North-Holland Publishing Company, Amsterdam, London, 1970) p. 2.
- [353] R.G. Nuckolls, C.L. Bailey, W.E. Bennett, T. Bergstrahl, H.G. Richards, J.H. Williams, Phys. Rev. **70** (1946) 805.
- [354] S. Obermanns, Diploma Thesis, Bochum 1989, unpublished.
- [355] W.T.H. van Oers, Proceedings of the VII International Conference on Few-Body Problems in Nuclear and Particle Physics, Dehli, 1976, eds. A.N. Mitra, I. Slaus, V.S. Bhasin, V.K. Gupta (North Holland, Amsterdam, 1976) p. 746.
- [356] K. Ogawa, H. Narumi, Y. Sunami, Prog. Theor. Phys. **63** (1980) 533.
- [357] G.O. Ohlsen, Rep. Prog. Phys. **35** (1972) 717.
- [358] G. G Ohlsen, Lecture Notes in Physics **87** (1978) 295.
- [359] G. G Ohlsen, R.E. Brown, F.D. Correl, R.A. Hardekopf, Nucl. Instr. Meth. **179** (1981) 283.
- [360] S. Okubo, Prog. Theor. Phys. **12** (1954) 603.
- [361] Electron-Nucleus Scattering, EIPC Italy 1993, eds. O. Benhar, A. Fabrocini, R. Schiavilla (World Scientific, Singapore, 1994).
- [362] S. Oryu, Prog. Theor. Phys. **52** (1974) 550.
- [363] S. Oryu, M. Araki, S. Satoh, Suppl. Prog. Theor. Phys. **61** (1977) 199.
- [364] S. Oryu, Lecture Notes in Phys. **273** (1987) 123.
- [365] J.N. Palmieri, Nucl. Phys. A 188 (1972) 72.
- [366] H. Patberg, PhD Thesis, Köln 1995, unpublished.
- [367] G. Paulette, F.D. Brooks, Nucl. Phys. A 255 (1975) 267.
- [368] G.L. Payne, J.L. Friar, B.F. Gibson, Phys. Rev. C 26 (1982) 1385.
- [369] G.L. Payne, Lecture Notes in Physics **273** (1987) 64.
- [370] G.L. Payne, private communication and G.L. Payne, W. Glöckle, in preparation.
- [371] M.T. Pena, H. Henning, P.U. Sauer, Phys. Rev. C 42 (1990) 855.
- [372] E.L. Petersen, M.I. Haftel, R.G. Allas, L.A. Beach, R.O. Boudelid, P.A. Treado, J.M. Lambert, M. Jain, J.M. Wallace, Phys. Rev. C 9 (1974) 508.
- [373] A.C. Phillips, Phys. Rev. **142** (1966) 984.
- [374] T.W. Phillips, B.L. Berman, J.D. Seagrave, Phys. Rev. C 22 (1980) 384.
- [375] A. Picklesimer, R.A. Rice, R. Brandenburg, Phys. Rev. C 44 (1991) 1359.
- [376] A. Picklesimer, R.A. Rice, R. Brandenburg, Phys. Rev. C 45 (1992) 547.
- [377] A. Picklesimer, R.A. Rice, R. Brandenburg, Phys. Rev. C 45 (1992) 2045.
- [378] A. Picklesimer, R.A. Rice, R. Brandenburg, Phys. Rev. C 45 (1992) 2624.
- [379] A. Picklesimer, R.A. Rice, R. Brandenburg, Phys. Rev. C 46 (1992) 1178.
- [380] A. Picklesimer, R.A. Rice, R. Brandenburg, Few-Body Systems **19** (1995) 47.
- [381] S.C. Pieper, Phys. Rev. Lett. **27** (1971) 1738.
- [382] S.C. Pieper, K.L. Kowalski, Phys. Rev. C 5 (1972) 306.
- [383] S.C. Pieper, Nucl. Phys. A 193 (1972) 519; A 193 (1972) 529; Phys. Rev. C 6 (1972) 1157.
- [384] S.C. Pieper, Phys. Rev. C 8 (1973) 1702.
- [385] W. Plessas in Few-Body Methods, proceedings of the International Symposium on Few-Body Methods and their Applications in Atomic, Molecular and Nuclear Physics and Chemistry, Nanning 1985) ed. T.K. Lim et al. (World Scientific, Singapore, 1986) p. 43.
- [386] W. Plessas, J. Haidenbauer, Y. Koike, Few-Body Systems, Suppl. **1** (1986) 172.
- [387] W. Plessas, Lecture Notes in Physics **273** (1987) 137.
- [388] D. Plümper, J. Flender, M.F. Gari, Phys. Rev. C 49 (1994) 2370.
- [389] W.N. Polyzou, Ann. Phys. **193** (1989) 367.

- [390] W.N. Polyzou, W. Glöckle, *Few-Body Systems* **9** (1990) 97.
- [391] H.L. Poss, E.O. Salant, G.A. Snow, L.C.L. Yuan, *Phys. Rev.* **87** (1952) 11.
- [392] H. Postma, R. Wilson, *Phys. Rev.* **121** (1961) 1229.
- [393] R.D. Present, *Phys. Rev.* **50** (1936) 635.
- [394] L.M. Quin, W. Boeglin, D. Fritsch, J. Goetz, J. Jourdan, G. Masson, S. Robinson, I. Sick, P. Trueb, M. Tuccillo, B. Zihlmann, H. Witala, J. Golak, W. Glöckle, D. Hüber, *Nucl. Phys. A* **587** (1995) 252.
- [395] M. Rauh, PhD Thesis, Mainz 1993, unpublished.
- [396] G. Rauprich, H.J. Hähn, M. Karus, P. Nießen, K.R. Nyga, H. Oswald, L. Sydow, H. Paetz gen. Schieck, Y. Koike, *Few-Body Systems* **5** (1988) 67.
- [397] G. Rauprich, S. Lemaitre, P. Niessen, K.R. Nyga, R. Reckensfelderbäumer, L. Sydow, H. Paetz gen. Schieck, H. Witała, W. Glöckle, *Nucl. Phys. A* **535** (1991) 313.
- [398] G. Rauprich, PhD Thesis, Köln 1991.
- [399] E.F. Redish, *Nucl. Phys. A* **225** (1974) 16.
- [400] R.V. Reid, *Ann. Phys.* **50** (1968) 411.
- [401] G.A. Retzlaff et al., *Phys. Rev. C* **49** (1994) 1263.
- [402] A.G. Reuber, K. Holinde, J. Speth, *Czech. J. Phys.* **42** (1992) 1115.
- [403] R.A.J. Riddle, A. Langsford, P.H. Bowen, G.C. Cox, *Nucl. Phys.* **61** (1965) 457.
- [404] Th. A. Rijken, R.A.M. Klomp J.J. deSwart in *Essays in Celebration of the Life of Robert Eugen Marshak*, ed. E.C.G. Sudershan (World Scientific, Singapore, 1995).
- [405] M.R. Robilotta, M.P. Isidro Filho, *Nucl. Phys. A* **414** (1984) 394.
- [406] M.R. Robilotta, M.P. Isidro Filho, H.T. Coelho, T.K. Das, *Phys. Rev. C* **31** (1985) 646.
- [407] M.R. Robilotta, M.P. Isidro Filho, *Nucl. Phys. A* **451** (1986) 581.
- [408] M.R. Robilotta, H.T. Coelho, *Nucl. Phys. A* **460** (1986) 645.
- [409] M.R. Robilotta, *Few-Body Systems, Suppl.* **2** (1987) 35.
- [410] L.S. Rodberg, R.M. Thaler, *Introduction to the Quantum Theory of Scattering* (Academic Press, New York, 1967) p. 123.
- [411] J.L. Romero, J.A. Jungerman, F.P. Brady, W.J. Knox, Y. Ishizaki, *Phys. Rev. C* **2** (1970) 2134.
- [412] J.L. Romero, J.L. Ullmann, F.P. Brady, J.D. Carlson, D.H. Fitzgerald, A.L. Sagle, T.S. Subramanian, C.I. Zanelli, N.S.P. King, M.W. McNaughton, B.E. Bonner, *Phys. Rev. C* **25** (1982) 2214.
- [413] H. Rühl, B. Dechant, J. Krug, W. Lübcke, G. Spangardt, M. Steinke, M. Stephan, D. Kamke, J. Balewski, K. Bodek, L. Jarczyk, A. Strzałkowski, W. Hajdas, St. Kistryn, R. Müller, J. Lang, R. Henneck, H. Witała, Th. Cornelius, W. Glöckle, *Nucl. Phys. A* **524** (1991) 377.
- [414] G. Rupp, J.A. Tjon, *Phys. Rev. C* **45** (1992) 2133.
- [415] C. Ruth et al., *Phys. Rev. Lett.* **72** (1994) 617.
- [416] K. Sagara, H. Oguri, S. Shimizu, K. Maeda, H. Nakamura, T. Nakashima, S. Morinobu, *Phys. Rev. C* **50** (1994) 576.
- [417] SAID program, Virginia Polytechnic Institute, Blacksburg, VA.
- [418] P. Salvisberg et al., *Phys. Rev. C* **46** (1992) 2172.
- [419] F. Sammarruca, D.P. Xu, R. Machleidt, *Phys. Rev. C* **46** (1992) 1636.
- [420] W. Sandhas, in *Few-Body Dynamics*, eds. A.N. Mitra et al. (North-Holland, Amsterdam, 1976) p. 540.
- [421] W. Sandhas, in *Few-Body Nuclear Physics*, eds. G. Pisent, V. Vanzani, L. Fonda (IAEA, Vienna, 1978) p. 3.
- [422] T. Sasakawa, S. Ishikawa, *Few-Body Systems* **1** (1986) 3.
- [423] T. Sasakawa, *Few-Body Systems, Suppl.* **1** (1986) 104.
- [424] T. Sasakawa, *Lecture Notes in Physics* **273** (1987) 53.
- [425] P.U. Sauer, W. Glöckle, *Europhysics News* **15** (1984) 5.
- [426] M. Sawada, S. Seki, K. Furuno, Y. Tagishi, Y. Nagashima, J. Schimizu, M. Ishikawa, T. Sugiyama, L.S. Chuang, W. Gruebler, J. Sanada, Y. Koike, Y. Taniguchi, *Phys. Rev. C* **27** (1983) 1932.
- [427] R.D. Schamberger, *Phys. Rev.* **85** (1952) 424.
- [428] L.H. Schick, J.H. Hetherington, *Phys. Rev.* **156** (1967) 1602.
- [429] P.A. Schmelzbach, W. Gruebler, R.E. White, V. Koenig, R. Risler, P. Marmier, *Nucl. Phys. A* **197** (1972) 273.
- [430] E.W. Schmid, H. Ziegelmann, *The Quantum Mechanical Three-Body Problem* (Pergamon Press, Oxford, 1974).

- [431] P. Schwarz, H.O. Klages, P. Doll, B. Haesner, J. Wilczynski, B. Zeitnitz, J. Kecskeméti, Nucl. Phys. A 398 (1983) 1.
- [432] R. Schiavilla, V.R. Pandharipande, R.B. Wiringa, Nucl. Phys. A 449 (1986) 219.
- [433] O. Schori, B. Gabioud, C. Joseph, J.P. Perroud, D. Rüegner, M.T. Tran, P. Truoel, E. Winkelmann, W. Dahme, Phys. Rev. C 35 (1987) 2252.
- [434] H. Paetz gen. Schieck, private communication.
- [435] J.D. Seagrave, R.L. Henkel, Phys. Rev. 98 (1955) 666.
- [436] J.D. Seagrave, J.C. Hopkins, D.R. Dixon, P.W. Keaton Jr., E.C. Kerr, A. Niler, R.H. Sherman, R.K. Walter, Ann. Phys. (N.Y.) 74 (1972) 250.
- [437] B. Sechi-Zorn, B. Kehoe, J. Twitty, Phys. Rev. 175 (1968) 1735.
- [438] R.G. Seyler, Nucl. Phys. A 124 (1969) 253.
- [439] D.L. Shannon, W. Breunlich, I. Slaus, J.W. Sunier, G. Anzelou, E. Tin, W.T.H. van Oers, M.B. Epstein, W. Ebenhoeh, Nucl. Phys. A 218 (1974) 381.
- [440] S. Shirato, N. Koori, Nucl. Phys. A 120 (1968) 387.
- [441] S. Shirato, K. Saitoh, N. Koori, R.T. Cahill, Nucl. Phys. A 215 (1973) 277.
- [442] H. Shimizu, K. Imai, N. Tamura, K. Nisimura, K. Hatanaka, T. Saito, Y. Koike, Y. Taniguchi, Nucl. Phys. A 382 (1982) 242.
- [443] S. Shirato, Y. Ishibe, K. Shibata in Book of Contributions, Conference on Few-Body Systems in Particle and Nuclear Physics, eds. T. Sasakawa et al., Suppl. Res. Rep. Tohoku Univ. 19. (1986) 412.
- [444] S. Shimizu, K. Sagara, H. Nakamura, K. Maeda, T. Miwa, N. Nishimori, S. Ueno, T. Nakashima, S. Morinobu, Phys. Rev. C 52 (1995) 1193.
- [445] Yu. A. Simonov, Sov. J. Nucl. Phys. 3 (1966) 461.
- [446] I. Slaus, Y. Akaishi, H. Tanaka, Phys. Rep. 173 (1989) 257.
- [447] I.H. Sloan, Phys. Rev. C 6 (1972) 1945.
- [448] F.T. Smith, Phys. Rev. 120 (1960) 1058.
- [449] F.T. Smith, J. Math. Phys. 3 (1962) 735.
- [450] L.C. Smith et al., Phys. Rev. C 40 (1989) 1347.
- [451] S.N. Sokolov, Theor. Mat. Fiz. 23 (1975) 355.
- [452] S.N. Sokolov, Dokl. Akad. Nauk. SSSR 233 (1977) 575.
- [453] S.N. Sokolov, A.N. Shatnii, Theor. Mat. Fiz. 37 (1978) 291.
- [454] J. Sowinski, D.D. Pun Casavant, L.D. Knutson, Nucl. Phys. A 464 (1987) 223.
- [455] F. Sperisen, W. Gruebler, V. Koenig, P.A. Schmelzbach, B. Jenny, K. Elsener, C. Schweizer, J. Ulbricht, P. Doleshall, Phys. Lett. B 102 (1981) 9.
- [456] F. Sperisen, W. Gruebler, V. Koenig, P.A. Schmelzbach, K. Elsener, B. Jenny, C. Schweizer, J. Ulbricht, P. Doleshall, Phys. Lett. B 110 (1982) 103.
- [457] F. Sperisen, W. Gruebler, V. Koenig, P.A. Schmelzbach, K. Elsener, B. Jenny, C. Schweizer, J. Ulbricht, P. Doleshall, Nucl. Phys. A 422 (1984) 81.
- [458] A. Stadler, W. Glöckle, P.U. Sauer, Phys. Rev. C 44 (1991) 2319.
- [459] A. Stadler, P.U. Sauer, Phys. Rev. C 46 (1992) 64.
- [460] A. Stadler, J. Adam Jr., H. Henning, P.U. Sauer, Phys. Rev. C 51 (1995) 2896.
- [461] A. Stadler, F. Gross, AIP Conference Proceedings 334 on Few-Body Problems in Physics, Williamsburg 1994, ed. F. Gross (AIP Press, New York, 1995) p. 867.
- [462] M. Stephan, K. Bodek, J. Krug, W. Lübcke, S. Obermanns, H. Rühl, M. Steinke, D. Kamke, H. Witała, Th. Cornelius, W. Glöckle, Phys. Rev. C 39 (1989) 2133.
- [463] C. Stolk, J.A. Tjon, Phys. Rev. Lett. 35 (1975) 985.
- [464] C. Stolk, J.A. Tjon, Nucl. Phys. A 295 (1978) 384.
- [465] C. Stolk, J.A. Tjon, Nucl. Phys. A 319 (1979) 1.
- [466] V.G.J. Stoks, R.A.M. Klomp, M.C.M. Rentmeester, J.J. de Swart, Phys. Rev. C 48 (1993) 792.
- [467] V.G.J. Stoks, R.A.M. Klomp, C.P.F. Terheggen, J.J. de Swart, Phys. Rev. C 49 (1994) 2950.
- [468] V.G.J. Stoks, private communication.
- [469] A. Stricker, Y. Saji, Y. Ishizaki, J. Kokame, H. Ogata, T. Suehiro, I. Nouaka, Y. Sugiyama, S. Shirato, N. Koori, Nucl. Phys. A 190 (1972) 284.

- [470] J. Strate, K. Geissdörfer, R. Lin, J. Cub, E. Finckh, K. Gebhardt, S. Schindler, H. Witała, W. Glöckle, Th. Cornelius, *J. Phys. G: Nucl. Phys.* **14** (1988) L229.
- [471] J. Strate, K. Geissdörfer, R. Lin, W. Bielmeier, J. Cub, A. Ebneth, E. Finckh, H. Friess, G. Fuchs, K. Gebhardt, S. Schindler, *Nucl. Phys. A* **501** (1989) 51.
- [472] J.H. Stuivenberg, R. van Wageningen, *Nucl. Phys. A* **304** (1978) 141.
- [473] J.P. Svenne, J. Birchall, M. de Jong, N.T. Okumusoglu, J.S.C. McKee, Fifth Int. Symp. on polarization phenomena in nuclear physics, ed. G.G. Ohlsen, R.E. Brown, N. Jarmie, W.W. McNaughton, G.M. Hale, (AIP, 1981) p. 1237.
- [474] L. Sydow, S. Lemaitre, P. Niessen, K.R. Nyga, G. Rauprich, R. Reckenfelderländer, S. Vohl, H. Paetz gen. Schieck, H. Witała, W. Glöckle, *Nucl. Phys. A* **567** (1994) 55.
- [475] T. Takemiya, *Progress Theor. Phys.* **74** (1985) 301.
- [476] L.H. Thomas, *Phys. Rev.* **47** (1935) 903.
- [477] J.H. Tinlot, R.E. Warner, *Phys. Rev.* **124** (1961) 890.
- [478] W. Tobocman, *Phys. Rev. C* **9** (1974) 2466.
- [479] W. Tobocman, *Phys. Rev. C* **11** (1975) 43.
- [480] W. Tornow, C.R. Howell, M. Alohal, Z.P. Chen, P.D. Felsher, J.M. Hanly, R.L. Walter, G. Mertens, I. Slaus, H. Witała, W. Glöckle, *Phys. Lett.* **257** (1991) 273.
- [481] W. Tornow, C.R. Howell, R.L. Walter, I. Slaus, *Phys. Rev. C* **45** (1992) 459.
- [482] W. Tornow, H. Witała, W. Glöckle, *Few-Body Systems* **13** (1992) 11.
- [483] W. Tornow, R.T. Braun, H. Witała, *Phys. Lett. B* **318** (1993) 281.
- [484] W. Tornow, H. Witała, R.T. Braun, to be published.
- [485] W. Tornow, private communication.
- [486] W. Tornow, C.R. Howell, R.T. Braun, Q. Chen, D.E. Gonzales Trotter, C.D. Roper, F. Salinas, H.R. Setze, R.L. Walter, H. Witała, *Few-Body Systems, Suppl.* **8** (1995) 163.
- [487] W. Tornow, R.T. Braun, H. Witała, N. Koori, preprint 1995.
- [488] R. de Tourreil, D.W.L. Sprung, *Nucl. Phys. A* **201** (1973) 193.
- [489] V. Vanzani, *Lett. Nuovo Cimento* **16** (1976) 1.
- [490] V. Vanzani, in *Few-Body Nuclear Physics* (IAEA, Wien, 1978) p. 57.
- [491] V. Vanzani, *Lett. Nuovo Cimento* **23** (1978) 586.
- [492] W.H. von Witsch, private communication.
- [493] H.S. Wall, *Continued Fractions* (Chelsea, New York 1967).
- [494] J.D. Walecka, *Nucl. Phys. A* **574** (1994) 271c.
- [495] R.E. Warner, J.H. Tinlot, *Phys. Rev.* **125** (1962) 1028.
- [496] K.M. Watson, *Phys. Rev.* **88** (1952) 1163.
- [497] K.M. Watson, *Phys. Rev.* **89** (1953) 575.
- [498] J.W. Watson, R. Garrett, F.P. Brady, D.H. Fitzgerald, J.L. Romero, J.L. Ullmann, C.I. Zanelli, *Phys. Rev. C* **25** (1982) 2219.
- [499] P. Weber et al., *Nucl. Phys. A* **501** (1989) 765.
- [500] P. Weber et al., *Nucl. Phys. A* **534** (1991) 541.
- [501] H.J. Weyer, *Phys. Rep.* **195** (1990) 295.
- [502] B.J. Wielinga, J.R. Balder, G.F.J. Blommestijn, R. van Dantzig, W.M. Kloet, J.A. Tjon, I. Slaus, *Nucl. Phys. A* **261** (1976) 13.
- [503] E. Wigner, *Phys. Rev.* **43** (1933) 252.
- [504] H.B. Willard, J.K. Bair, C.M. Jones, *Phys. Lett.* **9** (1964) 339.
- [505] R.B. Wiringa, R.A. Smith, T.L. Ainsworth, *Phys. Rev. C* **29** (1984) 1207.
- [506] R.B. Wiringa, *Phys. Rev. C* **43** (1991) 1585.
- [507] R.B. Wiringa, V.G.J. Stoks, R. Schiavilla, *Phys. Rev. C* **51** (1995) 38.
- [508] R.B. Wiringa, private communication.
- [509] W. von Witsch, B. Gomez Moreno, W. Rosenstock, K. Ettling, J. Bruinsma, *Nucl. Phys. A* **329** (1979) 141; *Phys. Lett.* **80B** (1979) 187.
- [510] H. Witała, W. Glöckle, Th. Cornelius, *Few-Body Systems, Suppl.* **2** (1987) 555.
- [511] H. Witała, Th. Cornelius, W. Glöckle, *Few-Body Systems* **3** (1988) 123.
- [512] H. Witała, Th. Cornelius, W. Glöckle, *Few-Body Systems* **5** (1988) 89.

- [513] H. Witała, W. Glöckle, Th. Cornelius, Nucl. Phys. A 491 (1989) 157.
- [514] H. Witała, W. Glöckle, Th. Cornelius, Nucl. Phys. A 496 (1989) 446.
- [515] H. Witała, W. Glöckle, Th. Cornelius, Few-Body Systems 6 (1989) 79.
- [516] H. Witała, W. Glöckle, Th. Cornelius, Phys. Rev. C 39 (1989) 384.
- [517] H. Witała, W. Glöckle, Nucl. Phys. A 528 (1991) 48.
- [518] H. Witała, W. Glöckle, H. Kamada, Phys. Rev. C 43 (1991) 1619.
- [519] H. Witała, W. Glöckle, Few-Body Systems, Suppl. 6 (1992) 291.
- [520] H. Witała, W. Glöckle, T. Takemiy, Prog. Theor. Phys. 88 (1992) 1015.
- [521] H. Witała, W. Glöckle, L.E. Antonuk, J. Arvieux, D. Bachelier, B. Bonin, A. Boudard, J.M. Cameron, H.W. Fielding, M. Garcon, F. Jourdan, C. Lapointe, W.J. McDonald, J. Pasos, G. Roy, I. The, J. Tinslay, W. Tornow, J. Yonnet, W. Ziegler, Few-Body Systems 15 (1993) 67.
- [522] H. Witała, D. Hüber, W. Glöckle, Phys. Rev. C 49 (1994) R14.
- [523] H. Witała, D. Hüber, W. Glöckle, W. Tornow, D.E. Gonzales Trotter, accepted for publication in Few-Body Systems.
- [524] H. Witała, W. Glöckle, J. Golak, D. Hüber, H. Kamada, W. Tornow, E.J. Stephenson, D.A. Low, accepted for publication in Phys. Rec. C.
- [525] H. Witała, D. Hüber, W. Glöckle, J. Golak, A. Stadler, J. Adam, Jr., Phys. Rev. C 52 (1995) 1254.
- [526] H. Witała, J. Golak, W. Tornow, W. Glöckle, D. Hüber, Phys. Rev. C 51 (1995) 1095.
- [527] Y. Wu, S. Ishikawa, T. Sasakawa, Few-Body Systems 15 (1993) 145.
- [528] O.A. Yakubovsky, Sov. J. Nucl. Phys. 5 (1967) 937.
- [529] T. Yuasa, H. Nakamura-Yokota, N. Fujiwara, Suppl. Prog. Theor. Phys. 61 (1977) 161.
- [530] M. Zadro, M. Bogovac, G. Calvi, M. Lattuada, D. Miljanic, D. Reudic, C. Spitaleri, B. Vlahovic, H. Witała, W. Glöckle, J. Golak, H. Kamada, Il Nuovo Cimento 107A (1994) 185.
- [531] J. Zamudio-Cristi, B.E. Bonner, F.P. Brady, J.A. Jungerman, J. Wang, Phys. Rev. Lett. 31 (1973) 1009.
- [532] H. Zankel, W. Plessas, J. Haidenbauer, Phys. Rev. C 28 (1983) 538.
- [533] H. Zankel, W. Plessas, Z. Phys. A 317 (1984) 45.
- [534] B. Zeitnitz, R. Maschuw, P. Suhr, Nucl. Phys. A 149 (1970) 449.
- [535] B. Zeitnitz, R. Maschuw, P. Suhr, W. Ebenhoeh, J. Bruinsma, J.H. Stuivenberg, Nucl. Phys. A 231 (1974) 13.
- [536] J. Zejma, PhD Thesis, Jagellonian University, Cracow 1995, unpublished.
- [537] W. Zickendraht, Ann. Phys. 35 (1965) 18.